Deciphering the functionality of the centrosomal protein PCMD-1 and its contribution to centrosome stability

Dissertation
zur Erlangung des Doktorgrades der Naturwissenschaften
der Fakultät für Biologie
der Ludwig-Maximilians-Universität München

Alina Jessica Schreiner
München, 2025

Diese Dissertation wurde angefertigt
unter der Leitung von Dr. Tamara Mikeladze-Dvali
im Bereich der Zell- und Entwicklungsbiologie
an der Ludwig-Maximilians-Universität München

Erstgutacherin:	PD Dr. Tamara Mikeladze-Dvali
Zweitgutacher:	Prof. Dr. Christof Osman
Tag der Abgabe:	17.12.2025
Tag der mündlichen Prüfung:	26.03.2026

Eidesstaatliche Erklärung:

Ich versichere hiermit an Eides statt, dass meine Dissertation selbstständig und ohne unerlaubte Hilfsmittel angefertigt worden ist. Weiterhin wurden alle Teile der Arbeit, die mit Hilfe von Werkzeugen der künstlichen Intelligenz de novo generiert wurden, durch Fußnote/Anmerkung an den entsprechenden Stellen kenntlich gemacht und die verwendeten Werkzeuge der künstlichen Intelligenz gelistet. Die genutzten Prompts befinden sich im Anhang. Diese Erklärung gilt für alle in der Arbeit enthaltenen Texte, Grafiken, Zeichnungen, Kartenskizzen und bildliche Darstellungen.

München, d. 17.12.2025

Alina Schreiner

Erklärung:

Hiermit erkläre ich, dass die vorliegende Dissertation weder ganz, noch teilweise bei einer Prüfkommission vorgelegt worden ist und, dass ich mich nicht anderweitig einer Doktorprüfung ohne Erfolg unterzogen habe.

München, d. 17.12.2025

Alina Schreiner

List of publications

Stenzel, L., **Schreiner, A**., Zuccoli, E., Üstüner, S., Mehler, J., Zanin, E., & Mikeladze-Dvali, T. (2021). PCMD-1 bridges the centrioles and the pericentriolar material scaffold in *C. elegans*. Development, 148(20). DOI: 10.1242/dev.198416

Schreiner, A., Heim, A., Pletschacher, L., Alznauer, L.-M., Schwenkert, S., Wolff, F., Zanin, E., Mikeladze-Dvali, T. (2025). PCMD-1 stabilizes the PCM scaffold and facilitates centriole separation. Journal of Cell Biology, 224(12). DOI: 10.1083/jcb.202411107

Abstract

Accurate spindle assembly and faithful chromosome segregation depend on the centrosome, whose pericentriolar material (PCM) must function as a robust, load-bearing matrix during metaphase while remaining sufficiently dynamic to disassemble as cells exit mitosis. In *C. elegans* centrosome integrity is shaped by an interplay between microtubule-generated pulling forces and posttranslational regulation of PCM components. Yet, the molecular principles that target the PCM to centrioles and endow the scaffold with the required mechanical properties remain incompletely understood. This thesis addresses these questions through the centriolar protein PCMD-1, previously identified as essential for seeding the core PCM and ensuring PCM integrity during mitosis. The overarching aim was to define how PCMD-1 establishes and maintains a functional centrosome by elucidating how PCMD-1 anchors core PCM to centrioles and testing how PCMD-1 cooperates with the mitotic kinase PLK-1 to control PCM structure and stability.

In the first study (Stenzel et al. 2021), PCMD-1 was defined as a centriole-to-PCM tether at the molecular level. Maternally provided PCMD-1 associates with sperm-derived centrioles early, preceding known PCM components. Interaction assays demonstrated that PCMD-1 can bind to both centriolar and PCM components. Moreover, it was shown that when PCMD-1 is targeted to an ectopic site, it can recruit PCM components there as well, underscoring its strong PCM-recruitment capacity. Mapping of functional regions of PCMD-1 supported a model in which centriolar docking is mediated primarily by the C-terminus via centriolar interaction, while additional regions contribute to efficient accumulation and PCM recruitment.

Building on this, the second study (Schreiner et al. 2025) dissected how PCMD-1 shapes the structure and mechanics of the mitotic PCM beyond core PCM recruitment. Both, stepwise reductions of PCMD-1 and disruption of specific PLK-1 docking to PCMD-1, separated its PCM-tethering function from PCM-organizing function. Although the PCM scaffold could still assemble, its morphology and integrity were compromised. In particular, impaired PCMD-1/PLK-1 docking produced a broadened and mechanically fragile PCM that was susceptible to force-dependent distortion and fragmentation, supporting a role for PCMD-1/PLK-1 docking in stabilizing a compact, load-bearing PCM scaffold. Unexpectedly, PLK-1 docking mutants also delayed centriolar separation at mitotic exit, suggesting that PCMD-1 contributes to mediating the force transmission from PCM to centrioles and/or a PLK-1-dependent licensing step for centriole disengagement.

Overall, this thesis establishes PCMD-1 as a key centriole-to-PCM tether and a determinant of PCM stability. This supports a model in which PCMD-1 contributes to centrosome regulation across the cell cycle by promoting efficient PCM recruitment, ensuring mechanical robustness during mitosis, and enabling the dynamic transitions of the PCM required for its disassembly.

Zusammenfassung

Für eine präzise Spindelbildung und eine zuverlässige Chromosomenseparation spielt das Zentrosom eine entscheidende Rolle. Seine pericentriolare Matrix (PCM) muss während der Metaphase als robuste, lasttragende Matrix fungieren und gleichzeitig ausreichend dynamisch bleiben, um sich am Ende der Mitose wieder aufzulösen. In *C. elegans* wird die Integrität von Zentrosomen durch zwei Faktoren geprägt: mikrotubuli-generierte Zugkräfte und die biochemische Regulierung der PCM-Komponenten. Dennoch sind die Prinzipien, wie die PCM an Zentriolen rekrutiert wird und wie die Matrix die erforderlichen mechanischen Eigenschaften erhält, nicht vollständig verstanden. Diese Thesis untersucht dies anhand des Proteins PCMD-1, das zuvor als essenziell für die Rekrutierung der PCM und deren Integrität während der Mitose beschrieben wurde. Ziel der Arbeit ist es, die Rolle von PCMD-1 bei der Etablierung eines funktionellen Zentrosoms zu definieren, wobei zwei Aspekte adressiert werden: Erstens, wie PCMD-1 die Core-PCM an Zentriolen rekrutiert, und zweitens, wie PCMD-1 zusammen mit der Kinase PLK-1 die PCM-Struktur und -Stabilität reguliert.

In der ersten Studie (Stenzel et al. 2021) wurde PCMD-1 auf molekularer Ebene als Zentriol-zu-PCM-Linker charakterisiert. PCMD-1 wird als eine der frühesten Komponenten an den Zentriolen rekrutiert, noch vor dem Auftreten bekannter PCM-Komponenten. Interaktionsstudien demonstrieren, dass PCMD-1 sowohl mit zentriolären als auch mit PCM-Komponenten interagieren kann. Zudem wurde gezeigt, dass PCMD-1 auch an ektopischen Stellen PCM-Proteine rekrutieren kann, was die ausgeprägte PCM-Rekrutierungsfähigkeit von PCMD-1 hervorhebt. Eine Struktur-Funktions-Analyse stützt ein Modell, in dem der C-Terminus hauptsächlich das zentrioläre Docking vermittelt und weitere Bereiche von PCMD-1 zur effizienten Akkumulation und zur PCM-Rekrutierung beitragen.

Die zweite Studie (Schreiner et al. 2025) untersuchte, wie PCMD-1 die Struktur und die mechanische Integrität der mitotischen PCM beeinflusst. Sowohl die abgestufte Reduktion von PCMD-1 als auch die spezifische Unterbrechung der Bindung von PLK-1 an PCMD-1 trennen die PCM-Rekrutierung von der PCM-Organisation: Obwohl sich das PCM-Gerüst weiterhin aufbauen kann, sind seine Morphologie und Integrität beeinträchtigt. Besonders deutlich zeigt sich dies bei gehindertem PCMD-1/PLK-1-Docking. Die PCM wurde breiter und mechanisch fragiler und war anfällig für kraftabhängige Verformungen sowie für Fragmentierung. Dies spricht dafür, dass das PCMD-1/PLK-1-Docking zur Stabilisierung eines kompakten, lasttragenden PCM-Gerüsts beiträgt. Überraschenderweise verzögern zudem PLK-1-Docking-Mutanten die Trennung der Zentriolen am Ende der Mitose. Dies deutet darauf hin, dass PCMD-1 die Kraftübertragung von PCM auf Zentriolen übernimmt und/oder einen PLK-1-abhängigen Lizenzierungsschritt für die Zentriolenentkopplung unterstützt.

Insgesamt etabliert diese Arbeit PCMD-1 als zentralen Zentriol-zu-PCM-Linker und als wichtigen Determinanten der PCM-Stabilität. PCMD-1 reguliert das Zentrosom über den Zellzyklus hinweg, indem es zunächst zur PCM-Rekrutierung beiträgt, im weiteren Verlauf die mechanische Robustheit garantiert und die Dynamik der PCM kontrolliert, die für den Abbau des PCM beim Mitoseaustritt notwendig ist.

List of figures

Abbreviations

General abbreviations

AA	Amino acid
AFM	Atomic force microscopy
C. elegans	*Caenorhabditis elegans*
CC domain	Coiled-coil domain
Centriculum	Centrosome-associated membrane reticulum
CM2 domain	Centrosomin-motif-2 domain
CRISPR	Clustered regularly interspaced short palindromic repeats
DIC	Differential interference contrast
DNA	Deoxyribonucleic acid
Drosophila	*Drosophila melanogaster*
EM	Electron microscopy
EMS	Ethyl methanesulfonate
ER	Endoplasmic reticulum
FLUCS	Focused light-induced cytoplasmic streaming
GFP	Green fluorescent protein
IDR	Intrinsically disordered region
LLPS	Liquid-liquid phase separation
MosSCI	Mos1-mediated single-copy insertion
M-phase	Mitotic phase
MTOC	Microtubule-organizing center
ncMTOC	Non-centrosomal MTOC
NEBD	Nuclear envelope breakdown
PA domain	PReM-associated domain
PACT domain	Pericentrin-AKAP450 centrosomal targeting domain
PBD	Polo-box domain
PCM	Pericentriolar material
PNMe	Pronuclear meeting
PNMi	Pronuclear migration
PP2A	Protein phosphatase 2A
PReM domain	Phosphoregulated multimerization domain
PTM	Posttranslational modification
RNA	Ribonucleic acid
RNAi	RNA interference

S-phase	DNA synthesis phase
TA	Translocation assay
TCP domain	T-complex protein 10 domain
Y2H	Yeast Two-Hybrid system
γ-TuRC	γ-Tubulin Ring Complex

Protein names and homology

C. elegans full protein name	*C. elegans*	*Drosophila*	*H. sapiens*
-	-	Asl	CEP152
Aurora kinase	AIR-1	Aurora A	Aurora A
Cyclin-dependent kinase 1	CDK-1	Cdk1	CDK1
G-protein regulator 1/2	GPR-1/2*	Pins	LGN/AGS3
Hydrolethalus-syndrome-homolog-1	HYLS-1	Hyls1	HYLS1
PP2A catalytic subunit let-92	LET-92	mts	PPP2CA/B
Spindle-apparatus protein lin-5	LIN-5	Mud	NuMA
Pericentriolar matrix deficient 1	PCMD-1*	Plp	PCNT
Polo-like kinase 1	PLK-1	Polo	Plk1
Polo-like kinase 2	PLK-2	Polo	Plk1
Spindle-assembly-abnormal-1	SAS-1	-	C2CD3
Spindle-assembly-abnormal-4	SAS-4	Sas-4	CPAP
Spindle-assembly-abnormal-5	SAS-5*	Ana2	STIL
Spindle-assembly-abnormal-6	SAS-6	Sas-6	SAS6
Spindle-assembly-abnormal-7	SAS-7	-	-
Separase	SEP-1	separase	Separase
Spindle-Defective 2	SPD-2	Spd-2	Cep192
Spindle-Defective 5	SPD-5	Cnn	CDK5RAP2
PP2A regulatory subunit sur-6	SUR-6	tws	PPP2RA/B/C/D
Transforming Acid CC-containing protein 1	TAC-1	TACC	TACC1/2/3
γ-tubulin	TBG-1	γTub37C	TUBG1
TPX2 domain-containing protein	TPXL-1	Tpx-2	TPX2
Zygote-defective 1	ZYG-1*	Plk4	PLK4
Zygote-defective-9	ZYG-9	Msps	XMAP215/ch-TOG

* functional homolog
- unknown

Table of contents

1. Introduction

Cell division is a universal and fundamental process that forms the basis of life. In unicellular organisms, it is the simplest form of reproduction, whereby a single cell gives rise to two genetically identical cells - two new organisms. In multicellular organisms, however, the impact of cell division is far more diverse. During development, cell division transforms a single cell into a complex organism comprising specialized cell communities that form tissues and organs. Furthermore, during adulthood, cell division replaces damaged or lost cells to maintain tissue integrity (Morgan 2007). By enabling growth, morphogenesis, and tissue homeostasis, cell division ensures the maintenance of an organism and, consequently, the continuance of a species. The total number of cell divisions completed by a multicellular organism can be substantial. For instance, an average human body contains approximately 30 trillion cells (Sender et al. 2016) and undergoes about 10,000 trillion cell division events over the course of a lifetime (Bansbach and Cortez 2011). To ensure its fidelity, cell division must be strictly controlled, both spatially and temporally. Malfunctions in this can result in developmental abnormalities, tissue degeneration, and uncontrolled proliferation, as observed in tumorigenesis (Morgan 2007). At the core of cell division is the assembly of the spindle apparatus, orchestrated by centrosomes in most animal cells. How centrosomes are formed and stabilized is a topic of intense research. In this PhD thesis, I use the first-cell embryo of the nematode *Caenorhabditis elegans* (*C. elegans*) to investigate molecular mechanisms facilitating centrosome integrity and thereby cell division fidelity.

1.1 The eukaryotic cell division

Eukaryotic cell division occurs in a cyclical process through distinct phases, interphase and the mitotic (M-) phase, which coordinate cell growth with genome duplication and division. During interphase, cells progress through G1, DNA synthesis (S-phase), and G2 to replicate their DNA, grow, and repair in preparation for mitosis (Morgan 2007). The following M-phase comprises nuclear division (mitosis) and cellular division (cytokinesis) (Morgan 2007). Mitosis starts with prophase, where chromosomes condense, and a highly organized bipolar spindle apparatus is formed, which, after nuclear envelope breakdown (NEBD) in prometaphase, interacts with the sister chromatids (Alberts et al. 2002b). By metaphase, the sister chromatids are aligned at the equatorial metaphase plate by the spindle apparatus (Alberts et al. 2002b). Anaphase begins once all chromosomes are correctly attached and aligned (Musacchio and Salmon 2007). Then, the link between sister chromatids is released, and the chromatids travel toward opposite poles as their attached spindle fibers shorten, while overlapping spindle fibers in the spindle midzone slide apart to push the poles further away (Scholey et al. 2016, McIntosh

2021). Telophase restores nuclear organization: the decondensed chromosomes reach the poles, nuclear envelopes reform, and the spindle disassembles (Morgan 2007). Cytokinesis then separates the cytoplasm and completes abscission to produce two independent daughter cells (Green et al. 2012). The accurate progression of the cell cycle is strictly regulated by a series of checkpoints that monitor DNA integrity, proper replication, and spindle attachment before the cell is allowed to proceed to the next phase (Morgan 2007). Notably, eukaryotic cell cycle programs are not invariant. Depending on the organism and context, phases can deviate from the canonical cycle: For example, in early embryos of some species (e.g., *Xenopus laevis, Drosophila melanogaster,* or *C. elegans*), blastomeres are lacking gap phases G1 and G2, and in turn divide in rapid S-M cycles (Newport and Kirschner 1982, Edgar and McGhee 1988, Farrell and O'Farrell 2014). Other than that, *C. elegans* intestinal and hypodermal cells undergo larval endoreduplication cycles in which DNA replicates without cytokinesis, generating highly polyploid tissue (van den Heuvel 2005).

An essential feature needed for the segregation of the duplicated genome during mitosis is the spindle apparatus. The spindle apparatus consists of dynamic microtubules that emanate from two opposite poles, the microtubule-organizing centers (MTOCs). Microtubules comprise three functional classes: kinetochore microtubules, which form end-on attachments to the kinetochores on the sister chromatids; interpolar microtubules, which overlap antiparallel in a central midzone; and astral microtubules, which project toward and are anchored at the cortex **(Figure 1)** (Meunier and Vernos 2012). Through these elements, the spindle not only captures, aligns, and segregates chromosomes (Prosser and Pelletier 2017), it also defines division geometry: spindle midzone and astral microtubules help to position the contractile ring and thereby determine the position of the future cleavage plane of the cell (Green et al. 2012; McNally 2013).

Across eukaryotes, MTOCs can take diverse forms: Recent work has elucidated many non-centrosomal MTOCs (ncMTOCs) (Sanchez and Feldman 2017). Well-known examples of ncMTOCs can be found in plants that assemble spindles from nuclear and cytoplasmic sites (Wu and Akhmanova 2017), or in many animal oocytes, including those of the nematode *C. elegans*, where acentrosomal spindles are formed during both meiosis I and meiosis II (Dumont and Desai 2012). Fungi provide yet another solution, using spindle pole bodies embedded in the nuclear envelope as MTOCs (Jaspersen and Winey 2004). Despite these alternatives, most animal cells rely on centrosome-based MTOCs to determine spindle architecture during mitosis (Prosser and Pelletier 2017). Centrosomes consist of two centrioles in their center - a mother and a daughter centriole - and a dynamic pericentriolar material (PCM) surrounding them **(Figure 1)**. During S-phase, each mother centriole templates the formation of one daughter centriole, ensuring that duplication occurs only once per cycle. At the onset of mitosis, the PCM expands in size, enabling robust microtubule nucleation and the

assembly of a bipolar spindle. After chromosome segregation, the PCM largely disassembles, the daughter centriole disengages and separates from the mother. Each disengaged centriole templates a new daughter centriole, and each newly formed cell inherits a pair of centrioles to begin the next cell cycle.

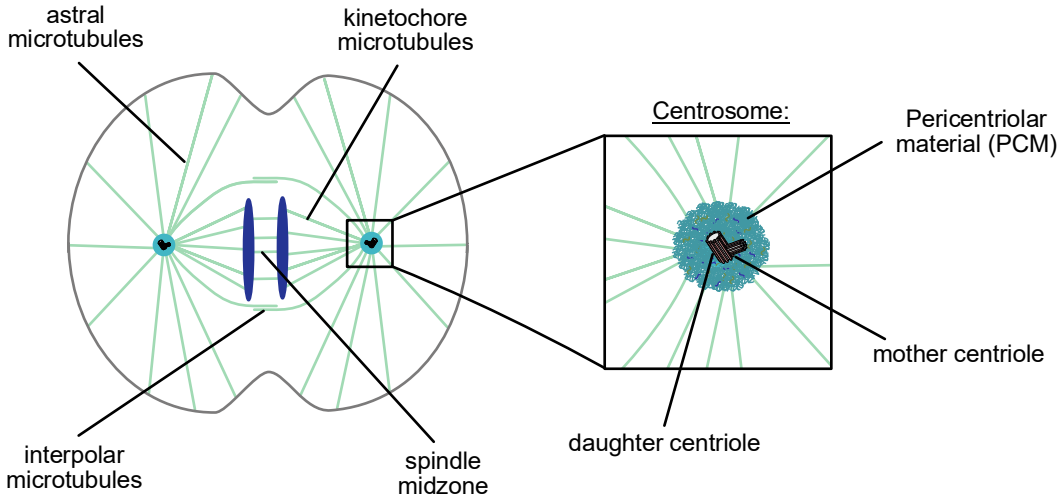

Figure 1: Mitotic spindle in an anaphase cell.
Centrosomes, each comprising a mother and daughter centriole pair surrounded by pericentriolar material (PCM), form the spindle poles. Three microtubule classes emanate from the poles: astral microtubules that extend toward the cell cortex; kinetochore microtubules that attach to kinetochores on condensed chromosomes; and interpolar microtubules that arise from both centrosomes and overlap in the spindle midzone. The spindle midzone forms between the segregating chromosome masses and facilitates chromosome segregation.

1.2 Discovery of the centrosome

Due to its minute size, the discovery and advances in understanding the structure of centrosomes go hand in hand with the development of microscopy techniques. From the late nineteenth century onward, the centrosome emerged from light microscopy studies of the anatomy and/or fertilization of different species. The first drawings were made by Walther Flemming in 1874/1875 on *Anodonta*, a freshwater mussel, and, one year later, by Edouard Van Beneden on the eggs of *Dycimella*, a kidney parasite of cephalopods. Van Beneden also named the tiny dot at each spindle pole - the “corpuscule polaire” (Gall 2004). Approximately ten years later, while studying the fertilization and cell division of the nematode *Ascaris megalocephala* (now renamed to *Parascaris equorum*), he described the positioning of these tiny dots at spindle poles and their duplication in later cell cycle stages (Gall 2004). At the same time (1888), Theodor Boveri recognized this body as a distinct, persistent organelle that organizes the spindle and coined the term “centrosome” (Boveri 1888). In Boveri’s following

studies, he also described associated “centroplasm,” a concept later replaced by the modern PCM, and a centered structure called “centrioles” (Scheer 2014). Moreover, he anticipated that centrosome and chromosome abnormalities could underlie malignant growth, insights later recognized as foundational to cancer genetics (Boveri 2008).

As instrumentation advanced, mid-twentieth-century electron microscopy (EM) turned qualitative light-microscope observations into ultrastructure: in 1954, the basal body (corresponding to a centriole) was first described by use of EM (Fawcett and Porter 1954, Guichard et al. 2018). Then, in 1955, the “centrosphére” (now termed PCM) was observed as a membraneless viscous mass surrounding centrioles (Policard and Bessis 1955), and in 1956, the centriole’s radially symmetric structure built from microtubules was resolved (De Harven and Bernhard 1956). At the same time, Shinya Inoué's optical innovation, which involved imaging a living cell with polarized-light microscopy, enabled the direct visualization of spindle fibers and their dynamics over the cell cycle in subsequent studies (Inoué 1953). Although historically, Boveri’s experiments in sea-urchin eggs showed that centrosomes form the two poles of the first mitotic spindle (Boveri 1902), phase-resolved EM then linked centrosome activity to spindle formation in mammalian cells (Robbins and Gonatas 1964). This led to a shift from a purely morphological ‘centrosome’ to the functional concept of the MTOC that emphasized spindle pole organization and accommodated later found non-centriolar sites such as the fungal spindle pole body and other ncMTOCs (Pickett-Heaps 1969, Brinkley 1985, Sanchez and Feldman 2017).

Over the last decades, genetics and live-cell imaging have revealed conserved molecular pathways that drive centrosome assembly and duplication; work in the *C. elegans* embryo was especially pivotal in identifying core duplication factors and the order of their recruitment, establishing a broadly conserved logic for centriole biogenesis (O’Connell 2001, Kirkham 2003, Delattre 2004, Kemp et al. 2004, Leidel et al. 2005, Delattre et al. 2006, Pelletier et al. 2006).

During the past century and a half, morphological, structural, and molecular studies have made the centrosome a well-researched and well-described organelle of animal cells. However, it is not yet fully understood how the centrosome changes dynamically during the cell cycle, from a regulatory but also a material perspective, hence it remains the subject of extensive investigation.

1.3 *Caenorhabditis elegans* as a model organism to study cell division

Our understanding of centrosome dynamics in the last decades has advanced substantially through work using *C. elegans* as a model organism (Conduit et al. 2015). This nematode serves as a powerful model to study cell division because it is a small, simple multicellular

organism with a well-developed genetic toolkit that enables efficient gene discovery, precise genetic manipulation, and quantitative imaging (Hattersley et al. 2018). Its compact, fully sequenced genome (~106 Mb, ~20,000 genes) (Ichikawa et al. 2025), with 41% of the genes predicted to have human orthologues (Kim et al. 2018), further contributes to its utility as an experimental system.

Many genes essential for cell division and centrosomal structure have been identified in *C. elegans* through systematic genetic screens (Pintard and Bowerman 2019). Reverse-genetic approaches based on RNA interference (RNAi), first established in *C. elegans* (Fire et al. 1998), became routine by using genome-wide RNAi libraries, which enabled high-throughput loss-of-function screening (Ashrafi et al. 2003, Kamath and Ahringer 2003). In parallel, classic forward-genetic screens, where mutagens such as ethyl methanesulfonate (EMS) (Brenner 1974) induce random point mutations and subsequent gene mapping rapidly pinpoints the causal gene (Wicks et al. 2001), have been highly effective. Complementing these screening approaches, the specific manipulation of identified target genes is possible via clustered regularly interspaced short palindromic repeats (CRISPR)-Cas9 (Friedland et al. 2013) or Mos1-mediated Single-Copy Insertion (MosSCI) (Frøkjaer-Jensen et al. 2008). While CRISPR-Cas9 enables highly specific modification of endogenous loci (Dickinson and Goldstein 2016), the MosSCI system enables the single-copy integration of defined constructs at characterized genomic landing sites, yielding stable expression levels and avoiding mosaic multi-copy arrays (Frøkjaer-Jensen et al. 2008). These approaches not only allow systematic perturbation of gene function but also enable the precise introduction of fluorescent tags, thereby directly linking defined molecular changes to observable phenotypes.

Several anatomical and optical features make *C. elegans* particularly well suited for qualitative microscopic analyses. The animal is transparent and ~1 mm long, which enables non-invasive live imaging of intact embryos, tissues, or even the whole adult by DIC (differential interference contrast) and fluorescence microscopy across all life stages (Meneely et al. 2019). In this context, *C. elegans* was also the first metazoan in which a GFP-tagged protein was expressed *in vivo* (Chalfie et al. 1994), establishing fluorescent reporters as routine readouts for gene expression and protein localization. Building on these general advantages for live imaging, the one-cell embryo of *C. elegans* is particularly powerful for studying cell division. It can be easily observed due to the transparent structure of the relatively large egg (50 × 20 µm) (Pintard and Bowerman 2019), which corresponds to a single cell in the first cell cycle. A remarkable consequence of this is that organelles such as the centrosome scale with cell size (Decker et al. 2011), making them exceptionally large and straightforward to observe.

1.4 The first cell division of *C. elegans*

The first mitotic division of *C. elegans* is highly reproducible in both timing and geometry in this autonomous single cell. Even subtle deviations from the stereotyped pattern can be readily detected and typically reflect a cell-division phenotype (Hattersley et al. 2018). The divisions proceed exclusively as S to M cycles, without GAP phases (Edgar and McGhee 1988, Oegema and Hyman 2006, Pintard and Bowerman 2019). Consequently, early checkpoints are unusually permissive: the DNA-damage response is silenced, and the spindle assembly checkpoint is weak, allowing embryos to continue cycling even in the face of major mitotic defects and thereby enabling the analysis of otherwise lethal perturbations (O'Connell 1999, Encalada et al. 2005, Holway et al. 2006, Galli and Morgan 2016). Together with the short duration of the first division (~20 minutes), these features make this process particularly amenable to analysis and have allowed it to be characterized in great detail (Pintard and Bowerman 2019).

C. elegans oocytes arrest at diakinesis of meiotic prophase I (Hirsh et al. 1976) and lack maternal centrioles as they are actively eliminated during oogenesis (Mikeladze-Dvali et al. 2012, Pierron et al. 2023). Fertilization reactivates oocyte meiosis (Hirsh et al. 1976), where an acentriolar spindle generates the maternal haploid genome by extrusion of two polar bodies **(Figure 2A)** (Kemphues and Strome 1997, Wignall and Villeneuve 2009). After completion of female meiosis II, maternal and paternal pronuclei, located at opposite ends of the embryo, enlarge and prepare for the first mitosis (Oegema and Hyman 2006). At fertilization, the sperm contributes a pair of centrioles, which mature into two centrosomes after the end of female meiosis (O'Connell 1999). These centrosomes separate while remaining associated with the male pronucleus, as they move along the nuclear envelope to opposite sides (Gönczy et al. 1999, Malone et al. 2003). While sperm-derived centrosomes separate, astral microtubules nucleating from them “capture” the maternal pronucleus and move the two pronuclei towards each other, in a process called pronuclear migration (PNMi) **(Figure 2B)** (Albertson 1984, Meaders and Burgess 2020). Simultaneously, chromosomes begin to condense (Oegema and Hyman 2006). The pronuclei meet posteriorly at the so-called pronuclear meeting (PNMe), with the centrosomes positioned on opposite sides of the pronuclear junctions **(Figure 2C)** (Meaders and Burgess 2020). The pronuclear-centrosome complex then moves to the center and rotates until the centrosomes are placed along the longitudinal axis (Hyman and White 1987). NEBD follows **(Figure 2D)**, a bipolar spindle assembles, and chromosomes align on a metaphase plate **(Figure 2E)** (Albertson 1984, Gönczy et al. 1999, Oegema and Hyman 2006). As the spindle gets positioned by the cell cortex-driven pulling forces, which are polarized with stronger net forces at the posterior cortex, the spindle becomes displaced posteriorly (Grill et al. 2001, Grill et al. 2003, Labbé et al. 2004). This imbalance arises from a patterned distribution of cortical force generators: the posterior recruits and activates more than the

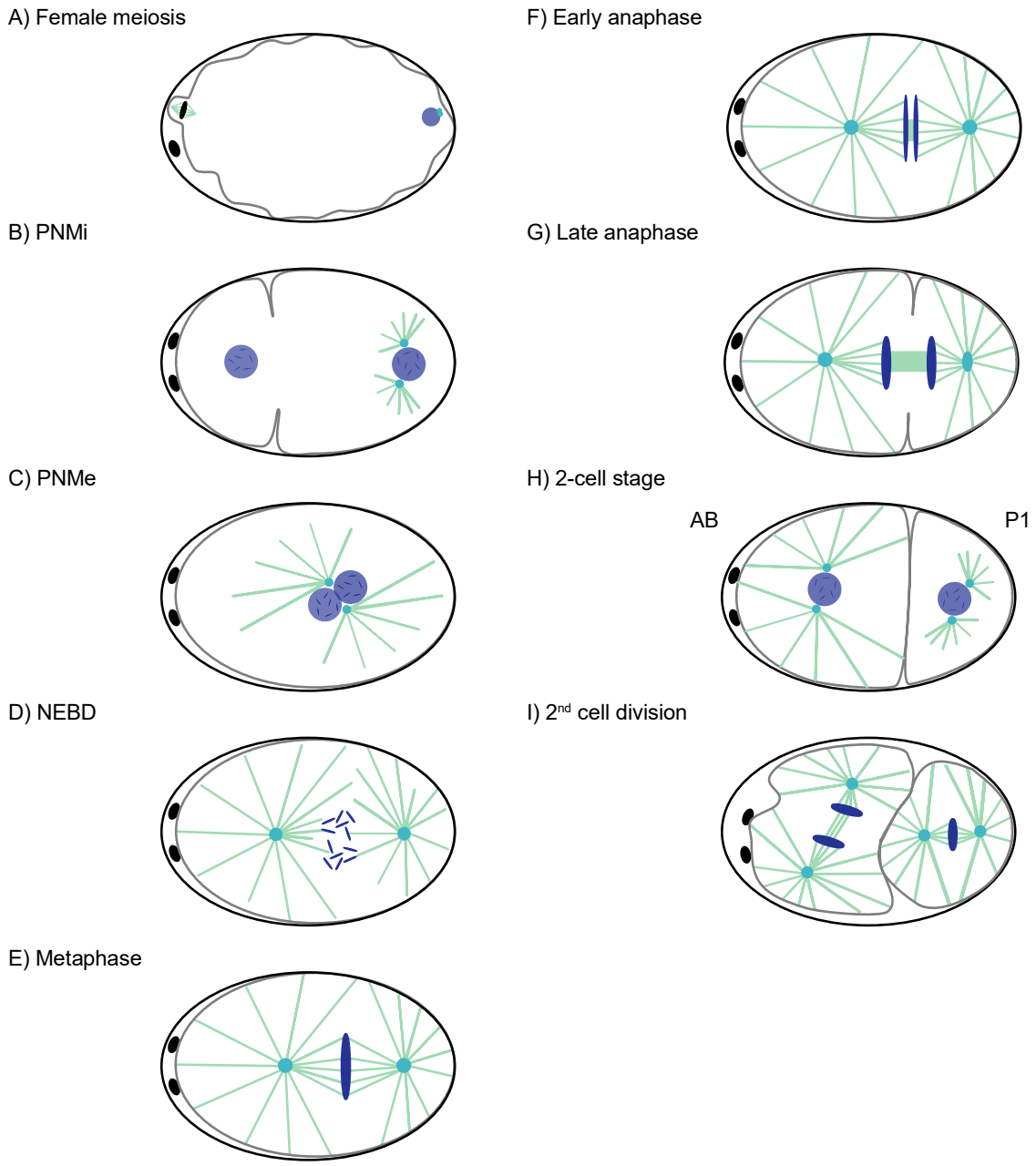

Figure 2: First cell division of a one-cell C. elegans zygote.
A) *Female meiosis: Upon fertilization, the sperm introduces a haploid set of chromosomes and two centrioles. Female meiosis resumes and extrudes two polar bodies.* ***B)*** *Pronuclear migration (PNMi): The centrioles mature into centrosomes, move along the pronuclear envelope, and begin to nucleate microtubules. These microtubules capture the female pronucleus, initiating the process of pronuclear migration.* ***C)*** *Pronuclear meeting (PNMe): The maternal and paternal pronuclei meet, rotate, and centrate.* ***D)*** *NEBD: The nuclear envelope of the pronuclei breaks down, and a bipolar spindle begins to form.* ***E)*** *Metaphase: Condensed chromosomes align at the metaphase plate.* ***F)*** *Early anaphase: The chromosomes start to segregate.* ***G)*** *Late anaphase: Furrow ingression initiates cytokinesis at the spindle midzone.* ***H)*** *Two-cell stage: Following chromosome decondensation, nuclear envelope reformation, and the completion of cytokinesis, a two-cell embryo forms, consisting of the larger anterior AB and the smaller posterior P1 cell.* ***I)*** *2nd cell division: Development proceeds, with the AB cell dividing before the P1 cell. In general, blue denotes DNA, green microtubules, and turquoise centrosomes. Schematic based on Hattersley et al. 2018.*

anterior during metaphase (Colombo et al. 2003, Grill et al. 2003, Park and Rose 2008). These force generators comprise an evolutionarily conserved ternary complex of Gα subunits, the GoLoco proteins G-protein regulator 1 and 2 (GPR-1/2; human LGN/AGS3; *Drosophila* Pins) and the coiled-coil (CC) scaffold Spindle-apparatus protein lin-5 (LIN-5; human NuMA; *Drosophila* Mud), which anchors dynein at the cortex to pull on astral microtubules and, by this in turn, on the spindle apparatus (Colombo et al. 2003, Srinivasan et al. 2003, Couwenbergs et al. 2007, Park and Rose 2008). With anaphase onset, the chromosomes start to segregate **(Figure 2F)** (Oegema and Hyman 2006). Cytokinesis initiates, and because the spindle is positioned off-center, the cleavage furrow ingresses asymmetrically **(Figure 2G)**. Two unequal daughter cells form, the larger anterior AB and the smaller posterior P1 **(Figure 2H)** (Sulston and Schierenberg 1983, Alberts et al. 2002a, Oegema and Hyman 2006). The embryo then proceeds into the next S-phase, with AB dividing reproducibly before P1 **(Figure 2I)** (Sulston and Schierenberg 1983). For all subsequent cell divisions to be successful, every daughter cell must assemble a new bipolar spindle, which critically depends on the duplication of the inherited centrosomes and, consequently, their centrioles.

1.5 Centriolar structure and assembly pathway

The assembly of a new centriole is a highly ordered, evolutionarily conserved pathway, which was first identified in *C. elegans* and subsequently in other species (Banterle and Gönczy 2017). Each centrosome consists of two centrioles, a mature “mother” centriole and the newly formed “daughter” or procentriole. They are barrel-shaped cylinders that are aligned orthogonally to each other. Centrioles are built on an almost universal ninefold radial symmetry, but their size and architecture can vary between species and sometimes even within a species (Winey and O'Toole 2014, Gottardo et al. 2015, Klena et al. 2020). Proximally, a cartwheel establishes this plan: a central hub with nine spokes that sets polarity and engages the nascent wall (Guichard et al. 2018). The cartwheel is most prominent during early procentriole growth; with centriolar maturation, it is typically removed in vertebrates (Izquierdo et al. 2014), and, as recently shown, also in *C. elegans* (Woglar et al. 2022, Tollervey et al. 2025). Nine microtubule units assemble in a ring-like manner around the cartwheel. In most animal cells, the units are composed of microtubule triplets in which a complete A-tubule templates a B- and C-tubule, yielding a stiff cylinder (Azimzadeh and Marshall 2010, Winey and O'Toole 2014). However, the number of tubules can also vary depending on species or tissue, as seen in *Drosophila*, where somatic cells have doublets, and the male germline has triplets (Gottardo et al. 2015). To mature into a mother, the centrioles in vertebrates acquire distal and subdistal appendages at the distal tip. These wedge-like structures dock the organelle to membranes and license ciliogenesis by organizing early trafficking into the nascent cilium (Ma et al. 2023).

In *C. elegans*, centrioles are much simpler and smaller in size (~100 nm in diameter and ~150 nm in length): The centriolar wall has long been described to consist of nine singlet A-tubules, but more recent in-situ cryo-electron tomography revealed that while procentrioles are indeed singlet-based, mature centrioles acquire short, incomplete B-tubules, which do not close into doublets (Pelletier et al. 2006, Tollervey et al. 2025). Furthermore, *C. elegans* centrioles lack canonical distal and subdistal appendages; instead, during ciliogenesis, the mother centriole converts into a basal body, and membrane docking proceeds via transition fibers at the ciliary base (Nechipurenko et al. 2017).

Centriole assembly in *C. elegans* begins at the proximal end of the mother centriole with the CC protein SPindle-Defective 2 (SPD-2; human CEP192; *Drosophila* Spd-2), which localizes to both centrioles and the PCM (Kemp et al. 2004, Murph et al. 2022). SPD-2 has several functions; the main one of which is to license centriole duplication by recruiting the polo kinase ZYGote-defective 1 (ZYG-1; human PLK4; *Drosophila* Plk4) **(Figure 3)** (Kemp et al. 2004, Pelletier et al. 2004, Delattre et al. 2006, Decker et al. 2011). ZYG-1 is an essential initiator of daughter-centriole formation (O'Connell 2001) as overexpression of its human or *Drosophila* homolog leads to the formation of additional centrioles (Nigg and Holland 2018). Similar observations have also been made in neuroectodermal cells of *C. elegans* (Wolf et al. 2018), as well as with misregulated ZYG-1 activity (Peel et al. 2017, Medley et al. 2023), confirming its regulatory role. ZYG-1 recruits a complex of Spindle-ASsembly-abnormal-5 (SAS-5; human STIL; *Drosophila* Ana2) and Spindle-ASsembly-abnormal-6 (SAS-6; human SAS6; *Drosophila* Sas-6) **(Figure 3)**, which likely pre-assembles in the cytoplasm (Leidel et al. 2005, Delattre et al. 2006, Qiao et al. 2012, Lettman et al. 2013). Structural studies have shown that SAS-6 molecules form a spiral arrangement with ninefold symmetry *in vitro*, which would contradict the ring-like cartwheel structure observed in vertebrates (Hilbert et al. 2013). However, recent research using improved imaging techniques has revealed that a cartwheel structure is also present in nematodes *in vivo*, with SAS-6 forming rings rather than the previously hypothesized spiral (Sugioka et al. 2017, Woglar et al. 2022, Tollervey et al. 2025). This discrepancy between *in vivo* and *in vitro* data is assumed to be due to the presence of SAS-6 interaction partners, such as SAS-5 (Woglar et al. 2022). Furthermore, ZYG-1 was shown to phosphorylate SAS-5 and SAS-6, respectively, to stably maintain both proteins at the procentriole and trigger cartwheel assembly (Kitagawa et al. 2009, Lettman et al. 2013, Sankaralingam et al. 2024). The SAS-5/SAS-6 module then recruits Spindle-ASsembly-abnormal-4 (SAS-4; human CPAP; *Drosophila* Sas-4) to the growing daughter **(Figure 3)**, as SAS-5 engages the conserved TCP (T-complex protein 10) domain of SAS-4 (Leidel and Gönczy 2003, Pelletier et al. 2006, Cottee et al. 2013, Zheng et al. 2014). SAS-4 initially exchanges dynamically with the cytoplasmic pool and requires γ-tubulin (TBG-1; human TUBG1; *Drosophila* γTub37C) as well as centriolar microtubules, which assemble from α- and

β-tubulin heteromeres, for its stable integration (Dammermann et al. 2008). The integration of centriolar microtubules around the cartwheel is facilitated by SAS-4 **(Figure 3)**, but also interaction with SAS-5 was observed (Pelletier et al. 2006, Bianchi et al. 2018). To become a mother and acquire the competence to duplicate, a centriole needs to mature. In *C. elegans,* centriole maturation is thought to be achieved by the assembly of an EM-dense structure called the paddlewheel on the microtubule wall under the control of Spindle-ASembly-abnormal-7 (SAS-7) **(Figure 3)** (Sugioka et al. 2017). Recent ultrastructural mapping suggested a set of proteins in the paddlewheel, among them SPD-2, SPindle-Defective-5 (SPD-5; human CDK5RAP2; *Drosophila* Cnn), and HYdroLethalus-Syndrome-homolog-1 (HYLS-1; human HYLS1; *Drosophila* Hyls1) (Woglar et al. 2022). HYLS-1 is a ciliary protein that is dispensable for centrosome maturation (Dammermann et al. 2009). However, recent cryo-EM data resolved this paddlewheel as the combination of the incomplete B-tubule, as mentioned before, together with an additional “outer star” structure surrounding A- and B-tubules (Tollervey et al. 2025). SAS-7, which sits on the centriolar surface (Woglar et al. 2022), probably as part of this star structure (Tollervey et al. 2025), recruits SPD-2 to the maturing organelle, effectively acting at both the beginning and end of the duplication program (Kemp et al. 2004, Pelletier et al. 2004, Sugioka et al. 2017). Although not part of the centriolar duplication pathway, Spindle-ASembly-abnormal-1 (SAS-1, human: C2CD3) is required to maintain centriolar integrity (von Tobel et al. 2014, Jha et al. 2025). In absence of SAS-1, the mature mother centriole is severely damaged or completely lost, while the daughter appears to be intact (Jha et al. 2025). Consistent with this, SAS-1 is the first player to be removed from centrioles in the centriolar elimination pathway during oogenesis in *C. elegans* (Pierron et al. 2023). Furthermore, the PCM was shown to promote centriolar assembly, although it is not required per se for centriolar duplication, by locally concentrating and providing TBG-1 to the daughter (Dammermann et al. 2004, Dammermann et al. 2008).

Genetic analyses in *C. elegans* first delineated the here described core centriole duplication pathway: SPD-2, ZYG-1, SAS-5, SAS-6, and SAS-4 (O’Connell 2001, Kirkham 2003, Delattre 2004, Pelletier et al. 2004, Leidel et al. 2005, Pelletier et al. 2006, Sugioka et al. 2017). Subsequent work in vertebrate and fly systems revealed that this module is highly conserved: In human cells, CEP192 and CEP152 recruit Plk4, which activates STIL to promote SAS-6 loading and subsequent CPAP-dependent centriole assembly (Habedanck et al. 2005, Strnad et al. 2007, Zhu et al. 2008, Kohlmaier et al. 2009, Vulprecht et al. 2012, Arquint and Nigg 2016). Although this core module is indeed conserved, work in human cells has revealed a considerably larger set of additional factors that modulate and fine-tune centriole biogenesis (Balestra et al. 2013). In *Drosophila*, the corresponding cascade involves Spd-2 and Asl upstream of Plk4, followed by Ana2, Sas-6, and Sas-4 (Bettencourt-Dias et al. 2005, Basto et al. 2006, Peel et al. 2007, Varmark et al. 2007, Giansanti et al. 2008, Stevens et al. 2010).

Thus, the centriole duplication pathway first uncovered in *C. elegans* provides a general blueprint that is remarkably similar from nematodes to insects and vertebrates.

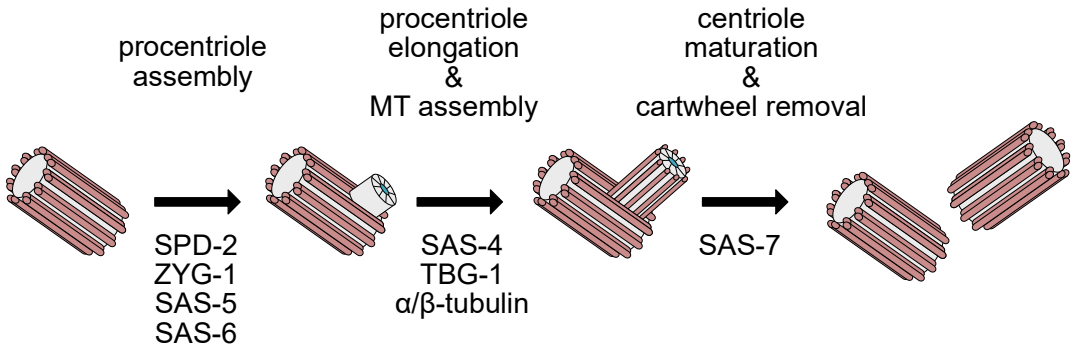

Figure 3: Schematic of the centriolar assembly and maturation pathway.
At the proximal side of the mother centriole, SPD-2 recruits ZYG-1, which in turn recruits the SAS-5/SAS-6 complex to assemble the centriolar cartwheel. The procentriole subsequently begins to elongate, and SAS-4 is recruited. SAS-4 is essential for the formation of nine symmetrically arranged microtubules (MT) around the procentriole. During centriolar maturation, the cartwheel disassembles, and a paddlewheel forms under the control of SAS-7. Adapted from Pintard and Bowerman 2019 and Tollervey et al. 2025.

1.6 Structure and assembly of the Pericentriolar Material

Centrioles are surrounded by a dynamic PCM, an amorphous and protein-rich matrix that expands several-fold during mitotic entry in a process known as centrosome maturation, which increases microtubule nucleation potential and supports bipolar spindle formation (Palazzo et al. 2000). This process transforms a small layer of interphase PCM (or core PCM), which initially coats the centrioles, into a substantial micron-scale scaffold through the regulated incorporation of multiple scaffolding proteins, primarily driven by phosphorylation events mediated by Polo-like kinases and other cell cycle regulators (Hannak et al. 2001, Conduit et al. 2010, Conduit et al. 2014, Woodruff et al. 2014, Woodruff et al. 2015). The PCM then serves as a structural platform for recruiting a variety of client proteins (Palazzo et al. 2000, Conduit et al. 2015).

In *C. elegans,* the PCM matrix is composed of the CC proteins SPD-5 and SPD-2, both essential for proper PCM assembly and centrosome function (Hamill et al. 2002, Kemp et al. 2004, Wueseke et al. 2014, Murph et al. 2022). SPD-2 and SPD-5 act as the primary structural components of the PCM, but only SPD-5, once integrated, remains stably associated with the matrix and does not exchange with the cytoplasmic pool, establishing it as the main matrix protein (Laos et al. 2015). *In vitro*, purified SPD-5 has been shown to self-assemble into large, interconnected networks - a property enhanced by Polo-like kinase 1 (PLK-1; human Plk1; *Drosophila* Polo) phosphorylation and the presence of SPD-2 (Woodruff et al. 2015). Moreover,

under crowding conditions, SPD-5 forms spherical condensates that can recruit client proteins and nucleate microtubules, recapitulating key PCM functions observed in embryos (Woodruff et al. 2017). *In vivo*, the cytoplasmic pools of SPD-5 and SPD-2 are mainly monomeric and remain unphosphorylated by PLK-1 (Wueseke et al. 2014). Upon proximity to the centrioles, SPD-2 recruits PLK-1 to the centrosome, enabling PLK-1 to phosphorylate SPD-5, which triggers SPD-5 self-assembly into higher-order structures within the PCM **(Figure 4)** (Woodruff et al. 2015, Wueseke et al. 2016, Cabral et al. 2019, Ohta et al. 2021). Polymerized SPD-5 forms the structural framework of the PCM, specifically serving as the scaffold for additional recruitment of SPD-2 and PLK-1 (Woodruff et al. 2015, Wueseke et al. 2016). This positive feedback loop of interacting SPD-5, SPD-2, and PLK-1 results in the enormous growth of the PCM scaffold during mitosis. Thus, SPD-5 exhibits two distinct states: an inactive, non-polymerizing form and an active form that, after phosphorylation by PLK-1, polymerizes and drives PCM scaffold expansion **(Figure 4)** (Wueseke et al. 2014, Woodruff et al. 2015, Wueseke et al. 2016, Nakajo et al. 2022).

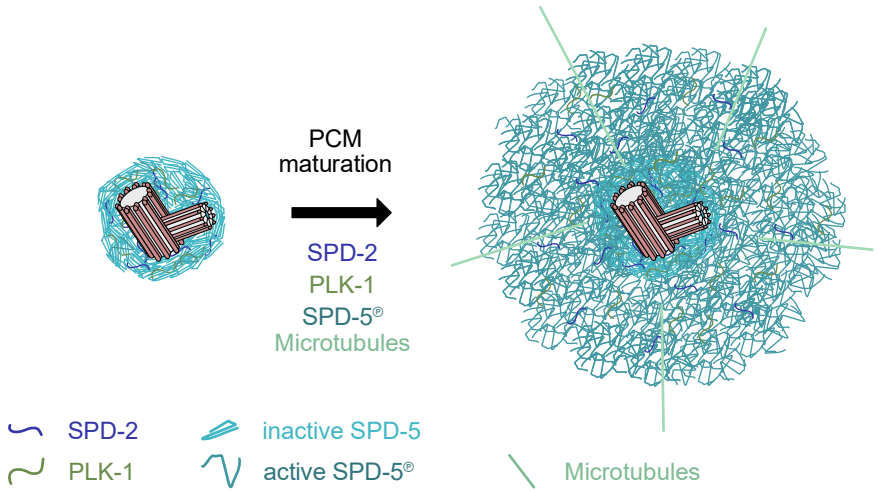

Figure 4: PCM maturation in C. elegans.
Before mitosis onset, the centrosome is small and contains predominantly non-polymerized SPD-5 with low levels of SPD-2 and PLK-1. Upon PCM maturation at mitotic entry, SPD-2 recruits PLK-1 to the centrosome, PLK-1 phosphorylates SPD-5, and active SPD-5 polymerizes into a large, stable scaffold. This SPD-5 matrix dramatically expands PCM size and efficiently nucleates microtubules. Model according to Woodruff et al. 2015, Wueseke et al. 2016, Cabral et al. 2019, and Ohta et al. 2021.

A very similar centrosome maturation module operates in other animals. In *Drosophila*, the SPD-5 homolog Centrosomin (Cnn) forms the principal PCM scaffold, and its incorporation and expansion are promoted by Polo-dependent phosphorylation and the centriolar targeting factor Spd-2, establishing a Cnn/Spd-2/Polo feedback loop (Alvarez-Rodrigo et al. 2019). In

vertebrates, CDK5RAP2 and CEP192 fulfill analogous roles as PCM scaffold protein and centriolar targeting factor, respectively, and their activities are modulated by PLK1 (Vasquez-Limeta and Loncarek 2021). Additionally, the CC scaffold components pericentrin (PCNT) in vertebrates and Pericentrin-like protein (Plp) in *Drosophila* are known to be required for forming an organized PCM (Lawo et al. 2012, Mennella et al. 2012). Still, for a long time, no *C. elegans* ortholog of these pericentrin-like proteins had been identified. Thus, despite organism-specific differences, PCM assembly in flies, worms, and humans appears to rely on a conserved principle: a PLK family kinase cooperates with a centriolar targeting factor and a large CC scaffold protein to drive the transition from a small core PCM to a polymerized, mitotic PCM matrix (Vasquez-Limeta and Loncarek 2021).

The molecular mechanism of SPD-5/Cnn/CDK5RAP2 multimerization is important for PCM matrix expansion and consequently has been intensely investigated in recent years (Feng et al. 2017, Nakajo et al. 2022, Rios et al. 2024, Rios et al. 2025). In *Drosophila,* Cnn's internal Phospho-Regulated Multimerization (PReM) domain is phosphorylated by Polo, enabling it to interact with Cnn's C-terminal Centrosomin-Motif-2 (CM2) domain via both intramolecular and intermolecular interactions (Feng et al. 2017). This triggers Cnn's multimerization and subsequent PCM scaffold assembly *in vitro* and *in vivo* (Feng et al. 2017, Alvarez-Rodrigo et al. 2019). In *C. elegans,* a systematic analysis of the functional regions of SPD-5 revealed similar domains: a PReM domain, which is phosphorylated by PLK-1, and a C-terminal PReM-Associated (PA) domain that interacts with a phosphorylated PReM domain (Nakajo et al. 2022). PLK-1 phosphorylation enhances both intramolecular and intermolecular interactions between SPD-5's PReM and PA domains, promoting SPD-5 multimerization and driving the formation and expansion of the PCM scaffold during mitosis (Nakajo et al. 2022). The critical phosphorylation sites - S530, S627, S653, and S658 - were identified through *in vitro* experiments; when these residues are rendered non-phosphorylatable, SPD-5, though still recruited to the centrioles, fails to expand into the mitotic scaffold (Woodruff et al. 2015, Ohta et al. 2021). Recently, the molecular interactions of the SPD-5 scaffold were detangled in detail by using crosslinking mass spectrometry (Rios et al. 2024). It was shown that SPD-5, in its inactive state, features long-range intramolecular contacts among its several CC domains. In the cytoplasm, these contacts stabilize the folded, inactive SPD-5 conformation and block multimerization, maintaining SPD-5 in an autoinhibited state. Once PLK-1 phosphorylates SPD-5 at the centrosome, these intramolecular restraints are relieved, resulting in a dramatic increase in intermolecular interactions between CC domains - including PReM-PReM and PReM-C-terminal associations (Rios et al. 2024). This transition enables rapid SPD-5 multimerization and consequently leads to the formation of a mechanically resilient polymeric scaffold. Thus, SPD-5's activation and assembly rely on a PLK-1 phosphorylation-dependent

switch that releases autoinhibition and, by this, orchestrates a multivalent CC-driven network expansion directly at the centrosome (Rios et al. 2024).

SPD-2 is the limiting factor for PCM growth (Decker et al. 2011). However, it is not fully elucidated how SPD-2 promotes PCM scaffolding (Pintard and Bowerman 2019, Murph et al. 2022). Although interaction with SPD-5 was demonstrated *in vitro* (Boxem et al. 2008, Woodruff et al. 2015), bleaching experiments of the mitotic PCM revealed substantial exchange of SPD-2 with the cytoplasmic pool (Laos et al. 2015). Furthermore, SPD-2 appears to be required only for PCM expansion, but not for maintaining the existing scaffold (Woodruff et al. 2015, Cabral et al. 2019). This suggests that SPD-2 does not play a primary structural role in scaffolding but rather functions in the regulation or stabilization of the PCM matrix. Current models propose that centrosomal SPD-2 recruits PLK-1 through direct interaction. This interaction requires the priming of the PLK-1 docking site on SPD-2 by Cyclin-dependent kinase 1 (CDK-1; human CDK1, *Drosophila* Cdk1) (Ohta et al. 2021). Centrosomal PLK-1 then phosphorylates SPD-5 (Decker et al. 2011, Cabral et al. 2019). This aligns with SPD-2's proposed function as a PCM size limiter by modulating the amount of PLK-1 recruited (Decker et al. 2011). Nevertheless, *in vitro* studies show that SPD-5 scaffolding accelerates in the presence of SPD-2, even in the absence of PLK-1 (Woodruff et al. 2015), suggesting that SPD-2's role extends beyond PLK-1 recruitment (Cabral et al. 2019). From a structural perspective, the C-terminal region of SPD-2 contains an ASH domain that, when expressed alone, localizes to the centrosome, supporting its recruitment role (Murph et al. 2022). In contrast, the N-terminal region of SPD-2 is highly unstructured, features multiple CC domains, and includes experimentally confirmed phosphorylation sites for PLK-1 and CDK-1 (Lu and Roy 2014, Murph et al. 2022). It is possible that phosphorylation of SPD-2 at the N-terminus modulates its conformational plasticity, enabling interactions with different binding partners, for PCM assembly, but also for centriolar duplication (Murph et al. 2022).

Interestingly, centrioles also play an active role in the assembly of the PCM, as their ablation has been shown to accelerate PCM disassembly (Cabral et al. 2019). Remarkably, this can be reversed through microtubule depolymerization, emphasizing the dependence of PCM integrity on the continued presence of centrioles (Cabral et al. 2019).

Beyond centrioles, additional kinases, such as CDK-1 and Aurora kinase (AIR-1; human Aurora A, *Drosophila* Aurora A), have emerged as important regulators of PCM dynamics. CDK-1 is required for PCM accumulation (Magescas et al. 2019), presumably indirectly. The inhibition of CDKs before metaphase leads to premature PCM disassembly. In contrast, inhibition at metaphase causes minimal effects (Magescas et al. 2019), consistent with CDK-1's natural inactivation shortly after metaphase (Begasse and Hyman 2011). Moreover, CDK-1 primes PLK-1 target proteins such as SPD-2 (Ohta et al. 2021) and cooperates with

AIR-1 to regulate PLK-1 activity (Tavernier et al. 2015). AIR-1 functions as another key kinase in PCM organization, as its loss was shown to impair PCM assembly (Hannak et al. 2001). Its active form localizes exclusively to centrosomes (Toya et al. 2011), where it is recruited by SPD-2 (Cabral et al. 2019). AIR-1 has been shown to bind SPD-5 in yeast two-hybrid (Y2H) assays (Boxem et al. 2008), although the functional relevance of this interaction is still unclear. AIR-1 activates PLK-1, likely at the onset of mitosis, which may represent its principal role in PCM assembly, since acute mitotic inhibition of AIR-1 does not disrupt ongoing PCM organization (Cabral et al. 2019).

Once mature, the PCM scaffold serves as a platform for recruiting diverse client proteins required for microtubule organization, microtubule stability, and spindle assembly. Principal among these clients is the γ-Tubulin Ring Complex (γ-TuRC), which is anchored to the PCM primarily through direct binding to SPD-5 (Moritz et al. 2000, Ohta et al. 2021, Tollervey et al. 2025). Interestingly, this interaction also involves PLK-1-mediated phosphorylation of SPD-5 at specific sites - T178 and T198 -, which are distinct from those required for PCM maturation (Ohta et al. 2021). Beyond γ-TuRC, the PCM scaffold also recruits other microtubule-associated proteins, including Transforming Acid CC-containing protein 1 (TAC-1; human TACC1/2/3; *Drosophila* TACC), ZYGote-defective 9 (ZYG-9; human: XMAP215/ch-TOG; *Drosophila* Msps), and TPX2 domain-containing protein (TPXL-1; human: TPX2, *Drosophila*: Tpx-2), which are essential for spindle assembly, microtubule stabilization, and organization (Matthews et al. 1998, Bellanger and Gönczy 2003, Le Bot et al. 2003, Özlü et al. 2005, Srayko et al. 2005). The recruitment and activity of these proteins are tightly coordinated and spatially regulated, allowing the centrosome to function as an organizer and regulator for microtubule nucleators. This ensures that spindle morphology and position are precisely controlled throughout mitosis (Conduit et al. 2015).

To date, many fundamental questions remain unanswered regarding the precise mechanisms that govern PCM recruitment, maturation, and organization. Despite the extensive characterization of scaffold components like SPD-5, it remains unclear how the hierarchical assembly of the PCM is temporally and spatially coordinated. Recent studies suggest that centriolar proteins such as SAS-7 are at the beginning of the cassette, as they interact with SPD-2 and are in turn required for both centriole duplication and PCM assembly (Sugioka et al. 2017). However, the exact mechanisms and protein linkers that integrate these events are still unknown, or their mode of action is not fully understood. The functional diversity of PCM proteins, their dynamic modifications, and potential crosstalk between structural and regulatory modules highlight the complexity of centrosome maturation.

1.7 PCMD-1, a linker between centrioles and PCM

In 2019, the conceptual gap in PCM recruitment in *C. elegans* was addressed by the identification of a previously uncharacterized protein PeriCentriolar Matrix Deficient 1 (PCMD-1) that acts as a dedicated PCM recruiter (Erpf et al. 2019). PCMD-1 is essential for non-mitotic PCM core recruitment **(Figure 5B)**, and its loss causes severe spindle assembly defects and early embryonic lethality (Erpf et al. 2019). The protein was originally discovered in an EMS mutagenesis screen that yielded temperature-sensitive mutant allele *pcmd-1(t3421)* (unpublished data from Nadine Memar and Ralph Schnabel), which introduces a premature stop codon at Q53. At restrictive temperature, this mutation results in 100% embryonic lethality, with 58% of embryos displaying a monopolar spindle at the first cell division and a tripolar spindle at the second (Erpf et al. 2019).

The *pcmd-1(c17d12.7)* gene encodes a 630 amino acid (AA) protein, which is predicted to have one CC domain and six intrinsically disordered regions (IDRs) **(Figure 5A)**. PCMD-1 localizes to centrosomes across all tissues, with the highest abundance in the syncytial germline, spermatheca, embryos, and sensory cilia in the head and tail. Analyzing the subcellular localization of PCMD-1 revealed that it predominantly associates with centrioles but can also be found in minor amounts at the PCM **(Figure 5B)** (Erpf et al. 2019). Consistent with this centriolar enrichment, a recent study suggested that PCMD-1, together with SPD-5, SPD-2, and HYLS-1, is a component of the centriolar paddlewheel (Woglar et al. 2022). Loss of PCMD-1 results in a previously unrecognized failure to recruit the core PCM to centrioles **(Figure 5C)**. Moreover, most embryos lacking PCMD-1 cannot assemble a mitotic PCM; those that do present highly disorganized and stretched PCM structures **(Figure 5C)** (Erpf et al. 2019). Besides SPD-5 recruitment failure, PLK-1 recruitment is also strongly decreased in the *pcmd-1(t3421)* mutant. The double depletion of PCMD-1 and SPD-2 completely abolishes centrosomal localization of both SPD-5 and PLK-1 (Erpf et al. 2019). On the contrary, the localization of PCMD-1 at the centriole is independent of the pericentriolar proteins SPD-2, SPD-5, and PLK-1 (Erpf et al. 2019). Based on its localization and function, PCMD-1 is therefore assumed to be the *C. elegans* functional homolog of human PCNT and *Drosophila* Plp (Erpf et al. 2019). In vertebrates and flies, PCNT/Plp similarly act as major PCM scaffold components that are required for efficient recruitment and organization of PCM factors around centrioles (Lawo et al. 2012, Mennella et al. 2012).

These findings demonstrate that PCMD-1, together with SPD-2, is essential for recruiting the PCM to the centrioles and orchestrating its proper organization **(Figure 5B)** (Erpf et al. 2019). When this process is disrupted, the PCM is either absent or loosely associated with centrioles at mitotic entry and appears highly disorganized during metaphase **(Figure 5C)**. As a result,

spindle formation is compromised, leading to defects in cell division and ultimately causing embryonic lethality.

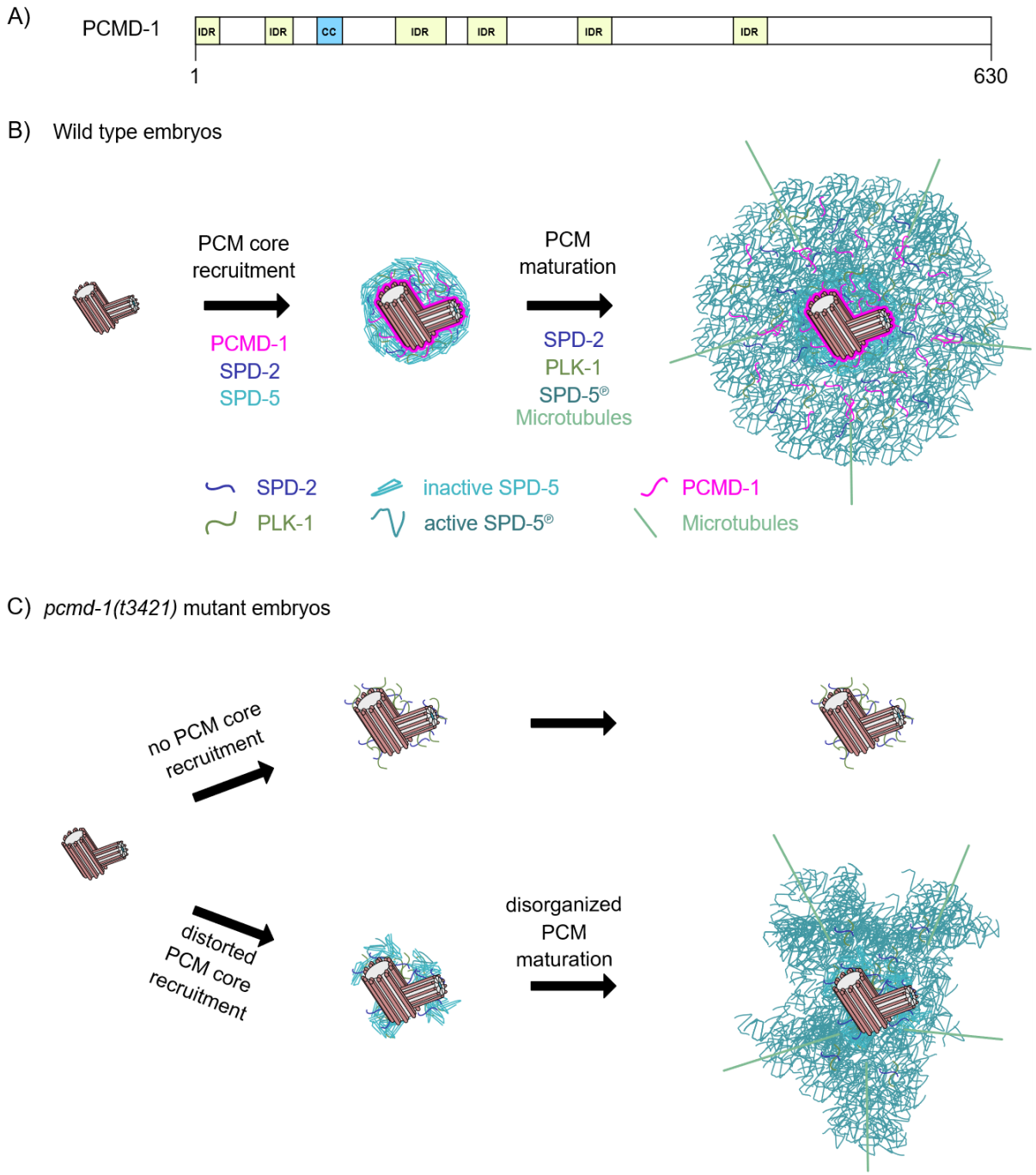

Figure 5: PCMD-1, a new player in the PCM recruitment pathway.
A) *Protein structure of C. elegans PCMD-1, a 630-AA protein with one predicted coiled-coil (CC) domain and multiple intrinsically disordered regions (IDRs).* ***B)*** *Schematic of PCM core recruitment. PCMD-1 localizes to centrioles and is required, together with SPD-2, for the recruitment of the core SPD-5 PCM before mitotic PCM maturation.* ***C)*** *PCM recruitment in pcmd-1(t3421) mutant embryos. In most embryos, core PCM fails to be recruited to centrioles. In the minority of cases where PCM is recruited, it is aberrant from the very beginning and forms a highly disorganized scaffold. Modified from Erpf et al. 2019.*

1.8 Disassembly of the PCM

To release centrioles from the PCM and enable the assembly of a new bipolar spindle in the subsequent cell cycle, the PCM must be disassembled as cells exit mitosis. Paradoxically, during metaphase, centrosomes first need to function as robust mechanical hubs that withstand strong tensile stresses generated by the cortical, microtubule-mediated pulling forces to position the spindle and ensure faithful chromosome segregation (Kotak and Gönczy 2013, Mittasch et al. 2020). Despite these substantial mechanical loads, centrosomes, which are not confined by a membrane, remain stable and spherical at this stage, with no detectable aberrations in shape. As anaphase proceeds, the very same forces that once maintained spindle positioning begin to deform the centrosomes, fracture the PCM, and ultimately drive its complete dissolution, a process here referred to as centrosome disassembly (Mittasch et al. 2020, Rios et al. 2024). This controlled disassembly releases the paired centrioles to permit their separation, ensuring that each daughter cell again harbors exactly two centrosomes for the next cell cycle (Cabral et al. 2013, Magescas et al. 2019).

How the structural and material integrity of the centrosome is regulated throughout the cell cycle to allow both robustness during metaphase and rapid breakdown from anaphase onward is still not completely understood. In *C. elegans*, current data show that centrosome stability relies on an interplay between mechanical forces exerted by cortex-bound microtubules and the structural composition and organization of the PCM scaffold (Enos et al. 2018, Mittasch et al. 2020). For instance, increased microtubule pulling forces at the posterior side of the *C. elegans* embryo lead to earlier and stronger PCM disassembly as compared to the anterior cell (Grill et al. 2003, Enos et al. 2018). However, mechanical tension alone cannot explain the observed transitions in centrosome structure. Although pulling forces rise sharply at metaphase-anaphase transition, centrosomes arrested in metaphase and still exposed to a similar increase in pulling forces, do not fracture and remain intact (Labbé et al. 2004, Laos et al. 2015, Cabral et al. 2019, Mittasch et al. 2020). Moreover, increasing microtubule-dependent pulling forces does not lead to premature PCM dissolution (Magescas et al. 2019). These findings suggest that centrosome disassembly is not a purely mechanical process but instead involves coordinated biochemical remodeling of PCM components, which modulate their interactions and lead to changes in the material properties of the entire structure.

The phosphorylation of the PCM scaffold component SPD-5 has been shown to catalyze assembly and stabilize the network (Woodruff et al. 2015), suggesting that its dephosphorylation, in contrast, serves as a molecular trigger for PCM fragmentation. *In vitro* assays demonstrated that the protein phosphatase 2A (PP2A) complex can directly dephosphorylate PLK-1-phosphorylated SPD-5, indicating that this phosphatase directly counteracts mitotic kinase signaling (Enos et al. 2018). Consistent with this, downregulation of

the PP2A catalytic subunit let-92 (LET-92; human PPP2CA/B; *Drosophila* mts) or PP2A regulatory subunit sur-6 (SUR-6; human: PPP2RA/B/C/D; *Drosophila* tws) was found to markedly slow PCM disassembly (Enos et al. 2018, Magescas et al. 2019). This effect becomes even more pronounced when cortical pulling forces are simultaneously inhibited, implying that biochemical and mechanical cues cooperate to drive centrosome disassembly (Enos et al. 2018, Magescas et al. 2019).

Temporal analyses of key PCM components reveal that SPD-2 and PLK-1 levels drop rapidly following metaphase, whereas PP2A remains stably associated with the PCM throughout this transition (Magescas et al. 2019, Mittasch et al. 2020). Such a pattern supports a model in which PP2A opposes PLK-1 activity (Enos et al. 2018, Mittasch et al. 2020). Dephosphorylation of SPD-5, coupled with the loss of the matrix stabilizer SPD-2, likely reduces the mechanical resilience of the PCM. In this weakened state, cortical pulling forces may even stretch the scaffold, exposing it to further phosphatases or enabling stabilizing components to diffuse away faster into the cytoplasm (Enos et al. 2018).

Together, these observations have led to a two-step model of PCM disassembly. In the first phase, SPD-2 and PLK-1 are released from the centrosome by gradual dissolution - a process also affected by PP2A activity but largely independent of cortical pulling forces **(Figure 6)** (Magescas et al. 2019). The second phase involves the physical rupture and tearing apart of the remaining SPD-5 scaffold, driven by combined cortical pulling forces and PP2A-mediated scaffold dephosphorylation, leading to the fragmentation of the PCM into small SPD-5-containing packets that later dissolve in the cytoplasm **(Figure 6)** (Magescas et al. 2019). Given that PLK-1 and SPD-2 exhibit higher cytoplasmic turnover rates compared to SPD-5 (Laos et al. 2015), their dynamic exchange may prevent their rupture. In contrast, the stably integrated SPD-5 molecules might require mechanical forces to detach from the scaffold and complete the disassembly process (Magescas et al. 2019).

This model has been substantially strengthened by findings from Mittasch et al. 2020, who directly assessed the changing material properties of the PCM throughout the cell cycle using focused light-induced cytoplasmic streaming (FLUCS) as an experimental perturbation. By applying this localized shear stress to centrosomes, they were able to probe how molecular regulation tunes the mechanical resilience of the PCM. They found that during metaphase, the PCM exists as a strong and ductile scaffold, robustly reinforced by high levels of SPD-2 and PLK-1, which FLUCS-induced forces could not deform or compromise (Mittasch et al. 2020).

As the cell cycle progresses into anaphase, the PCM becomes materially brittle and weak, making it susceptible to deformation by FLUCS. This material transition requires the decline of SPD-2 and PLK-1, as well as a functional PP2A (Mittasch et al. 2020). During telophase, microtubule-mediated pulling forces can fracture this PCM, thereby facilitating the final rupture

and disassembly of the PCM. This study established the concept of “PCM material aging”, the idea that the structural and physical properties of the PCM change transiently across the cell cycle, governed by the balance and turnover of SPD-2, PLK-1, and PP2A (Mittasch et al. 2020). This material transition enables centrosomes to withstand mitotic spindle forces, when necessary, but then to be effectively disassembled by the same types of forces as the cell exits mitosis.

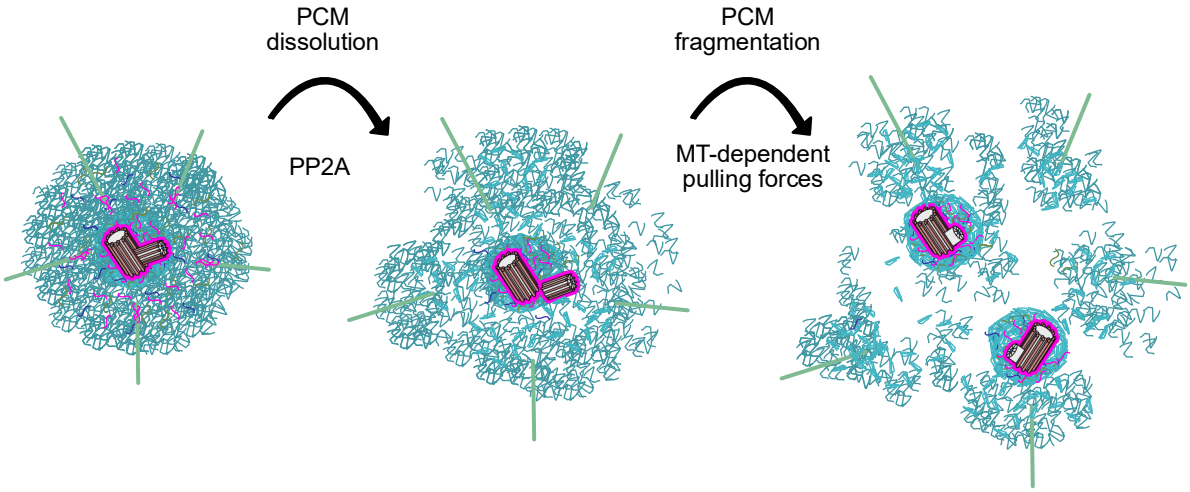

Figure 6: Disassembly of the PCM in C. elegans.
In the current model, PCM disassembly proceeds via a two-step mechanism (Magescas et al. 2019). In a first biochemical step, declining levels of the kinase PLK-1 from anaphase onwards, with approximately constant levels of the phosphatase PP2A, result in the dephosphorylation of the PCM scaffold, thereby loosening the matrix. In a second, mechanical step, the remaining PCM is ruptured and fragmented into small packages by microtubule-mediated pulling forces.

1.9 Centriolar separation

To guarantee the formation of bipolar spindles in each round of cell division, the separation of duplicated centrioles must be tightly regulated in space and time.

In vertebrates, procentrioles are assembled during S-phase and remain tightly associated with their mother centrioles until mitosis (Tsou and Stearns 2006). Centriole disengagement, the first step of their separation, occurs during mitotic exit **(Figure 7)** (Mardin and Schiebel 2012). At this stage, the orthogonal connection between the mother and daughter centrioles is lost, leaving them bonded only by a “loose” proteinaceous linker (Mardin and Schiebel 2012). The release of the daughter from the mother requires the proteolytic cleavage of this connection by separase (Tsou 2009). Separase is best known for triggering anaphase onset by cleaving cohesin complexes that hold sister chromatids together during mitosis (Uhlmann 2001). The centrosomal connection similarly consists of a cohesion complex, but also of PCNT, the latter of which must be phosphorylated to become a separase substrate (Schöckel et al. 2011, Lee and Rhee 2012, Kim et al. 2015). Together with the disassembly of the PCM (Seo et al. 2015),

this cleavage drives centriolar disengagement and licenses both centrioles for another round of duplication during the following S-phase **(Figure 7)** (Mardin and Schiebel 2012). The complete separation of the two centriolar pairs then occurs in a second step at G2/M transition, when the remaining centrosomal linker is resolved **(Figure 7)** (Mardin and Schiebel 2012). With this, each centriolar pair can build an MTOC for the formation of the bipolar spindle during mitosis **(Figure 7)**.

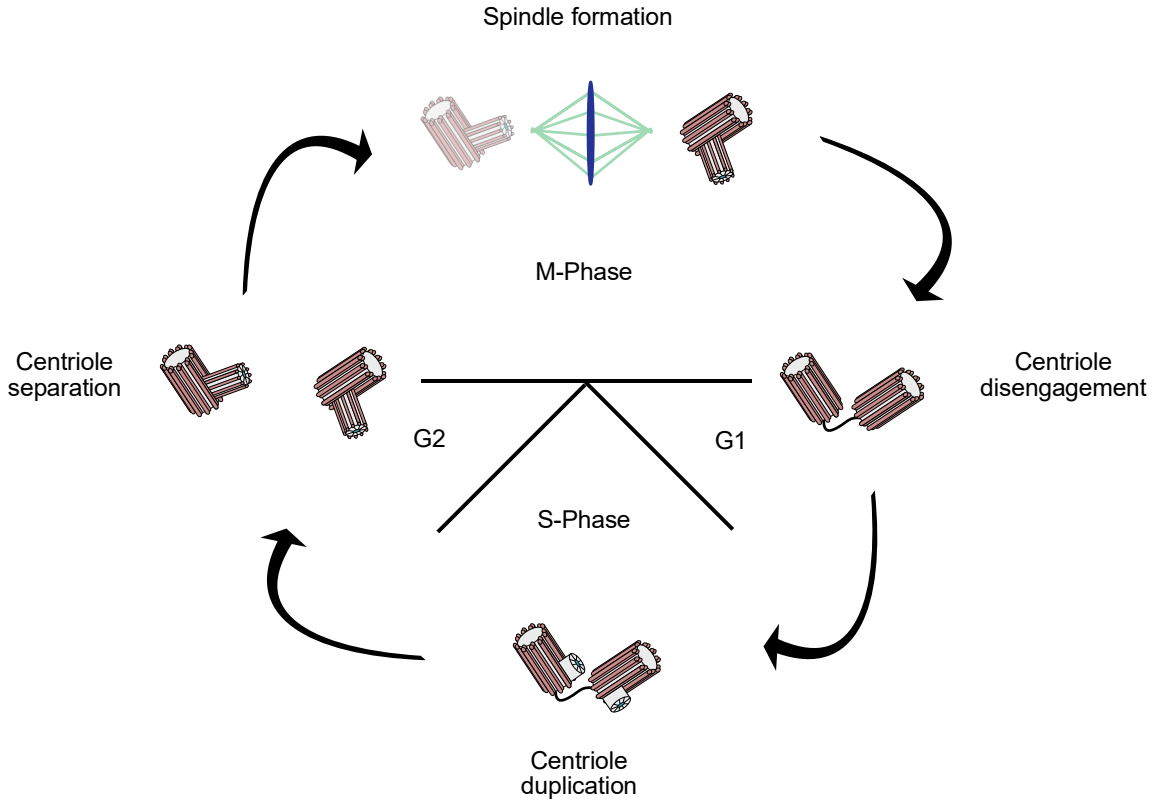

Figure 7: Centriolar separation in vertebrates.
During mitosis, two centrosomes, each consisting of a pair of orthogonally arranged centrioles, organize a mitotic spindle. Upon mitotic exit, the two centrioles within each centrosome disengage but remain connected by a flexible proteinaceous linker. This partial separation creates sufficient space for each centriole to duplicate and assemble a new procentriole during S-phase. At the G2/M transition, the linker is dissolved, allowing the two centriolar pairs (i.e., the two centrosomes) to fully separate and establish the bipolar spindle during mitosis. Adapted from Mardin and Schiebel 2012.

In *C. elegans*, centriolar separation has so far not been subdivided into distinct disengagement and separation phases. Mother and daughter centrioles appear to completely separate at the same time, which suggests either that disengagement is irrelevant, that it occurs almost simultaneously with separation, or that it has so far been experimentally indistinguishable. Notably, most observations derive from the first embryonic cell divisions. Because these early cleavages proceed through extremely rapid cell cycles that largely lack canonical gap phases, the mechanism of centriolar separation during this period may deviate from that operating in

later divisions. Nevertheless, it is useful to distinguish between the first centriolar separation event shortly after fertilization, hereafter referred to as the initial centriolar separation, and the subsequent separation events during later embryonic mitoses, hereafter referred to as mitotic centriolar separation **(Figure 8)**. This distinction reflects the idea that the underlying mechanisms and regulatory requirements of the initial separation differ from those operating during later mitotic cycles (Cabral et al. 2013).

During initial centriolar separation, centrioles contributed by the sperm are closely connected **(Figure 8A)** by a cohesin-like protein complex (Cabral et al. 2013). Similar to vertebrates (Tsou 2009), separase (SEP-1; human Separase; *Drosophila* separase) is essential for removing these engagement factors; depletion of separase impairs centriole separation and subsequent duplication (Cabral et al. 2013). Interestingly, increasing microtubule-mediated pulling forces can bypass this requirement for separase, allowing centrioles to separate and duplicate even when separase is deficient (Cabral et al. 2013). Upon successful separation, the centrosomes, which harbor only a thin core of PCM, undergo spatial re-localization along the nuclear envelope **(Figure 8A)** (Cabral et al. 2013, De Simone et al. 2016). This movement is orchestrated by dynein motor proteins, which are anchored at the nuclear envelope and the cell cortex, under the control of PP2A (De Simone et al. 2016, Boudreau et al. 2019). Dynein motors exert pulling forces on microtubules nucleated by the sperm-derived centrosomes, thereby directing the symmetric separation of the centrioles around the nuclear perimeter (De Simone et al. 2016). Once male and female pronuclei meet, centrosomes are positioned on opposite sides **(Figure 8A)**.

The subsequent rounds of centriolar separation, the mitotic separations, take place during mitotic exit. At metaphase, centriolar pairs are embedded within the PCM **(Figure 8B)**. As cells progress into anaphase and the PCM begins to disassemble, the individual centrioles separate and are released into the cytoplasm **(Figure 8B)**. Once the nuclear envelope has been reformed, the centrosomes re-establish their attachment to the nucleus **(Figure 8B)**. In contrast to vertebrates, these mitotic separations occur independently of separase (Cabral et al. 2013). Although the precise molecular mechanisms remain unclear, current evidence supports an essential role of PCM disassembly and microtubule-driven pulling forces in coordinating centriole separation. Compromised PCM assembly has been shown to induce premature centriole separation (Dammermann et al. 2004), whereas prolonged persistence of mitotic PCM, resulting from reduced cortical pulling forces, delays the process (Magescas et al. 2019). Centriole separation follows the same temporal pattern as PCM disassembly and is, therefore, polarity dependent. It consistently occurs in the posterior before the anterior side of the cell, corresponding with the stronger pulling forces (Grill et al. 2003, Cabral et al. 2013, Enos et al. 2018). This difference may stem from either asymmetric forces or PCM entrapment,

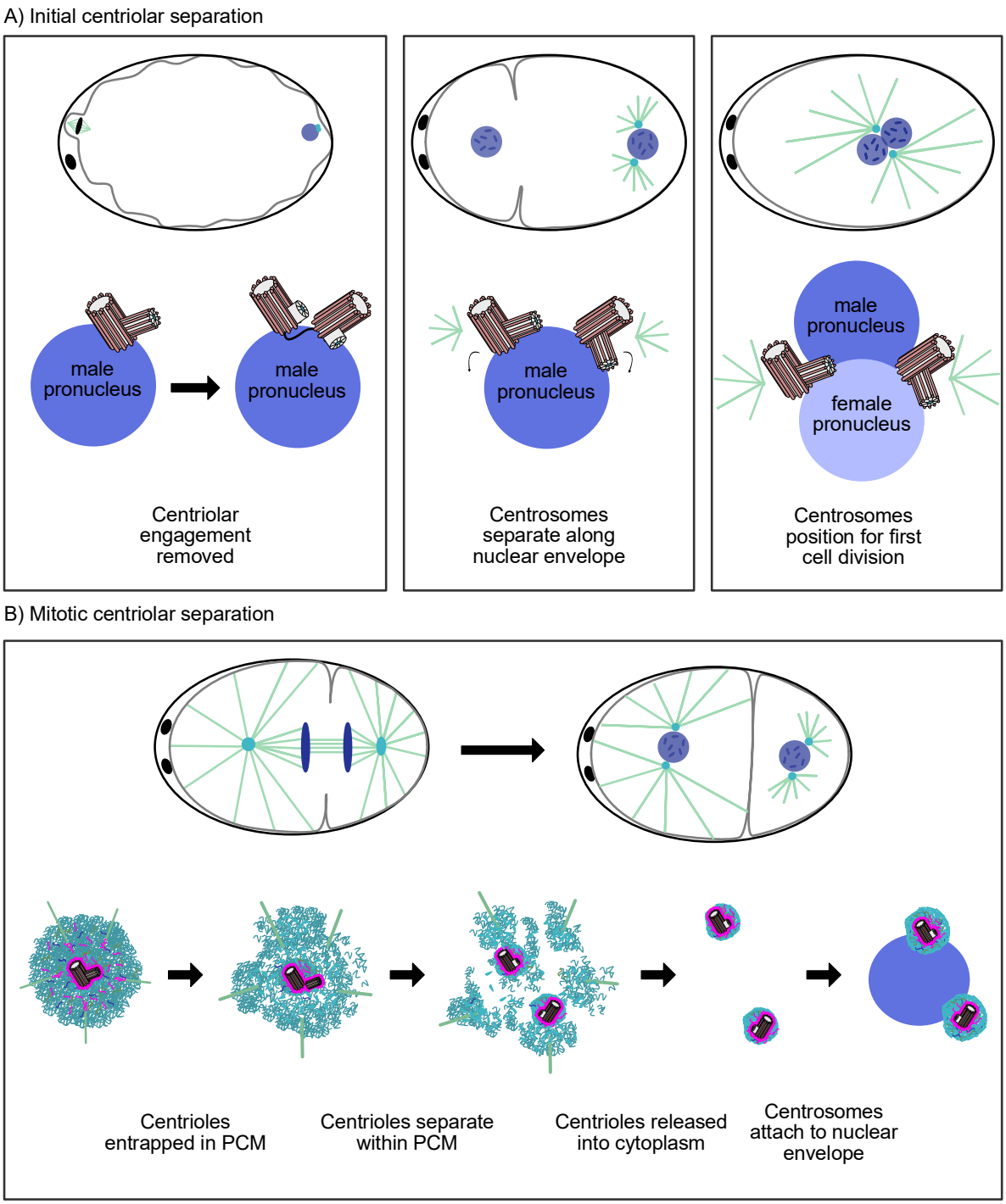

Figure 8: Centriolar separation in C. elegans.
A) *Upon fertilization, the sperm contributes a pair of closely apposed centrioles that are attached to the male pronucleus. According to current models, centrioles first begin to separate upon removal of engagement factors and subsequently slide apart along the surface of the nuclear envelope (Cabral et al. 2013, De Simone et al. 2016). As the male and female pronuclei migrate and meet, the two centrosomes become positioned on opposite sides of the joined pronuclei, thereby establishing the axis for the first embryonic division.* ***B)*** *During metaphase, the centriolar pair is embedded within the PCM. As mitosis progresses, the PCM disassembles and fragments, and the two centrioles gradually separate and move apart. Once the PCM is fully disassembled, the centriolar pairs are released into the cytoplasm. After the nuclear envelope is reassembled, the centrosomes reestablish their attachment to the nucleus.*

though the precise cause is still unknown (Cabral et al. 2013). Furthermore, mitotic kinases play a key role in regulating PCM dynamics and, in turn, potentially in the process of centriole separation. Depletion of AIR-1, for example, leads to premature centriole separation (Dammermann et al. 2004), suggesting either an indirect regulatory connection through PCM modification or a direct involvement in the separation process.

Collectively, in *C. elegans,* mitotic centriolar separation is regulated by PCM disassembly, microtubule pulling forces, and mitotic kinases, but the exact molecular mechanism remains unclear and requires further investigation.

1.10 The material properties of the centrosome

The centrosome is a membraneless organelle, and its functionality during the cell cycle relies on the biophysical properties of the PCM, which maintains its structural integrity despite the lack of a lipid membrane. PCM integrity is crucial for both dividing and non-dividing cells. During mitosis, loss of PCM integrity can lead to premature fragmentation of the PCM, generating extra, often acentriolar spindle poles (Maiato and Logarinho 2014). These aberrant MTOCs promote multipolar spindle formation, chromosome missegregation, and the production of aneuploid daughter cells (Maiato and Logarinho 2014). Although aneuploidy generally impairs proliferative capacity, the fact that many cancer cells are aneuploid suggests that defects in the centrosome and PCM may contribute to tumor development (Holland and Cleveland 2009). PCM integrity is also essential outside of mitosis, for example, during directed cell navigation. In migratory cells, such as immune cells, the centrosome is positioned in a mechanically demanding environment and experiences substantial forces arising from cell movement and confinement (Schmitt et al. 2025). If the PCM is structurally weakened, these forces can deform and fracture the centrosome, leading to the disruption of cell polarity and navigation, and in turn to physical entanglement with the surrounding microenvironment (Schmitt et al. 2025). Thus, the material properties that determine PCM cohesion, elasticity, and resistance to fracture directly control the cells' integrity under mechanical load.

These material properties and the ability of the PCM to maintain its integrity under mechanical load arise from the self-assembly of PCM proteins into a selective, permeable matrix. This matrix allows PCM components and their interaction partners to enter, diffuse, and interact within this complex environment. At the same time, the PCM must remain dynamic enough to assemble and disassemble rapidly, yet stable enough to resist the microtubule-mediated forces exerted during mitosis when it serves as the spindle anchor (Woodruff et al. 2017, Raff 2019). Although several molecular interactions underlying these properties have been elucidated, the precise mechanisms governing PCM architecture and biophysical behavior

remain only partially understood and are the subject of ongoing research (Raff 2019, Woodruff 2021). Most of the knowledge about how centrosomes maintain their structural integrity and how the mechanical properties of the PCM change over the cell cycle is based on experiments conducted on the one-cell embryo of *C. elegans* (Woodruff et al. 2017, Mittasch et al. 2020, Rios et al. 2024, Amato et al. 2025, Garcia-Baucells et al. 2025, Tollervey et al. 2025). Whether this also applies to centrosomes of other animals remains to be investigated.

Early EM studies of different species revealed that the mitotic PCM is electron-dense but lacks an ordered, crystalline organization, in stark contrast to the highly ordered centrioles at its core (Gould and Borisy 1977, O'Toole et al. 2002, Raff 2019). More recent cryo-electron tomography analyses on *C. elegans* centrosomes, which provide higher structural resolution, confirmed this observation (Tollervey et al. 2025). They further demonstrated that PCM architecture remains largely consistent throughout the cell cycle, with no major changes in pore size or lattice organization (Tollervey et al. 2025). This suggested that the centrosome is a membraneless scaffold that expands through the incorporation of newly assembled proteins. Advanced volumetric EM studies in *C. elegans* have uncovered an endoplasmic-reticulum (ER)-derived membrane network surrounding the centrosome in early embryos (Maheshwari et al. 2023). This structure, named the "centriculum" (from centrosome-associated membrane reticulum), forms a mesh-like shell around the PCM and could act as a selective filter or barrier that modulates which microtubules and molecular complexes can access or depart from the centrosome's core. Manipulation of the centriculum's structure affects PCM size, microtubule nucleation, and spindle morphology, indicating a regulatory interplay between the membrane network and centrosome function (Maheshwari et al. 2023). These observations support a model in which the PCM acts as a solid-like matrix encapsulated within an ER-derived membrane network **(Figure 9)**. However, this view is difficult to reconcile with the fact that the PCM maintains a spherical shape and expands isotropically during centrosome maturation (Laos et al. 2015). Additionally, structural studies have demonstrated that the PCM can form flexible and dynamic extensions when subjected to external stress (Mittasch et al. 2020). This property is incompatible with a rigid framework and indicates material adaptability.

A more plausible explanation is that the functional modulation of PCM material properties arises from regulated protein interactions via posttranslational modifications (PTMs), rather than from large-scale structural rearrangements of a scaffold. As described before, the phosphorylation of scaffold proteins like SPD-5 modulates PCM properties, tuning the network from a ductile, strong state during metaphase to a more brittle form when anaphase begins, supporting both robustness and flexibility (Mittasch et al. 2020). This molecular tuning enables the PCM to adapt to cell cycle stage-specific functional requirements. One hypothesis for how these biophysical needs can be achieved is that the PCM forms by liquid-liquid phase separation (LLPS) (Zwicker et al. 2014, Woodruff et al. 2017). LLPS describes the process by

which a single, homogenous liquid segregates into multiple, compositionally distinct droplets, analogous to oil separating from water. In biological systems, certain biomolecules can condense into dynamic, membraneless phases that often adopt spherical shapes due to surface tension (Ong and Torres 2020). Examples of such condensates include P-granules, the nucleolus, and stress granules (Bracha et al. 2019). Recent research highlights that not all condensates are permanently liquid. As condensates “age” or mature, they may transition to more solid-like or gel-like states that lose the capacity for internal rearrangement and fusion (Ong and Torres 2020). SPD-5 itself could be a driver central example of LLPS-mediated organization at the centrosome. This protein can spontaneously self-assemble into networks, but more importantly, into condensates when placed in a molecular crowded agent (supposed to mimic the crowded cytoplasm better) (Woodruff et al. 2015, Woodruff et al. 2017). These SPD-5 condensates exhibit liquid-like properties, such as fusion, fission, and internal rearrangement, and mature into more solid-like, gel states over time (Woodruff et al. 2017). This biophysical behavior could underpin the centrosome’s structural stability and mechanical integrity throughout the cell cycle, controlled by PLK-1-dependent phosphorylation **(Figure 9)** (Woodruff 2021).

Although LLPS provides an appealing concept to explain the assembly of membraneless organelles, direct evidence of a liquid-like centrosome scaffold *in vivo* remains elusive for *C. elegans* (Raff 2019, Woodruff 2021). A likely explanation is therefore that, similar to SPD-5 condensates observed *in vitro*, the PCM rapidly transitions into a gel-like or porous matrix *in vivo*. This transformation would obscure typical LLPS behaviors such as droplet fusion or fission (Woodruff 2021). Nevertheless, the assembled SPD-5 scaffold at the centrosome remains stably anchored and does not exchange with the cytoplasm, nor does it internally rearrange, further arguing against a simple LLPS-based PCM structure (Laos et al. 2015, Woodruff 2021).

Building on this, current models now combine the concepts of a stable scaffold and a gel-like matrix, describing the PCM as a viscoelastic material, displaying both elastic and viscous responses to deformation, much like memory foam **(Figure 9)** (Hyman et al. 2014, Woodruff 2021, Amato et al. 2025). Notably, the viscoelasticity of the SPD-5 scaffold varies according to its phosphorylation status. When SPD-5 is under-phosphorylated, the matrix is more dynamic and liquid-like, easily stretching or fragmenting, whereas, conversely, excessive phosphorylation results in a solid-like, irregular matrix with reduced mechanical integrity (Amato et al. 2025). Achieving the right balance of SPD-5 phosphorylation is thus vital for fine-tuning the scaffold’s material properties, a process orchestrated by kinases, as PLK-1, and phosphatases, as PP2A (Amato et al. 2025).

Interestingly, a recent preprint challenged this view by further exploring the mechanical nature of the centrosome using two complementary approaches: atomic force microscopy (AFM) on isolated centrosomes and Brillouin microscopy *in vivo*. Both analyses converged on a consistent result, a solid-like PCM that gradually softens rather than hardens during mitosis (Garcia-Baucells et al. 2025). This mechanical transition likely enables the centrosome to buffer fluctuations from cortical pulling forces while maintaining steady tension transmission to chromosomes (Garcia-Baucells et al. 2025). Excessive rigidity, by contrast, could amplify force spikes, potentially leading to chromosome missegregation and mitotic errors (Garcia-Baucells et al. 2025).

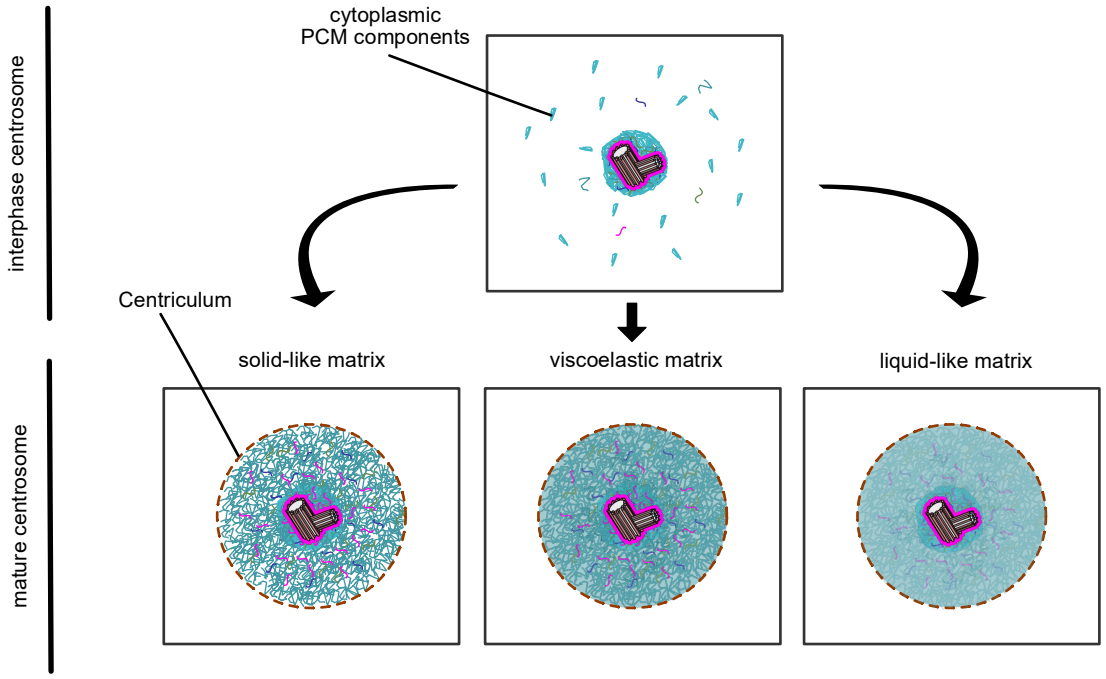

Figure 9: Models for material properties of the PCM.
The PCM grows by self-assembly of scaffold proteins that are progressively recruited from the cytoplasm, transforming a small interphase/core PCM into an expanded mitotic, "mature" PCM. Current models propose that this scaffold can behave as a solid-like matrix, in which PCM proteins form a relatively static, interconnected network (left), a viscoelastic matrix, which combines solid- and liquid-like behavior and can bear mechanical load but slowly flow and remodel over time (middle), or a liquid-like matrix, in which the PCM grows through the incorporation of new molecules via liquid-liquid phase separation (right). Adapted from Woodruff 2021.

Taken together, these data suggest a model in which the SPD-5 scaffold remains highly phosphorylated through PLK-1 activity and mechanically robust during early mitosis but gradually loses phosphorylation sites from anaphase onward through the activity of

phosphatases like PP2A, leading to a progressive softening of the PCM. This transition aligns well with the observed temporal and spatial dynamics of PLK-1 and PP2A at the centrosome.

Although recent findings increasingly portray the PCM as a dynamic, viscoelastic scaffold whose mechanical state is fine-tuned by reversible phosphorylation (Amato et al. 2025, Garcia-Baucells et al. 2025), the molecular principles that govern selective recruitment, concentration, and maintenance of PCM proteins at the centrosome remain unclear. Resolving how such organization emerges in the absence of a delimiting lipid membrane and enables centrosome assembly, its stability, and regulation over the cell cycle is a key challenge for the field.

1.11 Aims of this study

The function of the centrosome is tightly coordinated during the cell cycle for proper cell division to succeed. Therefore, it is of utmost importance to understand how its dynamics are regulated on a molecular level. While it has been established that PCMD-1 is required for the recruitment of interphase PCM and ensures integral stability of the mitotic PCM (Erpf et al. 2019), the molecular basis for these key functions remained elusive. The primary aim of this study is to investigate how PCMD-1 contributes to the establishment and maintenance of a stable and functional centrosome.

To achieve this, the first objective focuses on how PCMD-1 anchors the core PCM to centrioles. Therefore, I performed protein-protein interaction assays with main centriolar and pericentriolar matrix components, both *in vitro* and *in vivo*, to uncover direct and indirect molecular associations. Further, I conducted a structure-function analysis by generating truncations of PCMD-1. This allows me to analyze different protein regions for their contribution to centriolar localization and PCM recruitment.

The main goal of this study is to elucidate how PCMD-1 contributes to the structural integrity of the PCM. Building on interaction assays that identified a direct interaction between PCMD-1 and the key mitotic regulator PLK-1 in cellular and biochemical systems (Stenzel et al. 2021), I investigate whether these proteins collaboratively operate together to ensure proper PCM organization and stability, or if PLK-1 regulates PCMD-1 function via phosphorylation. Given that PCMD-1 and PLK-1 are indispensable for PCM integrity, this study tests the functional relevance of their interplay by generating targeted mutations in predicted PLK-1 binding sites on PCMD-1, thus blocking both physical interaction and potential phosphorylation. This approach allows me to analyze how the structure and dynamics of the PCM depend on the interaction between PCMD-1 and PLK-1. Moreover, it highlights how PLK-1-mediated phosphorylation influences the function of PCMD-1 at the centrosome.

Ultimately, this study aims to deepen our understanding of how a linker protein, mainly localized at the centrioles, governs the organizational integrity of the micron-scale PCM and, by doing so, supports faithful cell division. By integrating interaction assays, structural analyses, and functional mutagenesis, the study seeks to reveal new mechanistic insights into the molecular dynamics of centrosome structure and its implications for embryonic development.

2. Results

Publication I

PCMD-1 bridges the centrioles and the pericentriolar material scaffold in *C. elegans*

Lisa Stenzel, **Alina Schreiner**, Elisa Zuccoli, Sim Üstüner, Judith Mehler, Esther Zanin, Tamara Mikeladze-Dvali

Development (2021) - DOI: 10.1242/dev.198416

© 2021. Published by The Company of Biologists Ltd | Development (2021) 148, dev198416. doi:10.1242/dev.198416

RESEARCH ARTICLE

PCMD-1 bridges the centrioles and the pericentriolar material scaffold in *C. elegans*

Lisa Stenzel[1], Alina Schreiner[1], Elisa Zuccoli[1], Sim Üstüner[1], Judith Mehler[1], Esther Zanin[1,2] and Tamara Mikeladze-Dvali[1,*]

ABSTRACT

Correct cell division relies on the formation of a bipolar spindle. In animal cells, microtubule nucleation at the spindle poles is facilitated by the pericentriolar material (PCM), which assembles around a pair of centrioles. Although centrioles are essential for PCM assembly, the proteins that anchor the PCM to the centrioles are less known. Here, we investigate the molecular function of PCMD-1 in bridging the PCM and the centrioles in *Caenorhabditis elegans*. We demonstrate that the centrosomal recruitment of PCMD-1 is dependent on the outer centriolar protein SAS-7. The most C-terminal part of PCMD-1 is sufficient to target it to the centrosome, and the coiled-coil domain promotes its accumulation by facilitating self-interaction. We reveal that PCMD-1 interacts with the PCM scaffold protein SPD-5, the mitotic kinase PLK-1 and the centriolar protein SAS-4. Using an ectopic translocation assay, we show that PCMD-1 can selectively recruit downstream PCM scaffold components to an ectopic location in the cell, indicating that PCMD-1 is able to anchor the PCM scaffold proteins at the centrioles. Our work suggests that PCMD-1 is an essential functional bridge between the centrioles and the PCM.

KEY WORDS: PCM, PCMD-1, PLK-1, SPD-5, Centrioles, Centrosome

INTRODUCTION

Centrosomes are dynamic, non-membranous organelles that serve as the major microtubule-organizing centers in animal cells and are thus essential for biological processes ranging from polarity establishment to the orchestration of cell division. Centrosomes comprise a centriole pair and the surrounding pericentriolar material (PCM). The size and material properties of the PCM change dynamically during the cell cycle (Woodruff et al., 2015, 2017; Mittasch et al., 2020).

PCM expansion during mitosis facilitates bipolar spindle assembly. At the root of PCM expansion is a proteinaceous matrix that serves as a scaffold for the recruitment of regulatory proteins, including mitotic kinases and microtubule nucleators. In *Caenorhabditis elegans*, this scaffolding function is fulfilled by self-assembly of the coiled-coil protein SPD-5 (functional homolog of human CDK5RAP2), which is controlled by phosphorylation through Polo-like kinase PLK-1 (homolog of human PLK1) and interaction with the coiled-coil protein SPD-2 (homolog of human CEP192) (Hamill et al., 2002; Decker et al., 2011; Woodruff et al., 2015, 2017; Cabral et al., 2019). Our previous findings have revealed that PCMD-1, a protein with a predicted coiled-coil domain, regulates the spatial integrity of the PCM scaffold, and, together with SPD-2, is required for the recruitment of SPD-5 (Erpf et al., 2019). Centrioles serve as condensation centers for PCM proteins. During PCM expansion in mitosis, centrioles contribute to the growth and structural integrity of the PCM scaffold (Cabral et al., 2019). A limited set of centriolar core proteins has been described in *C. elegans* (O'Connell et al., 2001; Kirkham et al., 2003; Leidel and Gönczy, 2003; Dammermann et al., 2004; Delattre et al., 2004, 2006; Kemp et al., 2004; Pelletier et al., 2004, 2006; Leidel et al., 2005; Dammermann et al., 2008; Sugioka et al., 2017). From these proteins, SPD-2, SAS-4 (CPAP homolog) and SAS-7 have been proposed to functionally bridge the PCM and the centrioles (Varadarajan and Rusan, 2018). SAS-4, which localizes to the centrioles and the PCM, plays a crucial role in microtubule assembly around the central tube of a forming centriole (Kirkham et al., 2003; Leidel and Gönczy, 2003; Dammermann et al., 2008; Delattre et al., 2006; Pelletier et al., 2006). SAS-7 facilitates the formation of the paddlewheel structure on centriolar microtubules and recruits SPD-2, which in turn is needed for centriole duplication and mitotic PCM scaffold expansion (Sugioka et al., 2017).

PCMD-1 is predominantly a centriolar protein, yet its depletion affects SPD-5 recruitment and the structural integrity of the PCM (Erpf et al., 2019), raising the possibility that it connects the PCM scaffold functionally to the centrioles. However, the precise mechanisms of PCMD-1 centriolar targeting and how PCMD-1 recruits PCM components is still to be elucidated. Here, we investigate the function of PCMD-1 in functionally bridging centrioles and the PCM in *C. elegans* embryos.

RESULTS

SAS-7 maintains PCMD-1 at the centrioles in early embryos

PCMD-1 localizes weakly to the PCM and strongly to centrioles. PCMD-1 does not require the PCM scaffold protein SPD-5 for its localization in one-cell embryos (Erpf et al., 2019). This raises the questions of whether PCMD-1 is recruited to the centrosome via outer centriolar proteins and whether PCMD-1, in turn, has a role in maintaining these proteins at centrioles. One candidate for such interaction is SAS-7, which is needed for the formation of paddlewheels, the outermost centriolar structures known in *C. elegans* (Sugioka et al., 2017). We investigated the spatial relationship between PCMD-1 and SAS-7 by analyzing embryos expressing endogenously tagged GFP::PCMD-1 and RFP::SAS-7 using lattice structured illumination microscopy (SIM) (Fig. 1A). We found that PCMD-1 and SAS-7 signals largely overlapped on both centrioles at spindle poles of mitotic blastomeres in early embryos (Fig. 1A). This observation prompted us to test whether SAS-7 and PCMD-1 localization are interdependent. Live-cell

[1]Department Biology II, Ludwig-Maximilians-University, Munich, 82152 Planegg-Martinsried, Germany. [2]Department Biologie, Friedrich-Alexander-Universität Erlangen-Nürnberg, 91058 Erlangen, Germany.

*Author for correspondence (tmdvali@bio.lmu.de)

E.Z., 0000-0003-1450-8684; T.M., 0000-0002-9449-3218

Handling Editor: Swathi Arur
Received 10 November 2020; Accepted 15 September 2021

Development (2021) 148, dev198416. doi:10.1242/dev.198416

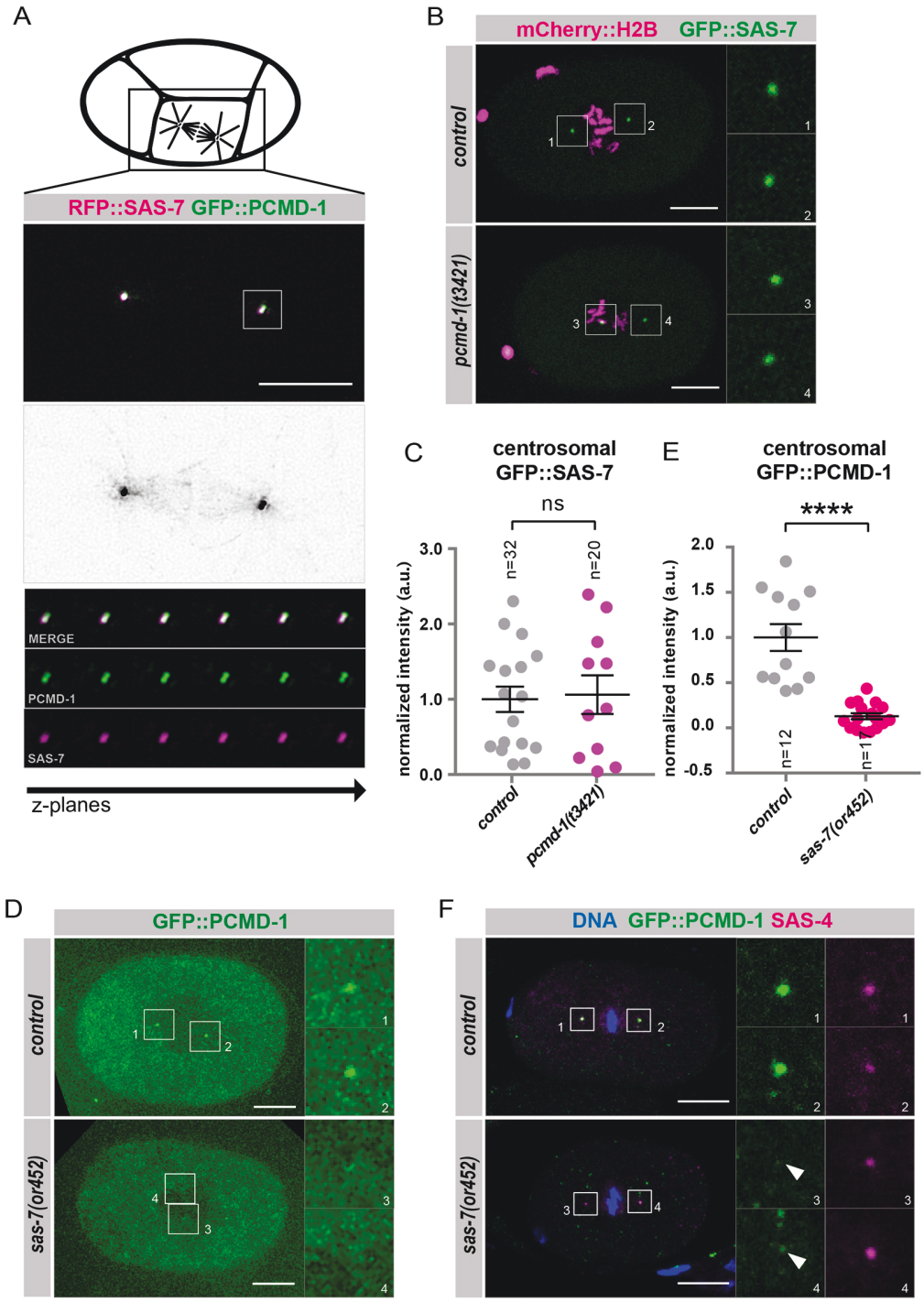

Fig. 1. SAS-7 recruits PCMD-1 to the centrioles. (A) Mitotic centrosomes of the EMS cell of a 4-cell embryo (schematic) expressing GFP::PCMD-1 and RFP::SAS-7 (*n*=6 centrosomes). Note that some GFP signals decorated astral and kinetochore microtubules of the mitotic spindle (middle panels). Lower panels represent a montage of different *z*-planes spanning a centriole pair. (B) Stills of time-lapse spinning disk confocal images of *mCherry::h2b;gfp::sas-7* (*n*=16) and *pcmd-1(t3421);mCherry::h2b;gfp::sas-7* (*n*=10) embryos during nuclear envelope break-down (NEB). Insets show centrosomes. (C) Normalized centrosomal GFP::SAS-7 signal intensities in control and *pcmd-1(t3421)* mutant embryos at NEB. Two-sample *t*-test, *n*=number of analyzed centrosomes. (D) Stills of time-lapse spinning disk confocal images of *gfp::pcmd-1* (*n*=6) and *gfp::pcmd-1;sas-7(or452)* (*n*=10) embryos during pronuclear meeting. Centrosomal areas are shown enlarged for the GFP::PCMD-1 signal. (E) Normalized centrosomal GFP::PCMD-1 signal intensities in control and *sas-7(or452)* embryos at NEB. Two-sample *t*-test, *n*=number of analyzed centrosomes. (F) Representative confocal images of fixed *gfp::pcmd-1* (*n*=8) and *gfp::pcmd-1;sas-7(or452)* (*n*=11) one-cell embryos in prometaphase stained for DNA, GFP and SAS-4. Insets represent single channels of the centrioles. Arrowheads indicate the GFP::PCMD-1 signal. Error bars denote s.e.m. ****P<0.0001; ns, not significant (P>0.05). a.u., arbitrary units. Scale bars: 10 µm.

Development (2021) 148, dev198416. doi:10.1242/dev.198416

imaging of GFP::SAS-7 in *pcmd-1(t3421)* mutant embryos revealed that GFP::SAS-7 levels at centrioles are comparable to that of control embryos (Fig. 1B,C). We concluded that PCMD-1 is not involved in the recruitment of SAS-7 to the centrioles. To test inversely whether SAS-7 is required for PCMD-1 recruitment to the centrosome, we crossed an in-locus-tagged *gfp::pcmd-1* with *sas-7(or452)* mutant animals. Whereas GFP::PCMD-1 at the centrosome was apparent in all control embryos, the centrosomal GFP::PCMD-1 signal was significantly reduced in *sas-7(or452)* one-cell embryos (Fig. 1D,E). Interestingly, a GFP::PCMD-1 signal was consistently detected at sperm-derived *sas-7(or452)* centrioles during pronuclear migration (Fig. S1A). Shortly thereafter, this signal decreased close to the detection limit (Fig. 1E, Fig. S1A). As an alternative means to address the SAS-7-dependent localization of PCMD-1, we performed immunostaining using antibodies against GFP and SAS-4 to mark the centrioles. In one-cell control embryos, all centrosomal SAS-4 foci colocalized with a clear GFP::PCMD-1 signal (Fig. 1F). In contrast, only a very weak GFP::PCMD-1 signal was observed at SAS-4 foci in *sas-7(or452)* embryos (Fig. 1F), probably reflecting the hypomorphic nature of the *sas-7(or452)* allele (Sugioka et al., 2017). Note that centrosomal GFP::PCMD-1 signal was detectable in *sas-7(or452)* multicellular embryos (Fig. S1B). In these late embryos, PCMD-1 could be recruited through a SAS-7-independent mechanism, as is the case at the ciliary base (Garbrecht et al., 2021; Magescas et al., 2021). Thus, SAS-7 is necessary to maintain PCMD-1 at the centrosome during the first cell division.

PCMD-1 bridges centriolar and PCM scaffold proteins

The genetic dependency of PCMD-1 centrosomal localization on SAS-7 raises the possibility that PCMD-1 is recruited to the centriole by direct interaction with SAS-7. To determine whether PCMD-1 and SAS-7 interact with each other and with other centrosomal proteins such as SAS-4, SPD-2, SPD-5 and PLK-1, we performed a candidate-based yeast two-hybrid screen (Fields and Song, 1989). We generated bait plasmids containing the cDNAs of SAS-7 and PCMD-1 and prey plasmids for the candidate proteins SAS-4, SAS-7, PCMD-1, SPD-2, SPD-5 and PLK-1. The readouts of positive interactions were growth and the expression of a GFP reporter. We categorized proteins showing both readouts on day 3 as strong interactors and on day 5 as weak interactors.

Previous yeast two-hybrid screens identified SAS-7 as a binding partner of SPD-2 (Sugioka et al., 2017; Boxem et al., 2008; Li et al., 2004) and SAS-4 (Boxem et al., 2008). We used these interactions to validate our yeast two-hybrid assay. As previously reported, we found that SAS-7 interacts with SPD-2 and SAS-4 (Fig. 2A,B). However, we could not detect an interaction between SAS-7 and PCMD-1 using either protein as bait or prey. Therefore, we tested whether PCMD-1 could interact with the centriolar proteins SAS-4 or SPD-2. We observed strong interaction of PCMD-1 with SAS-4 but not with SPD-2. Next, we tested whether PCMD-1 could bind to the PCM scaffold protein SPD-5, the kinase PLK-1 or itself. We detected strong interaction of PCMD-1 with itself and a weaker interaction with SPD-5 and PLK-1. In turn, SAS-7 did not interact with SPD-5 or with PLK-1 (Fig. 2A,B).

To confirm the interactions between the PCMD-1 bait and SAS-4, PLK-1 and SPD-5 preys, we reversed bait and prey. Again, we observed that PLK-1 and SAS-4 interacted with PCMD-1 (Fig. 2C). Because SPD-5 bait autoactivated, we turned to an alternative assay to confirm this interaction. We expressed *C. elegans* PCMD-1 tagged with EGFP (EGFP::PCMD-1) and SPD-5 tagged with mCherry and 6xHis (mCherry::SPD-5::6xHis) in human HEK293T cells and performed a co-immunoprecipitation. We successfully co-immunoprecipitated EGFP::PCMD-1 with SPD-5, confirming our yeast two-hybrid observation (Fig. 2D).

The yeast two-hybrid assay revealed no interaction of PCMD-1 with SAS-7 or SPD-2. However, both PCMD-1 and SAS-7 interact with SAS-4. Thus, rather than direct recruitment of PCMD-1 by SPD-2 or SAS-7, SAS-4 could theoretically act as a linker between PCMD-1 and SAS-7. However, in accordance with previous studies we found that in *sas-7(or452)* mutant embryos, where no PCMD-1 is found at the centrosome, SAS-4 foci are still present (Fig. 1F) (Sugioka et al., 2017). Therefore, it is highly unlikely that SAS-4 is accountable for the loss of PCMD-1 centrosomal localization in *sas-7(or452)* embryos.

In summary, PCMD-1 interacts with the centriolar protein SAS-4, the PCM protein SPD-5, the mitotic kinase PLK-1, and with itself. We propose that PCMD-1 acts as a functional bridge between the centrioles and the PCM scaffold.

PCMD-1 recruits SPD-5 and PLK-1 to an ectopic location

PCMD-1 is required to recruit SPD-5 to the centrosome (Erpf et al., 2019). This finding is strongly supported by our yeast-two hybrid interaction data, which indicates that PCMD-1 anchors the PCM scaffold to the centriole. Therefore, we investigated whether PCMD-1 is also able to recruit SPD-5 to an ectopic location. To address this, we established a 'translocation assay' by targeting PCMD-1 to an ectopic location in the cell and testing whether PCMD-1 is capable of recruiting SPD-5 to this cellular location. To tether PCMD-1 to the plasma membrane, we fused the mkate2::PCMD-1 reporter to the plcδ1PH-domain and expressed it under a heat-shock promoter. Upon heat shock, PH::mkate2::PCMD-1 was expressed and reliably translocated to the plasma membrane (Fig. 3A,B).

We tested whether membrane-bound PH::mkate2::PCMD-1 could recruit GFP::SPD-5 in the *pcmd-1(t3421)* mutant, which has a premature stop codon, and in the presence of wild-type PCMD-1. In *pcmd-1(t3421)* animals, recruitment of SPD-5 to the centrosome is compromised owing to the lack of endogenous PCMD-1 (Erpf et al., 2019). Therefore, more GFP::SPD-5 is expected in the cytoplasm. In control embryos without heat shock, GFP::SPD-5 was never detected at the plasma membrane. Induction of PH::mkate2::PCMD-1 by heat shock resulted in GFP::SPD-5 localization to the plasma membrane in 95.2% of the *pcmd-1(t3421)* and 68.4% of the wild-type embryos (Fig. 3B,C, Fig. S2A,B).

Because PLK-1 is also a PCM component and interacts with PCMD-1 in the yeast two-hybrid assay, we tested whether the in-locus-tagged PLK-1::sGFP translocates to the plasma membrane in a PCMD-1-dependent manner. Similar to GFP::SPD-5, PLK-1::sGFP localized to the plasma membrane in 41.4% of *pcmd-1(t3421)* and 26.3% of wild-type embryos after heat shock but did not localize to the membrane without heat shock (Fig. 3B,C, Fig. S2A, B). Note that the PLK-1::sGFP signal at the membrane was much weaker compared with the GFP::SPD-5 signal.

SPD-5 phosphorylation by PLK-1 is essential for PCM maturation (Woodruff et al., 2015). In the absence of PLK-1 phosphorylation at four specific residues, SPD-5 only forms a centrosome core but fails to assemble the mitotic scaffold. Therefore, we tested whether the translocation of SPD-5 to the membrane requires phosphorylation by PLK-1 at these residues. For this, we used a strain carrying RNAi-resistant GFP::SPD-5(4A), in which the four PLK-1 phosphorylation sites were substituted by alanine residues (Woodruff et al., 2015). To eliminate the endogenous SPD-5, embryos were treated with RNAi against *spd-5*. We found that GFP::SPD-5(4A) was still able to translocate

Development (2021) 148, dev198416. doi:10.1242/dev.198416

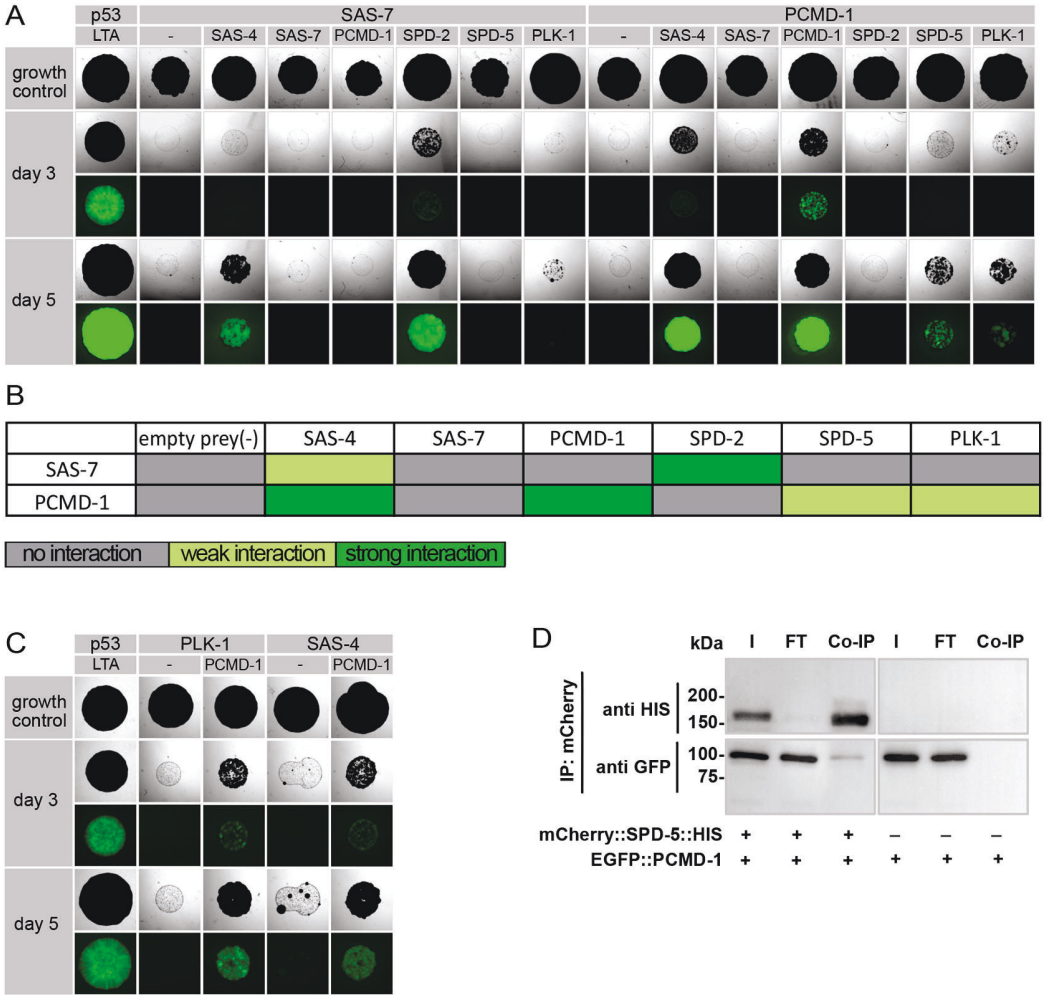

Fig. 2. PCMD-1 interacts with centriolar and PCM scaffold proteins. (A) Images of representative yeast two-hybrid colonies. Interaction of bait proteins SAS-7 and PCMD-1 with centrosomal proteins SAS-4, SAS-7, PCMD-1, SPD-2, SPD-5 and PLK-1 as preys, respectively. The top panel represents growth control, middle panels represent colonies screened on day 3 for growth on the selection medium and expression of the GFP-reporter, and the bottom panels represent colonies screened on day 5 for growth on the selection medium and expression of the GFP-reporter. (B) Summary of protein-protein interactions observed categorized by the strength of their interactions. (C) Images of representative yeast two-hybrid colonies. Interaction of bait proteins PLK-1 and SAS-4 with PCMD-1 prey. p53 with LTA was used as a positive control. (D) Co-immunoprecipitation of *C. elegans* EGFP::PCMD-1 and mCherry::SPD-5::6xHIS expressed in HEK293T cells using an RFP-trap. Co-IP, co-immunoprecipitation; FT, flow-through; I, input fraction.

efficiently to the membrane (96.8%; Fig. 3D,E), indicating that the membrane-bound GFP::SPD-5 pool does not resemble the mitotic PCM scaffold of SPD-5. Membrane translocation of PLK-1 could be mediated through SPD-5. To test this possibility, we performed the experiment in the *spd-5(RNAi)* background. PLK-1::sGFP recruitment still took place (45.9%; Fig. 3D,E). Thus, PCMD-1 can recruit PLK-1 independently of SPD-5.

Next, we tested whether PCMD-1 can also induce translocation of centriolar proteins. Interestingly, PH::mkate2::PCMD-1 was unable to translocate GFP::SAS-4, GFP::SAS-7 or GFP::PCMD-1 in any of the analyzed *pcmd-1(t3421)* embryos (Fig. 3B,C). This was unexpected, especially for SAS-4, because the interaction in the yeast two-hybrid assay was very strong. One explanation could be that a centriole tethering of SAS-4 prevents membrane translocation by PCMD-1. To test this hypothesis, we used a GFP::SAS-4 construct that lacks the conserved T complex protein 10 (TCP) domain, needed for its binding to SAS-5 (Cottee et al., 2013). When endogenous SAS-4 is eliminated by RNAi, the RNAi resistant GFP::SAS-4(ΔTCP) protein is not tethered to the centrioles but still localizes to the PCM (Cottee et al., 2013) (Fig. S2C). In the translocation assay, PCMD-1 was unable to recruit GFP::SAS-4(ΔTCP) to the membrane (Fig. S2C,D), raising the possibility that the interaction between SAS-4 and PCMD-1 is not through the PCM pool and may require the local environment at the centrioles. Therefore, the ability of PCMD-1 to ectopically anchor proteins to the plasma membrane is specific to the PCM scaffold proteins SPD-5 and PLK-1. Alternatively, the deletion of the TCP domain could compromise the interaction between SAS-4 and PCMD-1.

PCMD-1 is recruited to the centrioles prior to SPD-5

Our findings suggest that PCMD-1 could recruit the initial PCM core to the PCM-less sperm centrioles in the *C. elegans* one-cell embryo. Therefore, we investigated whether PCMD-1 is loaded onto the sperm centrosomes before SPD-5. In the *C. elegans* zygote, SPD-5 is recruited to the sperm-derived centrioles after the completion of meiosis II of the female pronucleus and concomitant with the ability of the centrosome to nucleate microtubules (McNally et al., 2012). This paradigm allows us to

Development (2021) 148, dev198416. doi:10.1242/dev.198416

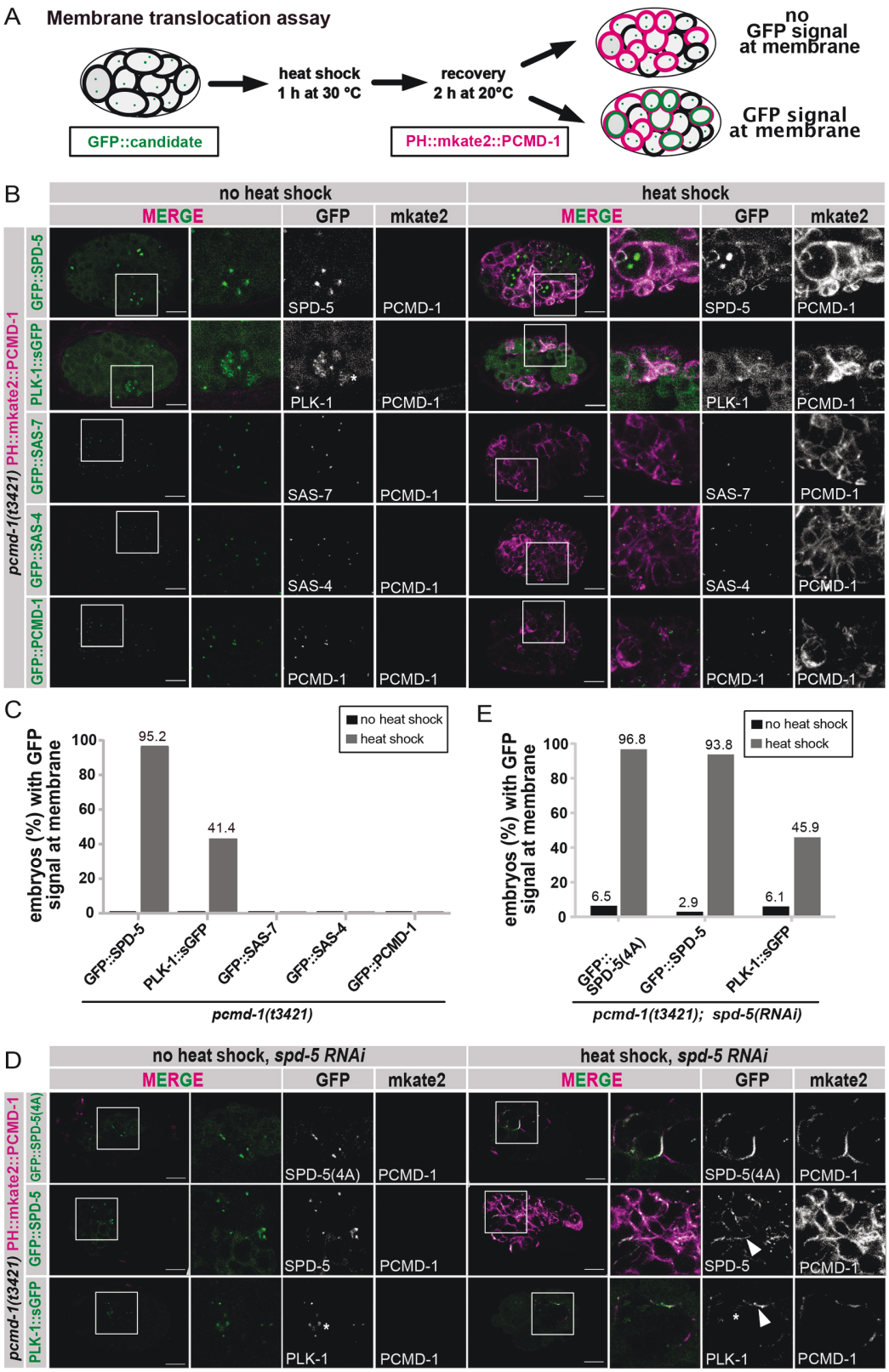

Fig. 3. See next page for legend.

investigate whether PCMD-1 is loaded to the centrioles prior to SPD-5 recruitment using marked mating experiments in which only the sperm or the oocyte expresses a fluorescent marker. First, we tested whether paternal GFP::PCMD-1 could be detected at the centrosome after fertilization. For this, we mated *fog-2(q71)* females lacking sperms with GFP::PCMD-1-expressing males, thus labeling

Development (2021) 148, dev198416. doi:10.1242/dev.198416

Fig. 3. PCMD-1 targets SPD-5 and PLK-1 to the plasma membrane. (A) Schematic of the 'translocation assay'. After 1 h heat shock to induce expression and 2 h recovery, PH::mkate2::PCMD-1 is expressed and binds to the plasma membrane of a multicellular embryo. If PH::mkate2::PCMD-1 recruits GFP-tagged candidate proteins, they will also localize to the plasma membrane (bottom embryo). If PH::mkate2::PCMD-1 is not able to recruit, the localization of the GFP-tagged candidate proteins will not change upon PH::mkate2::PCMD-1 expression (top embryo). (B) Representative multicellular embryos of the 'translocation assay' for GFP::SPD-5 (*n*=17 no heat shock; *n*=21 heat shock), PLK-1::sGFP (*n*=21 no heat shock; *n*=29 heat shock), GFP::SAS-7 (*n*=20 no heat shock; *n*=23 heat shock), GFP::SAS-4 (*n*=28 no heat shock; *n*=28 heat shock) and GFP::PCMD-1 (*n*=25 no heat shock; *n*=27 heat shock) fusion proteins in the *pcmd-1(t3421)* background with and without heat shock. Selected regions (boxed) are enlarged and shown as merge and single channels. Note that PLK-1::sGFP signal at the plasma membrane is less intense than GFP::SPD-5. Scale bars: 10 µm. (C) Quantification of B showing the percentage of embryos with GFP signal at the membrane after heat shock in the *pcmd-1(t3421)* background. (D) Representative multicellular embryos of the 'translocation assay' using GFP::SPD-5 (*n*=31 no heat shock; *n*=31 heat shock), GFP::SPD-5(4A) (*n*=34 no heat shock; *n*=32 heat shock) and PLK-1::sGFP (*n*=33 no heat shock; *n*=37 heat shock) in a *pcmd-1(t3421);spd-5(RNAi)* background. Selected regions (boxed) are enlarged and shown as merge and single channels. Arrowheads indicate the membrane-localized GFP signal. Asterisks indicate kinetochore localization of PLK-1::sGFP. Scale bars: 10 µm. (E) Quantification of D showing the percentage of embryos with GFP signal at the membrane after heat shock in the *pcmd-1(t3421); spd-5(RNAi)* background.

sperm centrioles (Fig. S3A) (Erpf et al., 2019). We could not detect GFP::PCMD-1 at centrioles in any of the analyzed embryos after the completion of meiosis II. Second, we mated GFP::PCMD-1 females, treated with *fem-1(RNAi)* to block sperm production, with control *fog-2(n71)* males with unlabeled sperm centrioles. We found that the GFP::PCMD-1 signal was detected at the centrosomes in all analyzed embryos during the first mitotic division (Fig. S3C). These results suggest that sperm-derived PCMD-1 is not maintained and that the maternal PCMD-1 is recruited to the centrioles after fertilization.

To determine exactly when maternal PCMD-1 is recruited to the centriole after fertilization and to temporally map its loading with respect to SPD-5, we immunostained embryos from GFP::PCMD-1 females mated with males with unlabeled sperm centrioles (Fig. S3C,D), using antibodies against SPD-5 and GFP. In meiosis I embryos, neither GFP::PCMD-1 nor SPD-5 foci were present at the centrioles (Fig. S3E), indicating that maternal GFP::PCMD-1 was not yet incorporated in the centrioles. During meiosis II, we found that a GFP::PCMD-1 focus, without any detectable SPD-5, was visible at 90.5% of sperm centrioles (Fig. S3D,E). In the remaining 9.5% of embryos, categorized as early meiosis II, neither GFP::PCMD-1 nor SPD-5 foci were present (Fig. S3D). Therefore, we conclude that maternal GFP::PCMD-1 is recruited to the sperm centrioles at meiosis II. After meiosis II, when sperm pronuclei are decondensed, SPD-5 colocalized with GFP::PCMD-1 at the centrosomes in 87% of the embryos (Fig. S3D,E). We never observed embryos with centrosomes only labeled by SPD-5.

In summary, our results are consistent with a model in which maternal GFP::PCMD-1 is recruited to the sperm-derived centrioles shortly after fertilization and subsequently recruits SPD-5 and PLK-1 to form the centrosome core. These findings strengthen the hypothesis that PCMD-1 bridges centriolar and PCM proteins.

The coiled-coil domain promotes PCMD-1 loading to the centrosome and self-interaction

To determine how PCMD-1 is anchored to the centrosome, we next examined which part of the protein is necessary for its centrosomal targeting. PCMD-1 is predicted to have a single coiled-coil domain and six intrinsically disordered regions (IDRs 1-6), which partially overlap with low complexity regions (Fig. 4A) (UniProt Consortium, 2019; Schultz et al., 2000; Letunic and Bork, 2018). Coiled-coil domains often mediate protein-protein interactions, including oligomerization, and these interactions can have regulatory functions for centrosomal proteins (Leidel et al., 2005; Kitagawa et al., 2011; Qiao et al., 2012; Hilbert et al., 2013; Lettman et al., 2013; Rogala et al., 2015). Therefore, we set out to investigate the function of the coiled-coil domain in PCMD-1.

To examine the function of the coiled-coil domain, we deleted the sequence from E86 up to and including F118, predicted as the coiled-coil domain by the COILS program (Lupas et al., 1991; Lupas, 1996), using CRISPR/Cas9 in the in-locus-tagged GFP::PCMD-1 protein. We refer to this deletion as *gfp::pcmd-1(ΔCC)* (Fig. 4A). In a lethality test, 97.5% of the *gfp::pcmd-1* embryos and 87.6% of the *gfp::pcmd-1(ΔCC)* embryos survived at 25°C (Fig. 4B). Thus, the deletion of the predicted coiled-coil domain compromised viability.

Next, we investigated whether the GFP::PCMD-1(ΔCC) protein could localize to the centrosome. We performed live-cell imaging on worms expressing GFP::PCMD-1 and GFP::PCMD-1(ΔCC). Whereas GFP::PCMD-1 efficiently localized to the centrosomes in all analyzed embryos, the GFP::PCMD-1(ΔCC) signal on average appeared much weaker (Fig. 4C, Movies 1 and 2). Measuring the mean centrosomal GFP signal intensity confirmed that PCMD-1 without the coiled-coil domain was significantly reduced at the centrosomes in comparison with wild-type PCMD-1, whereas cytoplasmic levels remained unchanged (Fig. 4D,E). Thus, the coiled-coil domain is necessary for efficient centrosomal loading of PCMD-1 but is not essential for the viability of the embryos. Given that coiled-coil domains are often implicated in the oligomerization of centrosomal proteins, we asked whether PCMD-1 self-interaction was compromised in the absence of the coiled-coil domain. To this end, we expressed PCMD-1(ΔCC) as a bait plasmid and probed its interaction with the PCMD-1(ΔCC) prey (Fig. 4F). In the absence of the coiled-coil domain, PCMD-1 self-interaction was lost (Fig. 4F).

This raises the question of how embryos with reduced centrosomal PCMD-1 levels can divide. To investigate whether these animals could still recruit the PCM scaffold, we immunostained GFP::PCMD-1(ΔCC) embryos using antibodies against GFP and SPD-5 and performed live-cell imaging of RFP::SPD-5. We found that SPD-5 was still recruited to the centrosome in all analyzed embryos, even in embryos in which GFP::PCMD-1(ΔCC) was almost undetectable (Fig. 4G, Fig. S4A). Although overall centrosomal RFP::SPD-5 levels remained similar to the control embryos in the absence of the coiled-coil domain (Fig. S4A,B), the SPD-5 centrosome matrix appeared to be much more dispersed and disorganized (Fig. 4G). To quantify the degree of disorganization, we measured centrosome circularity using immunofluorescence staining and found that mean centrosome circularity values were significantly lower in *gfp::pcmd-1(ΔCC)* embryos (Fig. 4H).

We propose that the coiled-coil domain facilitates PCMD-1 self-interaction and thereby promotes efficient PCMD-1 accumulation at the centrosome and the maintenance of PCM scaffold integrity.

Regions in the C-terminal part of PCMD-1 target the protein to the centrosome and cilia

The fact that GFP::PCMD-1(ΔCC) could still be recruited to the centrosome indicates that protein regions other than the coiled-coil

Development (2021) 148, dev198416. doi:10.1242/dev.198416

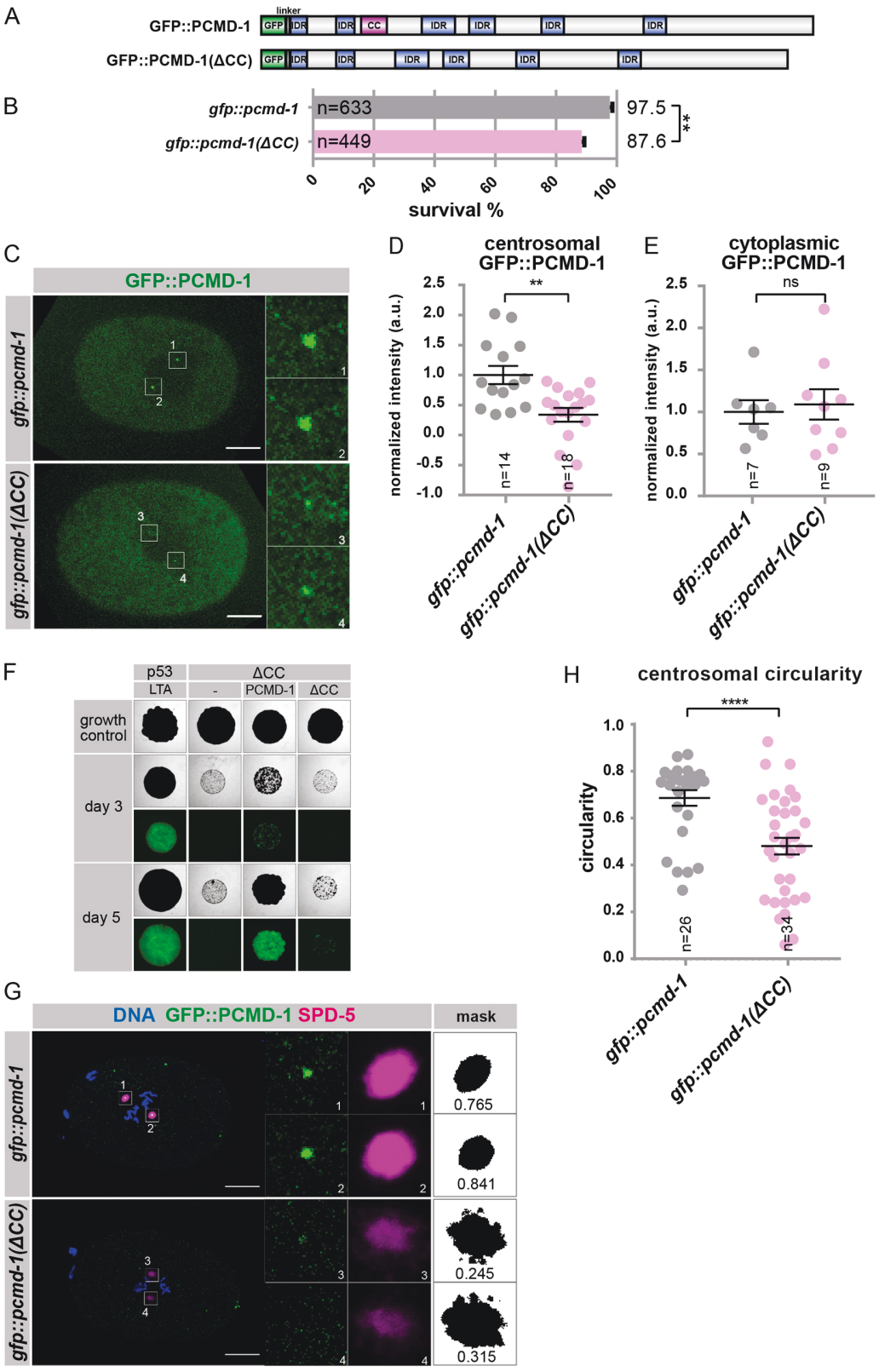

Fig. 4. See next page for legend.

domain might play a role in centrosomal anchoring. To map which part of the protein is involved, we used a previously established single-copy replacement system (Erpf et al., 2019). *pcmd-1(t3421)* mutant animals carry a stop codon before the coiled-coil domain and are lethal at 25°C (Fig. S5A). Reconstituting a single copy of the PCMD-1 cDNA under the regulatory elements of the *mai-2* gene

Development (2021) 148, dev198416. doi:10.1242/dev.198416

Fig. 4. The coiled-coil domain promotes PCMD-1 accumulation at the centrosome and PCM scaffold integrity. (A) Top: Schematic of the domain structure of endogenously tagged GFP::PCMD-1 protein (aa 2-630), with predictions of the coiled-coil domain (CC) and six IDRs. Bottom: Schematic of the domain structure of a truncated version, with the deleted coiled-coil domain (Δ86-117). All domains except GFP are represented on a relative scale. (B) Survival of *gfp::pcmd-1* and *gfp::pcmd-1(ΔCC)* animals at 25°C. *P*-values were calculated by Mann–Whitney *U*-Test, *n*=number of analyzed embryos. (C) Stills of time-lapse imaging of *gfp::pcmd-1* (*n*=7) and *gfp::pcmd-1(ΔCC)* (*n*=9) embryos at NEB. Centrosomal areas were determined by DIC imaging and are shown enlarged for the GFP::PCMD-1 signal. See Movies 1 and 2. (D) Normalized centrosomal GFP signal intensities in embryos expressing *gfp::pcmd-1* and *gfp::pcmd-1(ΔCC)* at NEB. *P*-values were calculated by Mann–Whitney *U*-test. *n*=number of analyzed centrosomes. (E) Normalized cytoplasmic GFP signal intensities in embryos expressing *gfp::pcmd-1* and *gfp::pcmd-1(ΔCC)* at NEB. *P*-values were calculated by two-sample *t*-test. *n*=number of analyzed embryos. (F) Images of representative yeast two-hybrid colonies. Interaction of bait proteins PCMD-1(ΔCC) with PCMD-1 and PCMD-1(ΔCC) as preys. p53 with LTA was used as a positive control. (G) Representative images of fixed embryos of the indicated genotype stained for DNA, GFP and SPD-5. Centrosomes are enlarged in individual channels and the corresponding masks of the SPD-5 signal. Values of centrosomal circularity are indicated. (H) Quantification of SPD-5 circularity in *gfp::pcmd-1* and *gfp::pcmd-1(ΔCC)* embryos. *P*-values were calculated by Mann–Whitney *U*-Test, *n*=number of analyzed centrosomes. Error bars denote s.e.m. ***P*<0.01, *****P*<0.0001; ns, not significant (*P*>0.05). a.u., arbitrary units. Scale bars: 10 µm.

rescues survival rates to 96.2% (Fig. S5A). We used this assay to test the functionality and localization of different truncations of the PCMD-1 protein. GFP::PCMD-1(N) spans the region E2-N117, including the first two IDRs and the coiled-coil domain. GFP::PCMD-1(C) comprises amino acids F118 to the stop codon, spanning the remaining IDRs (Fig. 5A). In the survival assay, GFP::PCMD-1(C) could rescue the lethality of *pcmd-1(t3421)* to 90.8% survival, whereas GFP::PCMD-1(N) was not sufficient to rescue viability (0.3%) (Fig. S5A). Interestingly, GFP::PCMD-1(N) even had a dominant-negative effect on the viability of *pcmd-1(t3421)* at the permissive temperature of 15°C, reducing it from 41% to 28% (Fig. S5B).

Next, we assessed the ability of these constructs to localize to the centrosome by live-cell imaging. Centrosomal GFP signal was detected in all GFP::PCMD-1(C) embryos, albeit with slightly reduced GFP signal intensities compared with control animals (Fig. 5B,C). In contrast, we could not detect any GFP signal at the centrosome in embryos expressing the GFP::PCMD-1(N) constructs, even though the cytoplasmic levels were much higher (Fig. 5B, Fig. S5C). Therefore, the C-terminal part of PCMD-1, excluding the coiled-coil domain and IDR1 and IDR2, is sufficient for PCMD-1 anchoring to the centrosome.

To further map the part of PCMD-1 that targets the protein to the centrosome, we subdivided the C-terminal part into two fragments spanning F118-D342 (C1) and G343-stop codon (C2) (Fig. 5A). In the survival assay, neither GFP::PCMD-1(C1) nor GFP::PCMD-1(C2) rescued the lethality of *pcmd-1(t3421)* (Fig. S5A). However, GFP::PCMD-1(C2) still localized to the centrosome, whereas GFP::PCMD-1(C1) did not (Fig. 5B,C). This raises the possibility that the C2 part of the PCMD-1 could be interacting with SAS-4. Therefore, we expressed the PCMD-1(C2) as a bait together with SAS-4 as a prey in the yeast two-hybrid assay (Fig. 5D). The PCMD-1(C2) bait strongly interacted with the SAS-4 prey. A similarly strong interaction was detected between the SAS-4 bait and the PCMD-1(C2) prey (Fig. 5D).

Similar to the centrosomes in the embryo, only GFP::PCMD-1, GFP::PCMD-1(C) and GFP::PCMD-1(C2) localized to the ciliary base of adult animals (Fig. S6). In particular, signals from GFP::PCMD-1(C) and GFP::PCMD-1(C2) appeared stronger than the control, extending along the cilia (Fig. S6).

In *pcmd-1(t3421)* mutant animals, SPD-5 recruitment to the centrosome is severely compromised (Erpf et al., 2019). Therefore, we tested whether the truncated parts of PCMD-1 that localize to the centrosome can restore SPD-5 recruitment. In animals expressing GFP::PCMD-1(C), levels of RFP::SPD-5 at metaphase were similar to those in animals carrying the full-length GFP::PCMD-1. However, in GFP::PCMD-1(C2)-expressing animals, RFP::SPD-5 levels were largely reduced (Fig. S5C,D). Thus, the C2 part of PCMD-1, including IDR6, is sufficient to target PCMD-1 to the centrosome but is insufficient to recruit the PCM scaffold composed of SPD-5.

The fact that PCMD-1(C2) strongly localizes to the centrosome prompted us to test a construct that lacks the C2 part (GFP::PCMD-1(ΔC2) E2-D342). Surprisingly, GFP::PCMD-1(ΔC2) could still localize to the centrosome, although the centrosomal levels were reduced by 60% in comparison with the full-length construct (Fig. 5B,C). However, GFP::PCMD-1(ΔC2) fully rescued the viability of *pcmd-1(t3421)* and recruited RFP::SPD-5 to the centrosome (Fig. S5A,D,E).

Intriguingly, we could not detect GFP::PCMD-1(ΔC2) at the cilia, indicating that the C2 part is absolutely essential for ciliary base targeting (Fig. S6). Given that the C2 part contains IDR6, we generated a worm strain that expresses GFP::PCMD-1(ΔC2.2) E2-G514, a construct in which IDR6 is included. Centrosomal GFP::PCMD-1(ΔC2.2) levels were comparable to GFP::PCMD-1(ΔC2); however, the ciliary targeting was restored (Fig. S6).

In summary, multiple parts of PCMD-1 contribute to the centrosomal localization of PCMD-1. The PCMD-1(C2) region can bind SAS-4 and is sufficient for anchoring to the centrosome. The N-terminal construct lacking C2 can still localize to the centrosome, suggesting the presence of a second centrosome targeting region. The centrosomal PCMD-1(C2) is insufficient to recruit SPD-5 and for embryonic development. By contrast, the N-terminal construct lacking the C2 localizes to the centrosome at largely reduced levels and can restore centrosomal SPD-5 levels and function. The C2 part, and specifically the amino acids between D342 and G514 encompassing IDR6, are necessary for cilia localization.

DISCUSSION

In this study, we examine the mechanism by which PCMD-1 anchors the PCM scaffold to the centriole. We demonstrate that PCMD-1 interacts with the PCM scaffold protein SPD-5, the mitotic kinase PKL-1 and the centriolar protein SAS-4. Furthermore, tethering PCMD-1 at an ectopic cellular location is sufficient to recruit SPD-5 and PKL-1. In turn, the centrosomal localization of PCMD-1 depends on the outer centriolar protein SAS-7. Together with previous findings that PCMD-1 is required for SPD-5 recruitment to the PCM core in the one-cell embryo, these findings place the function of PCMD-1 between the centrioles and the PCM.

Our analysis revealed that PCMD-1 interacts with SPD-5. A similar protein-protein interaction has been established for pericentrin/Plp, the putative homolog of PCMD-1, and CDK5RAP2/Cnn the functional homolog of SPD-5 in vertebrates and *Drosophila*, respectively (Buchman et al., 2010; Lerit et al., 2015; Galletta et al., 2016). This interaction is especially important in *C. elegans* for the initial formation of the PCM core in the one-cell embryo. Paternally contributed centrioles in the one-cell embryo are deficient of the PCM core. SPD-5, which renders the

Development (2021) 148, dev198416. doi:10.1242/dev.198416

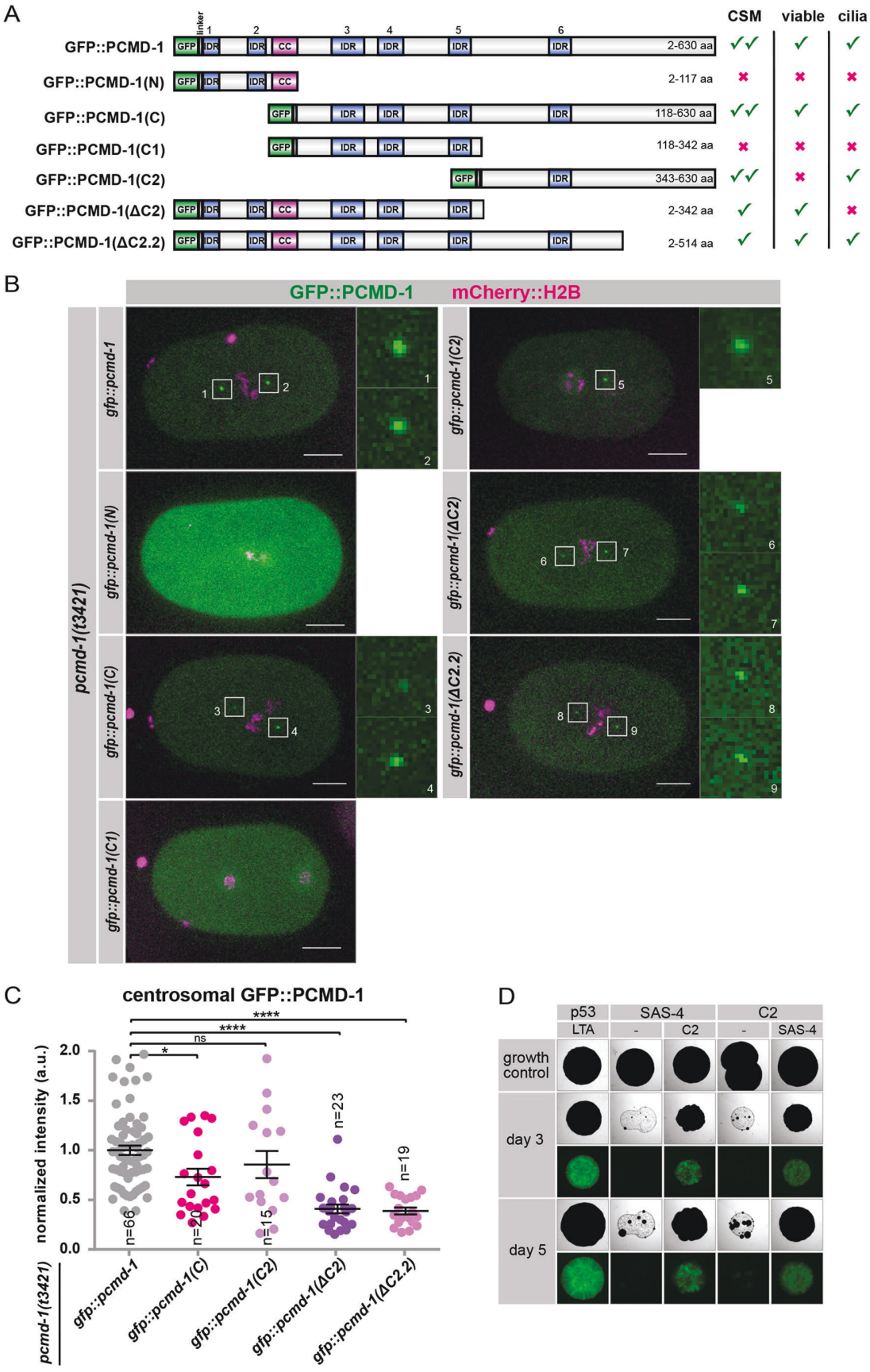

Fig. 5. See next page for legend.

Development (2021) 148, dev198416. doi:10.1242/dev.198416

Fig. 5. The C-terminal region targets PCMD-1 to the centrosome and binds SAS-4. (A) Domain structure of different GFP-tagged PCMD-1 constructs. All domains except GFP are represented to a relative scale. All constructs are expressed under the regulatory elements of the *mai-2* gene. Summary of localization and viability. CC, coiled-coil domain; CSM, centrosome. (B) Stills of time-lapse imaging of embryos expressing *gfp::pcmd-1* (*n*=12), *gfp::pcmd-1(N)* (*n*=7), *gfp::pcmd-1(C)* (*n*=10), *gfp::pcmd-1(C1)* (*n*=8), *gfp::pcmd-1(C2)* (*n*=9), *gfp::pcmd-1(ΔC2)* (*n*=12) and *gfp::pcmd-1(ΔC2.2)* (*n*=10) in combination with the *mCherry::h2b* in the *pcmd-1(t3421)* background at NEB. Enlarged are the two centrosomes. *n*=number of embryos. (C) Normalized centrosomal GFP signal intensities of embryos represented in B. *P*-values were determined for multiple comparisons with Kruskal–Wallis test and post-hoc Dunn's test adjusted with Holm correction; *n*=number of analyzed centrosomes. (D) Images of representative yeast two-hybrid colonies. Interaction of bait proteins SAS-4 and PCMD-1(C2) with SAS-4 and PCMD-1(C2) as preys. Error bars denote s.e.m. **P*<0.05, *****P*<0.0001; ns, not significant (*P*>0.05). a.u., arbitrary units. Scale bars: 10 µm.

centrioles' microtubule-organizing activity, is recruited from the maternal pool after female meiosis (McNally et al., 2012). Our findings that PCMD-1 is associated with centrioles prior to SPD-5 recruitment and that tethering of PCMD-1 at the plasma membrane is sufficient to recruit SPD-5 suggest that PCMD-1 is needed for SPD-5 accumulation and the formation of the PCM core after fertilization. In the translocation assay, PCMD-1 was consistently more effective at recruiting SPD-5 and PLK-1 to the plasma membrane in the absence of an endogenous PCMD-1. In the *pcmd-1(t3421)* mutant background, SPD-5 and PLK-1 are not efficiently recruited to the centrosome and are expected to be more abundant in the cytoplasm. This finding suggests a 'tug-of-war' between the centrosomal and membrane-bound PCMD-1 pools for the recruitment of SPD-5 and PLK-1. Membrane-bound PCMD-1 can also efficiently recruit a phospho-deficient version of SPD-5 in which the four residues that are phosphorylated by PLK-1 and that play a key role in the expansion and maturation of the mitotic PCM scaffold are mutated (Woodruff et al., 2015). Therefore, we speculate that PLK-1 phosphorylation of these residues is not required for PCMD-1 to recruit SPD-5 and that the membrane-targeted SPD-5 is analogous to the PCM core. The fact that PLK-1 can be translocated to the membrane in the absence of SPD-5 confirms our previous findings that PCMD-1 contributes to the formation of the PLK-1 pool at the centrosome independently of SPD-5 (Erpf et al., 2019). By bringing together PLK-1 and SPD-5, PCMD-1 facilitates the initiation of the centrosome maturation process.

In contrast to the PCM proteins, PCMD-1 was unable to relocate itself and the centriolar proteins SAS-4 and SAS-7 to the plasma membrane. This is consistent with observations that the centriolar localization of both SAS-4 and SAS-7 is independent of PCMD-1 (this study; Erpf et al., 2019). At the same time, this is puzzling especially in the case of PCMD-1 and SAS-4, for which we found a strong protein-protein interaction in the yeast two-hybrid system. Assays such as the yeast two-hybrid system do not indicate exactly where and when these interactions occur. In the case of PCMD-1, this could be due to a stronger binding of PCMD-1 to other centrosomal proteins, which prevent delocalization.

The fact that PCMD-1 could not recruit SAS-4(ΔTCP) raises the possibility that the PCMD-1/SAS-4 interaction may need a specific local environment or modification, which is provided at the centrioles but is absent at the cytoplasmic pool of the proteins. As the TCP domain of SAS-4 associates with SAS-5 and the centrioles, SAS-4(ΔTCP) only represents the PCM fraction of SAS-4 (Cottee et al., 2013). Even though we cannot exclude the formal possibility that the deletion of the TCP domain additionally disrupts the interaction with PCMD-1, we consider it highly unlikely. We favor the possibility that either another protein bridges SAS-4 and PCMD-1 or that the proteins are post-translationally modified in the yeast two-hybrid system and at the centrosome, but not on the plasma membrane.

The outer centriolar protein SAS-7 is genetically upstream and required for PCMD-1 centrosomal recruitment in the one-cell embryo. This interaction could be direct or mediated through the known SAS-7 binding partners SPD-2 and SAS-4 (Sugioka et al., 2017). It has been shown previously that SAS-7 recruits SPD-2 to the centrosome, and that SAS-7 and PCMD-1 do not rely on a functional SPD-2 for their centrosomal localization (Sugioka et al., 2017; Erpf et al., 2019). In the yeast two-hybrid assay, PCMD-1 did not interact with SAS-7 or SPD-2. Thus, SPD-2 is an unlikely mediator of this interaction. As both PCMD-1 and SAS-7 interact with SAS-4 in the yeast two-hybrid assay, one could assume that the interaction is mediated through SAS-4. The absence of a fully formed daughter centriole in *sas-4(RNAi)* embryos does not allow us to make a conclusion about the requirement of SAS-4 for PCMD-1 localization. However, SAS-4 foci are still present in *sas-7(or452)* mutant embryos (Sugioka et al., 2017), in which little or no PCMD-1 is found at the centrosome. Although we cannot exclude the formal possibility that in *sas-7(or452)* mutant embryos SAS-4 changes its conformation or lacks a post-translational modification, which would hinder the interaction with PCMD-1, we do not favor a model in which SAS-4 is the only anchor for PCMD-1 on the centriole. We suggest that the interaction between SAS-7 and PCMD-1 is either indirect, through an unknown protein or an additional co-factor, or that a modification is required for interaction in the yeast two-hybrid and translocation assay. Structurally intact paddlewheels, which are altered in *sas-7(or452)* mutant animals, might be a prerequisite for PCMD-1 anchoring (Sugioka et al., 2017).

The presence of multiple IDRs in PCMD-1 suggests high conformational plasticity of the protein (Uversky, 2019). Our structure-function analysis revealed that multiple regions of PCMD-1 contribute to centrosomal targeting. The PCMD-1(C2) fragment, including IDR6, is sufficient for the centrosomal localization of PCMD-1. In the yeast two-hybrid assay, the same fragment strongly interacts with SAS-4, suggesting an interaction site with the centrioles (Fig. 6A). At the same time, centrosomal SPD-5 levels in the PCMD-1(C2) background are highly reduced and are comparable to the *pcmd-1(t3421)* mutants (Erpf et al., 2019). Thus, the PCMD-1(C2) fragment alone is insufficient to recruit SPD-5 and as a result does not support embryonic development. Therefore, we suggest that N-terminal parts of the protein are needed for SPD-5 recruitment and function (Fig. 6A). In accordance with this, constructs lacking the C-terminal region [PCMD-1(ΔC2) and PCMD-1(ΔC2.2)], which localize to the centrosome at much-reduced levels, are sufficient to accumulate SPD-5 and sustain viability.

The coiled-coil domain and IDR1 and IDR2 alone are insufficient for centrosomal targeting. Combination with the adjacent IDRs 3-5 restores localization and function. Therefore, the PCMD-1(C1) fragment reconstitutes major functional units. The dominant-negative effect on the viability of the coiled-coil domain and IDR1 and IDR2 could be explained by binding or sequestration of PCMD-1 interaction partners. In the context of the full-length protein, the coiled-coil domain significantly contributes to the accumulation of PCMD-1 at the centrosome and is required to form an organized PCM. The fact that the deletion of the coiled-coil

Development (2021) 148, dev198416. doi:10.1242/dev.198416

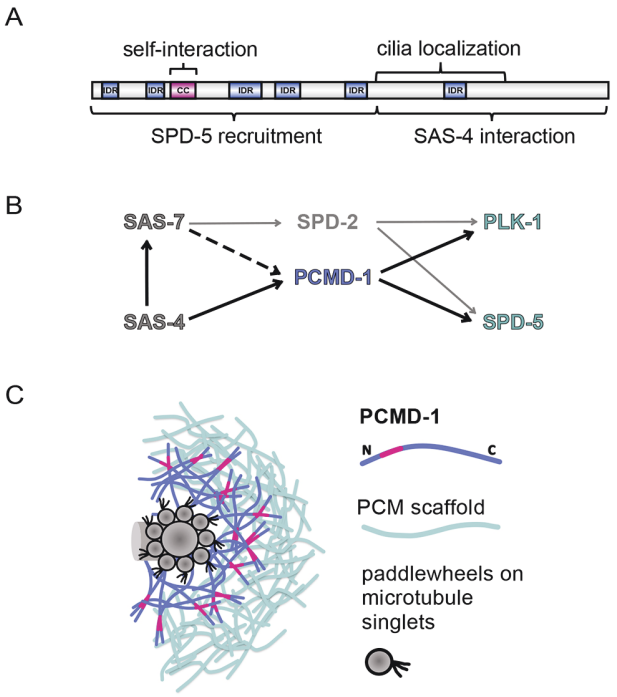

Fig. 6. Model of how PCMD-1 bridges the centrioles and PCM. (A) Structure of PCMD-1 with interaction sites indicated. CC, coiled-coil domain. (B) Genetic interactions of PCMD-1. PCMD-1 is genetically downstream of SAS-7 and SAS-4. SAS-7 itself interacts with SAS-4 and SPD-2. PCMD-1 acts genetically upstream of SPD-5 and PLK-1. Proteins other than PCMD-1, such as SPD-2, are involved in SPD-5 and PLK-1 recruitment to the centrosome. Interactions identified in this study are indicated by black arrows. Dashed arrow indicates genetic dependency. Gray arrow indicates interactions found in other studies. (C) Proposed model: PCMD-1 interacts with both centriolar and PCM proteins and thereby bridges the two centrosomal components. PCMD-1 is tethered to the centrioles through its C-terminal region, whereas the N-terminal region, including the coiled-coil domain (pink section), plays a role in PCMD-1 self-interaction and PCM formation.

domain only partially compromises viability is not surprising given that even the complete absence of an expanded SPD-5 scaffold at mitosis does not affect the viability (Woodruff et al., 2015). In animals with the deleted coiled-coil domain, SPD-5 levels are not altered, but the PCM appears more dispersed. This could be a direct effect of the coiled-coil domain on SPD-5 or an indirect effect as a result of the reduced PCMD-1 levels at the centrosome. In the yeast two-hybrid assay, we identified a strong self-interaction of PCMD-1, pointing to a tendency towards dimerization or formation of higher-order structures. Self-association is frequently found in centrosomal proteins. This has also been demonstrated for Plp in flies (Galletta et al., 2016). The self-interaction is abolished in the absence of the coiled-coil domains in both bait and prey but not when the coiled-coil domain is only deleted in the bait. This might indicate that PCMD-1/PCMD-1 self-interaction is mediated through binding of the coiled-coiled domain to a different part of the protein, rather than a dimerization of the coiled-coil domain. We speculate that the self-interaction of PCMD-1 plays a significant role in the PCM scaffold integrity. It would be interesting to investigate how exactly the physical properties of the mitotic PCM change in the absence of the coiled-coil domain of PCMD-1.

Recently it was shown that PCMD-1 and SPD-5 play an important role in the function of sensory cilia (Garbrecht et al., 2021; Magescas et al., 2021). After initial recruitment, PCMD-1 and SPD-5 maintain each other at the ciliary base through a positive-feedback loop (Garbrecht et al., 2021). Through our structure-function analysis, we could separate the cilia localization of PCMD-1 from the centrosome localization. A part of the C2 region, missing in PCMD-1(ΔC2) but present in PCMD-1(ΔC2.2) restores PCMD-1 at the ciliary base (Fig. S6). Interestingly, this region comprises the most C-terminal IDR (IDR6), suggesting a potential role in targeting the C2 construct to the cilia. Our observation that PCMD-1 localizes to astral and spindle microtubules (Fig. 1A), could indicate binding to microtubules or a microtubule-binding protein. The enhanced localization of the GFP::PCMD-1(C2) along the length of the cilium may reflect increased microtubule binding, which in the cilia is limited by the N-terminal region in the full-length PCMD-1.

Together we propose a model (Fig. 6B,C) in which PCMD-1 is recruited to the centriole via two anchor points: SAS-7, either directly or indirectly, and SAS-4. The C-terminal part, especially the C2 part of PCMD-1, is sufficient for its centrosomal recruitment and interacts with SAS-4. We speculate that SAS-4 acts in parallel to SAS-7 and that this interaction needs the local environment at the centrioles. Centrosomal PCMD-1 recruits SPD-5 through its N-terminal parts, including IDR3-5. By bringing together SPD-5 and PLK-1, PCMD-1 facilitates PCM core formation and PCM maturation. The coiled-coil domain enhances PCMD-1 centrosomal accumulation through its self-interaction and contributes to the stabilization of the mitotic PCM scaffold. Given that proteins other than PCMD-1, such as SPD-2, play a role in SPD-5 scaffold formation during mitosis, this model might be cell-cycle specific or needed for the initial recruitment of SPD-5 to the PCM core. In summary, we propose that PCMD-1 is one of the proteins that anchors the PCM to the centrioles and functionally bridges the two centrosomal components.

MATERIALS AND METHODS

C. elegans strains maintenance

Worms were maintained on NGM plates seeded with the OP50 *Escherichia coli* strain under standard conditions at 15°C (Brenner, 1974). All worm strains used in this work are listed in Table S1. Unless indicated otherwise, for experimental use, progeny of worms shifted to 25°C at the L4 stage for 16-20 h, were analyzed. *gfp::pcmd-1; sas-7(or452)/hT2* worms were allowed to lay eggs for 3 h at 25°C. The laid eggs developed into adults at 25°C for 68 h. Progeny of *gfp::pcmd-1;sas-7(or452)* worms were used for further analysis.

Worm strain generation

Worms carrying single-copy transgene insertions were generated by the Universal MosSCI system, according to previously published protocols (Frøkjær-Jensen et al., 2008). Transgenes with the pCFJ350 backbone were injected into EG6699 or EG8081 and the progeny were selected using selection markers. Insertions were verified by PCR. Multiple independent insertion lines were screened for expression of the transgenes.

The *pcmd-1(syb1285 syb486[gfp::pcmd-1(ΔCC)])I* allele was generated by SunyBiotech by deleting 33 amino acids from E86 including F118, spanning the coiled-coil domain ranging from amino acids E86 to N117, predicted by the COILS program (see below). The deletion was verified by PCR amplification using the oligos GCGCTCCGTTGAGAATCTCGTA and CACAAACGAGCCCGCACGGA and sequencing.

Protein domain prediction and illustration

IDRs were annotated based on information provided by the UniProt Consortium (UniProt Consortium, 2019). The coiled-coil domain was defined via the COILS program with a 28-residue window comparing both MTK and MTIDK matrices (weighted and unweighted) (Lupas et al., 1991; Lupas, 1996). The domain structures were illustrated using DOG2.0 (Ren et al., 2009).

Development (2021) 148, dev198416. doi:10.1242/dev.198416

Yeast strains, media and transformation

Growth and genetic manipulation of the *Saccharomyces cerevisiae* strain EGY 48/194 (MATα, trp 1, his 3, ura 3, leu2::2/4 LECAop-LEU2) were performed using standard genetic techniques. The yeast strain was transformed with plasmids using lithium acetate (1 M). The selection of the different plasmids was conducted with complete minimal medium lacking histidine/uracil/tryptophane/leucine. Yeast two-hybrid assays were performed using the Grow'N'Glow GFP Yeast Two-Hybrid System (Mobitech) according to the manufacturer's protocol. Full-length cDNA of *C. elegans* SAS-7, PCMD-1, PCMD-1(ΔCC), PCMD-1(C2), SPD-5, PLK-1 and SAS-4 were inserted into the bait vector pEG202 containing the DNA-binding domain LexA. pEG202_SPD-5 could not be used owing to autoactivation. The cDNA of the different candidates PCMD-1, PCMD-1(ΔCC), PCMD-1(C2), SPD-2, SPD-5, PLK-1, SAS-7 and SAS-4 were cloned into the prey vector pJG45 comprising the B42 transcription activation domain. The third plasmid transformed into the yeast was pGNG1-GFP containing the reporter gene *gfp*. pEG202-p53 with pJG45-LTA was used as a positive control, whereas pJG45 without an insert was used as a negative control. The presence of the plasmids in yeast was verified by plasmid extraction, followed by PCR amplification of the inserts and sequencing. Expression of the prey proteins was verified by immunoblotting against an HA-tag.

Cell lines and culture conditions

Human embryonic kidney (HEK) 293T cells were cultured at 37°C (5% CO_2) in Dulbecco's modified Eagle's medium (DMEM) supplemented with 10% fetal bovine serum (FBS; Biochrom), 100 units/ml penicillin and 100 µg/ml streptomycin (Gibco).

Co-immunoprecipitation

HEK293T cells were transfected with 4 µg DNA of pTMD143 and/or pTMD144. After 24 h, cells were chilled to 4°C. To prepare cell extracts, cells were washed once with 1×PBS and pelleted by centrifugation at 1000 ***g*** for 5 min. Cell pellets were lysed using 100 µl lysis buffer [10 mM Tris-HCl (pH8.0), 50 mM NaF, 0.3 mM Na_3VO_4, 10 mM sodium pyrophosphate, 5 mM β-glycerolphosphate, 120 mM NaCl, 0.25% NP40] containing protease and phosphatase inhibitors (PhosSTOP, Pefabloc, cOmplete Mini, Pepstatin A, Leupeptin, Sigma-Aldrich; Aprotinin, Carl Roth) by incubating them for 30 min at 4°C. Crude extracts were clarified by centrifugation at 12,000 ***g*** for 12 min at 4°C and incubated with RFP-trap agarose beads (ChromoTek). Beads were pre-blocked in 3% bovine serum albumin and washed three times in 500 µl lysis buffer before use. Beads were then collected by centrifugation at 2500 ***g*** for 5 min at 4°C, washed 1× in lysis buffer and resuspended in SDS gel loading buffer. The double volume was loaded for the CoIP compared with input (I) and flow-through (FT). Immunoblotting was performed by using primary antibodies mouse anti-GFP (1:1000; 11814460001, Sigma-Aldrich) and mouse anti-His (1:1000; MA1-135, Thermo Scientific) and HRP-linked anti-mouse secondary antibody [1:7500; Goat Anti-Mouse IgG (H+L)-HRP Conjugate, 170-6516, Bio-Rad)] and detected using ECL Prime Western Blotting Detection Reagent (Amersham).

Translocation assay

L4 stage worms of different strains carrying the construct with the heat-shock promoter (TMD151, TMD157, TMD158, TMD159, TMD162, TMD165, TMD168, TMD167, TMD183 and TMD184) were shifted to 25°C for 15 h. Subsequently, worms laid eggs for 2 h at 25°C. The embryos were mounted on a 2% agarose pad and heat-shocked at 30°C for 1 h (Thermocycler, Bio-Rad). After 2 h recovery at 20°C, embryos were imaged using a SP5 Leica confocal microscope (see 'Microscopy' section). Control embryos were incubated at 20°C without heat shock. Feeding RNAi against *spd-5* was performed for 20 h at 25°C by using I-2G08 for TMD168 and the pTMD118 feeding clone constructed against the re-encoded region (Woodruff et al., 2015, 2017; Mittasch et al., 2020) for TMD151 and TMD162. Soaking RNAi against *sas-4* for TMD183 and TMD184 was performed against the re-encoded region (Cottee et al., 2013). dsRNA was made using the MEGAscript T7 Kit (Invitrogen) and primers TAATACGACTCACTATAGATGGCTTCCGATGAAAATATCGGTGC and TAATACGACTCACTATAGGCAGCGTGCTGTCCACTGTGGC. Worms were incubated in 1 µg/µl dsRNA for 48 h at 20°C and allowed to recover for 24 h at 25°C. Both RNAi treatments were validated on N2 worms by lethality tests and differential interference contrast (DIC) imaging. Embryos with a minimum of two cells in the case of a weak GFP signal or one cell with the GFP signal surrounding the whole circumference of this cell were considered as positive.

Marked mating experiments

To mark the sperm centrioles in marked mating experiments *fog-2(q71)*, females were mated with TMD119 males at 20°C and the progeny imaged by 4D microscopy. For the converse experiment, TMD119 L4 worms were fed *fem-1(RNAi)* overnight. The hatched progeny were raised on *fem-1(RNAi)* to block sperm production. Feminized animals were mated with *fog-2(q71)* males at 20°C. Progeny of the crosses were either imaged by 4D microscopy or used for indirect immunofluorescence. Meiotic stages of embryos in fixed samples were staged by the condensation state of the female DNA and the presence of the polar bodies.

Indirect immunofluorescence

Indirect immunofluorescence was performed using a protocol by Delattre et al. (2004). Hermaphrodite worms were cut in M9 buffer, covered with a coverslip, and placed on ice blocks. After freeze-cracking, slides were fixed in methanol, followed by incubation with primary antibodies anti-SAS-4 (1:500; sc-98949, Santa Cruz Biotechnology), anti-SPD-5 (1:1000, a generous gift from B. Bowerman; Hamill et al., 2002) and anti-GFP (1:500; 11814460001, Roche) overnight at 4°C and with Alexa 488-conjugated (1:500; A32723, Invitrogen Molecular Probes) and Alexa 568-conjugated (1:500; A-11011, Invitrogen Molecular Probes) secondary antibodies and Hoechst 33258 (1:1000, Sigma-Aldrich) at room temperature for 1 h.

Microscopy

Embryos treated for the translocation assay and indirect immunofluorescence samples were imaged at a resolution of 1024×1024 pixels with an HCX PL APO Lambda Blue 63×1.4 oil objective and a step size of 0.7 µm on a SP5 Leica confocal microscope using LAS software. For live-cell imaging, young adult worms were either dissected in 6 µl M9 and mounted on 2% agar pads or dissected in Polybead Microspheres 20.00 µm (diluted 1:10 in M9). Live-cell imaging was performed on an inverted Nikon Eclipse Ti spinning disc confocal microscope using an Andor DU-888 X-11056 camera (1024×1024 pixels), a 100×1.45-NA Plan-Apochromat oil immersion objective and controlled by NIS Elements 4.51 software. *z*-stacks were taken every 30 s with a step size of 0.7 µm and with 2×2 binning. Embryos for marked mating experiments were imaged using a Zeiss Axio Imager.M2 equipped with epifluorescence and 'Time to Live' software from Caenotec. Twenty-five DIC *z*-stacks were taken throughout the volume of the embryo every 35 s, and fluorescence scans were taken at required time points.

For SIM of live *C. elegans* embryos, we used the ZEISS Elyra 7 system in the Lattice SIM mode equipped with a Plan Apochromat 63×/1.40 oil immersion objective. Images were acquired with two pco.edge sCMOS 4.2 cameras simultaneously, using the ZEISS DuoLink adapter. Acquired *z*-stacks with a voxel size of 63×63×110 nm^3 and field of view size of 1024×1024 pixels were processed using the SIM processing algorithm of ZEN Black 3.0 software. SIM processed *z*-stacks have a voxel size of 31.5×31.5×110 nm^3. Yeast colonies were acquired using a Leica Stereomicroscope M205 FA, controlled by the Leica Application Suite software (3.2.0.9652) and equipped with a 1×2.11 NA Plan Apo lens and a Leica DigitalDFC340x FX camera.

Fluorescence intensity measurements

GFP and RFP intensities were measured on raw images by analyzing *z*-stacks with ManualTrackMate in Fiji (Tinevez et al., 2017). The time point was either defined through the DNA condensation visualized by the mCherry::H2B marker (for EU3000, TMD107, TMD165, TMD166,

TMD175, TMD177, TMD181, TMD202, TMD210) or through corresponding DIC recordings (for TMD119, TMD123, PHX1285, TMD178, TMD179, TMD203, TMD214, TMD216, TMD217). When there was no clear GFP signal recognizable, the centrosomal position was determined by DIC. A fixed radius was applied to measure all fluorescent signals (GFP::PCMD-1: 0.762 µm for Fig. 1E and 0.788 µm for all other figures, GFP::SAS-7: 0.828 µm, RFP::SPD-5: 4.062 µm), background signal, and cytoplasmic background signal outside the embryo, in 3D. Intensities were calculated for each centrosome as: intensity=(C-B)−(CS-B). The total intensity of the background (B) was subtracted from the total intensity of the centrosome (C) and from the total intensity of the cytoplasmic signal (CS). The cytoplasmic signal without background was then subtracted from the centrosomal signal without background. For GFP::SAS-7, the sum of the centrosomal fluorescence intensities per embryo was used to calculate the mean centrosomal fluorescence intensities because of separation defects in some *pcmd-1(t3421)* embryos. For cytoplasmic GFP values, the background (B) was subtracted from the cytoplasmic signal (CS).

Statistical analysis was performed by using R Studio version 1.2.5003 (R Core Team, 2014). Shapiro–Wilk test was used to test for normality. Levene's test was performed to compare variances. Depending on the normality, variance, and number of groups in the data sets, different comparison tests were performed (see figure legends). Mean values with the standard error of mean were plotted in Prism v6.

Circularity measurements

Centrosomal circularities were evaluated in one-cell embryos ranging from NEB to metaphase that were immunostained with an antibody against SPD-5. The cell stage was defined by DNA condensation, visualized with Hoechst staining. Image analysis was performed in Fiji (Schindelin et al., 2012). Maximum *z*-projections were created and the PCM shapes were converted into black/white outlines using the 'Huang' threshold. Statistical analysis was performed by using R Studio version 1.2.5003 (R Core Team, 2014). Shapiro–Wilk test was used to test for normality. Levene's test was performed to compare variances. Mann–Whitney *U*-Test was used for the comparison of circularity values. Mean values with the standard error of mean were plotted with Prism v6.

Statistical analysis for survival

L4 worms were singled and maintained at the indicated temperature for 16-20 h; laid eggs and hatched adult worms were counted. Statistical analysis was performed in R Studio version 1.2.5003 (R Core Team, 2014). Shapiro–Wilk test was used to test for normality. Levene's test was used to test for homogeneity of variances. Depending on the normality, variance, and number of groups in the data sets, different comparison tests were performed (see figure legends).

Acknowledgements

We thank the laboratories of C. Osman and N. Wagener for help with the yeast two-hybrid experiments; the laboratory of A. Böttger for help with the cell culture; M. Antoniolli, N. Sharma, A. Trinca and M. Plotnikova for generating tools; A. Bezler for critical comments on the manuscript; the imaging facility CALM, especially H. Harz and J. Ryan for help with imaging, the whole Zeiss-team and especially M. Gorelashvili for giving us the opportunity to image using the Lattice SIM; N. Lebedeva and M. Nöcker for excellent technical assistance; P. Gönczy, K. Oegema and J. Feldman for providing worm strains; B. Bowerman for the anti-SPD-5 antibody; the LSM graduate school. Some strains used in this study were provided by the *Caenorhabditis* Genetic Center (CGC), which is funded by the NIH Office of Research Infrastructure Programs (P40 OD010440).

Competing interests

The authors declare no competing or financial interests.

Author contributions

Conceptualization: E. Zanin, T.M.-D.; Methodology: L.S., A.S., E. Zanin, T.M.-D.; Validation: L.S., A.S., E. Zuccoli, T.M.-D.; Formal analysis: L.S., A.S., E. Zuccoli, T.M.-D.; Investigation: L.S., A.S., E. Zuccoli, S.Ü., J.M., T.M.-D.; Resources: L.S., A.S., E. Zuccoli, S.Ü., J.M., T.M.-D.; Data curation: T.M.-D.; Writing - original draft: L.S., T.M.-D.; Writing - review & editing: L.S., A.S., E. Zuccoli, E. Zanin, T.M.-D.; Visualization: L.S., A.S., E. Zuccoli, T.M.-D.; Supervision: L.S., T.M.-D.; Project administration: T.M.-D.; Funding acquisition: T.M.-D.

Funding

This work was funded by the Deutsche Forschungsgemeinschaft (DFG MI 1867/3 to T.M.-D.) and (DFG ZA/619/3 to E. Zanin).

Peer review history

The peer review history is available online at https://journals.biologists.com/dev/article-lookup/doi/10.1242/dev.198416

References

Boxem, M., Maliga, Z., Klitgord, N., Li, N., Lemmens, I., Mana, M., de Lichtervelde, L., Mul, J. D., van de Peut, D., Devos, M. et al. (2008). A protein domain-based interactome network for *C. elegans* early embryogenesis. *Cell* **134**, 534-545. doi:10.1016/j.cell.2008.07.009

Brenner, S. (1974). The genetics of *Caenorhabditis elegans*. *Genetics* **77**, 71-94. doi:10.1093/genetics/77.1.71

Buchman, J. J., Tseng, H.-C., Zhou, Y., Frank, C. L., Xie, Z. and Tsai, L.-H. (2010). Cdk5rap2 interacts with pericentrin to maintain the neural progenitor pool in the developing neocortex. *Neuron* **66**, 386-402. doi:10.1016/j.neuron.2010.03.036

Cabral, G., Laos, T., Dumont, J. and Dammermann, A. (2019). Differential requirements for centrioles in mitotic centrosome growth and maintenance. *Dev. Cell* **50**, 355-366.e6. doi:10.1016/j.devcel.2019.06.004

Cottee, M. A., Muschalik, N., Wong, Y. L., Johnson, C. M., Johnson, S., Andreeva, A., Oegema, K., Lea, S. M., Raff, J. W. and van Breugel, M. (2013). Crystal structures of the CPAP/STIL complex reveal its role in centriole assembly and human microcephaly. *eLife* **2**, 23-30. doi:10.7554/eLife.01071

Dammermann, A., Müller-Reichert, T., Pelletier, L., Habermann, B., Desai, A. and Oegema, K. (2004). Centriole assembly requires both centriolar and pericentriolar material proteins. *Dev. Cell* **7**, 815-829. doi:10.1016/j.devcel.2004.10.015

Dammermann, A., Maddox, P. S., Desai, A. and Oegema, K. (2008). SAS-4 is recruited to a dynamic structure in newly forming centrioles that is stabilized by the gamma-tubulin-mediated addition of centriolar microtubules. *J. Cell Biol.* **180**, 771-785. doi:10.1083/jcb.200709102

Decker, M., Jaensch, S., Pozniakovsky, A., Zinke, A., O'Connell, K. F., Zachariae, W., Myers, E. and Hyman, A. A. (2011). Limiting amounts of centrosome material set centrosome size in *C. elegans* embryos. *Curr. Biol.* **21**, 1259-1267. doi:10.1016/j.cub.2011.06.002

Delattre, M., Leidel, S., Wani, K., Baumer, K., Bamat, J., Schnabel, H., Feichtinger, R., Schnabel, R. and Gönczy, P. (2004). Centriolar SAS-5 is required for centrosome duplication in *C. elegans*. *Nat. Cell Biol.* **6**, 656-664. doi:10.1038/ncb1146

Delattre, M., Canard, C. and Gönczy, P. (2006). Sequential protein recruitment in *C. elegans* centriole formation. *Curr. Biol.* **16**, 1844-1849. doi:10.1016/j.cub.2006.07.059

Erpf, A. C., Stenzel, L., Memar, N., Antoniolli, M., Osepashvili, M., Schnabel, R., Conradt, B. and Mikeladze-Dvali, T. (2019). PCMD-1 organizes centrosome matrix assembly in *C. elegans*. *Curr. Biol.* **29**, 1324-1336.e6. doi:10.1016/j.cub.2019.03.029

Fields, S. and Song, O.-K. (1989). A novel genetic system to detect protein-protein interactions. *Nature* **340**, 245-246. doi:10.1038/340245a0

Frøkjær-Jensen, C., Davis, M. W., Hopkins, C. E., Newman, B. J., Thummel, J. M., Olesen, S.-P., Grunnet, M. and Jorgensen, E. M. (2008). Single-copy insertion of transgenes in *Caenorhabditis elegans*. *Nat. Genet.* **40**, 1375-1383. doi:10.1038/ng.248

Galletta, B. J., Fagerstrom, C. J., Schoborg, T. A., McLamarrah, T. A., Ryniawec, J. M., Buster, D. W., Slep, K. C., Rogers, G. C. and Rusan, N. M. (2016). A centrosome interactome provides insight into organelle assembly and reveals a non-duplication role for Plk4. *Nat. Commun.* **7**, 12476. doi:10.1038/ncomms12476

Garbrecht, J., Laos, T., Holzer, E., Dillinger, M. and Dammermann, A. (2021). An acentriolar centrosome at the *C. elegans* ciliary base. *Curr. Biol.* **31**, 12476. doi:10.1016/j.cub.2021.03.023

Hamill, D. R., Severson, A. F., Carter, J. C. and Bowerman, B. (2002). Centrosome maturation and mitotic spindle assembly in *C. elegans* require SPD-5, a protein with multiple coiled-coil domains. *Dev. Cell* **3**, 673-684. doi:10.1016/S1534-5807(02)00327-1

Hilbert, M., Erat, M. C., Hachet, V., Guichard, P., Blank, I. D., Flückiger, I., Slater, L., Lowe, E. D., Hatzopoulos, G. N., Steinmetz, M. O. et al. (2013). *Caenorhabditis elegans* centriolar protein SAS-6 forms a spiral that is consistent with imparting a ninefold symmetry. *Proc. Natl. Acad. Sci. USA* **110**, 11373-11378. doi:10.1073/pnas.1302721110

Kemp, C. A., Kopish, K. R., Zipperlen, P., Ahringer, J. and O'Connell, K. F. (2004). Centrosome maturation and duplication in *C. elegans* require the coiled-coil protein SPD-2. *Dev. Cell* **6**, 511-523. doi:10.1016/S1534-5807(04)00066-8

Kirkham, M., Müller-Reichert, T., Oegema, K., Grill, S. and Hyman, A. A. (2003). SAS-4 is a *C. elegans* centriolar protein that controls centrosome size. *Cell* **112**, 575-587. doi:10.1016/S0092-8674(03)00117-X

Kitagawa, D., Vakonakis, I., Olieric, N., Hilbert, M., Keller, D., Olieric, V., Bortfeld, M., Erat, M. C., Flückiger, I., Gönczy, P. et al. (2011). Structural basis of the 9-fold symmetry of centrioles. *Cell* **144**, 364-375. doi:10.1016/j.cell.2011.01.008

Leidel, S. and Gönczy, P. (2003). SAS-4 is essential for centrosome duplication in *C. elegans* and is recruited to daughter centrioles once per cell cycle. *Dev. Cell* **4**, 431-439. doi:10.1016/S1534-5807(03)00062-5

Leidel, S., Delattre, M., Cerutti, L., Baumer, K. and Gönczy, P. (2005). SAS-6 defines a protein family required for centrosome duplication in *C. elegans* and in human cells. *Nat. Cell Biol.* **7**, 115-125. doi:10.1038/ncb1220

Lerit, D. A., Jordan, H. A., Poulton, J. S., Fagerstrom, C. J., Galletta, B. J., Peifer, M. and Rusan, N. M. (2015). Interphase centrosome organization by the PLP-Cnn scaffold is required for centrosome function. *J. Cell Biol.* **210**, 79-97. doi:10.1083/jcb.201503117

Lettman, M. M., Wong, Y. L., Viscardi, V., Niessen, S., Chen, S.-H., Shiau, A. K., Zhou, H., Desai, A. and Oegema, K. (2013). Direct binding of SAS-6 to ZYG-1 recruits SAS-6 to the mother centriole for Cartwheel Assembly. *Dev. Cell* **25**, 284-298. doi:10.1016/j.devcel.2013.03.011

Letunic, I. and Bork, P. (2018). 20 years of the SMART protein domain annotation resource. *Nucleic Acids Res.* **46**, D493-D496. doi:10.1093/nar/gkx922

Li, S., Armstrong, C. M., Bertin, N., Ge, H., Milstein, S., Boxem, M., Vidalain, P.-O., Han, J.-D. J., Chesneau, A., Hao, T. et al. (2004). A map of the interactome network of the metazoan *C. elegans*. *Science* **303**:540-543. doi:10.1126/science.1091403

Lupas, A., Van Dyke, M. and Stock, J. (1991). Predicting coiled coils from protein sequences. *Science* **252**, 1162-1164. doi:10.1126/science.252.5009.1162

Lupas, A. (1996). Prediction and analysis of coiled-coil structures. *Meth. Enzymol.* **266**, 513-525. doi:10.1016/s0076-6879(96)66032-7

Magescas, J., Eskinazi, S., Tran, M. V. and Feldman, J. L. (2021). Centriole-less pericentriolar material serves as a microtubule organizing center at the base of *C. elegans* sensory cilia. *Curr. Biol.* **31**, 2410-2417.e6. doi:10.1016/j.cub.2021.03.022

McNally, K. L. P., Fabritius, A. S., Ellefson, M. L., Flynn, J. R., Milan, J. A. and McNally, F. J. (2012). Kinesin-1 prevents capture of the oocyte meiotic spindle by the sperm aster. *Dev. Cell* **22**, 788-798. doi:10.1016/j.devcel.2012.01.010

Mittasch, M., Tran, V. M., Rios, M. U., Fritsch, A. W., Enos, S. J., Ferreira Gomes, B., Bond, A., Kreysing, M. and Woodruff, J. B. (2020). Regulated changes in material properties underlie centrosome disassembly during mitotic exit. *J. Cell Biol.* **219**, 623-647. doi:10.1083/jcb.201912036

O'Connell, K. F., Caron, C., Kopish, K. R., Hurd, D. D., Kemphues, K. J., Li, Y. and White, J. G. (2001). The *C. elegans zyg*-1 gene encodes a regulator of centrosome duplication with distinct maternal and paternal roles in the embryo. *Cell* **105**, 547-558. doi:10.1016/S0092-8674(01)00338-5

Pelletier, L., Özlü, N., Hannak, E., Cowan, C., Habermann, B., Ruer, M., Müller-Reichert, T. and Hyman, A. A. (2004). The *Caenorhabditis elegans* centrosomal protein SPD-2 is required for both pericentriolar material recruitment and centriole duplication. *Curr. Biol.* **14**, 863-873. doi:10.1016/j.cub.2004.04.012

Pelletier, L., O'Toole, E., Schwager, A., Hyman, A. A. and Müller-Reichert, T. (2006). Centriole assembly in *Caenorhabditis elegans*. *Nature* **444**, 619-623. doi:10.1038/nature05318

Qiao, R., Cabral, G., Lettman, M. M., Dammermann, A. and Dong, G. (2012). SAS-6 coiled-coil structure and interaction with SAS-5 suggest a regulatory mechanism in *C. elegans* centriole assembly. *EMBO J.* **31**, 4334-4347. doi:10.1038/emboj.2012.280

R Core Team. (2014). *R: A Language and Environment for Statistical Computing*. Vienna, Austria: R Foundation for Statistical Computing. URL http://www.R-project.org/.

Ren, J., Wen, L., Gao, X., Jin, C., Xue, Y. and Yao, X. (2009). DOG 1.0: illustrator of protein domain structures. *Cell Res.* **19**, 271-273. doi:10.1038/cr.2009.6

Rogala, K. B., Dynes, N. J., Hatzopoulos, G. N., Yan, J., Pong, S. K., Robinson, C. V., Deane, C. M., Gönczy, P. and Vakonakis, I. (2015). The *Caenorhabditis elegans* protein SAS-5 forms large oligomeric assemblies critical for centriole formation. *eLife* **4**, e07410. doi:10.7554/eLife.07410

Schindelin, J., Arganda-Carreras, I., Frise, E., Kaynig, V., Longair, M., Pietzsch, T., Preibisch, S., Rueden, C., Saalfeld, S., Schmid, B. et al. (2012). Fiji: an open-source platform for biological-image analysis. *Nat. Meth.* **9**, 676-682. doi:10.1038/nmeth.2019

Schultz, J., Copley, R. R., Doerks, T., Ponting, C. P. and Bork, P. (2000). SMART: a web-based tool for the study of genetically mobile domains. *Nucleic Acids Res.* **28**, 231-234. doi:10.1093/nar/28.1.231

Sugioka, K., Hamill, D. R., Lowry, J. B., McNeely, M. E., Enrick, M., Richter, A. C., Kiebler, L. E., Priess, J. R. and Bowerman, B. (2017). Centriolar SAS-7 acts upstream of SPD-2 to regulate centriole assembly and pericentriolar material formation. *eLife* **6**, e20353. doi:10.7554/eLife.20353

Tinevez, J.-Y., Perry, N., Schindelin, J., Hoopes, G. M., Reynolds, G. D., Laplantine, E., Bednarek, S. Y., Shorte, S. L. and Eliceiri, K. W. (2017). TrackMate: An open and extensible platform for single-particle tracking. *Methods* **115**, 80-90. doi:10.1016/j.ymeth.2016.09.016

UniProt Consortium. (2019). UniProt: a worldwide hub of protein knowledge. *Nucleic Acids Res.* **47**, D506-D515. doi:10.1093/nar/gky1049

Uversky, V. N. (2019). Intrinsically disordered proteins and their "Mysterious" (Meta)physics. *Front. Phys.* **7**, 1-18. doi:10.3389/fphy.2019.00010

Varadarajan, R. and Rusan, N. M. (2018). Bridging centrioles and PCM in proper space and time. *Essays Biochem.* **62**, 793-801. doi:10.1042/EBC20180036

Woodruff, J. B., Wueseke, O., Viscardi, V., Mahamid, J., Ochoa, S. D., Bunkenborg, J., Widlund, P. O., Pozniakovsky, A., Zanin, E., Bahmanyar, S. et al. (2015). Regulated assembly of a supramolecular centrosome scaffold in vitro. *Science* **348**, 808-812. doi:10.1126/science.aaa3923

Woodruff, J. B., Gomes, B. F., Widlund, P. O., Mahamid, J., Honigmann, A. and Hyman, A. A. (2017). The centrosome is a selective condensate that nucleates microtubules by concentrating tubulin. *Cell* **169**, 1066-1071.e10. doi:10.1016/j.cell.2017.05.028

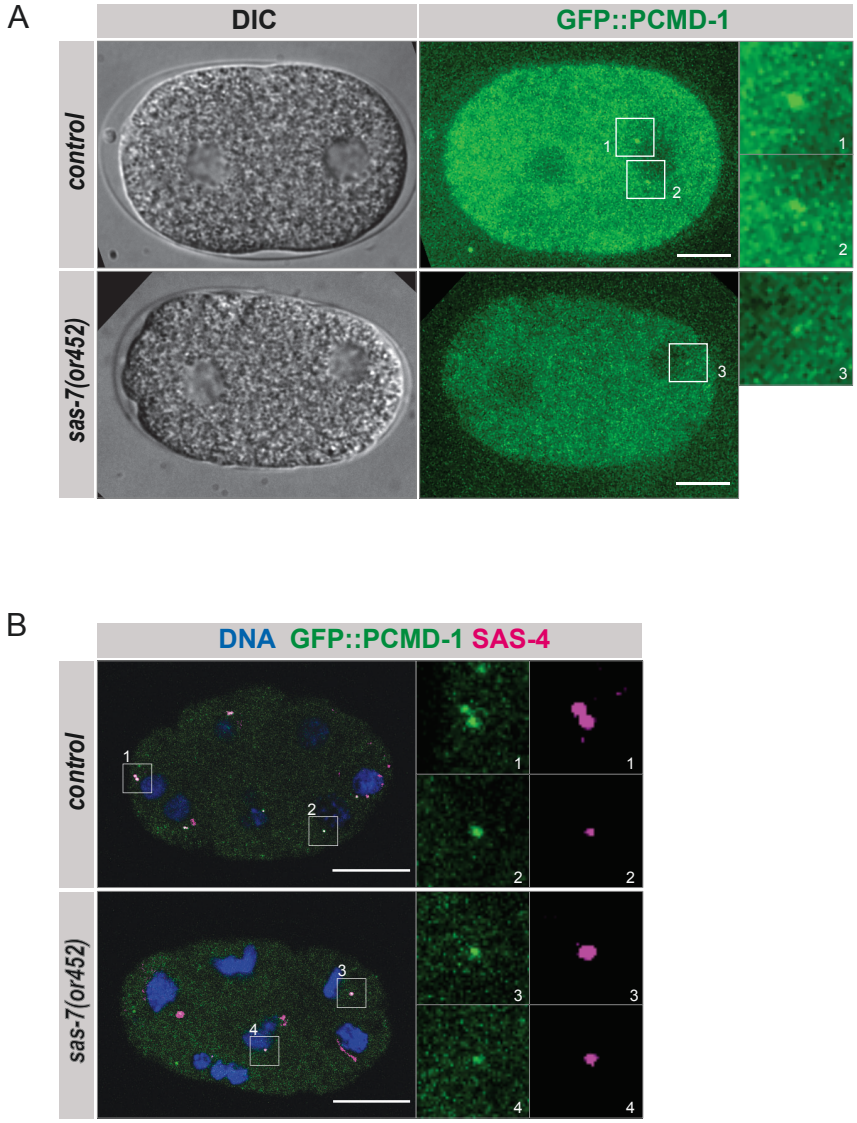

Fig. S1. SAS-7 recruits PCMD-1 to the centrioles in early embryos
(A) Stills of time-lapse spinning disc confocal images of *gfp::pcmd-1* (n=6) and *gfp::pcmd-1;sas-7(or452)* (n=8) embryos during pronuclear migration. Centrosomes are shown enlarged for the GFP::PCMD-1 signal.
(B) Representative confocal images of fixed *gfp::pcmd-1* (n=3) and *gfp::pcmd-1;sas-7(or452)* (n=8) embryos (>6 nuclei) stained for DNA, GFP and SAS-4. Insets represent single channels of the centrioles.
In all panels, scale bars are 10 µm.

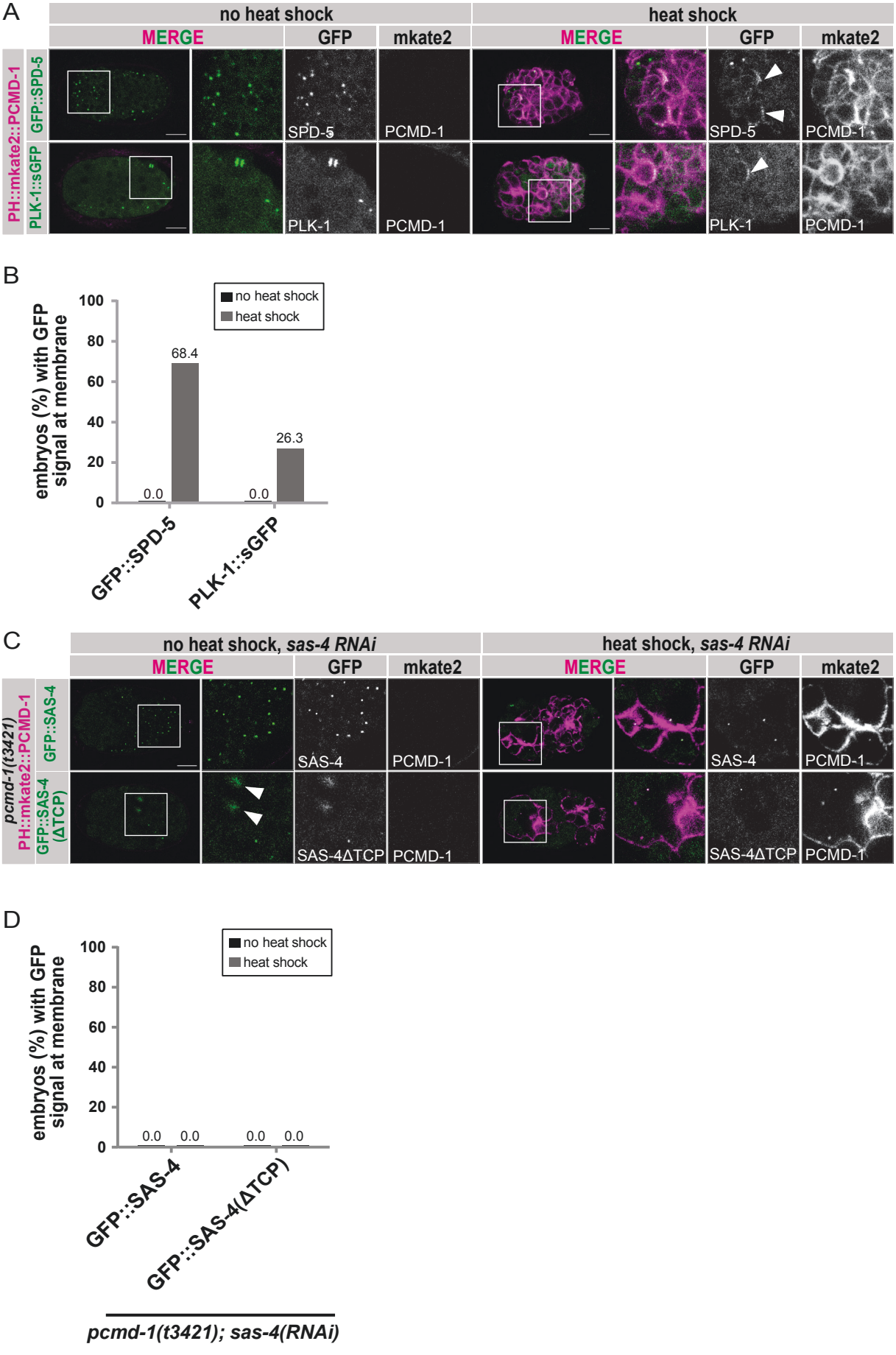

Fig. S2. PCMD-1 targeting of SPD-5 and PLK-1 to the plasma membrane in the presence of endogenous PCMD-1 is less efficient

(A) Representative multicellular embryos of the 'translocations assay' using GFP::SPD-5 (n=19 no heat shock; n=19 heat shock), and PLK-1::sGFP (n=20 no heat shock; n=19 heat shock) in a wild-type background. Selected regions are enlarged and shown as merge and single channels. Note that plasma membrane-localized PLK-1::sGFP is faint. Scale bars are 10 µm.

(B) Quantification of (A); the percentage of embryos (%) with GFP signal at the membrane after heat shock in the wild-type background.

(C) Representative multicellular embryos of the 'translocations assay' using GFP::SAS-4 (n=33 no heat shock; n=36 heat shock), and GFP::SAS-4(deltaTCP) (n=30 no heat shock; n=29 heat shock) in a *pcmd-1(t3421)* background and treated with *sas-4(RNAi)*. Selected regions are enlarged and shown as merge and single channels. Scale bars are 10 µm.

(D) Quantification of (C); the percentage of embryos (%) with GFP signal at the membrane after heat shock in the *sas-4(RNAi)* background.

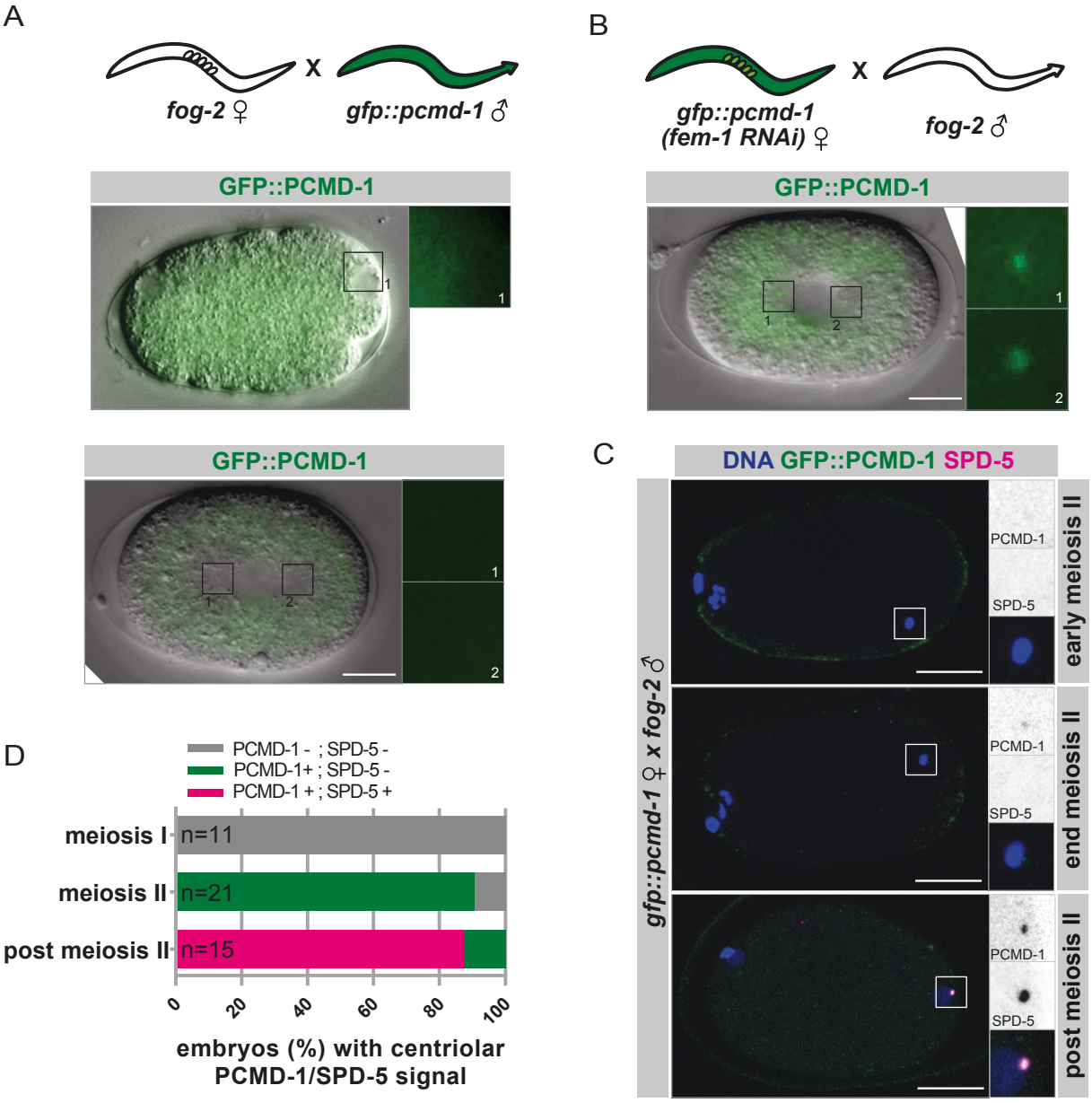

Fig. S3. PCMD-1 is recruited before SPD-5 to sperm-derived centrioles
(A) Schematic representation of a marked mating experiment where *fog-2(n71)* females were mated with *gfp::pcmd-1* males. The images below represent one-cell embryos taken by live-cell imaging shortly after meiosis II (n=6) and at metaphase (n=11). Centrosomal areas were determined by DIC imaging and are shown enlarged for the GFP::PCMD-1 signal.
(B) Schematic representation of a marked mating experiment where *fem-1(RNAi)*-treated *gfp::pcmd-1* females were mated with *fog-2(n71)* males (n=10). The image below represents a one-cell embryo taken by live-cell imaging. Centrosomal areas were determined by DIC imaging and are shown enlarged for the GFP::PCMD-1 signal.
(C) Images of fixed embryos in different stages of meiosis II, derived from the cross indicated in (B) and stained for DNA, GFP and SPD-5. Enlarged are sperm-associated centrosomal signals merged and as single channels.
(D) Quantification of (C) percentage of embryos (%).
Scale bars in all panels are 10 µm.

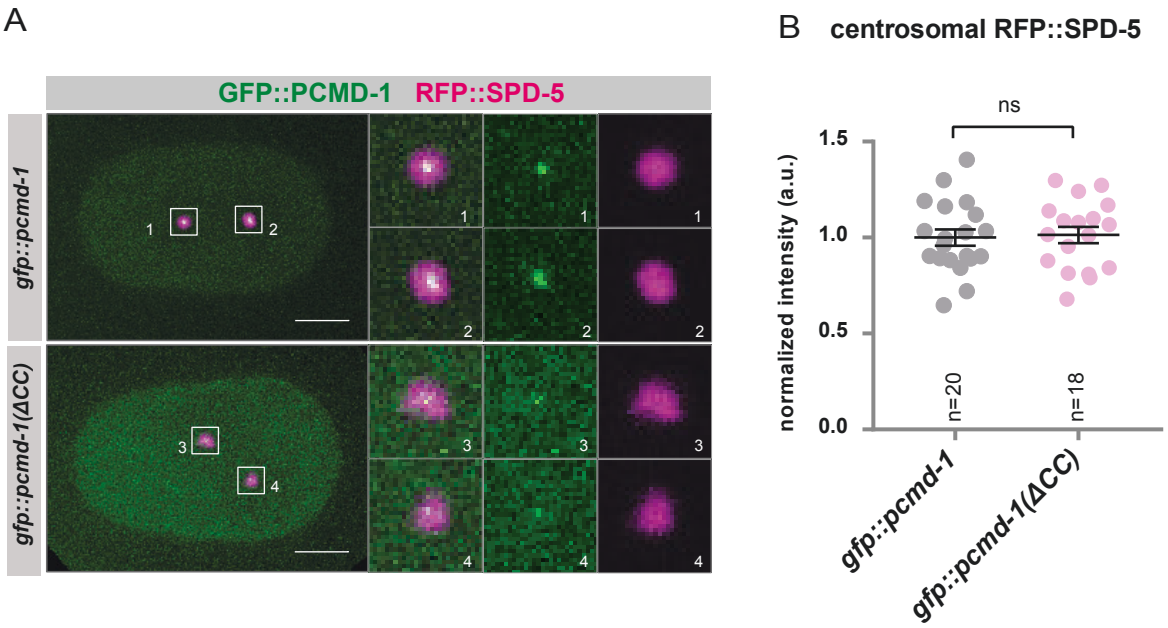

Fig. S4. Deletion of the coiled-coil domain PCMD-1 does not affect centrosomal SPD-5 levels
(A) Stills of time-lapse imaging of embryos expressing *rfp::spd-5 gfp::pcmd-1* (n=10) and *rfp::spd-5 gfp::pcmd-1(deltaCC)* (n=9) at metaphase. Centrosomal areas are shown enlarged as merge and for the RFP::SPD-5, GFP::PCMD-1 signal. n=number of embryos.
(B) Normalized centrosomal RFP signal intensities in embryos expressing *rfp::spd-5 gfp::pcmd- 1* and *rfp::spd-5 gfp::pcmd-1(deltaCC)* at metaphase. Two Sample t-test. n=number of analyzed centrosomes. ns p>0.05. Scale bars are 10 µm.

A

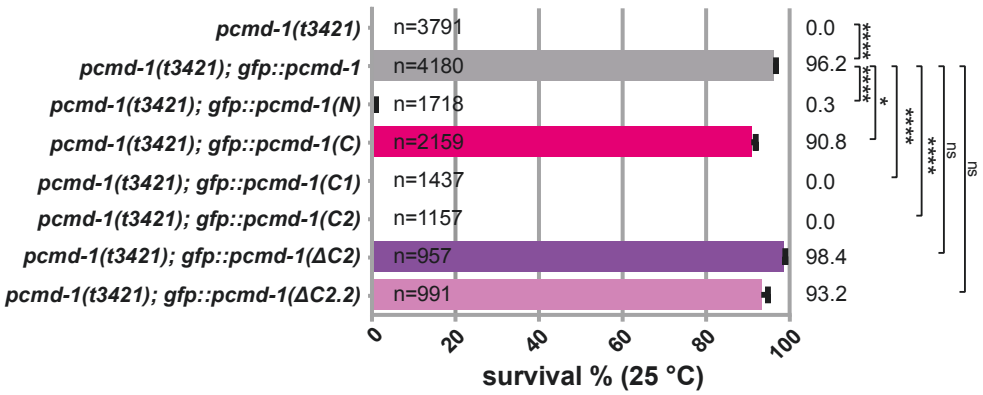

B

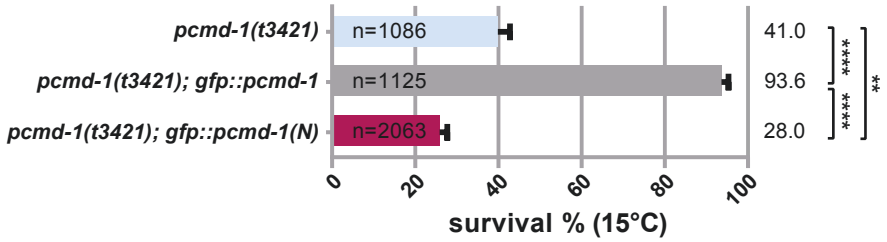

C

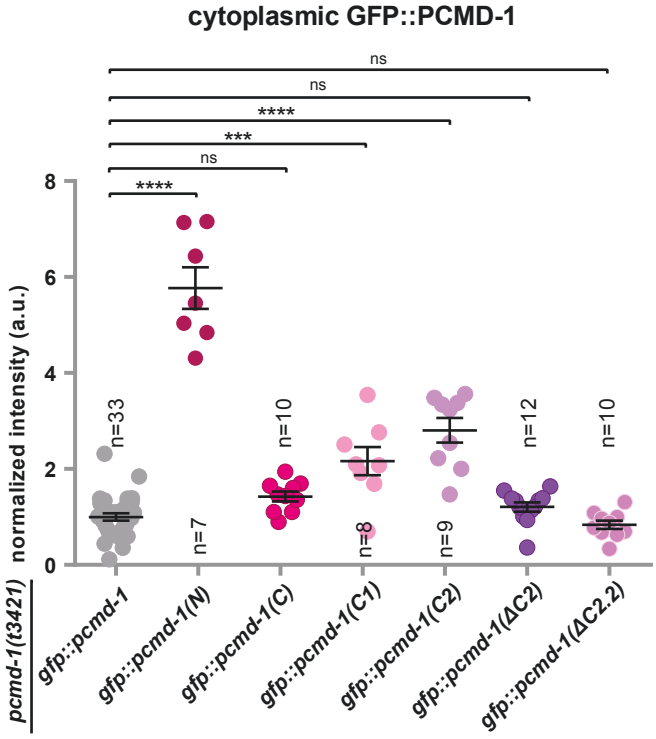

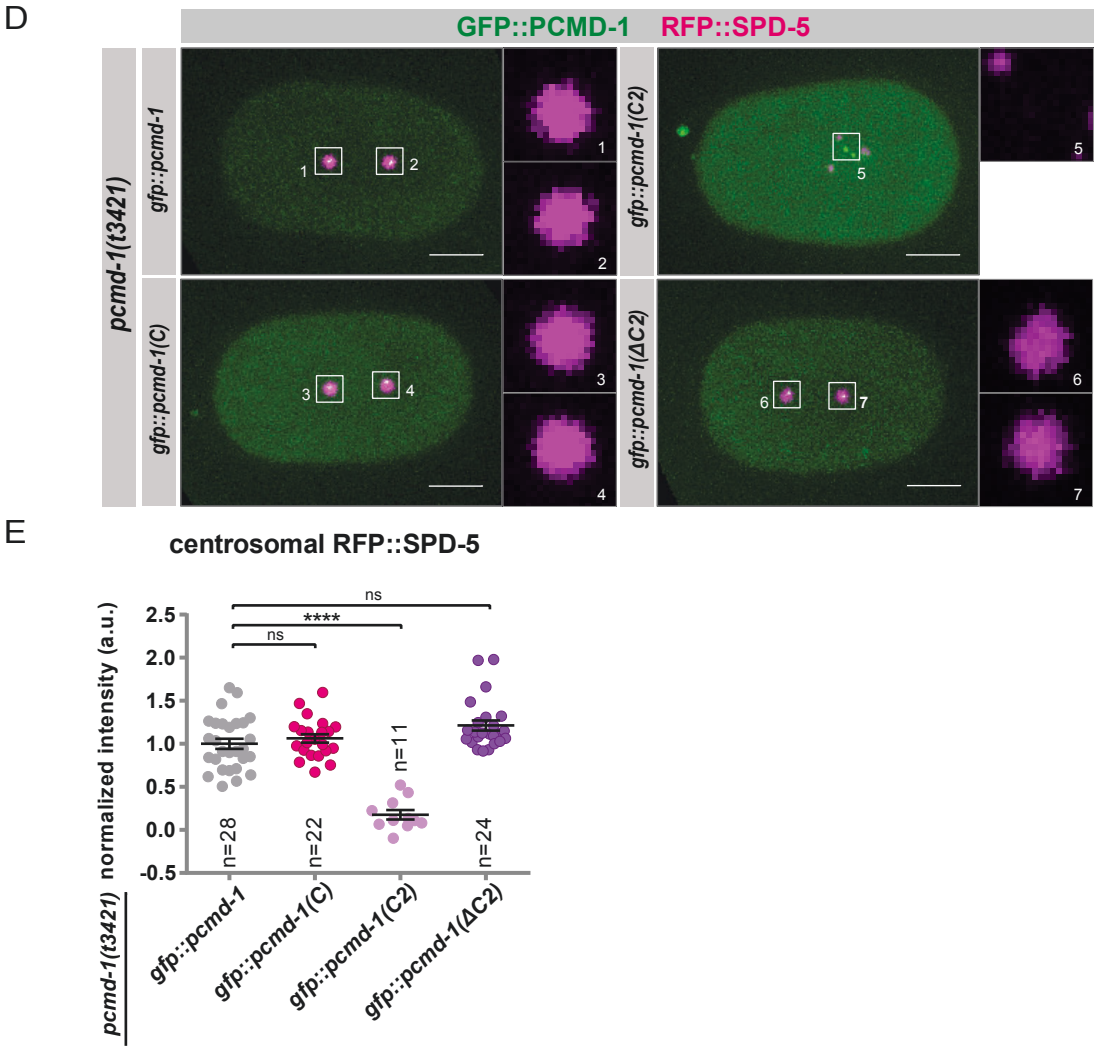

Fig. S5. The C2-region of PCMD-1 is insufficient to recruit SPD-5 to the centrosome
(A) Survival (%) of *gfp::pcmd-1, gfp::pcmd-1(N), gfp::pcmd-1(C), gfp::pcmd-1(C1), gfp::pcmd-1(C2), gfp::pcmd-1(deltaC2)* and *gfp::pcmd-1(deltaC2.2)* in the *pcmd-1(t3421)* background at 25C. Multiple Comparison with Kruskal Wallis test and post-hoc Dunn's test adjusted with Holm correction. n=number of analyzed embryos.
(B) Survival (%) of *gfp::pcmd-1* and *gfp::pcmd-1(N)* embryos in the *pcmd-1(t3421)* background at 15C. P-values were determined with multiple Comparison with Kruskal Wallis test and post-hoc Dunn's test adjusted with Holm correction, n=number of analyzed embryos.
(C) Normalized cytoplasmic GFP signal intensities of *gfp::pcmd-1, gfp::pcmd-1(N), gfp::pcmd-1(C), gfp::pcmd-1(C1), gfp::pcmd-1(C2), gfp::pcmd-1(deltaC2)* and *gfp::pcmd-1(deltaC2.2)* embryos, in combination with the *mCherry::h2b* in the *pcmd-1(t3421)* background at NEB. P-values were determined with multiple Comparison with Kruskal Wallis test and post-hoc Dunn's test adjusted with Holm correction, n=number of analyzed embryos.
(D) Stills of time-lapse imaging of *rfp::spd-5; gfp::pcmd-1* (n=14) and *rfp::spd-5; gfp::pcmd-1(C)* (n=11), *rfp::spd-5; gfp::pcmd-1(C2)* (n=9) and *rfp::spd-5; gfp::pcmd-1(deltaC2)* (n=12) of embryos in the *pcmd-1(t3421)* background at metaphase. Note that in two *rfp::spd-5; gfp::pcmd-1(C2) embryos* the PCM does not co-localize with the centrioles. Centrosomal areas are shown enlarged as merge and for the RFP::SPD-5, GFP::PCMD-1 signal. n=number of embryos.
(E) Normalized centrosomal RFP::SPD-5 signal intensities at metaphase of embryos in (D). p-values were determined with Multiple Comparison with Kruskal Wallis test and post-hoc Dunn's test adjusted with Holm correction, n=number of analyzed centrosomes.
In all panels error bars denote s.e.m. p-values represent: **p<0.01, ***p<0.001, ****p<0.0001, ns p>0.05. Scale bars are 10 µm.

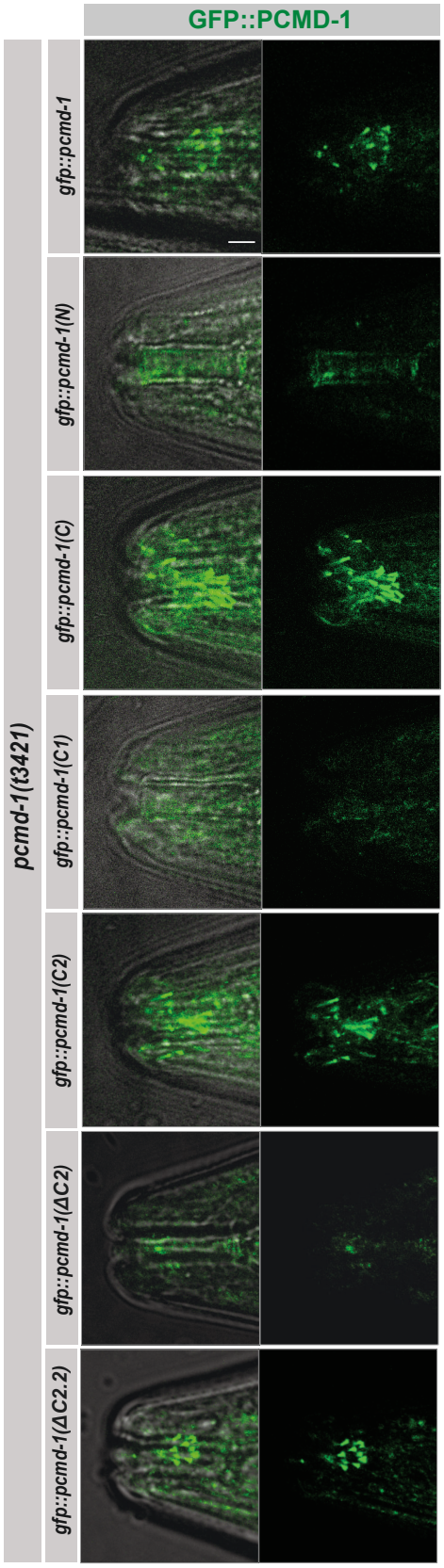

Fig. S6. The region spanning the IDR6 is necessary for ciliary targeting of PCMD-1
Localization of GFP::PCMD-1, GFP::PCMD-1(N), GFP::PCMD-1(C), GFP::PCMD-1(C1), GFP::PCMD-1(C2), GFP::PCMD-1(deltaC2) and GFP::PCMD-1(deltaC2.2) to the ciliary base in adult animals. n=5 animals for each condition.
Scale bars are 10 μm.

Table S1. Strains and materials used in the study.

Click here to download Table S1

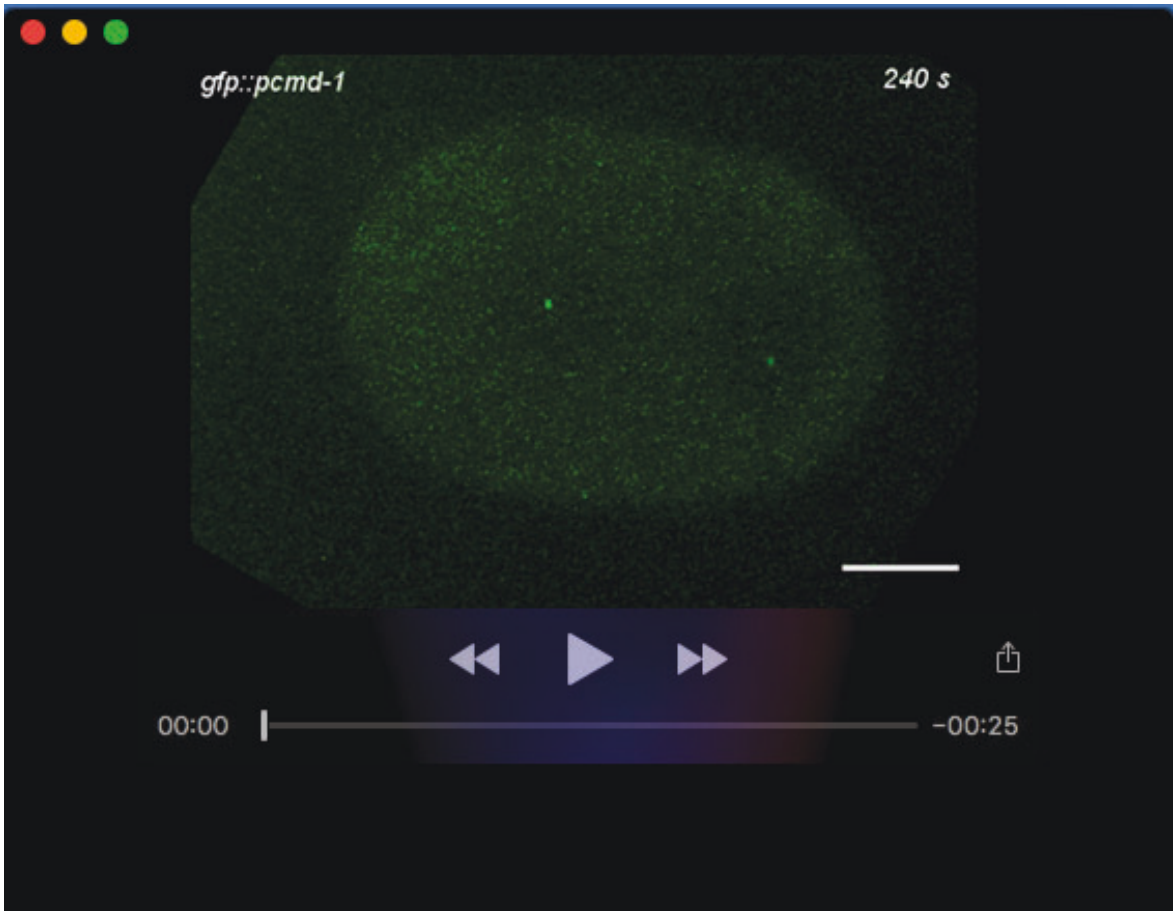

Movie 1. Time-lapse of the first cell cycle of a GFP::PCMD-1 expressing embryo (related to figure 4C). In the control embryo, GFP::PCMD-1 localizes to the centrosome throughout the first cell cycle. Live-cell spinning disk microscopy. The scale bar is 10 μm.

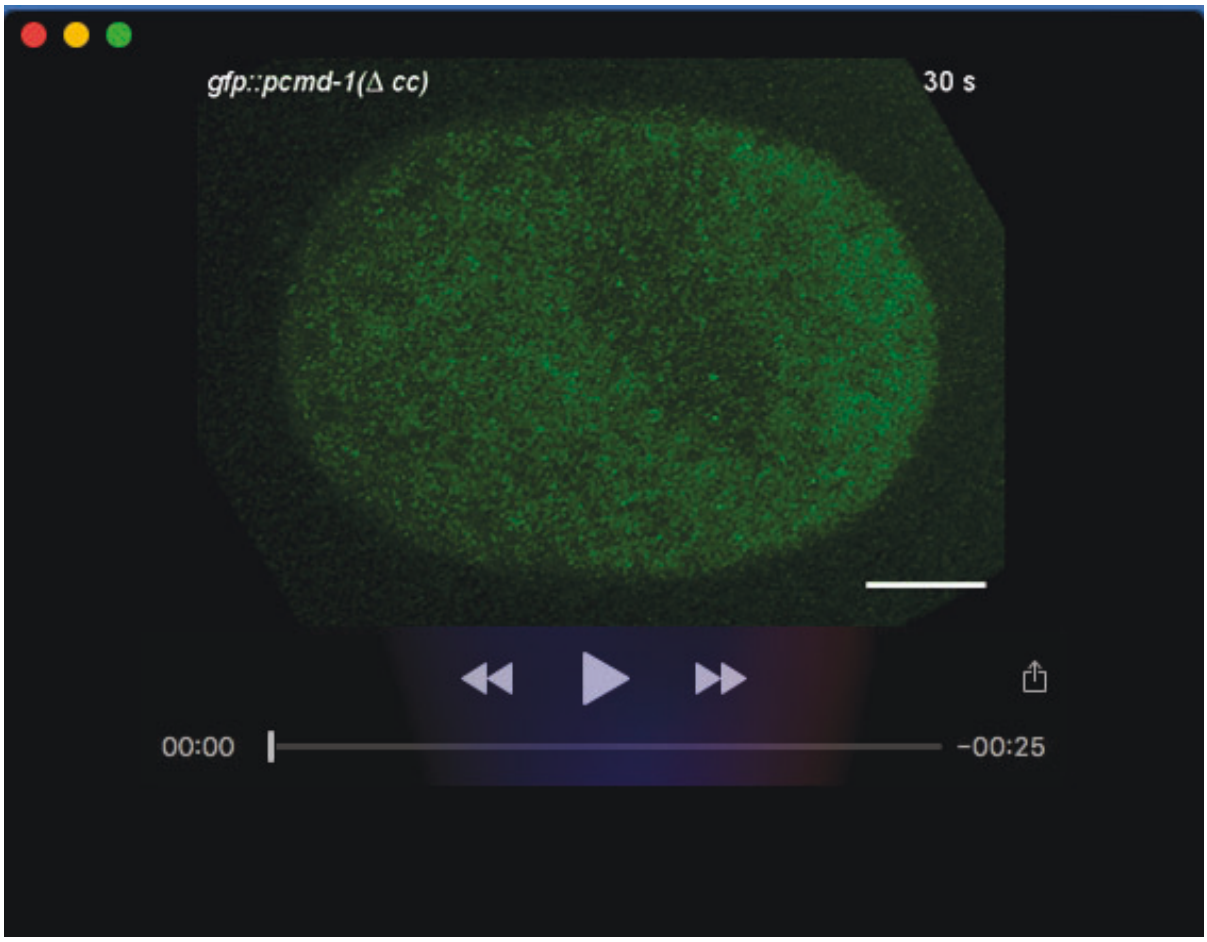

Movie 2. Time-lapse of the first cell cycle of a GFP::PCMD-1 expressing embryo lacking the predicted coiled-coil domain (related to figure 4C) In the *gfp::pcmd-1(ΔCC)* embryo, GFP::PCMD-1(ΔCC) localizes to the centrosome with reduced levels. Live-cell spinning disk microscopy. The scale bar is 10 μm.

Publication II

PCMD-1 stabilizes the PCM scaffold and facilitates centriole separation

Alina Schreiner, Astrid Heim, Luisa Pletschacher, Lisa-Marie Alznauer, Serena Schwenkert, Friederike Wolff, Esther Zanin, Tamara Mikeladze-Dvali

Journal of Cell Biology (2025) - DOI: 10.1083/jcb.202411107

JCB Journal of Cell Biology

ARTICLE

PCMD-1 stabilizes the PCM scaffold and facilitates centriole separation

Alina Schreiner[1], Astrid Heim[1], Luisa Pletschacher[1], Lisa-Marie Alznauer[1], Serena Schwenkert[1], Friederike Wolff[2], Esther Zanin[2], and Tamara Mikeladze-Dvali[1]

Centrosomes are highly dynamic organelles, and maintaining their stability is crucial for spindle pole integrity and bipolar spindle formation. Centrosomes consist of a pair of centrioles surrounded by the PCM. In *Caenorhabditis elegans*, interactions between the scaffold protein SPD-5 and kinase PLK-1 are essential for PCM formation. However, how PCM stability is established and maintained remains unclear. We address this by analyzing the function of PCMD-1, a protein mainly localizing to centrioles. We show that CDK-1 primes PCMD-1 for PLK-1 phosphorylation. Mutations in PLK-1 docking sites abolish PCMD-1 phosphorylation and SPD-5 binding *in vitro* and destabilize the PCM scaffold *in vivo*. As a result, microtubule-pulling forces cannot be relayed to centrioles, delaying their separation. Our findings reveal that PCMD-1 is critical for PCM stability and timely centriole separation during PCM disassembly. We propose that PCMD-1 initiates scaffold assembly by biasing the PCM core toward intrinsic order, acting as a seed that propagates throughout the scaffold to ensure structural integrity.

Introduction

Centrosomes are the main microtubule-organizing centers of dividing animal cells and orchestrate the assembly of a bipolar spindle during cell division. Centrosomes comprise a pair of centrioles surrounded by the pericentrosomal material (PCM). While the PCM nucleates and tethers spindle microtubules, it must also withstand extremely high pulling forces exerted on the centrosome by emanating microtubules (Grill et al., 2003; Laan et al., 2012). Ensuring a stable and intact centrosome is pivotal for coordinated cell division and faithful chromosome segregation. Several different mechanisms can cause the formation of a spindle apparatus with multiple poles, which is a source of aneuploidy and has been often observed in cancer cells (Ganem et al., 2009; Holland and Cleveland, 2009). Multipolar spindles can be the result of numerical aberrations or premature separation of centrioles, or alternatively be caused by the fragmentation of an unstable and weakened PCM, leading to the assembly of extra, acentriolar poles (Maiato and Logarinho, 2014). How PCM stability is achieved, such that it can withstand microtubule-pulling forces without fragmentation, is still not fully understood. The PCM is a proteinaceous matrix, undergoing dynamic changes during the cell cycle. The interphase PCM forms a highly structured core around centrioles (Fu and Glover, 2012; Lawo et al., 2012; Mennella et al., 2012; Sonnen et al., 2012). Upon mitotic entry, the PCM undergoes a maturation process and expands to its maximum extent at metaphase. Research in *Caenorhabditis elegans* led to the proposal that the centrosome can be best described as a viscoelastic entity, with physical properties reminiscent of a non-Newtonian fluid (Mittasch et al., 2020; Woodruff, 2021). According to the current model, after maturation and growth, the PCM transitions from a strong, more ductile physical state at metaphase to a weak, deformable one in anaphase. The physical properties at metaphase allow the PCM to withstand deformation by microtubule-pulling forces. The same forces can easily disassemble the brittle PCM in anaphase and release the entrapped pair of centrioles (Magescas et al., 2019).

Posttranslational modifications of PCM components drive this dynamic process and are intrinsically intervened with PCM stabilization during mitosis. Aurora A and PLK1 (polo-like kinase) are two multifunctional mitotic kinases linked to centrosome integrity. In human cells, the decrease of Aurora A activity and its substrate ch-TOG leads to the loss of centrosome stability and formation of extra spindle poles (De Luca et al., 2008; Foraker et al., 2012; Ou et al., 2018). Along with its diverse roles in cell division, such as the promotion of mitotic entry, nuclear envelope breakdown (NEBD), sister chromatid separation, and cytokinesis, PLK1 promotes centrosome maturation and centriole separation (Joukov and De Nicolo, 2018). Increased PCM fragmentation has been observed in PLK1-inhibited cultured and zebrafish cells (Aljiboury et al., 2022; Rathbun et al., 2020). A possible substrate for PLK1 in terms of centrosome stability is Kizuna (Novarino et al., 2011; Oshimori et al., 2006; Thomas

[1]Faculty of Biology, Ludwig-Maximilians-Universität München, München, Germany; [2]Department Biologie, Friedrich-Alexander-Universität Erlangen-Nürnberg, Erlangen, Germany.

Correspondence to Tamara Mikeladze-Dvali: tmdvali@biologie.uni-muenchen.de.

et al., 2014). Kiz tethers the PCM to the centrioles, and its phosphorylation by PLK1 is needed to maintain spindle pole integrity. Other key substrates of PLK1 are the centrosome proteins Cdk5Rap2, Cep192, and pericentrin (PCNT) (Barrera et al., 2010; Lee and Rhee, 2012; Pagan et al., 2015; Santamaria et al., 2011). Cdk5Rap2 (spindle-defective-5 [SPD-5] in *C. elegans*, centrosomin (Cnn) in *Drosophila melanogaster*), Cep192 (SPD-2 in *C. elegans*, Spd-2 in *D. melanogaster*), and PLK1 form an evolutionary conserved module, which drives PCM expansion and maturation during mitotic entry (Alvarez-Rodrigo et al., 2019; Conduit et al., 2014; Decker et al., 2011; Dobbelaere et al., 2008; Haren et al., 2009; Joukov et al., 2014; Lee and Rhee, 2011; Meng et al., 2015; Ohta et al., 2021; Wong et al., 2025; Wong et al., 2022; Woodruff et al., 2015). Phosphorylation of PCNT by PLK1 is a prerequisite for its separase-based cleavage toward mitotic exit. This leads to timely PCM disassembly and subsequent centriole disengagement and separation (Kim et al., 2019; Lee and Rhee, 2012; Matsuo et al., 2012; Tsou et al., 2009). In agreement with this, in HeLa cells depleted of PCNT, centrioles separate prematurely (Kim et al., 2019). Premature centriole separation was also observed in PCNT-like protein (PLP) mutant sensory organ precursors of *D. melanogaster* (Roque et al., 2018). Interestingly, PLP mutant embryos recruit PCM to the centrosomes but exhibit a highly fragmented and flared PCM, indicating that proper PLP levels are not only necessary for timely centriole separation, but also to maintain centrosome stability (Richens et al., 2015).

SPD-5 and PLK-1 are major drivers of PCM dynamics in *C. elegans*. SPD-5 is the main scaffold protein of the PCM matrix that can self-assemble and form micron-scale networks *in vitro* (Hamill et al., 2002; Woodruff et al., 2015). Network formation of purified SPD-5 is highly accelerated by the structural protein SPD-2 and by PLK-1 phosphorylation. SPD-5 contains a phospho-regulated multimerization (PReM) domain and a C-terminal centriole-targeting sequence. The PReM domain, originally discovered in Cnn, mediates the interaction of SPD-5 with PLK-1, and phosphorylation by PLK-1 fine-tunes the complex landscape of SPD-5 macromolecular self-interactions *in vitro* (Conduit et al., 2014; Feng et al., 2017; Nakajo et al., 2022; Rios et al., 2024; Woodruff et al., 2015).

In vivo SPD-2, along with the kinases PLK-1 and AIR-1 (Aurora A), is required for the centrosome scaffold assembly and maturation (Cabral et al., 2019; Hannak et al., 2001; Kemp et al., 2004; Özlü et al., 2005; Pelletier et al., 2004). PLK-1 is recruited to the centrioles by SPD-2 (Decker et al., 2011). The polo-box domains (PBD) of PLK-1 bind a docking site in SPD-2 primed by CDK-1 (Ohta et al., 2021). Subsequent phosphorylation of SPD-5 by PLK-1 at four residues drives PCM expansion at mitotic entry (Woodruff et al., 2015; Wueseke et al., 2016). When these residues are rendered phosphodeficient, SPD-5 still seeds the PCM core around the centrioles but is unable to assemble an expanded micron-scale scaffold. PLK-1, in contrast to AIR-1 and SPD-2, is not only needed for centrosome maturation but also to maintain an already assembled PCM (Cabral et al., 2019). Acute inhibition of PLK-1 at metaphase causes rapid PCM dispersal and disassembly. Centrosomal PLK-1 is downregulated at anaphase in a CDK-1–dependent manner (Cabral et al., 2019), and concomitant with this, the PCM weakens and disassembles. The switch between PLK-1 activity at the centrosome and its counteracting phosphatase PP2A is thought to trigger PCM fragmentation and dissolution by microtubule-pulling forces (Enos et al., 2018; Magescas et al., 2019; Mittasch et al., 2020). Interestingly, when centrioles are ablated at early time points of centrosome maturation, the remaining PCM cannot recover; it disperses prematurely even before anaphase onset. The dispersal can be reversed by microtubule depolymerization, indicating that a fragile and untethered PCM scaffold dissipates in a microtubule-dependent manner; however, the PCM still retains its intrinsic ability to form a spherical entity under these conditions (Cabral et al., 2019).

While much progress has been made in understanding the role of the scaffold protein SPD-5 and PLK-1 in regulating dynamical changes in the mechanical properties of the PCM, how other centrosomal proteins contribute to this process and how a weakened PCM affects centriole separation is less well understood.

The PCM scaffold is tethered to the centrioles by the intrinsically disordered protein pericentriolar matrix deficient-1 (PCMD-1) (Erpf et al., 2019; Stenzel et al., 2021). One-cell embryos mutant for *pcmd-1* are 100% embryonically lethal due to the failure of SPD-5 recruitment to the centrioles, absence of the PCM core formation, and failure of PCM scaffold self-assembly. Occasionally, SPD-5 forms an extremely compromised PCM, necessitating an analysis of PCMD-1 function in maintaining PCM integrity. We have previously shown that PCMD-1 binds SPD-5 and PLK-1, and is also able to recruit SPD-5 and PLK-1 to an ectopic cellular location (Erpf et al., 2019; Stenzel et al., 2021). Centrosomal PLK-1 levels are decreased in *pcmd-1(t3421)* mutant embryos, suggesting that, along with SPD-2, PCMD-1 contributes to PLK-1 recruitment to the centrosome and thereby facilitates its centrosome-related functions (Erpf et al., 2019; Stenzel et al., 2021).

Here we show that PCMD-1 is primed by CDK-1 and phosphorylated by PLK-1, and that this interaction is necessary to establish a coherent and stable PCM. When predicted PLK-1–binding sites are mutated in PCMD-1, phosphorylation of PCMD-1 by PLK-1 is abolished, and the recruited PCM scaffold assembles into a fragile and distorted network that cannot withstand microtubule-pulling forces. The fragile PCM is easily deformed by exaggerated forces applied to spindle poles. As a consequence of a weakened PCM scaffold, pulling forces are not relayed to the entrapped centriole pair, resulting in a delayed centriole separation in anaphase, suggesting a key role of PCMD-1 in centriole separation.

Results

Mutating putative PLK-1–binding sites in PCMD-1 leads to severe PCM scaffold disorganization

Downregulating PLK-1 function has pleiotropic effects on the embryo and does not allow us to test the functional importance of the PLK-1–PCMD-1 interaction. To overcome this, we set out to identify and mutate predicted PLK-1 PBD-binding sites in PCMD-1. PLK-1 PBD sites are phosphorylation sites, usually primed by PLK-1 itself or another kinase (Garcia-Alvarez et al., 2007).

Using a prediction algorithm and manual annotation, we identified 23 potential PBD consensus sites in PCMD-1 and rendered all sites phosphodeficient by changing them to alanines (Table S1), further referred to as PCMD-1-PBD^{m} (for PBD mutant) throughout the manuscript (Fig. 1 A).

We used the previously established "single-copy-replacement-system" to assess the functionality of the modified protein in *C. elegans* (Stenzel et al., 2021). In short, N-terminally GFP-tagged PCMD-1-PBD^{m} was crossed into the *pcmd-1(syb975)* null mutant background, and the WT version (GFP::PCMD-1^{WT}) was used as a control. We assessed the functionality of GFP::PCMD-1-PBD^{m} by scoring rescue of embryonic viability. Compared with WT worms, none of the embryos laid by *pcmd-1(syb975)* mutant worms hatch at restricted temperature (Fig. S1 A). Re-introduction of GFP::PCMD-1^{WT} rescued embryonic viability to 97.7%. In comparison, only 86.4% of GFP::PCMD-1-PBD^{m} embryos were viable (Fig. S1 A). This indicates that by mutating PLK-1-PBD sites the protein lost some of its functionality. Then, we analyzed recruitment of GFP::PCMD-1-PBD^{m} by measuring relative GFP intensities at the centrosome (Fig. 1, C and D). GFP::PCMD-1-PBD^{m} centrosomal levels were at 27% compared with the GFP::PCMD-1^{WT}. A reduction in expression of the transgene in whole worm lysates was apparent (Fig. S1 B). Although not significant, it might still contribute to the reduction at the centrosome.

Most of the *pcmd-1* mutant embryos fail to recruit the PCM core to centrioles prior to mitotic entry (Erpf et al., 2019; Stenzel et al., 2021). To test whether the reduced lethality of PCMD-1-PBD^{m} transgenes could be explained by a failed or compromised PCM recruitment of *pcmd-1(syb975)* mutants, we introduced RFP::SPD-5. To test whether SPD-5 was recruited to the PCM core, we treated animals with *spd-2(RNAi)*, where PCM scaffold does not assemble, leaving behind the PCM core around the centrioles. *spd-2(RNAi)* treatment revealed that SPD-5 was still detected at the PCM core of both, PCMD-1^{WT} and PCMD-1-PBD^{m} strains (Fig. S1 C). Next, to analyze changes in the mitotic PCM scaffold, we performed live-cell imaging during the first cell cycle (Fig. 1 B; and Videos 1, and 2). Similar to the control, in all GFP::PCMD-1-PBD^{m} embryos, centrosomes were able to recruit SPD-5. PCM mass at metaphase was not decreased, indicating that WT levels of RFP::SPD-5 PCM were recruited to the centrosome (Fig. 1, B, C, and E). Therefore, mutating predicted PBD sites did not significantly interfere with the PCM tethering function of PCMD-1 in embryos. However, we noticed that the PCM scaffold recruited by GFP::PCMD-1-PBD^{m} was severely disorganized, showing flared extensions. To better characterize the distortion of PCM scaffold, we quantified PCM shape parameters, such as circularity and area, at prometaphase (−150 s), metaphase (0 s), and late anaphase (120 s) by creating masks of RFP::SPD-5 (Fig. 1 F). In control embryos, the centrosome is almost circular with a circularity value close to 1 in prometaphase. Mean circularity slightly decreases from 0.9 in metaphase to 0.8 when centrosomes enter anaphase (Fig. 1, F and G). In GFP::PCMD-1-PBD^{m} embryos, the PCM scaffold fails to assemble into a spherical structure from the beginning. A mean circularity of 0.8 at prometaphase is comparable with the mean circularity of control centrosomes in anaphase, and it decreases even more dramatically when embryos progress to anaphase (Fig. 1, F and G). Accordingly, the area of the PCM scaffold is larger than the control at every time point analyzed (Fig. 1, F and H).

In summary, this indicates that embryos expressing PCMD-1-PBD^{m} are viable, albeit viability is lower than in control embryos. PCMD-1-PBD^{m} is less efficiently recruited to centrioles; however, these levels are sufficient to tether and assemble the PCM. Recruited PCM appears distorted and severely disorganized. Thus, by mutating predicted PBD sites of PLK-1 in PCMD-1, we have created a setting where the PCM is recruited to centrioles, and therefore, it allows us to analyze the role of PLK-1–binding sites of PCMD-1 in PCM scaffold assembly.

Phosphorylation by CDK-1 primes PLK-1 docking sites in PCMD-1

Previously, we demonstrated that PCMD-1 binds PLK-1 in a yeast two-hybrid system (Stenzel et al., 2021). We used the same assay to test whether, by mutating PLK-1–binding sites, PLK-1 binding is disrupted. When using PLK-1 as a bait and PCMD-1^{WT} or PCMD-1-PBD^{m} as preys, we found that the mutant version of PCMD-1 showed a compromised binding to PLK-1 (Fig. 2 A).

PLK-1 docking on a substrate requires priming of PBD-binding sites by PLK-1 itself or another kinase, such as CDK-1 (Garcia-Alvarez et al., 2007). Interestingly, four of the predicted PLK-1 PBD sites overlapped with phosphorylation motifs of CDK-1 (Table S1). We argued that CDK-1 could be a potential priming kinase for PLK-1 docking on PCMD-1. To test this, we purified PCMD-1^{WT} and PCMD-1-PBD^{m} from *Escherichia coli* and performed an *in vitro* kinase assay (Fig. 2 B). Here PCMD-1^{WT} was barely phosphorylated by hsPLK1 alone. Instead, hsCDK1 strongly phosphorylated PCMD-1^{WT}. This signal was reduced to background levels in PCMD-1-PBD^{m}, indicating that PCMD-1-PBD^{m} is lacking functional hsCDK1 phosphorylation sites. Interestingly, when both kinases were used in combination, phosphorylation signal was highly increased and a strong upward shift of the band was detected. No phosphorylation was detected in PCMD-1-PBD^{m}. These results indicate that PCMD-1 is primed by hsCDK1, which in turn facilitates hsPLK1 docking and phosphorylation, and that this phosphorylation is abolished in the mutated PCMD-1-PBD^{m} protein.

PLK-1 is reduced at the PCMD-1-PBD^{m} centrosome

PLK-1 levels at the centrosome are reduced, but not entirely eliminated, when PCMD-1 function is compromised (Erpf et al., 2019). Remaining PLK-1 in *pcmd-1(t3421)* mutant embryos is recruited by SPD-2. To explore whether by mutating PBD sites in PCMD-1, recruitment and maintenance of PLK-1 at the centrosome is affected, we made use of a strain expressing an endogenously mCherry-tagged PLK-1. In PCMD-1^{WT} embryos, PLK-1::mCherry is recruited to the centrosome during prophase and reaches its maximal levels at metaphase (0 s) (Fig. 2 C). Although cytoplasmic PLK-1 levels are higher at the anterior part of the embryo (Budirahardja and Gonczy, 2008; Rivers et al., 2008), we did not detect any difference between PLK-1 levels at the anterior versus posterior centrosome at metaphase (Fig. 2 C and Fig. S2 A). In late anaphase (120 s), PLK-1 levels at both centrosomes dropped and were undetectable (Fig. 2 C). To better visualize

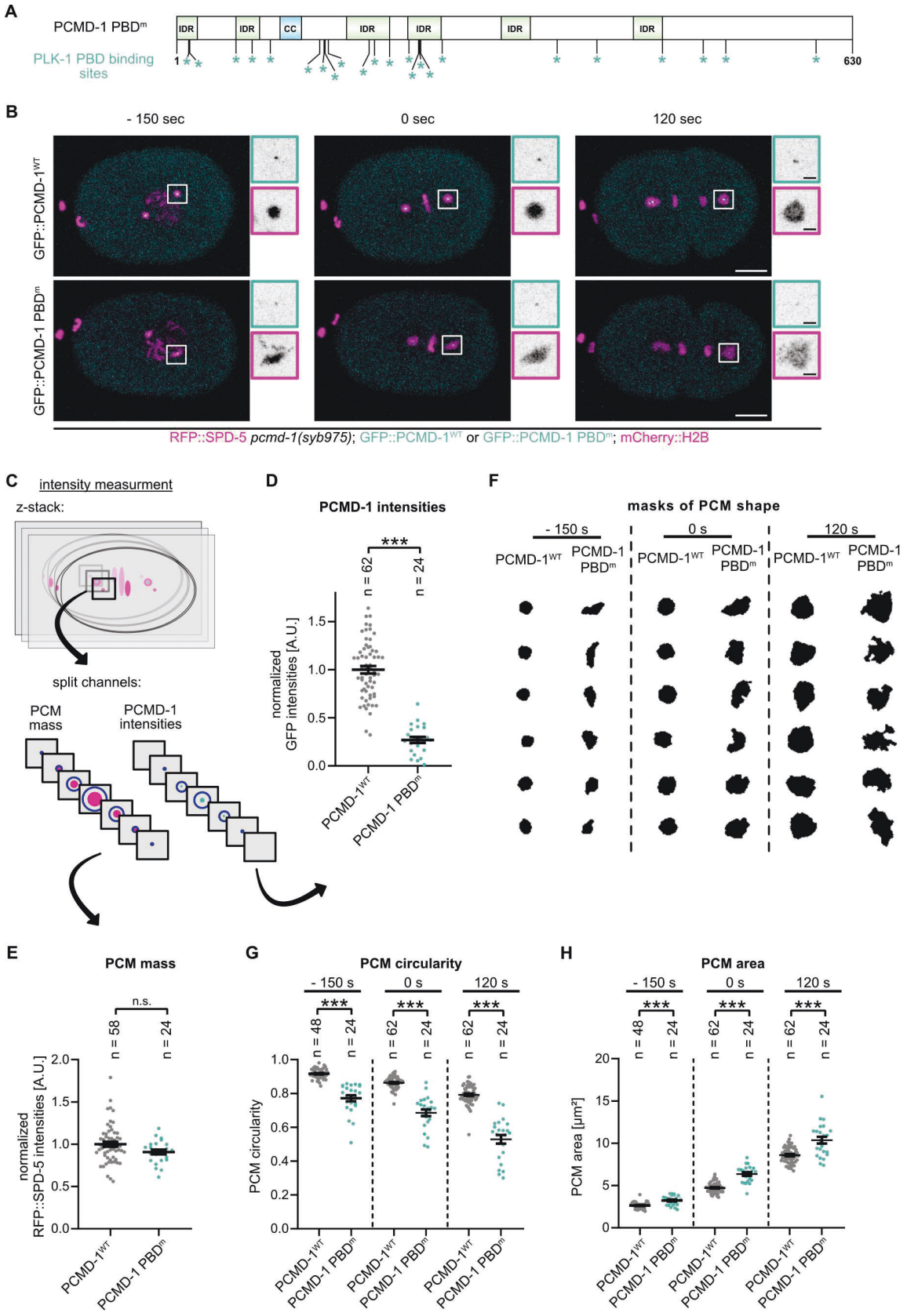

Figure 1. **PCMD-1-PBD^m leads to severe PCM scaffold disorganization. (A)** Schematic representation of PCMD-1^{WT} structure, with predicted IDRs (Varadi et al., 2024) in green and the coiled-coil region (CC) in blue. The position of the mutated PBD^m-binding sites is indicated by asterisks under the protein structure.

(B) Stills of time-lapse movies of embryos expressing GFP::PCMD-1^{WT} and GFP::PCMD-1-PBD^{m} in combination with mCherry::H2B and RFP::SPD-5 in the *pcmd-1(syb975)* background. Centrosomal areas are shown enlarged in insets. White scale bar = 10 µm; black scale bar = 2 µm. **(C)** Schematics of quantifications of PCM mass and PCMD-1 intensities. **(D)** Normalized GFP intensity values of GFP::PCMD-1^{WT} and GFP::PCMD-1-PBD^{m} at metaphase. **(E)** Normalized PCM mass at the centrosome during metaphase. **(F)** Representative examples of PCM shapes at the indicated time points. **(G)** Quantification of PCM circularities at the indicated time points. **(H)** Quantification of PCM area at indicated time points. For all movies, 0 s is metaphase. *n* = number of analyzed centrosomes. P values: n.s. >0.05 > * >0.01 > ** >0.001 > ***. Quantifications represent a subset of a larger dataset, fully presented in Figs. 7 and S5 (including corresponding statistics). See also Fig. S1; and Videos 1 and 2.

how PCMD-1^{WT} and PCMD-1-PBD^{m} levels correlate with PLK-1 levels at the centrosome, we plotted individual datapoints at early prophase (−240 s) and metaphase (0 s) (pink line, Fig. 2, D and E). At prophase, PLK-1 levels in PCMD-1-PBD^{m}–expressing embryos did not significantly differ from the controls. However, at this time point PLK-1 centrosomal levels were in general relatively low, which hinders a reliable comparison. At metaphase, the difference became more evident. In PCMD-1-PBD^{m} embryos, centrosomal PLK-1 levels were significantly reduced by nearly 30%.

To test whether this reduction was due to lower GFP::PCMD-1-PBD^{m} levels, we subjected GFP::PCMD-1^{WT} embryos to GFP RNAi (Fig. S2 B). Indeed, in GFP RNAi-treated embryos, where GFP::PCMD-1^{WT} levels were highly reduced (Fig. S2 C), PLK-1 levels were also low and comparable with the ones in GFP::PCMD-1-PBD^{m} (green and pink lines, Fig. 2, D and E). Therefore, PCMD-1 is needed to maintain WT PLK-1 levels at the mitotic centrosome. It is accountable for a part of PLK-1, with the remaining fraction being recruited by SPD-2 (Decker et al., 2011). The analyzed PLK-1 levels represent a sum of PLK-1 at the PCM core and PCM scaffold. When PLK-1–docking sites are mutated in SPD-2, centrosomal PLK-1 levels are highly reduced, but not fully abolished (Decker et al., 2011; Ohta et al., 2021). The remaining PLK-1 represents the PCMD-1–dependent fraction at the PCM core (Erpf et al., 2019). To specifically address PLK-1 recruitment to the PCM core in PCMD-1-PBD^{m} embryos, we subjected the embryos to *spd-2(RNAi)*. Live-cell imaging of control and PCMD-1-PBD^{m} embryos at prophase showed that PLK-1::mCherry is still being recruited to the PCM core in both strains (Fig. S2 D). In summary, recruitment of PLK-1 to the PCM core is unaffected by the absence of phosphorylation at the mutated PBD sites. This could be mediated by residual binding (Fig. 2 A) or by the remaining SPD-5 found at the PCM core in this background (Fig. S1 C). Unfortunately, due to the collapse of the mitotic spindle in *spd-2(RNAi)*, we could not assess PLK-1 at the PCM core during metaphase.

Since PLK-1 plays a key role in nuclear envelope breakdown, altered PLK-1 levels could impact cell cycle entry and progression (Martino et al., 2017). To rule out this possibility, we measured the length of the first two cell cycles of the PCMD-1^{WT} and PCMD-1-PBD^{m} embryos and found no significant difference in cell cycle progression between the two strains (Fig. S2 E).

Mutating putative CDK-1-phosphorylation sites in PCMD-1 does not lead to PCM scaffold disorganization

In vitro, hsCDK1 primes PCMD-1^{WT} for hsPLK1 phosphorylation, and in PCMD-1-PBD^{m}, where all four putative CDK-1 phosphorylation sites are mutated, phosphorylation by hsCDK1 is fully abolished (Fig. 2 B). To assess the extent to which CDK-1 phosphorylation sites contribute to PCM disorganization *in vivo*, we generated a strain expressing a PCMD-1 construct in which four previously identified CDK-1 sites, along with two additional predicted sites not included in the PCMD-1-PBD^{m} mutant, were mutated to alanine (Fig. 3 A). These additional sites, selected using a lower selection cutoff, were included to ensure the generation of a phosphodeficient CDK-1 mutant form of PCMD-1. Interestingly, in GFP::PCMD-1-CDK-1^{m} background, centrosomal PCMD-1 levels were reduced to 78% (Fig. 3 C); however, PCM mass and PCM shape parameter appeared largely unaffected (Fig. 3, B and D–F).

To identify sites that are phosphorylated by hsCDK1 in PCMD-1, we subjected the *in vitro* phosphorylated protein to mass spectrometry (MS) (Fig. 3 G). A total of four sites were recovered at least two times, with a 73% coverage of the protein, and they represent four of the six mutated sites in GFP::PCMD-1-CDK-1^{m}.

We conclude that *in vivo* phosphorylation by CDK-1 is required to recruit PCMD-1 to the centrosome at WT levels. However, in addition to the six mutated sites, CDK-1 phosphorylation at non-consensus sites or phosphorylation by other kinases may contribute to priming PCMD-1 for subsequent phosphorylation by PLK-1.

Distorted PCM scaffold responds to the modulation of microtubule-pulling forces

A labile PCM scaffold could fail to resist forces exerted by microtubules, which might explain its disorganization and flaring at different mitotic stages. To test this hypothesis, we decided to alter pulling forces exerted by the microtubules.

To decrease microtubule-pulling forces, we used RNAi treatment against the G protein activators GPR-1/2 (Colombo et al., 2003; Gotta et al., 2003; Grill et al., 2003; Tsou et al., 2003) and mock RNAi as a negative control (Fig. 4, A and B). If microtubule-pulling forces are responsible for PCM scaffold distortion, we expect that circularity and PCM area will be restored when these forces are reduced. The effectiveness of *gpr-1/2* RNAi was confirmed by failed posterior spindle displacement at metaphase (Panbianco et al., 2008) (Fig. S3 A). Interestingly, at prometaphase and metaphase, mean circularity of the PCM in *gpr-1/2* RNAi-treated PCMD-1-PBD^{m} embryos was not significantly different from mock-treated ones, meaning that diminished microtubule-pulling forces are unable to restore circularity (Fig. 4, C and D). Mean circularity at both stages had a lower value than that of the PCMD-1^{WT} embryos. In anaphase, in PCMD-1^{WT} embryos treated with *gpr-1/2* RNAi, circularity was restored to values of metaphase. Similarly, mean circularity in *gpr-1/2* RNAi-treated PCMD-1-PBD^{m} embryos was restored, albeit to a value comparable with a disassembling PCM in mock-

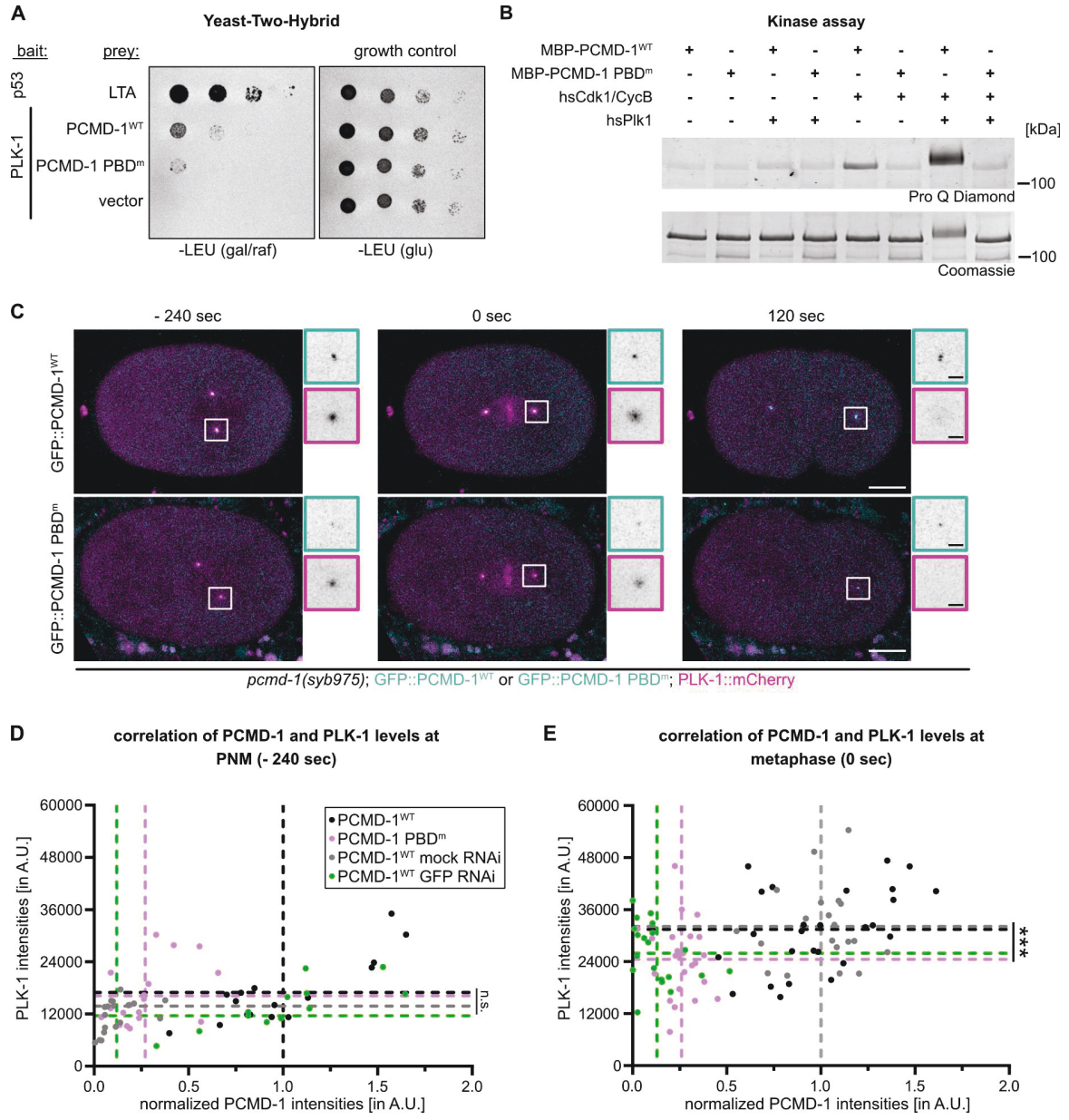

Figure 2. **CDK-1 priming facilitates PCMD-1 phosphorylation by PLK-1. (A)** PLK-1 bait interaction with PCMD-1^{WT} and PCMD-1-PBD^{m} preys in a yeast two-hybrid assay. p53 bait and LTA prey are positive controls. **(B)** Kinase assay of *in vitro* purified MBP::PCMD-1^{WT} and MBP::PCMD-1-PBD^{m} with active kinases hsPLK1 and hsCDK1/CycB. **(C)** Stills of time-lapse movies of embryos expressing GFP::PCMD-1^{WT} and GFP::PCMD-1-PBD^{m} in combination with PLK-1::mCherry in the *pcmd-1(syb975)* background. Centrosomal areas are shown enlarged in insets. 0 s is metaphase. White scale bar = 10 µm; black scale bar = 2 µm. **(D and E)** Correlation plots of PLK-1 levels and PCMD-1 levels at −240 and 0 s, respectively. Dashed lines indicate respective means. P values from Wilcoxon rank-sum test or two sample *t* test. Scale bar = 10 µm, *n* = number of analyzed centrosomes. P values: n.s. >0.05 > * >0.01 > ** >0.001 > ***. See also Fig. S2. Source data are available for this figure: SourceData F2.

treated PCMD-1^{WT} embryos. A similar trend was observed with the PCM area (Fig. 4, C and E). No significant changes were observed in PCMD-1-PBD^{m} embryos with *gpr-1/2 (RNAi)* in prometaphase and metaphase. In late anaphase, mean values of *gpr-1/2* RNAi-treated PCMD-1-PBD^{m} embryos were restored and fell slightly under the ones of mock-treated PCMD-1^{WT}.

PCM scaffold deformation could reflect changes in microtubule dynamics. To test whether microtubule dynamics were altered by introducing PBD mutations in PCMD-1, we crossed in the microtubule plus-end marker EBP-2::GFP and monitored astral microtubule dynamics (Fig. S3, B and C) (Wang et al., 2015). The number of EBP-2::GFP comets passing a fixed line shortly before metaphase was comparable between PCMD-1^{WT} and PCMD-1-PBD^{m} embryos, indicating that the microtubule nucleation rate from the distorted PCM is not altered.

A labile PCM scaffold should be easier to deform in the presence of increased microtubule-pulling forces. To increase microtubule-pulling forces, we knocked down casein kinase 1

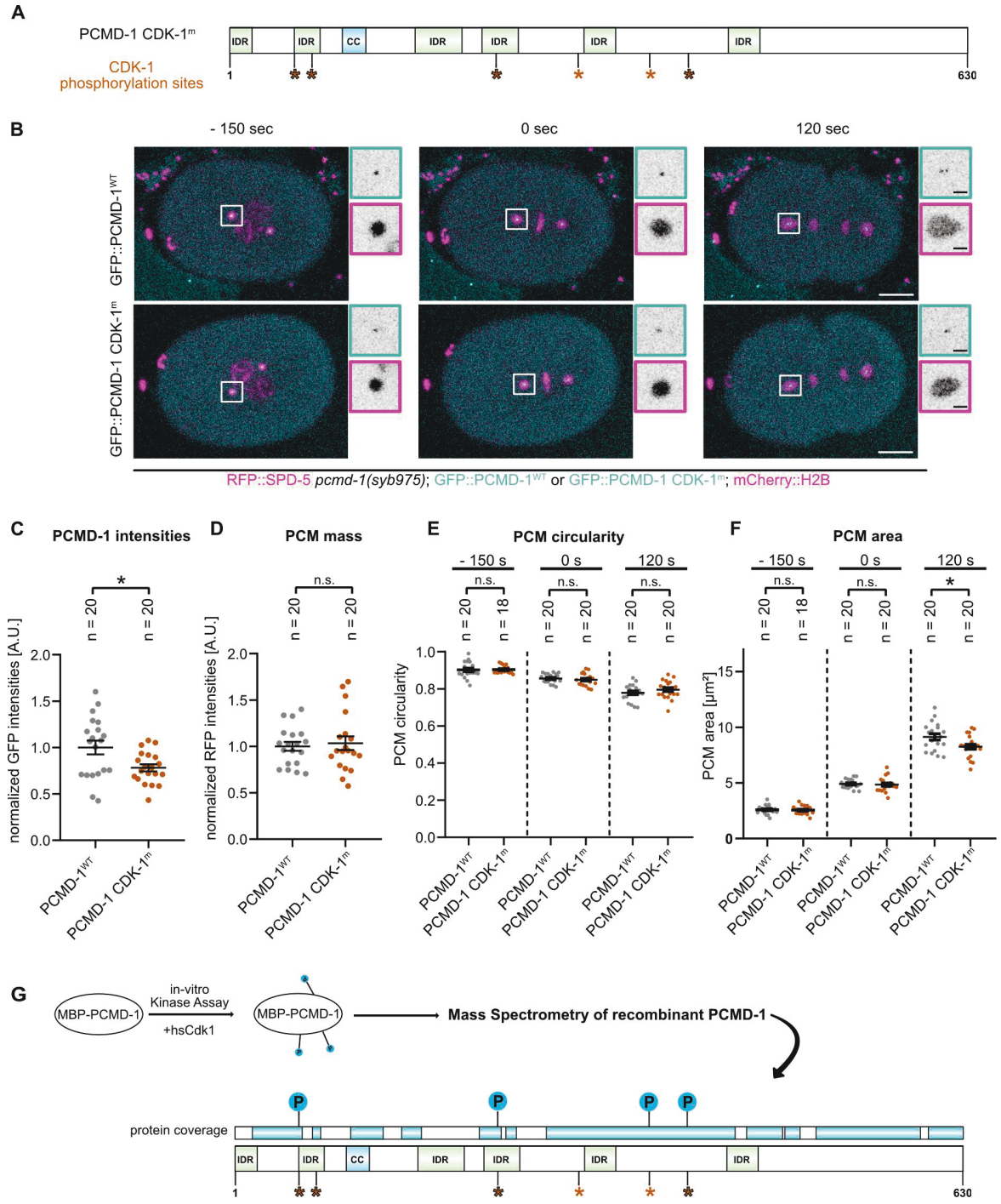

Figure 3. **Mutation of predicted and identified CDK-1 phosphorylation sites do not affect PCM shape. (A)** Schematic representation of the domain structure of PCMD-1 CDK-1^{m}, with predicted CDK-1^{m} phosphorylation sites indicated by asterisks under the protein structure. Bold asterisks indicate the CDK-1 phosphorylation sites that overlap with GFP::PCMD-1-PBD^{m}. **(B)** Stills of time-lapse movies of embryos expressing GFP::PCMD-1^{WT} and GFP::PCMD-1 CDK-1^{m} in combination with mCherry::H2B and RFP::SPD-5 in the *pcmd-1(syb975)* background. Centrosomal areas are shown enlarged in insets. White scale bar = 10 µm; black scale bar = 2 µm. **(C)** Normalized GFP intensities at the centrosome during metaphase. P value from Welch two sample *t* test. **(D)** Normalized PCM mass at the centrosome during metaphase. P value from Wilcoxon rank-sum test. **(E)** Quantification of PCM circularities at the indicated time points. P values from two sample *t* test or Wilcoxon rank-sum test. **(F)** Quantification of PCM area at indicated time points. P values from two sample *t* test. **(G)** Schematics of MS, coverage, and recovered hsCDK1 phosphorylation sites of PCMD-1^{WT}. For all movies; 0 s is metaphase. *n* = number of analyzed centrosomes. P values: n.s. >0.05 > * >0.01 > ** >0.001 > ***. CC, coiled-coil region.

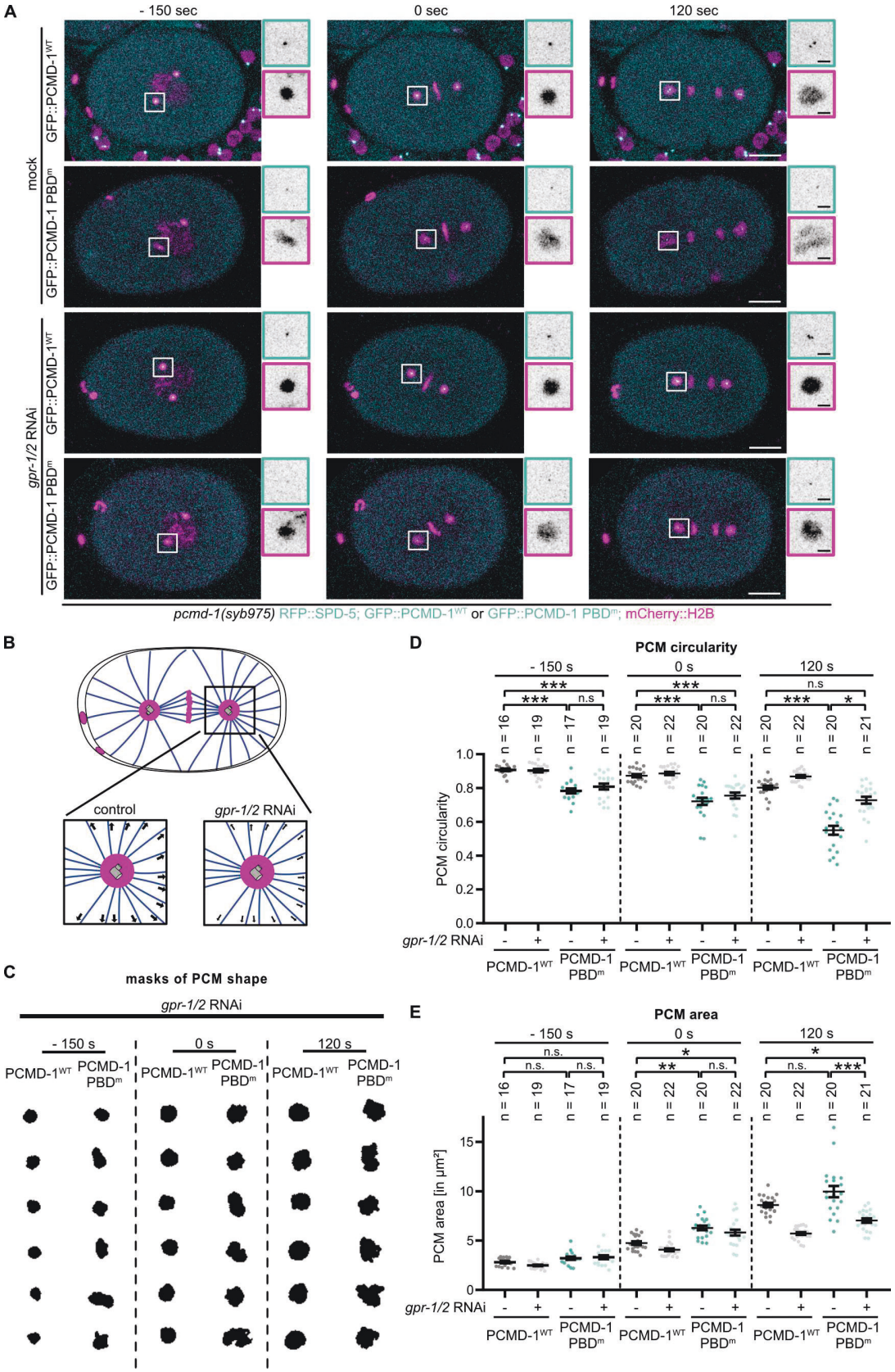

Figure 4. **Decreased microtubule-pulling forces partially rescue PCM scaffold distortion of PCMD-1-PBD^m centrosomes. (A)** Stills of time-lapse movies of embryos expressing GFP::PCMD-1^{WT} and GFP::PCMD-1-PBD^m in combination with mCherry::H2B and RFP::SPD-5 in the *pcmd-1(syb975)* background and

treated with mock or *gpr-1/2* RNAi. Centrosomal areas are shown enlarged in insets. White scale bar = 10 µm; black scale bar = 2 µm. **(B)** Schematics of change in microtubule-pulling forces in embryos treated with mock or *gpr-1/2* RNAi. **(C)** Representative examples of PCM shapes under *gpr-1/2* RNAi at the indicated time points. **(D)** Quantification of PCM circularities at the indicated time points. P values from Kruskal–Wallis test with Dunn post hoc. **(E)** Quantification of PCM area at indicated time points. P values from Kruskal–Wallis test with Dunn post hoc. For all movies, 0 s is metaphase. *n* = number of analyzed centrosomes. P values: n.s. >0.05 > * >0.01 > ** >0.001 > ***. See also Fig. S3.

gamma (CSNK-1), a kinase negatively regulating GPR-1/2 localization to the cortex. In *csnk-1* RNAi, cortical levels of GPR-1/2 are elevated and equalized, leading to an increase of pulling forces exerted at both spindle poles (Panbianco et al., 2008) (Fig. 5, A and B).

In PCMD-1^{WT} embryos, the PCM scaffold progressively deforms and shows decreased mean circularity and increased area values when higher pulling forces are applied (Fig. 5, D and E). Interestingly, circularity values of *csnk-1(RNAi)*-treated PCMD-1^{WT} centrosomes at prometaphase and metaphase showed less distortion compared with mock RNAi-treated PCMD-1-PBD^{m} centrosomes. This indicates that even increased microtubule-pulling forces are unable to distort the WT PCM to the same degree as PCMD-1-PBD^{m} centrosome.

When microtubule-pulling forces were increased in PCMD-1-PBD^{m} embryos, the already compromised PCM deformed even more dramatically (Fig. 5, A and C–E). From prometaphase going into metaphase, an extremely high degree of variability in mean circularity and area became evident. However, the impact was most obvious in anaphase, when the *csnk-1* RNAi-treated PCMD-1-PBD^{m} PCM dissembled and dissolved extremely rapidly (Fig. 5 C). It almost seemed to be torn apart by exerted pulling forces, showing a significantly lower value of circularity and increased area than the PCMD-1^{WT} control (Fig. 5, D and E).

In summary, microtubule-pulling forces are not the only cause for the shape distortion of the maturing PCM scaffold in PCMD-1-PBD^{m} at prometaphase and metaphase, and their reduction only partially restores the shape of a disassembling PCM in anaphase. *csnk-1(RNAi)* experiments revealed that the distorted PCM scaffold in the PCMD-1-PBD^{m} mutant is extremely labile and unable to withstand an increase in microtubule-pulling forces.

Reducing PCMD-1 levels leads to compromised PCM scaffold formation

We found centrosomal PCMD-1 levels to be decreased by 73% in PCMD-1-PBD^{m} embryos (Fig. 1 D), and this decrease could directly or indirectly cause the distortion of the PCM scaffold. To test this possibility, we decreased PCMD-1 levels by treating animals expressing GFP-tagged PCMD-1^{WT} with RNAi against GFP (Fig. 6 A). To achieve a stepwise decrease of PCMD-1^{WT} levels, we used a weak and a strong RNAi condition. Upon strong RNAi-treatment, mean PCMD-1 levels at the centrosome decreased to 12.6% of the mock-treated controls (Fig. 6 B). These levels were lower than the decrease caused by mutations in PCMD-1-PBD^{m}. The PCM mass was comparable with mock-treated embryos (Fig. 6 C); however, similar to PCMD-1-PBD^{m}, the PCM scaffold appeared more disorganized (Fig. 6, D and E). In weak GFP RNAi-treated embryos, PCMD-1^{WT} levels decreased to 35% of mock-treated embryos and showed an intermediate level of PCM scaffold disorganization (Fig. 6, B, D, and E). This indicates that a gradual decrease in PCMD-1 levels at the centrosome is followed by a progressive PCM disorganization.

To better illustrate how the degree of PCMD-1 levels relates to the PCM scaffold circularity in RNAi-treated PCMD-1^{WT} and PCMD-1-PBD^{m} embryos, we individually plotted all datapoints on a scatterplot (Fig. 6 F). For mock-treated or untreated PCMD-1^{WT} embryos, mean circularity values were close to 0.9 (gray and black dotted line). In strong and weak GFP RNAi-treated PCMD-1^{WT} controls, mean circularity dropped just below 0.8 (red dotted line) and 0.84 (light red dotted line), respectively. Interestingly, although the centrosomal intensities of PCMD-1-PBD^{m} were higher than in strong GFP RNAi-treated PCMD-1^{WT} embryos, PCM appeared more distorted, with mean circularity values dropping to 0.7 (blue dotted line). Further, we would like to point out that some of PCMD-1-PBD^{m} centrosomes (Fig. 6 F, blue dots circled with black line) with PCMD-1 levels higher than the mean of weak RNAi-treated embryos showed a very high degree of PCM disorganization. To directly compare PCM shape parameters of GFP RNAi-treated PCMD-1^{WT} centrosomes with PCMD-1-PBD^{m}, we selected datapoints that were close to the values of PCMD-1-PBD^{m} (±10% of mean levels) (Fig. 6 G). The mean intensity values were not different between the two datasets, while the PCM circularity and PCM area significantly dropped in PCMD-1-PBD^{m}.

Cumulatively, these results suggest that lowering PCMD-1 levels at the centrosome destabilizes the PCM scaffold. However, the degree of disorganization in PCMD-1-PBD^{m} exceeds the one caused by a simple decrease in PCMD-1 levels, pointing toward an additional layer of PCM scaffold destabilization caused by the introduced mutations at PBD sites in PCMD-1.

PCM fragmentation caused by SPD-5(Δ734–918) does not affect PCMD-1 recruitment to the centrosome

While PCMD-1 recruits and tethers SPD-5 to the centrioles, in turn SPD-5 can also recruit PCMD-1 to the ciliary base in a positive feedback loop (Garbrecht et al., 2021). Therefore, a labile PCM scaffold could potentially impair PCMD-1 recruitment to the centrosome and be an indirect cause of lowered PCMD-1-PBD^{m} levels at the centrosome. To test this possibility, we used the Δ734–918 deletion in the C-terminal "coiled-coil-long" domain in the endogenously tagged SPD-5 protein (Rios et al., 2024). In this mutant background, the PCM exhibits microtubule-dependent PCM fragmentation due to an aberrant self-interaction of SPD-5. We combined this strain with an endogenously GFP-tagged PCMD-1 and tested whether PCMD-1 levels were affected in this background.

As shown by Rios et al. (2024), in SPD-5(Δ734–918) mutant embryos, the PCM mass is largely diminished compared with control embryos, and the PCM scaffold has an irregular and

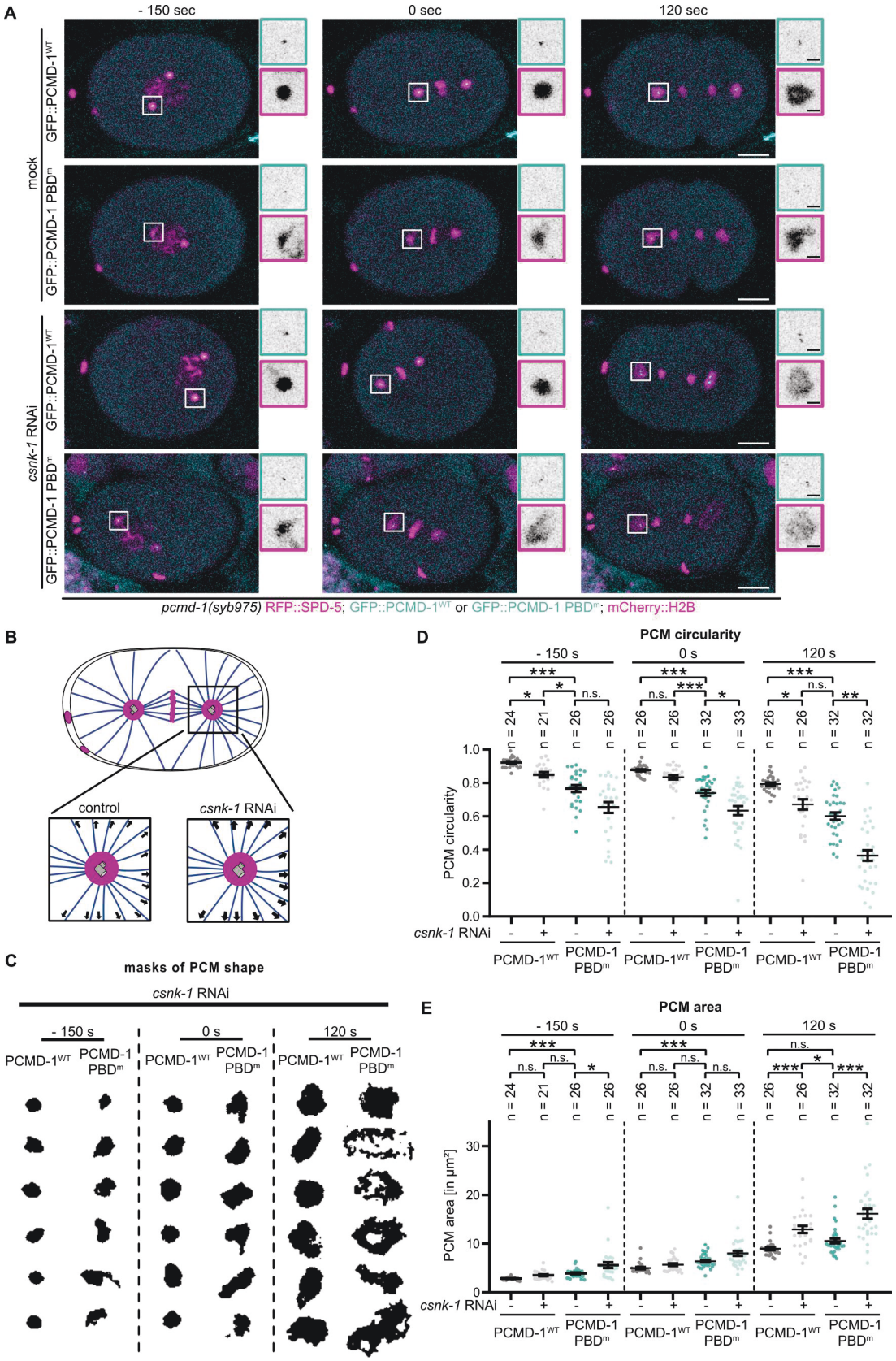

Figure 5. **PCMD-1-PBD^{m} centrosomes cannot counteract increased microtubule-pulling forces. (A)** Stills of time-lapse movies of embryos expressing GFP::PCMD-1^{WT} and GFP::PCMD-1-PBD^{m} in combination with mCherry::H2B and RFP::SPD-5 in the *pcmd-1(syb975)* background and treated with mock or *csnk-1*

RNAi. Centrosomal areas are shown enlarged in insets. White scale bar = 10 µm; black scale bar = 2 µm. **(B)** Schematics of change in microtubule-pulling forces in embryos treated with mock or *csnk-1* RNAi. **(C)** Representative examples of PCM shapes under *csnk-1* RNAi at the indicated time points. **(D)** Quantification of PCM circularities at the indicated time points. P values from Kruskal–Wallis test with Dunn post hoc. **(E)** Quantification of PCM area at indicated time points. P values from Kruskal–Wallis test with Dunn post hoc. For all movies, 0 s is metaphase. *n* = number of analyzed centrosomes. P values: n.s. >0.05 > * >0.01 > ** >0.001 > ***.

distorted shape (Fig. S4, A, C, and D). In prometaphase, when PCMD-1-PBD^{m} is already disordered, SPD-5(Δ734–918) PCM scaffold appeared spherical and comparable with the control (compare Fig. 1 G and Fig. S4 D). Deviations in mean circularity of SPD-5(Δ734–918) PCM became apparent at metaphase and increased during anaphase, coincidental with the increased tension exerted by microtubule-pulling forces (Fig. S4, C and D). At metaphase, mean circularity values dropped from 0.9 to 0.7 in the SPD-5(Δ734–918) embryos. Despite a less dense and more disorganized PCM in SPD-5(Δ734–918) animals, PCMD-1 levels were similar to the ones of a WT SPD-5 PCM. Therefore, a disorganized PCM does not lead to failed PCMD-1 recruitment to the centrosome.

PBD sites in the N-terminal part of PCMD-1 are needed to form a stable PCM scaffold

To further discriminate between these two levels of regulation and to narrow down regions playing a role in PCM stabilization, we set out to create a mutant version of PCMD-1 that would uncouple its function in centrosome destabilization from centrosome localization. In our previous studies, we have shown that the C-terminal part of PCMD-1 is needed for its robust loading to the centrosome (Stenzel et al., 2021). We reasoned that mutations in the C-terminal part of the protein could be responsible for low PCMD-1 levels at the centrosome, and swapping the mutant C terminus with a WT sequence would potentially lead to increased PCMD-1 levels at the centrosome. Therefore, we created a transgene harboring 17 mutated PLK-1–binding sites only in the N-terminal part (PCMD-1-PBD^{m}N^{ter}) and a complementary transgene carrying six mutations in the C-terminal part (PCMD-1-PBD^{m}C^{ter}) (Fig. 7 A and Table S1). Indeed, by reintroducing WT-binding sites in the C-terminal part of the protein, we could elevate centrosomal levels of PCMD-1-PBD^{m}N^{ter} to 51% of PCMD-1^{WT} controls (Fig. 7, B and C; and Fig. S1 B). Mean centrosomal levels in the PCMD-1-PBD^{m}C^{ter} transgene were reduced, but not significantly different from the PCMD-1^{WT} ones.

Interestingly, in PCMD-1-PBD^{m}N^{ter} embryos, the PCM scaffold still appeared very labile and deformed (Fig. 7 D; and Fig. S5, A and B). The PCM disorganization started from prometaphase and increased at metaphase and anaphase. Mean PCM circularity and area at prometaphase, metaphase, and anaphase were still comparable with the ones of PCMD-1-PBD^{m}. In contrast, in PCMD-1-PBD^{m}C^{ter} embryos, dynamics of the PCM shape were largely unaffected over time. Mean PCM area and circularity of PCMD-1-PBD^{m}C^{ter} at metaphase and anaphase were not different from control embryos (Fig. 7 D; and Fig. S5, A and B). PCM mass was unaffected in PCMD-1-PBD^{m}N^{ter}; however, it slightly dropped in PCMD-1-PBD^{m}C^{ter} (Fig. S5 C). Together, these data suggest that the 17 residues in the N terminus are critical to stabilize the PCM.

We previously showed that the most N-terminal part of PCMD-1, spanning the first two intrinsically disordered regions (IDRs) and including two predicted CDK-1 priming sites, was dispensable for PCMD-1 function (Stenzel et al., 2021). To further narrow down mutated residues, we created a transgene where mutations in the first 100 amino acids were changed back to their WT versions and named this construct PCMD-1-PBD^{m}N^{terShort} (Fig. 7 A). PCMD-1-PBD^{m}N^{terShort} contains 12 mutated residues, including only one CDK-1 priming site, T228 (Fig. S5 E, bold). When PCMD-1-PBD^{m}N^{terShort} was tested for PCMD-1 levels and PCM shape properties, we found that PCMD-1 levels were not significantly different from PCMD-1-PBD^{m}C^{ter}; however, PCM circularity and area were comparable with the ones of PCMD-1-PBD^{m}N^{ter} embryos (Fig. 7, B–D; and Fig. S5, A and B).

To better visualize the impact of reduced number of PBD-binding sites in PCMD-1 on PCM disorganization, we plotted individual datapoints of centrosomal PCMD-1 levels of the PCMD-1-PBD^{m}N^{ter}, PCMD-1-PBD^{m}C^{ter}, and PCMD-1-PBD^{m}N^{terShort} against PCM circularity (Fig. S5 D). In PCMD-1-PBD^{m}N^{ter}, with 51% of control intensity levels, the PCM is still highly disorganized (gray and dark blue dotted lines). Interestingly, for PCMD-1-PBD^{m}C^{ter}, where the mean intensity was reduced to 76%, PCM circularity was just below 0.9, exactly the same as in the control embryos (gray and light blue dotted lines). Instead, for PCMD-1-PBD^{m}N^{terShort} (pink dotted lines), centrosomal intensity was not significantly different from PCMD-1-PBD^{m}C^{ter}; its mean PCM circularity was below the 0.8 mark, exactly overlaying with the one of PCMD-1-PBD^{m}N^{ter}. Therefore, besides PCMD-1 centrosomal levels, mutations in the PBD-binding sites have an impact on the PCM structure, and the 12 residues, falling into a completely unstructured region of PCMD-1, are critical to stabilize the PCM scaffold (Fig. S5 E and Video 3).

Taken together, these data support the previously suggested two layers of PCM dysregulation in PCMD-1-PBD^{m}, one caused by the decreased levels of PCMD-1 at the centrosome and a second one, which is induced by the mutations in potential PLK-1 docking sites.

PBD sites in the N-terminal part of PCMD-1 are needed for PLK-1 and SPD-5 interaction in HEK293T cells

By mutating the predicted PLK-1–binding sites in PCMD-1, we significantly disrupted PCM stability but only reduced PLK-1 and did not change SPD-5 levels at the centrosome (Fig. 1 E and Fig. 2 E). In *C. elegans* PCMD-1-PBD^{m} embryos, PLK-1 and SPD-5 recruitment to centrosome could be mediated by redundant pathways and therefore mask a change in the interaction between PCMD-1 with PLK-1 or SPD-5. To systematically assess the impact of PBD mutations on PLK-1 and SPD-5 binding, we transiently expressed WT and modified PCMD-1 proteins in human HEK293T cells. EGFP-tagged PCMD-1^{WT} localized to

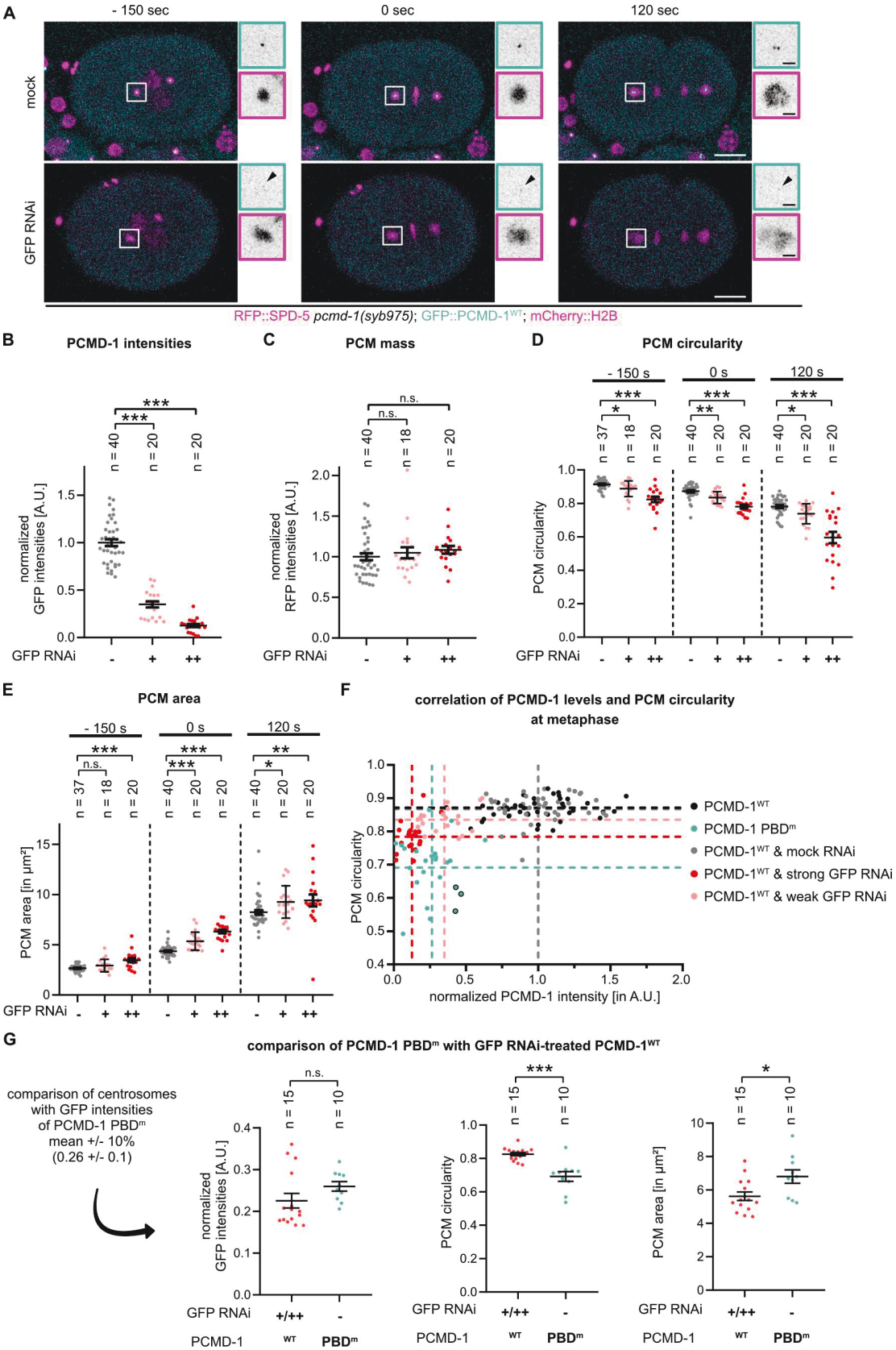

Figure 6. **Reducing PCMD-1^{WT} levels leads to a compromised PCM scaffold formation. (A)** Stills of time-lapse movies of embryos expressing GFP::PCMD-1^{WT} in combination with mCherry::H2B and RFP::SPD-5 in the *pcmd-1(syb975)* background treated with mock and strong GFP RNAi. Centrosomal areas are

shown enlarged in insets. White scale bar = 10 µm; black scale bar = 2 µm. **(B)** Normalized GFP intensities at the centrosome during metaphase. P value from a Kruskal–Wallis test with Dunn post hoc. **(C)** Normalized PCM mass at the centrosome during metaphase. P value from Kruskal–Wallis test with Dunn post hoc. **(D)** Quantification of PCM circularities at the indicated time points. P values from a Kruskal–Wallis test with Dunn post hoc. **(E)** Quantification of PCM area at indicated time points. P values from a Kruskal–Wallis test with Dunn post hoc. **(F)** Scatter plot correlating normalized GFP intensities and PCM circularities at metaphase of PCMD-1-PBD^{m} and GFP::PCMD-1^{WT} treated with mock, weak, and strong GFP RNAi. Dashed lines indicate the mean of the corresponding condition. Circled dots highlight datapoints with intermediate GFP::PCMD-1-PBD^{m} levels and a high level of PCM disorganization. **(G)** Direct comparison of GFP::PCMD-1-PBD^{m} levels and PCM scaffold parameters with similar, weak, and strong GFP RNAi-treated GFP::PCMD-1^{WT} centrosomes from F. For all movies, 0 s is metaphase. *n* = number of analyzed centrosomes; + indicates weak and ++ strong GFP RNAi. P values: n.s. >0.05 > * >0.01 > ** >0.001 > ***. See also Fig. S4.

microtubules (Fig. 8, A and B) and was able to recruit mCherry::PLK-1 and mCherry::SPD-5 to this ectopic location in 88% and 86% of the cells, respectively. Interestingly, EGFP::PCMD-1-PBD^{m} localized to microtubules with the same efficiency, however, it was less efficient in recruiting its binding partners (Fig. 8, A and B). mCherry::PLK-1 localized to ectopic locations in only 24% of the cells to EGFP::PCMD-1-PBD^{m}–decorated microtubules. mCherry::SPD-5 was recruited in 4% of cells and additionally formed spherical aggregates in the cytoplasm, which are reminiscent of Cdk5Rap2 condensates in cells (Fong et al., 2008; Yoo et al., 2025). Interestingly, EGFP::PCMD-1-PBD^{m}C^{ter} recruited PLK-1 and SPD-5 with an efficiency similar to PCMD-1^{WT}, while EGFP::PCMD-1-PBD^{m}N^{ter} and EGFP::PCMD-1-PBD^{m}N^{terShort} bind slightly better than EGFP::PCMD-1-PBD^{m} (Fig. 8, A and B). This corresponds to the performance of PCMD-1-PBD^{m}N^{ter}, PCMD-1-PBD^{m}C^{ter}, and PCMD-1-PBD^{m}N^{terShort} in terms of PCM stability in the *C. elegans* embryos.

To test for reciprocal binding, we used a "bead recruitment assay" (Qi et al., 2025). Lysates of the HEK293T cells were applied to an RFP-Trap (Fig. 8 C). mCherry::PLK-1 and mCherry::SPD-5 did bind to the RFP-Trap beads and acted as a bait for the recruitment of EGFP-tagged PCMD-1 protein variants. Similar to microtubules, EGFP::PCMD-1^{WT} and EGFP::PCMD-1-PBD^{m}C^{ter} strongly decorated both mCherry::PLK-1 and mCherry::SPD-5–bound beads, while EGFP::PCMD-1-PBD^{m}, EGFP::PCMD-1-PBD^{m}N^{ter}, and EGFP::PCMD-1-PBD^{m}N^{terShort} levels at the beads were close to the background. These assays further strengthen our hypothesis that by mutating PBD-binding sites in PCMD-1, we compromise the interaction with PLK-1 and SPD-5. Since PCMD-1-PBD^{m}N^{ter} and PCMD-1-PBD^{m}N^{terShort} in all assays behave comparably with PCMD-1-PBD^{m}, we can assume that residues critical for these interactions are located in the N terminus of PCMD-1. Of the 17 mutated PBD sites in the N terminus, three sites have a phosphorylation motif of CDK-1. To verify that these sites are still primed by CDK-1 and phosphorylated by PLK-1, we purified the N-terminal fragment of protein spanning from amino acids 2–262 (PCMD-1$^{WT(2–262)}$) and the corresponding mutated version (PCMD-1-PBD$^{m(2–262)}$) and performed an *in vitro* kinase assay (Fig. 8 D). While PCMD-1$^{WT(2–262)}$ was primed by hsCDK1 and highly phosphorylated by hsPLK1, mutated PCMD-1-PBD$^{m(2–262)}$ did not show any phosphorylation. Curiously, the shift of the phosphorylated PCMD-1$^{WT(2–262)}$ band shows three distinct bands, which could reflect the three CDK-1 phosphorylation sites in PCMD-1$^{WT(2–262)}$ (Fig. 8 D).

In summary, in HEK293T cells, mutations of PBD sites in the N-terminal part of PCMD-1, which are deficient in hsCDK1 priming and hsPLK1 phosphorylation, strongly disrupt its interaction with both PLK-1 and SPD-5.

Centrosome separation is delayed in PCMD-1-PBD^{m}N^{ter}

In vertebrates, centriole separation depends on cleavage of PCNT by separase at anaphase onset (Kim et al., 2015; Lee and Rhee, 2012; Matsuo et al., 2012). In *C. elegans*, separase does not play a role in centriole separation. According to the current model, pericentriolar material traps the centriole pair at the spindle pole (Cabral et al., 2013). At anaphase, PCM weakening and disassembly by microtubule-pulling forces allow centrioles to separate. Whether this release is a passive process and merely a consequence of PCM disassembly or, alternatively, requires a relay of microtubule-pulling forces to the centrioles is not known. The PCM scaffold in PCMD-1-PBD^{m}N^{ter} is weakened and labile and is therefore an ideal setting to test whether a compromised PCM can still relay the tension generated by the pulling forces to the centrioles.

Therefore, we set out to measure and analyze centriole separation dynamics in a 3D volume at each spindle pole in PCMD-1-PBD^{m}N^{ter} embryos (Fig. 9 A), as the intermediate PCMD-1 levels allow us to track the centrioles easily over time. In control embryos, starting from 60 s after metaphase, two slightly separated but still largely overlapping foci were evident. We consider this time period as "centriole disengagement." On average, the first time point at which one could clearly discriminate two independent centriole foci was at 150 s for the anterior pole and 120 s for the posterior. We set the distance of 0.6 µm as a threshold and determined this time point as the "onset of centriole separation" (Fig. 9, B and C). We scored centriole separation until the newly formed centrosomes touched the nuclear envelope, where other dynein-dependent mechanisms could influence centriole movement (De Simone et al., 2016). Centriole separation dynamics differ at the two poles and correlate with differences in microtubule-pulling forces and PCM disassembly dynamics. At the anterior, centrioles separate slowly, with a flatter curve over time. Instead, at the posterior pole, where microtubule-pulling forces are higher, centriole separation started faster and slightly plateaued around 300 s after metaphase (Fig. 9, B and C).

In PCMD-1-PBD^{m}N^{ter} embryos, centriole separation was significantly delayed. Two distinct foci could be first discriminated at 270 s at the anterior and at 240 s at the posterior pole (Fig. 9 A [lower panel], Fig. 9, B and C). The two foci remained in close proximity for a longer period of time and eventually moved apart, but within the timeframe of our analysis, they never reached the same distance as the control embryos. Interestingly, the posterior pair separated with a similar dynamic as the pair at the anterior pole. In contrast, in PCMD-1-PBD^{m}C^{ter}, where the PCM is not disorganized, centrioles separated similarly to the control ones (Fig. 9 A [lower panel], Fig. 9, B and C). Centrioles

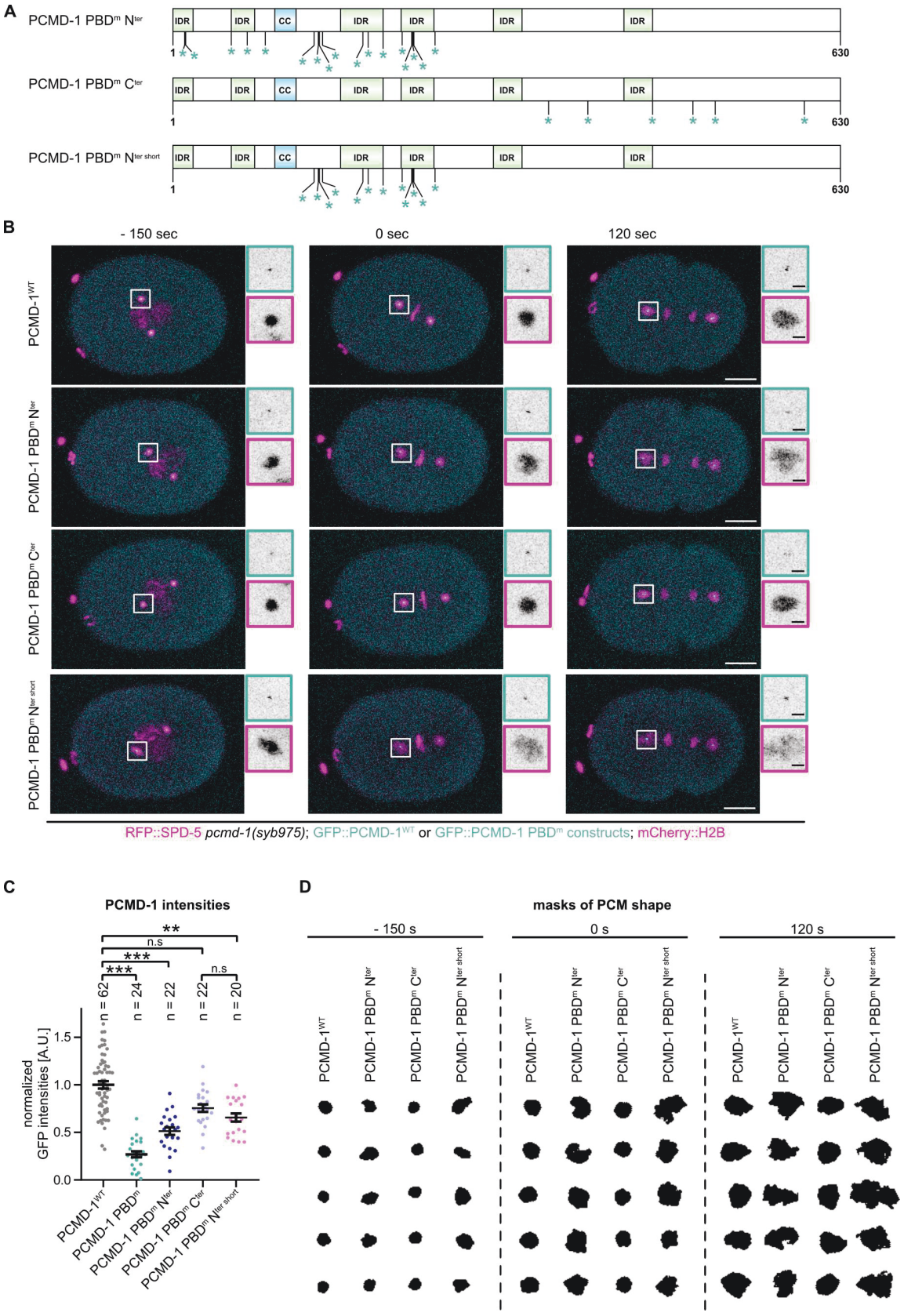

Figure 7. **PBD sites in the N-terminal part of PCMD-1 are needed to form a stable PCM scaffold. (A)** Schematic representation of the domain structure of PCMD-1-PBD^{m}N^{ter}, PCMD-1 -PBD^{m}C^{ter}, and PCMD-1-PBD^{m}N^{terShort}, with predicted PLK-1-PBD^{m}–binding sites indicated by asterisks under the protein

structure. **(B)** Stills of time-lapse movies of embryos expressing GFP::PCMD-1^{WT}, GFP::PCMD-1-PBD^{m}N^{ter}, PCMD-1-PBD^{m}C^{ter}, and PCMD-1-PBD^{m}N^{terShort} in combination with mCherry::H2B and RFP::SPD-5 in the *pcmd-1(syb975)* background. Centrosomal areas are shown enlarged in insets. White scale bar = 10 µm; black scale bar = 2 µm. **(C)** Normalized GFP intensities at the centrosome during metaphase. P value Kruskal–Wallis test with Dunn post hoc. **(D)** Representative examples of PCM shapes of GFP::PCMD-1^{WT}, PCMD-1-PBD^{m}N^{ter}, PCMD-1-PBD^{m}C^{ter}, and PCMD-1-PBD^{m}N^{terShort} at the indicated time points. For all movies, 0 s is metaphase. *n* = number of analyzed centrosomes. P values: n.s. >0.05 > * >0.01 > ** >0.001 > ***. See also Fig. S5. CC, coiled-coil region.

disengagement and separation started around the same time as in control embryos. The general separation dynamics were similar to the control, with the exception that at the anterior pole, separation was somewhat delayed at later time points.

These data speak for a model where a strong and ductile PCM scaffold relays microtubule-pulling forces to the centrioles during separation. If so, we would expect that any kind of weakening of the PCM should have a similar effect on centriole separation.

To test this idea, we once again turned to the SPD-5(Δ734–918) mutant embryos and analyzed centriole separation in this background (Fig. S4 E). To our surprise, we found that centriole separation was largely unaffected. Mean time points of the onset of centriole separation at both poles coincided with the one of the control embryos, and separation dynamics were comparable with controls. Only at the posterior pole, centrioles separate with a higher variability, and on average, did not separate to the same extent as in the control embryos.

In summary, at the poles of PCMD-1-PBD^{m}N^{ter} embryos, centrioles fail to separate in a timely manner, and the delay in separation cannot be explained solely by the disorganization of the PCM scaffold. Mutated PBD-binding sites in PCMD-1 could act as a part of the relay mechanism by which centrioles are separated during PCM disassembly.

Discussion

Here we show that PLK-1 binds and phosphorylates CDK-1 primed PCMD-1 and that this interaction contributes to PCM integrity and centriole separation.

Over the course of mitosis, the PCM scaffold isotopically grows and undergoes changes in its physical properties (Laos et al., 2015; Mittasch et al., 2020). It transitions from a strong and ductile state, resisting microtubule-pulling forces at metaphase, to a labile or more brittle state in anaphase, where it undergoes dispersal and dissolution (Mittasch et al., 2020). Interestingly, recent cryo-ET analysis could not reveal any structural differences of the PCM over the cell cycle (Tollervey et al., 2025), suggesting that the described alterations in physical properties are driven by qualitative modulations of PCM components. The switch to a brittle scaffold that is less resistant to microtubule forces and more prone to disassembly coincides with a reduction in PLK-1 centrosomal levels, and chemical inhibition of PLK-1 at metaphase triggers premature PCM disassembly (Cabral et al., 2019; Mittasch et al., 2020). It has been proposed that the balance between PLK-1 phosphorylation and dephosphorylation by the counteracting PP2A phosphatase drives the abovementioned changes in material properties of the PCM (Magescas et al., 2019; Mittasch et al., 2020).

In our previous work, we showed that PCMD-1, a protein with several IDRs, interacts with SPD-5 and PLK-1 (Stenzel et al., 2021). However, the impact of these interactions on PCM scaffold dynamics had not been explored. Here, we show that *in vitro* PCMD-1 is primed by hsCDK1 and subsequently highly phosphorylated by hsPLK1. When putative PLK-1 docking sites are mutated in PCMD-1, both hsCDK1 priming and hsPLK1 phosphorylation are reduced to background levels, indicating that PLK-1 binds and phosphorylates PCMD-1, and CDK-1 is a priming kinase.

However, mutating CDK-1 phosphorylation sites *in vivo* did not lead to the same disorganization of the PCM. Although the PCMD-1-PBD^{m} construct harboring four of the six mutated CDK-1 phosphorylation sites and is not phosphorylated by hsCDK1, we might have missed additional CDK-1 sites *in vivo*. Alternatively, CDK-1 might not be the only priming kinase for PCMD-1 *in vivo*. PLK-1 itself or other mitotic kinases, such as Aurora A, could also contribute to PCMD-1 priming, along with CDK-1 in *C. elegans* embryos.

When PBD-binding sites in PCMD-1 are mutated, PLK-1 levels at the PCM scaffold during metaphase are reduced by approximately one-third. Similarly, strong RNAi-mediated depletion of WT PCMD-1 results in a comparable reduction in PLK-1 levels. These findings suggest that sufficient centrosomal PCMD-1 is necessary to maintain PLK-1 at the centrosome, while the remaining PLK-1 is likely recruited through SPD-2 activity.

In contrast to PLK-1, SPD-5 is recruited to the centrosome comparable with WT levels in PCMD-1-PBD^{m}, while the scaffold assembles in an aberrant manner. A distorted and flared PCM scaffold is already evident during PCM maturation when the cell transitions from prophase to metaphase. Compared with PCMD-1-PBD^{m}, in SPD-5(Δ734–918) the PCM mass is much lower, indicating a less efficient scaffold recruitment. Nevertheless, the low amount of PCM mass does not translate into a higher degree of disorganization at prometaphase. PCM maturation of the SPD-5(Δ734–918) scaffold seems to be unaffected, and defects in the PCM scaffold are only revealed at the metaphase when microtubule-pulling forces become most active and displace the spindle. In contrast, in PCMD-1-PBD^{m} the scaffold seems to assemble in an abnormal way from the moment of its recruitment to the centrioles.

How aberrant the PCM scaffold actually is, is best described by its response to the modulation of microtubule-pulling forces. PCM distortion at prometaphase and metaphase is evident by exaggerated deformation of its shape parameters when higher pulling forces are applied under *csnk-1 RNAi*. In contrast, when pulling forces are decreased by using *gpr-1/2 RNAi*, the shape of the distorted centrosome is not restored to WT circularity. Although we cannot entirely rule out that residual microtubule-pulling forces act on the PCM, PCM scaffold shapes do not change significantly, despite the failed posterior displacement of the metaphase spindle, which is a readout for the decreased

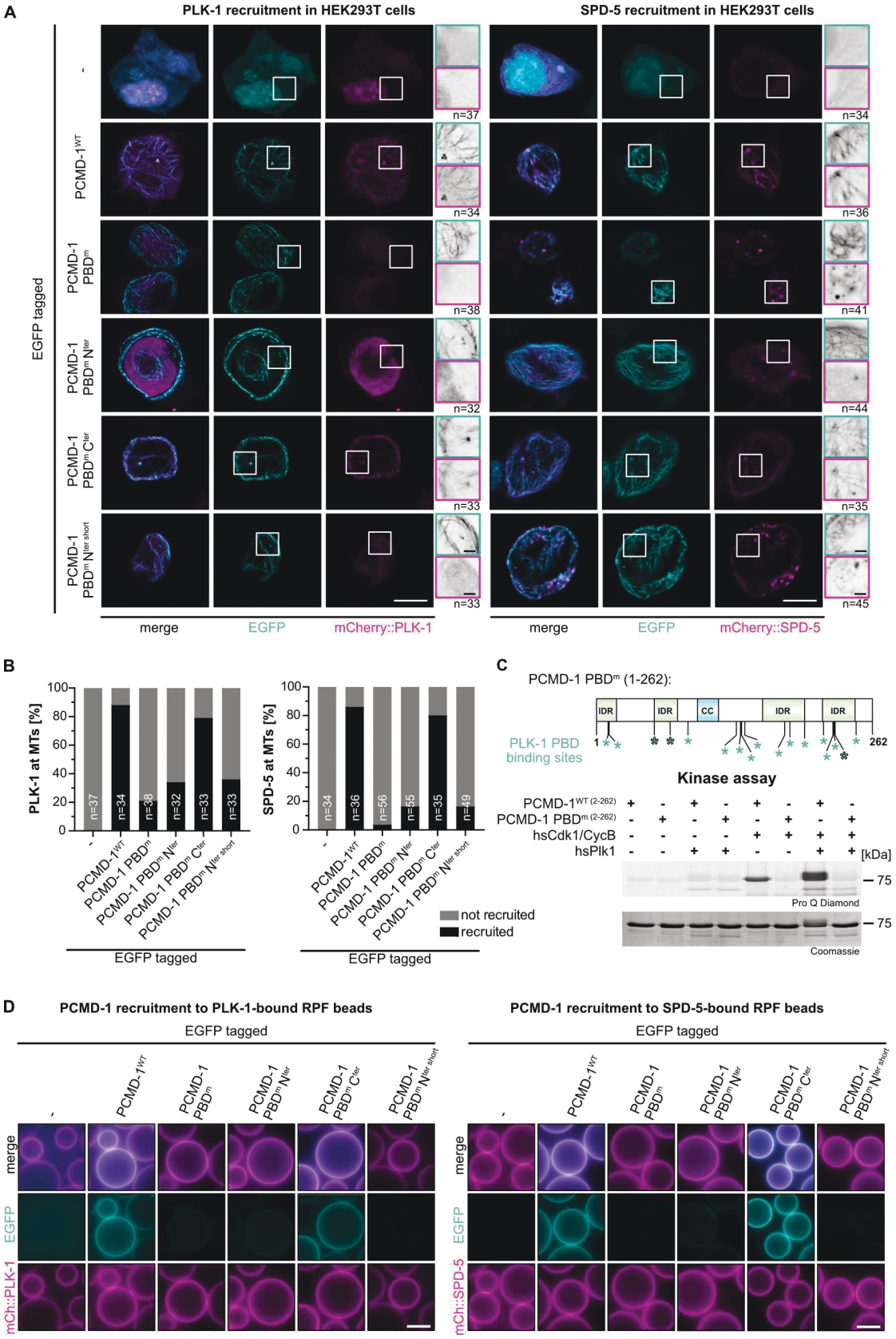

Figure 8. **PBD sites in the N-terminal part of PCMD-1 are needed for PLK-1 and SPD-5 recruitment. (A)** Representative images of HEK293T cells expressing EGFP::PCMD-1^{WT}, EGFP::PCMD-1-PBD^{m}, EGFP::PCMD-1-PBD^{m}N^{ter}, EGFP::PCMD-1-PBD^{m}C^{ter}, EGFP::PCMD-1-PBD^{m}N^{terShort}, or cytoplasmic EGFP, in

combination with mCherry::PLK-1 or mCherry::SPD-5, respectively. White scale bar = 10 µm; black scale bar = 2 µm. **(B)** Quantifications of % of cells recruiting either mCherry::PLK-1 or mCherry::SPD-5, respectively, to the microtubules. *n* = number of cells. **(C)** Kinase assay of *in vitro* purified N-terminal 262 amino acids of MBP::PCMD-1^{WT} and MBP::PCMD-1-PBD^{m} with active kinases hsPLK1 and hsCDK1/CycB. **(D)** Bead recruitment assay of immobilized mCherry::PLK-1 or mCherry::SPD-5 in combination with cytoplasmic EGFP, EGFP::PCMD-1^{WT}, EGFP::PCMD-1-PBD^{m}, EGFP::PCMD-1-PBD^{m}N^{ter}, EGFP::PCMD-1-PBD^{m}C^{ter}, or EGFP::PCMD-1-PBD^{m}N^{terShort}. Analyses were done on ≥50 fields in three independent replicates. Scale bar = 50 µm. Source data are available for this figure: SourceData F8.

microtubule-pulling forces at this time point. Together, this indicates that the PCM in PCMD-1-PBD^{m} is formed in a less condensed manner; the initial shape distortion of the PCM cannot entirely be attributed to microtubule-pulling forces and is most likely a result of an intrinsically aberrant assembly of the scaffold. In anaphase, the already structurally weakened PCM is completely unable to counteract increased microtubule-pulling forces. The scaffold is literally torn apart and dispersed. The disorganized PCM scaffold in prometaphase very much resembles the one caused by centriole ablation before NEBD (Cabral et al., 2019). Due to the ablation, the PCM scaffold seems to have lost its tether at the center and disperses in a microtubule-dependent manner. However, in contrast to centriole ablation, in PCMD-1-PBD^{m}, reduction of microtubule-pulling forces does not restore PCM circularity, supporting the possibility that the PCM scaffold has intrinsically different properties from the moment of its formation.

PCMD-1 levels at the centrosome are highly reduced in PCMD-1-PBD^{m} and, to a lesser extent, in PCMD-1-CDK-1^{m} (Fig. 1 D and Fig. 3 C). As PCMD-1 is an intrinsically disordered protein, alterations in its sequence or in posttranslational modifications by PLK-1 or CDK-1 might tune its self-interaction or interaction with partners recruiting it to the centrosome. By reintroducing WT phosphorylation sites in PCMD-1-PBD^{m}N^{ter}, we could elevate centrosomal levels, which confirms our previous finding that the main residues critical for centrosome targeting of PCMD-1 are located in the C terminus (Stenzel et al., 2021).

By modulating WT PCMD-1 levels by strong and weak GFP RNAi, and by mutating the PBD-binding sites only in the N or C terminus of PCMD-1, we could reveal a two-tier regulation of scaffold shape and integrity. The first tier is explained by the reduced level of PCMD-1 at the centrosome. A gradual reduction of WT PCMD-1 by GFP RNAi results in progressively increasing PCM distortion. However, even at its peak, the level of disorganization does not match that seen in PCMD-1-PBD^{m}. The extremely high degree of PCM distortion in PCMD-1-PBD^{m} can only be explained by the additional impact of the mutated binding sites. This is particularly evident in the PCMD-1-PBD^{m}N^{ter} and PCMD-1-PBD^{m}N^{terShort} variants, where PCMD-1 levels are similar to those in PCMD-1-PBD^{m}C^{ter}, yet PCM integrity remains severely compromised.

The changes in PCM properties allow us, for the first time, to test the model put forward for centriole separation in *C. elegans* (Cabral et al., 2013; Magescas et al., 2019). According to the current model, centrioles are trapped in the PCM and passively released and separated upon PCM disassembly in late anaphase. Based on this model, we would expect centrioles embedded in a softer and more labile PCM to separate prematurely. Instead, our measurements in PCMD-1-PBD^{m} showed a delay in centriole separation. This can be explained by two mutually nonexclusive mechanisms. First, PCMD-1, similar to the human PCNT, could serve as a linker, and this linker requires PLK-1 binding for a timely cleavage. Failure in proper PLK-1 binding and phosphorylation at metaphase could delay the process of separation in late anaphase. Alternatively, after PCM disassembly in late anaphase, timely centriole separation could require a direct tethering or relay mechanism that transmits the forces generated by the astral microtubules to the centrioles at the moment of PCM rupture. In PCMD-1-PBD^{m}, this relay mechanism could be dysfunctional, allowing for PCM to be torn apart easily while leaving behind the centrioles to be separated by their own slow kinetics (Fig. 9 D).

We cannot exclude that by mutating putative PLK-1 docking sites in the PCMD-1 and thereby drastically reducing phosphorylation by PLK-1, we alter its interaction with SPD-5. PCMD-1 is an intrinsically disordered protein, the structure of which is poorly predicted and can change upon binding with different partners or in response to posttranslational modifications. We identified the PCMD-1-PBD^{m}N^{terShort} region as the critical segment required for maintaining PCM stability. This region, which harbors only 12 mutated PBD sites, falls into the highly disordered N terminus of the protein and was shown to interact with SPD-5 (Nakajo et al., 2022).

Unlike in the *C. elegans* embryo, when expressed in HEK293T cells, PCMD-1-PBD^{m}N^{terShort}, similar to PCMD-1-PBD^{m}N^{ter} and PCMD-1-PBD^{m}, fails to recruit SPD-5 to microtubules and abolishes binding in the bead assay. This indicates that the interaction between PCMD-1 and SPD-5 is compromised, potentially due to the PBD site mutations. We speculate that this particular region exhibits an intrinsic binding flexibility that is modulated via PLK-1 binding and/or phosphorylation. In *C. elegans* embryos, this change in PCMD-1 and SPD-5 binding is masked due to additional factors, such as SPD-2, that recruit SPD-5 to centrosomes. However, an altered interaction mode with PCMD-1 may compromise scaffold stability, regardless of SPD-5's recruitment efficiency or abundance. Similar to PCMD-1 and SPD-5, interaction between Cnn and PLP is required for centrosome scaffold integrity in *Drosophila* (Lerit et al., 2015; Richens et al., 2015).

How could PCMD-1, which is mostly concentrated at the centrioles, affect the integrity of a micron-scale structure? We previously used super-resolution microscopy to describe low or close-to-detection-limit signals of PCMD-1 along SPD-5 fibers, which could potentially stabilize the entire scaffold (Erpf et al., 2019). Alternatively, we propose that PLK-1-bound and phosphorylated PCMD-1 forms a complex with SPD-5 close to the centrioles that facilitates PCM maturation and biases the PCM to

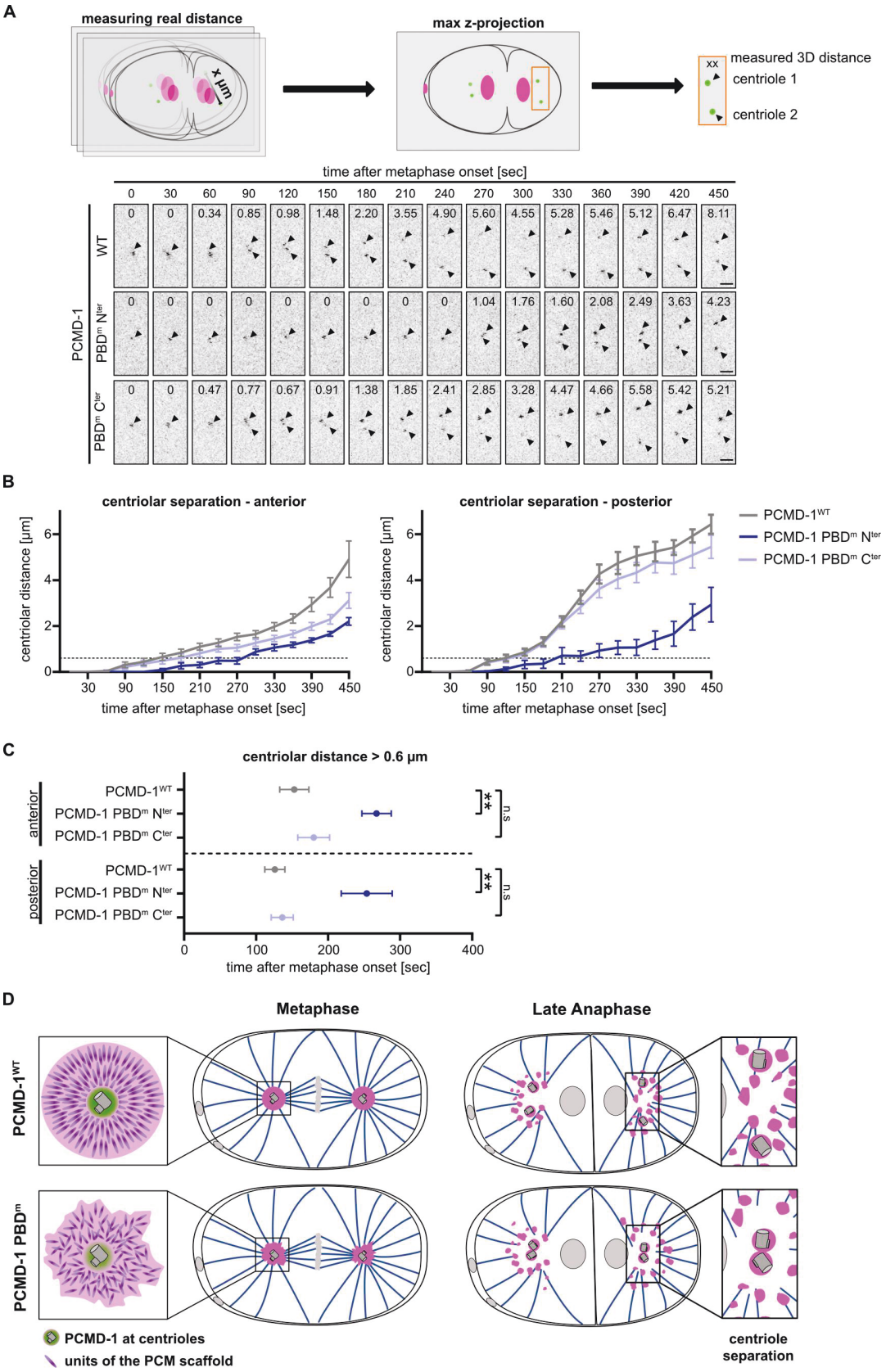

Figure 9. **Centrosome separation is delayed in PCMD-1-PBD^{m}N^{ter}. (A)** Schematics of 3D measurement of centriole separation. Analysis was performed at the anterior and posterior spindle poles. Representative time-lapse images of centriole separation at the posterior pole of GFP::PCMD-1^{WT}, GFP::PCMD-1-

PBD^{m}N^{ter}, and PCMD-1-PBD^{m}C^{ter}. Black scale bar = 2 µm. **(B)** Quantification of the centriolar distance during the first cell division at the anterior and posterior spindle poles of GFP::PCMD-1^{WT} (n = 10), GFP::PCMD-1-PBD^{m}N^{ter} (n = 11), and GFP::PCMD-1-PBD^{m}C^{ter} (n = 11) embryos. For all movies, 0 s is metaphase. Bold lines represent the mean ± SEM. Dashed lines indicate centrioles at a distance of 0.6 µm, a threshold defined as the onset of visible centriole separation. **(C)** Quantification of the time point of onset of centriolar separation at the anterior and posterior spindle poles, defined as a distance of 0.6 µm. P values from a Kruskal–Wallis test with Dunn post hoc and an ANOVA with subsequent Tukey HSD. n = number of analyzed centrosomes. P values: n.s. >0.05 > * >0.01 > ** >0.001 > ***. **(D)** Model of PCM scaffold destabilization and delayed centriole separation in PCMD-1-PBD^{m} embryos. Left panels: Close to the centrioles, PCMD-1^{WT} together with PLK-1 (not shown) biases the multimodal self-interactions of SPD-5 toward a certain intrinsic order. A rotational symmetry propagates this order along the entire PCM scaffold, giving the PCM strength and integrity. PCMD-1-PBD^{m} fails to bias the macromolecular interactions during PCM seeding and maturation, leading to a scaffold formation by randomized macromolecular self-interaction, which in turn leads to a destabilized PCM. Right panels: After PCM disassembly in late anaphase, pulling forces from astral microtubules are relayed to the centrioles, allowing for a timely centriole separation. In PCMD-1-PBD^{m}, the disorganized and labile PCM is torn apart easily, leaving behind the centrioles to separate by their own slow kinetics in the absence of a functional relay mechanism. Note: centrioles and the PCM scaffold units are not drawn to scale. See also Fig. S4.

assemble into a strong and ductile scaffold. The centrosome was speculated to behave as a non-Newtonian liquid, such as a liquid crystal with physical properties that fall between ordinary liquids and solids (Woodruff, 2021). The properties of a liquid crystal are dependent on the spatial orientation of its units or molecules. If so, one could envision that PCMD-1 seeds the PCM scaffold in the close vicinity of the centrioles by bringing together SPD-5 and PLK-1. At the centrioles, PCMD-1 and PLK-1 would bias the multimodal self-interactions of SPD-5 toward a certain intrinsic order (Rios et al., 2024). A rotational or translational symmetry could propagate this order along the entire PCM scaffold, giving the PCM strength and integrity (Fig. 9 D). The failure to bias the macromolecular interactions during centrosome seeding and maturation, be it due to lowered PLK-1 levels, aberrant SPD-5 binding, or a combination of both, could result in a scaffold built by randomized macromolecular self-interaction, which in turn leads to a destabilized PCM with more liquid-like properties.

In summary, our findings demonstrate that PCMD-1 plays a stabilizing role during PCM scaffold formation and that its function is essential for timely centriole separation at late anaphase.

Materials and methods

C. elegans strain maintenance and generation

C. elegans strains (Table S2) were maintained under standard conditions on NGM plates seeded with *E. coli* (OP50) at 15°C (Brenner, 1974). If not indicated otherwise, worms were shifted to 25°C at the late L3–L4 stage for 16–20 h for experimental usage. Transgenic worm strains were generated by single-copy integration of the respective transgenes using the MosSCI system (Frokjaer-Jensen et al., 2008). Transgenes were cloned into the pCFJ350 vector and injected into the EG6699 (chromosome II).

Prediction of CDK-1 phosphorylation or PBD-binding sites of PCMD-1

PLK-1-PBD–binding sites of PCMD-1 were predicted by searching for the consensus polo-binding motif S-S/T (Alvarez-Rodrigo et al., 2019) and by using the GPS-PBS (Guo et al., 2020) and the GPS-Polo (Liu et al., 2013) prediction programs with a medium threshold. All predicted sites were selected and mutated.

Potential CDK-1 phosphorylation sites were identified using the kinase-specific phosphorylation prediction system GPS 5.0 with a medium threshold (Wang et al., 2020) and by searching for the consensus motif S-T/P. All identified sites were mutated. The predicted 3D structure of PCMD-1 (UniProt: O62071) presented in Fig. S5 E was retrieved from the AlphaFold Protein Structure Database (Jumper et al., 2021; Varadi et al., 2024). The twelve mutated sites were manually annotated.

Embryonic survival assay

L4 worms were singled and incubated at 25°C for 16–20 h. The laid eggs were counted and compared with the hatched larvae after 48 h to assess the embryonic lethality.

RNA-mediated interference

RNAi experiments against GFP, *spd-2* and *gpr-1/2* were performed after feeding worms with the bacterial clones L4440_GFPi, I-4O08 and III-5C03, respectively, for 16–20 h at 25°C (Kamath and Ahringer, 2003; Lebedev et al., 2023; von Tobel et al., 2014). A weak GFP RNAi condition was achieved by mixing GFP RNAi bacteria with bacteria carrying the empty pL4440 vector 1:4. For RNAi against *csnk-1*, an L4440 vector was generated carrying the CDS of *csnk-1* using primers 5′-ATGACGAACACACGCGGG-3′ and 5′-CTATTTTTGTGTAGCTGGGGTCGCAT-3′, transformed into *E. coli* HT115(DE3) bacteria, and worms were fed for 48 h at 25°C. Bacteria carrying the empty pL4440 vector were used as negative control (mock).

Microscopy

Young adult worms were immobilized and dissected in 4 µl 2.5 µM Levamisole in M9 buffer to extract the embryos and mounted on 4% agarose pads. Live-cell imaging was performed at 25°C on an inverted Leica Stellaris 5 Point Scanning Confocal Microscope with a resolution of 512 × 512 pixels using a 100× HC PL APO oil immersion objective and controlled by LAS X software. Z-stacks were taken every 30 s with a step size of 0.7 µm and 2 × 2 binning. For representative images from one-cell embryos. Maximum z-projections of a fixed volume of 20 slices were generated.

Protein overexpression and purification

Recombinant proteins were expressed in BL21(DE3) bacteria. At an OD600 of 0.4–0.6, the bacterial culture was subjected to cold shock and protein expression was induced for 20 h at 17°C with 0.1 mM IPTG. Bacterial pellets were harvested, washed with cold PBS, and snap frozen in liquid nitrogen. Bacterial pellets were

resuspended in lysis buffer (50 mM Tris-HCl, pH 8.0, 500 mM NaCl, 10 mM imidazole, 4 mM ß-mecapthoethanol, 2 mM PMSF, 10% glycerol, and 0.2% Triton X-100) and lysed by applying it three times on a high-pressure cell homogenizer. Cleared lysates ran over Ni-NTA resin (30210; QIAGEN) with a flow-rate of ∼1 ml/min. Agarose beads were washed two times in lysis buffer with 10 column volumes. Protein was eluted (50 mM Tris-HCl, pH 8.0, 500 mM NaCl, 500 mM imidazole, 4 mM ß-mecapthoethanol, and 10% glycerol) and buffer exchange (25 mM Tris-HCl, pH 8.0, 250 mM NaCl, 2 mM DTT, and 10% glycerol) was performed three times while protein concentration (UCF8100; Merck) took place. Concentrated protein was eluted and stored at −80°C until further usage.

Kinase assay

Kinase assays were performed using ∼1 mg of recombinant protein and ∼200 ng human PLK1 kinase (Cat. No.: PV3501; Thermo Fisher Scientific) and/or ∼100 ng human CDK1/Cyclin B kinase (Cat. No.: PV3292; Thermo Fisher Scientific) in kinase buffer (50 mM Tris-HCl, pH 8.0, 10 mM $MgCl_2$, 1 mM DTT, 125 mM NaCl, 20 mM ATP, PhosSTOP [Roche], and cOmplete Mini [Roche]) for 30 min at 30°C. Assays were analyzed using SDS-PAGE with ProQ Diamond phosphoprotein staining (P33301; Thermo Fisher Scientific) and subsequent Coomassie staining.

MS

For sample preparation, a total of 1 µg of protein was reduced with 2 mM DTT for 30 min at 37°C, followed by alkylation with 5 mM iodoacetamide for 30 min at room temperature in the dark. Proteins were digested overnight at 37°C with trypsin at a 1:50 (wt/wt) enzyme-to-substrate ratio. Resulting peptides were desalted using home-made C18 StageTips, as described by Rappsilber et al. (2003).

For liquid chromatography–tandem MS peptides were analyzed on a nanoElute2 LC system (Bruker Daltonics) coupled to a timsTOF HT mass spectrometer (Bruker Daltonics) equipped with a CaptiveSpray nano-electrospray ionization source. Chromatographic separation was performed using a PepMap Neo trap column (C18, 300 µm × 5 mm; Thermo Fisher Scientific) and a PepSep Ultra analytical column (C18, 25 cm × 75 µm, 1.5 µm particle size; Bruker Daltonics). Peptides were eluted with a linear gradient from 5 to 37% acetonitrile (vol/vol) over 30 min at a flow rate of 250 nl/min, with the column maintained at 50°C. Data-dependent acquisition was carried out using the "DDA PASEF-standard_1.1.sec_cycletime.m" method with default instrument parameters. Raw MS data were analyzed using MaxQuant (version 2.4.14.0 [Cox and Mann, 2008]). Spectra were searched against the *E. coli* reference proteome (UniProt, Proteomes, UP000000625), supplemented with custom sequences for MBP-PCMD-1-His and hsCdk1. Default search parameters were used, with phosphorylation of serine, threonine, and tyrosine specified as a variable modification. Sites were scored as phosphorylated when at least 2 phosphorylated peptides/site were detected.

Immunoblotting

For immunoblotting, a fixed number of 100 worms per sample was picked in M9 buffer and washed four times. Buffer volume was reduced, and the respective amount of 2× Laemmli buffer was added. Samples were incubated at 95°C for 10 min, sonicated for 10 min, and again incubated at 95°C for 10 min (adapted from Lebedev et al. [2025]). After applying samples on an SDS-PAGE and western blotting, PCMD-1 transgene proteins with a GFP-tag were probed with a GFP antibody (mouse monoclonal 1:600; Roche) or an α-tubulin antibody (mouse monoclonal 1:7,500; Sigma-Aldrich). Proteins of interest were detected using HRP-conjugated secondary antibodies against mouse (1:7,500; Bio-Rad Laboratories). The proteins were visualized using Amersham ECL Prime Western Blotting Detection Reagent (GE Healthcare).

Cell cycle length measurements

Young adult worms were immobilized and dissected in 4 µl 2.5 µM Levamisol in M9 buffer to extract the embryos and mounted on 4% agarose pads. Live-cell imaging was performed on a Zeiss Axio Imager.M2 and "Time to Live" software. Every 35, s z-stacks were acquired through the embryos using a 0.7 µm step size in a total volume of 25 µm, from pronuclear migration until the end of the second cell cycle. Time from NEBD in the one-cell embryo until NEBD in the AB cell was measured.

Measuring spindle positioning

Spindle position was measured in Fiji (Schindelin et al., 2012) at metaphase by drawing a linescan from the anterior to posterior cortex of the embryo. mCherry-H2B intensities along the linescan were measured to identify the position of the DNA metaphase plate relative to embryo length.

Fluorescence intensity analysis

GFP, RPF, and mCherry intensities were measured on raw images by analyzing z-stacks with ManualTrackMate in Fiji (Schindelin et al., 2012; Tinevez et al., 2017). The time point of measurement was determined by the DNA condensation pattern visualized by the mCherry::H2B marker. Fluorescent signals were measured in a sphere with a fixed radius (GFP: 0.782 µm, RFP::SPD-5: 3.328 µm, and PLK-1::mCherry: 1.505 µm). A sphere with the same radius was used to measure the cytoplasmic background signal and the background signal outside the embryo. For each datapoint, the cytoplasmic background signal was subtracted from the fluorescent signal. To take into account the cytoplasmic gradient of PLK-1::mCherry in the one-cell embryo, cytoplasmic background levels were measured in the anterior and posterior sides of the embryo and subtracted from the respective centrosomal signal.

PCM shape analysis

PCM circularity and area were measured at the indicated time points. Maximum z-projections of the RFP::SPD-5 channel were created, and PCM was extracted by removing outliers (radius 2; threshold: 5) and despeckling the whole stack. PCM shape was then converted into black/white outlines using the "Otsu white" threshold. Circularity and area were measured by the Fiji software (Schindelin et al., 2012). Circularity of a shape is defined as $4\pi x(\text{area}/\text{perimeter}^2)$, whereas 1.0 indicates a perfect circle.

Quantification of EBP-2 dynamics

To assess microtubule nucleation rate, EBP-2::GFP was imaged at the posterior centrosome in 1.3-second intervals for a period of 78 s before metaphase (Mangal et al., 2018). EBP-2::GFP signals were extracted in Fiji (Schindelin et al., 2012) by using a median filter (radius = 2) to reduce background noise. The stack was duplicated, and the copy was subjected to background subtraction with a rolling ball radius of 15. The processed stack was subtracted from the original using Image Calculator. To stabilize the moving centrosome, rigid body registration was applied using StackReg (Thevenaz et al., 1998), and the LUT was inverted for visualization. An arc (15.7 µm length) was drawn 5 µm away from the centrosome, from which a kymograph was generated using the "Live Kymographer" Plugin. EBP-2::GFP dots were automatically counted by using the "Find Maxima" function with a prominence of 10.

Measuring centriolar distance

Centriolar distance was measured in 4D stacks after metaphase using the TrackMate Plugin (Ershov et al., 2022) in Fiji (Schindelin et al., 2012). Centrioles were detected using the DoG detector with an estimated object diameter of 1 µm, a quality threshold of 5, and subpixel localization. Signals were contrast-filtered (0.3 and above), and missed centrioles, especially due to weak signals, were manually added. To track their separation, LAP Tracker was used with a frame-to-frame linking of 10 µm. Track segment gap closing with a distance of 10 µm with a maximal two-frame gap and track segment splitting with a maximal distance of 10 µm. Tracks were manually adjusted if required; centriolar positions were measured by Fiji, and centriolar distance at all analyzed time points was calculated by Pythagoras' theorem in 3D.

Cell culture, transfection, and imaging of staining and bead assay

Human embryonic kidney (HEK) 293T cells were cultured in Dulbecco's Modified Eagle Medium (DMEM) supplemented with 10% fetal calf serum, penicillin (100 U/ml), and streptomycin (100 µg/ml) at 37°C, 5% CO_2. For microscopy, the cells were grown to 50–70% confluence on glass coverslips and transfected with expression plasmids using Lipofectamine 2000 (Invitrogen) or jetOPTIMUS (Sartorius) according to the manufacturer's instructions. 24 h after transfection, cells were fixed with 4% paraformaldehyde (15 min at room temperature), permeabilized with 1% Triton X-100 in PBS, and stained with 4′,6-diamidino-2-phenylindole (DAPI, 10 µg/ml). Cells were imaged at the Leica SP5 point scanning confocal microscope with the HCX PL APO Lambda Blue 63× 1.4 oil objective and 1,024 × 1,024 pixel resolution.

For the bead recruitment assay, HEK293T cells were transfected with 4 µg DNA. After 24 h, cells were chilled to 4°C. To prepare cell extracts, cells were washed once with 1×PBS and pelleted by centrifugation at 1,000 *g* for 5 min. Cell pellets were lysed using 100 µl lysis buffer (10 mM Tris-HCl [pH8.0], 50 mM NaF, 0.3 mM Na_3VO_4, 10 mM sodium pyrophosphate, 5 mM β-glycerol phosphate, 120 mM NaCl, and 0.5% NP40) containing protease and phosphatase inhibitors (PhosSTOP, Pefabloc, cOmplete Mini, Pepstatin A, and Leupeptin, Sigma-Aldrich; Aprotinin, Carl Roth) by incubating them for 30 min at 4°C. Crude extracts were clarified by centrifugation at 12,000 *g* for 12 min at 4°C and incubated with RFP-trap agarose beads (ChromoTek). Cell lysate was loaded on beads for 90 min, and the buffer was exchanged to equilibration buffer (150 mM NaCl and 10 mM Tris-HCl) before imaging. Microscopy was performed on a Nikon Ti2-Eclipse microscope equipped with a CFI Apochromat TIRF 100×/1.49 numerical aperture (NA) oil objective and a Photometrics Prime 95B 25-mm camera.

Yeast two-hybrid

Growth and genetic manipulation of the *Saccharomyces cerevisiae* strain were performed using standard genetic techniques. Yeast two-hybrid assays were performed using the Grow'N'Glow GFP Yeast Two-Hybrid System (Mobitech) according to the manufacturer's protocol (Stenzel et al., 2021). pEG202 containing the DNA-binding domain LexA and the cDNA for PLK-1 was used as a bait. cDNAs of PCMD-1^{WT} and PCMD-1-PBD^{m} were inserted into the prey vector pJG45 comprising the B42 transcription activation domain. pEG202-p53 with pJG45-LTA was used as a positive control, whereas pJG45 without an insert was used as a negative control.

Statistical analysis

The statistical analyses were performed using the software R (Posit team, 2024). RStudio: Integrated Development Environment for R. Posit Software, PBC. URL https://www.rstudio.com/) and the packages car (Fox and Weisberg, 2019) and FSA (Ogle et al., 2017). Data were tested for normal distribution using the Shapiro–Wilk test and for equal variances using the Levene's test. Datasets with two groups and parametric conditions were analyzed by Student's (equal variances) or Welch (unequal variances) *t* test, and nonparametric conditions by the Wilcoxon rank-sum test. For data with multiple groups and parametric conditions, an ANOVA was performed, and P values were calculated subsequently with Tukey honest significant differences. For multiple groups and nonparametric conditions, a Kruskal–Wallis rank-sum test with Dunn post hoc was performed. The statistical test used is indicated in the figure legends. In the analysis of Fig. 1, G and H; Fig. 3, E and F; Fig. 4, D and E; Fig. 5, D and E; Fig. 6, D and E; Fig. S4 D; and Fig. S5, and B, an independent statistical test was performed for each time point. P values: n.s. >0.05 > * >0.01 > ** >0.001 > ***.

Online supplemental material

Fig. S1 shows results related to Fig. 1 (PCMD-1-PBD^{m} leads to severe PCM scaffold disorganization). Fig. S2 shows results related to Fig. 2 (CDK-1 priming facilitates PCMD-1 phosphorylation by PLK-1). Fig. S3 shows results related to Fig. 4 (decreased microtubule-pulling forces partially rescue PCM scaffold distortion of PCMD-1-PBD^{m} centrosomes). Fig. S4 shows results related to Fig. 6 (reducing PCMD-1^{WT} levels leads to a compromised PCM scaffold formation) and Fig. 8 (centrosome separation is delayed in PCMD-1-PBD^{m}N^{ter}). Fig. S5 shows results related to Fig. 7 (PBD sites in the N-terminal part of PCMD-1 are needed to form a stable PCM scaffold). Table S1 shows mutated sites in PCMD-1-PBD^{m}, PCMD-1-PBD^{m}N^{ter}, PCMD-1-PBD^{m}N^{terShort}, PCMD-1-PBD^{m}C^{ter}, and CDK-1^{m} and PCR primers and oligos used to introduce these mutations. Table S2 shows the *C. elegans* strains used in this study. Video 1 shows PCM scaffold dynamics in PCMD-1^{WT} and is related to

Fig. 1. Video 2 shows PCM scaffold dynamics in PCMD-1-PBD^{m} and is related to Fig. 1. Video 3 shows the AlphaFold model of PCMD-1 with 12 mutated PBD-binding sites and is related to Fig. S5.

Data availability

The MS proteomics data have been deposited to the ProteomeXchange Consortium via the PRIDE partner repository with the dataset identifier PXD067573. All data generated or analyzed during this study are included in this published article and its supplementary information files.

Acknowledgments

We thank the CALM facility for support during live-cell imaging and the MSBioLMU core facility for support with mass spectroscopy. We like to express our deep gratitude to Monica Gotta (University of Geneva, Geneva, Switzerland) for sharing the unpublished strain expressing *plk-1(syb2781)::mCherry*, to Lionel Pintard (Institut Jacques Monod, Paris, France) for sharing the cePLK-1 kinase, Saskia Hütten for the support with protein purification, Christof Osman for giving access to the Nikon microscope, and to Jeff Woodruff (UT Southwestern, Dallas, TX, USA) for sharing the strain expressing *spd-5(wow36_syb5737[D734-918])*. Some strains were provided by the CGC, which is funded by the National Institutes of Health Office of Research Infrastructure Programs (P40 OD010440). We would also like to thank Felicia Haxel, Disha Shenai, Sasha Degtyareva, and Alex Schilder for support with building the worm strains and conducting the experiments.

The project was funded by the support of the Deutsche Forschungsgemeinschaft (MI 1867/3-1) to Tamara Mikeladze-Dvali.

Author contributions: Alina Schreiner: conceptualization, data curation, formal analysis, investigation, methodology, project administration, software, validation, visualization, and writing—original draft, review, and editing. Astrid Heim: investigation and validation. Luisa Pletschacher: investigation and validation. Lisa-Marie Alznauer: investigation and validation. Serena Schwenkert: investigation. Friederike Wolff: investigation and validation. Esther Zanin: conceptualization and writing—review and editing. Tamara Mikeladze-Dvali: conceptualization, data curation, formal analysis, funding acquisition, investigation, methodology, project administration, resources, supervision, validation, visualization, and writing—original draft, review, and editing.

Disclosures: The authors declare no competing interests exist.

Submitted: 14 November 2024
Revised: 14 July 2025
Accepted: 9 September 2025

References

Aljiboury, A., A. Mujcic, E. Curtis, T. Cammerino, D. Magny, Y. Lan, M. Bates, J. Freshour, Y.H. Ahmed-Braimeh, and H. Hehnly. 2022. Pericentriolar matrix (PCM) integrity relies on cenexin and polo-like kinase (PLK)1. *Mol. Biol. Cell*. 33:br14. https://doi.org/10.1091/mbc.E22-01-0015

Alvarez-Rodrigo, I., T.L. Steinacker, S. Saurya, P.T. Conduit, J. Baumbach, Z.A. Novak, M.G. Aydogan, A. Wainman, and J.W. Raff. 2019. Evidence that a positive feedback loop drives centrosome maturation in fly embryos. *Elife*. 8:e50130. https://doi.org/10.7554/eLife.50130

Barrera, J.A., L.-R. Kao, R.E. Hammer, J. Seemann, J.L. Fuchs, and T.L. Megraw. 2010. CDK5RAP2 regulates centriole engagement and cohesion in mice. *Dev. Cell*. 18:913–926. https://doi.org/10.1016/j.devcel.2010.05.017

Brenner, S. 1974. The genetics of *Caenorhabditis elegans*. *Genetics*. 77:71–94. https://doi.org/10.1093/genetics/77.1.71

Budirahardja, Y., and P. Gönczy. 2008. PLK-1 asymmetry contributes to asynchronous cell division of *C. elegans* embryos. *Development*. 135:1303–1313. https://doi.org/10.1242/dev.019075

Cabral, G., T. Laos, J. Dumont, and A. Dammermann. 2019. Differential requirements for centrioles in mitotic centrosome growth and maintenance. *Dev. Cell*. 50:355–366.e6. https://doi.org/10.1016/j.devcel.2019.06.004

Cabral, G., S.S. Sans, C.R. Cowan, and A. Dammermann. 2013. Multiple mechanisms contribute to centriole separation in *C. elegans*. *Curr. Biol.* 23:1380–1387. https://doi.org/10.1016/j.cub.2013.06.043

Colombo, K., S.W. Grill, R.J. Kimple, F.S. Willard, D.P. Siderovski, and P. Gönczy. 2003. Translation of polarity cues into asymmetric spindle positioning in *Caenorhabditis elegans* embryos. *Science*. 300:1957–1961. https://doi.org/10.1126/science.1084146

Conduit, P.T., Z. Feng, J.H. Richens, J. Baumbach, A. Wainman, S.D. Bakshi, J. Dobbelaere, S. Johnson, S.M. Lea, and J.W. Raff. 2014. The centrosome-specific phosphorylation of Cnn by Polo/Plk1 drives Cnn scaffold assembly and centrosome maturation. *Dev. Cell*. 28:659–669. https://doi.org/10.1016/j.devcel.2014.02.013

Cox, J., and M. Mann. 2008. MaxQuant enables high peptide identification rates, individualized p.p.b.-range mass accuracies and proteome-wide protein quantification. *Nat. Biotechnol.* 26:1367–1372. https://doi.org/10.1038/nbt.1511

De Luca, M., L. Brunetto, I.A. Asteriti, M. Giubettini, P. Lavia, and G. Guarguaglini. 2008. Aurora-A and ch-TOG act in a common pathway in control of spindle pole integrity. *Oncogene*. 27:6539–6549. https://doi.org/10.1038/onc.2008.252

De Simone, A., F. Nédélec, and P. Gönczy. 2016. Dynein transmits polarized actomyosin cortical flows to promote centrosome separation. *Cell Rep.* 14:2250–2262. https://doi.org/10.1016/j.celrep.2016.01.077

Decker, M., S. Jaensch, A. Pozniakovsky, A. Zinke, K.F. O'Connell, W. Zachariae, E. Myers, and A.A. Hyman. 2011. Limiting amounts of centrosome material set centrosome size in *C. elegans* embryos. *Curr. Biol.* 21:1259–1267. https://doi.org/10.1016/j.cub.2011.06.002

Dobbelaere, J., F. Josué, S. Suijkerbuijk, B. Baum, N. Tapon, and J. Raff. 2008. A genome-wide RNAi screen to dissect centriole duplication and centrosome maturation in *Drosophila*. *PLoS Biol.* 6:e224. https://doi.org/10.1371/journal.pbio.0060224

Enos, S.J., M. Dressler, B.F. Gomes, A.A. Hyman, and J.B. Woodruff. 2018. Phosphatase PP2A and microtubule-mediated pulling forces disassemble centrosomes during mitotic exit. *Biol. Open*. 7:bio029777. https://doi.org/10.1242/bio.029777

Erpf, A.C., L. Stenzel, N. Memar, M. Antoniolli, M. Osepashvili, R. Schnabel, B. Conradt, and T. Mikeladze-Dvali. 2019. PCMD-1 organizes centrosome matrix assembly in *C. elegans*. *Curr. Biol.* 29:1324–1336.e6. https://doi.org/10.1016/j.cub.2019.03.029

Ershov, D., M.-S. Phan, J.W. Pylvänäinen, S.U. Rigaud, L. Le Blanc, A. Charles-Orszag, J.R.W. Conway, R.F. Laine, N.H. Roy, D. Bonazzi, et al. 2022. TrackMate 7: Integrating state-of-the-art segmentation algorithms into tracking pipelines. *Nat. Meth.* 19:829–832. https://doi.org/10.1038/s41592-022-01507-1

Feng, Z., A. Caballe, A. Wainman, S. Johnson, A.F.M. Haensele, M.A. Cottee, P.T. Conduit, S.M. Lea, and J.W. Raff. 2017. Structural basis for mitotic centrosome assembly in flies. *Cell*. 169:1078–1089.e13. https://doi.org/10.1016/j.cell.2017.05.030

Fong, K.W., Y.-K. Choi, J.B. Rattner, and R.Z. Qi. 2008. CDK5RAP2 is a pericentriolar protein that functions in centrosomal attachment of the gamma-tubulin ring complex. *Mol. Biol. Cell*. 19:115–125. https://doi.org/10.1091/mbc.e07-04-0371

Foraker, A.B., S.M. Camus, T.M. Evans, S.R. Majeed, C.-Y. Chen, S.B. Taner, I.R. Corrêa Jr., S.J. Doxsey, and F.M. Brodsky. 2012. Clathrin promotes centrosome integrity in early mitosis through stabilization of centrosomal ch-TOG. *J. Cell Biol.* 198:591–605. https://doi.org/10.1083/jcb.201205116

Fox, J., and S. Weisberg. 2019. An R Companion to Applied Regression. SAGE, Los Angeles. 577.

Frøkjaer-Jensen, C., M.W. Davis, C.E. Hopkins, B.J. Newman, J.M. Thummel, S.-P. Olesen, M. Grunnet, and E.M. Jorgensen. 2008. Single-copy

insertion of transgenes in *Caenorhabditis elegans*. *Nat. Genet.* 40: 1375–1383. https://doi.org/10.1038/ng.248
Fu, J., and D.M. Glover. 2012. Structured illumination of the interface between centriole and peri-centriolar material. *Open Biol.* 2:120104. https://doi.org/10.1098/rsob.120104
Ganem, N.J., S.A. Godinho, and D. Pellman. 2009. A mechanism linking extra centrosomes to chromosomal instability. *Nature*. 460:278–282. https://doi.org/10.1038/nature08136
Garbrecht, J., T. Laos, E. Holzer, M. Dillinger, and A. Dammermann. 2021. An acentriolar centrosome at the *C. elegans* ciliary base. *Curr. Biol.* 31: 2418–2428.e8. https://doi.org/10.1016/j.cub.2021.03.023
García-Alvarez, B., G. de Cárcer, S. Ibañez, E. Bragado-Nilsson, and G. Montoya. 2007. Molecular and structural basis of polo-like kinase 1 substrate recognition: Implications in centrosomal localization. *Proc. Natl. Acad. Sci. USA*. 104:3107–3112. https://doi.org/10.1073/pnas.0609131104
Gotta, M., Y. Dong, Y.K. Peterson, S.M. Lanier, and J. Ahringer. 2003. Asymmetrically distributed *C. elegans* homologs of AGS3/PINS control spindle position in the early embryo. *Curr. Biol.* 13:1029–1037. https://doi.org/10.1016/s0960-9822(03)00371-3
Grill, S.W., J. Howard, E. Schäffer, E.H.K. Stelzer, and A.A. Hyman. 2003. The distribution of active force generators controls mitotic spindle position. *Science*. 301:518–521. https://doi.org/10.1126/science.1086560
Guo, Y., W. Ning, P. Jiang, S. Lin, C. Wang, X. Tan, L. Yao, D. Peng, and Y. Xue. 2020. GPS-PBS: A deep learning framework to predict phosphorylation sites that specifically interact with phosphoprotein-binding domains. *Cells*. 9:1266. https://doi.org/10.3390/cells9051266
Hamill, D.R., A.F. Severson, J.C. Carter, and B. Bowerman. 2002. Centrosome maturation and mitotic spindle assembly in *C. elegans* require SPD-5, a protein with multiple coiled-coil domains. *Dev. Cell*. 3:673–684. https://doi.org/10.1016/s1534-5807(02)00327-1
Hannak, E., M. Kirkham, A.A. Hyman, and K. Oegema. 2001. Aurora-A kinase is required for centrosome maturation in *Caenorhabditis elegans*. *J. Cell Biol.* 155:1109–1116. https://doi.org/10.1083/jcb.200108051
Haren, L., T. Stearns, and J. Lüders. 2009. Plk1-dependent recruitment of gamma-tubulin complexes to mitotic centrosomes involves multiple PCM components. *PLoS One*. 4:e5976. https://doi.org/10.1371/journal.pone.0005976
Holland, A.J., and D.W. Cleveland. 2009. Boveri revisited: Chromosomal instability, aneuploidy and tumorigenesis. *Nat. Rev. Mol. Cell Biol.* 10: 478–487. https://doi.org/10.1038/nrm2718
Joukov, V., and A. De Nicolo. 2018. Aurora-PLK1 cascades as key signaling modules in the regulation of mitosis. *Sci. Signal.* 11:eaar4195. https://doi.org/10.1126/scisignal.aar4195
Joukov, V., J.C. Walter, and A. De Nicolo. 2014. The Cep192-Organized Aurora A-Plk1 Cascade is essential for centrosome cycle and bipolar spindle assembly. *Mol. Cell*. 55:578–591. https://doi.org/10.1016/j.molcel.2014.06.016
Jumper, J., R. Evans, A. Pritzel, T. Green, M. Figurnov, O. Ronneberger, K. Tunyasuvunakool, R. Bates, A. Žídek, A. Potapenko, et al. 2021. Highly accurate protein structure prediction with AlphaFold. *Nature*. 596: 583–589. https://doi.org/10.1038/s41586-021-03819-2
Kamath, R.S., and J. Ahringer. 2003. Genome-wide RNAi screening in *Caenorhabditis elegans*. *Methods*. 30:313–321. https://doi.org/10.1016/s1046-2023(03)00050-1
Kemp, C.A., K.R. Kopish, P. Zipperlen, J. Ahringer, and K.F. O'Connell. 2004. Centrosome maturation and duplication in *C. elegans* require the coiled-coil protein SPD-2. *Dev. Cell*. 6:511–523. https://doi.org/10.1016/s1534-5807(04)00066-8
Kim, J., J. Kim, and K. Rhee. 2019. PCNT is critical for the association and conversion of centrioles to centrosomes during mitosis. *J. Cell Sci.* 132: jcs225789. https://doi.org/10.1242/jcs.225789
Kim, J., K. Lee, and K. Rhee. 2015. PLK1 regulation of PCNT cleavage ensures fidelity of centriole separation during mitotic exit. *Nat. Commun.* 6: 10076. https://doi.org/10.1038/ncomms10076
Laan, L., N. Pavin, J. Husson, G. Romet-Lemonne, M. van Duijn, M.P. López, R.D. Vale, F. Jülicher, S.L. Reck-Peterson, and M. Dogterom. 2012. Cortical dynein controls microtubule dynamics to generate pulling forces that position microtubule asters. *Cell*. 148:502–514. https://doi.org/10.1016/j.cell.2012.01.007
Laos, T., G. Cabral, and A. Dammermann. 2015. Isotropic incorporation of SPD-5 underlies centrosome assembly in *C. elegans*. *Curr. Biol.* 25: R648–R649. https://doi.org/10.1016/j.cub.2015.05.060
Lawo, S., M. Hasegan, G.D. Gupta, and L. Pelletier. 2012. Subdiffraction imaging of centrosomes reveals higher-order organizational features of pericentriolar material. *Nat. Cell Biol.* 14:1148–1158. https://doi.org/10.1038/ncb2591
Lebedev, M., F.-Y. Chan, A. Lochner, J. Bellessem, D.S. Osório, E. Rackles, T. Mikeladze-Dvali, A.X. Carvalho, and E. Zanin. 2023. Anillin forms linear structures and facilitates furrow ingression after septin and formin depletion. *Cell Rep.* 42:113076. https://doi.org/10.1016/j.celrep.2023.113076
Lebedev, M., F.-Y. Chan, E. Rackles, J. Bellessem, T. Mikeladze-Dvali, A. Xavier Carvalho, and E. Zanin. 2025. Anillin mediates unilateral furrowing during cytokinesis by limiting RhoA binding to its effectors. *J. Cell Biol.* 224:e202405182. https://doi.org/10.1083/jcb.202405182
Lee, K., and K. Rhee. 2011. PLK1 phosphorylation of pericentrin initiates centrosome maturation at the onset of mitosis. *J. Cell Biol.* 195:1093–1101. https://doi.org/10.1083/jcb.201106093
Lee, K., and K. Rhee. 2012. Separase-dependent cleavage of pericentrin B is necessary and sufficient for centriole disengagement during mitosis. *Cell Cycle*. 11:2476–2485. https://doi.org/10.4161/cc.20878
Lerit, D.A., H.A. Jordan, J.S. Poulton, C.J. Fagerstrom, B.J. Galletta, M. Peifer, and N.M. Rusan. 2015. Interphase centrosome organization by the PLP-Cnn scaffold is required for centrosome function. *J. Cell Biol.* 210:79–97. https://doi.org/10.1083/jcb.201503117
Liu, Z., J. Ren, J. Cao, J. He, X. Yao, C. Jin, and Y. Xue. 2013. Systematic analysis of the Plk-mediated phosphoregulation in eukaryotes. *Brief. Bioinform.* 14:344–360. https://doi.org/10.1093/bib/bbs041
Magescas, J., J.C. Zonka, and J.L. Feldman. 2019. A two-step mechanism for the inactivation of microtubule organizing center function at the centrosome. *Elife*. 8:e47867. https://doi.org/10.7554/eLife.47867
Maiato, H., and E. Logarinho. 2014. Mitotic spindle multipolarity without centrosome amplification. *Nat. Cell Biol.* 16:386–394. https://doi.org/10.1038/ncb2958
Mangal, S., J. Sacher, T. Kim, D.S. Osório, F. Motegi, A.X. Carvalho, K. Oegema, and E. Zanin. 2018. TPXL-1 activates Aurora A to clear contractile ring components from the polar cortex during cytokinesis. *J. Cell Biol.* 217: 837–848. https://doi.org/10.1083/jcb.201706021
Martino, L., S. Morchoisne-Bolhy, D.K. Cheerambathur, L. Van Hove, J. Dumont, N. Joly, A. Desai, V. Doye, and L. Pintard. 2017. Channel nucleoporins recruit PLK-1 to nuclear pore complexes to direct nuclear envelope breakdown in *C. elegans*. *Dev. Cell*. 43:157–171.e7. https://doi.org/10.1016/j.devcel.2017.09.019
Matsuo, K., K. Ohsumi, M. Iwabuchi, T. Kawamata, Y. Ono, and M. Takahashi. 2012. Kendrin is a novel substrate for separase involved in the licensing of centriole duplication. *Curr. Biol.* 22:915–921. https://doi.org/10.1016/j.cub.2012.03.048
Meng, L., J.E. Park, T.-S. Kim, E.H. Lee, S.-Y. Park, M. Zhou, J.K. Bang, and K.S. Lee. 2015. Bimodal interaction of mammalian polo-like kinase 1 and a centrosomal scaffold, Cep192, in the regulation of bipolar spindle formation. *Mol. Cell. Biol.* 35:2626–2640. https://doi.org/10.1128/MCB.00068-15
Mennella, V., B. Keszthelyi, K.L. McDonald, B. Chhun, F. Kan, G.C. Rogers, B. Huang, and D.A. Agard. 2012. Subdiffraction-resolution fluorescence microscopy reveals a domain of the centrosome critical for pericentriolar material organization. *Nat. Cell Biol.* 14:1159–1168. https://doi.org/10.1038/ncb2597
Mittasch, M., V.M. Tran, M.U. Rios, A.W. Fritsch, S.J. Enos, B. Ferreira Gomes, A. Bond, M. Kreysing, and J.B. Woodruff. 2020. Regulated changes in material properties underlie centrosome disassembly during mitotic exit. *J. Cell Biol.* 219:e201912036. https://doi.org/10.1083/jcb.201912036
Nakajo, M., H. Kano, K. Tsuyama, N. Haruta, and A. Sugimoto. 2022. Centrosome maturation requires phosphorylation-mediated sequential domain interactions of SPD-5. *J. Cell Sci.* 135:jcs259025. https://doi.org/10.1242/jcs.259025
Novarino, G., N. Akizu, and J.G. Gleeson. 2011. Modeling human disease in humans: The ciliopathies. *Cell*. 147:70–79. https://doi.org/10.1016/j.cell.2011.09.014
Ogle, D.H., P. Wheeler, and A. Dinno. 2017. FSA: Fisheries stock analysis. *R. Package Version 0*. 17:636.
Ohta, M., Z. Zhao, D. Wu, S. Wang, J.L. Harrison, J.S. Gómez-Cavazos, A. Desai, and K.F. Oegema. 2021. Polo-like kinase 1 independently controls microtubule-nucleating capacity and size of the centrosome. *J. Cell Biol.* 220:e202009083. https://doi.org/10.1083/jcb.202009083
Oshimori, N., M. Ohsugi, and T. Yamamoto. 2006. The Plk1 target Kizuna stabilizes mitotic centrosomes to ensure spindle bipolarity. *Nat. Cell Biol.* 8:1095–1101. https://doi.org/10.1038/ncb1474
Ou, S., M.-H. Tan, T. Weng, H. Li, and C.-G. Koh. 2018. LIM kinase1 regulates mitotic centrosome integrity via its activity on dynein light intermediate chains. *Open Biol.* 8:170202. https://doi.org/10.1098/rsob.170202
Özlü, N., M. Srayko, K. Kinoshita, B. Habermann, E.T. O'Toole, T. Müller-Reichert, N. Schmalz, A. Desai, and A.A. Hyman. 2005. An essential

function of the *C. elegans* ortholog of TPX2 is to localize activated Aurora A kinase to mitotic spindles. *Dev. Cell*. 9:237–248. https://doi.org/10.1016/j.devcel.2005.07.002

Pagan, J.K., A. Marzio, M.J.K. Jones, A. Saraf, P.V. Jallepalli, L. Florens, M.P. Washburn, and M. Pagano. 2015. Degradation of Cep68 and PCNT cleavage mediate Cep215 removal from the PCM to allow centriole separation, disengagement and licensing. *Nat. Cell Biol.* 17:31–43. https://doi.org/10.1038/ncb3076

Panbianco, C., D. Weinkove, E. Zanin, D. Jones, N. Divecha, M. Gotta, and J. Ahringer. 2008. A casein kinase 1 and PAR proteins regulate asymmetry of a PIP(2) synthesis enzyme for asymmetric spindle positioning, *Dev. Cell*. 15:198–208. https://doi.org/10.1016/j.devcel.2008.06.002

Pelletier, L., N. Özlü, E. Hannak, C. Cowan, B. Habermann, M. Ruer, T. Müller-Reichert, and A.A. Hyman. 2004. The *Caenorhabditis elegans* centrosomal protein SPD-2 is required for both pericentriolar material recruitment and centriole duplication. *Curr. Biol.* 14:863–873. https://doi.org/10.1016/j.cub.2004.04.012

Qi, F., S. Yin, X. Yang, N. Ju, B. Liu, X. Zhang, Z. Zhu, L. Ji, F. Zhang, L. Zhao, et al. 2025. Dynamic SAS-6 phosphorylation aids centrosome duplication and elimination in *C. elegans* oogenesis. *EMBO Rep.* 26:3411–3444. https://doi.org/10.1038/s44319-025-00485-7

Rappsilber, J., Y. Ishihama, and M. Mann. 2003. Stop and go extraction tips for matrix-assisted laser desorption/ionization, nanoelectrospray, and LC/MS sample pretreatment in proteomics. *Anal. Chem.* 75:663–670. https://doi.org/10.1021/ac026117i

Rathbun, L.I., A.A. Aljiboury, X. Bai, N.A. Hall, J. Manikas, J.D. Amack, J.N. Bembenek, and H. Hehnly. 2020. PLK1- and PLK4-Mediated asymmetric mitotic centrosome size and positioning in the early zebrafish embryo. *Curr. Biol.* 30:4519–4527.e3. https://doi.org/10.1016/j.cub.2020.08.074

Richens, J.H., T.P. Barros, E.P. Lucas, N. Peel, D.M.S. Pinto, A. Wainman, and J.W. Raff. 2015. The *Drosophila* pericentrin-like-protein (PLP) cooperates with Cnn to maintain the integrity of the outer PCM. *Biol. Open*. 4:1052–1061. https://doi.org/10.1242/bio.012914

Rios, M.U., M.A. Bagnucka, B.D. Ryder, B. Ferreira Gomes, N.E. Familiari, K. Yaguchi, M. Amato, W.E. Stachera, Ł.A. Joachimiak, and J.B. Woodruff. 2024. Multivalent coiled-coil interactions enable full-scale centrosome assembly and strength. *J. Cell Biol.* 223:e202306142. https://doi.org/10.1083/jcb.202306142

Rivers, D.M., S. Moreno, M. Abraham, and J. Ahringer. 2008. PAR proteins direct asymmetry of the cell cycle regulators Polo-like kinase and Cdc25. *J. Cell Biol.* 180:877–885. https://doi.org/10.1083/jcb.200710018

Roque, H., S. Saurya, M.B. Pratt, E. Johnson, and J.W. Raff. 2018. Drosophila PLP assembles pericentriolar clouds that promote centriole stability, cohesion and MT nucleation. *PLoS Genet.* 14:e1007198. https://doi.org/10.1371/journal.pgen.1007198

Santamaria, A., B. Wang, S. Elowe, R. Malik, F. Zhang, M. Bauer, A. Schmidt, H.H. Silljé, R. Körner, and E.A. Nigg. 2011. The Plk1-dependent phosphoproteome of the early mitotic spindle. *Mol. Cell. Proteomics*. 10:M110.004457. https://doi.org/10.1074/mcp.M110.004457

Schindelin, J., I. Arganda-Carreras, E. Frise, V. Kaynig, M. Longair, T. Pietzsch, S. Preibisch, C. Rueden, S. Saalfeld, B. Schmid, et al. 2012. Fiji: An open-source platform for biological-image analysis. *Nat. Methods*. 9:676–682. https://doi.org/10.1038/nmeth.2019

Sonnen, K.F., L. Schermelleh, H. Leonhardt, and E.A. Nigg. 2012. 3D-structured illumination microscopy provides novel insight into architecture of human centrosomes. *Biol. Open*. 1:965–976. https://doi.org/10.1242/bio.20122337

Stenzel, L., A. Schreiner, E. Zuccoli, S. Üstüner, J. Mehler, E. Zanin, and T. Mikeladze-Dvali. 2021. PCMD-1 bridges the centrioles and the pericentriolar material scaffold in *C. elegans*. *Development*. 148:dev198416. https://doi.org/10.1242/dev.198416

Thevenaz, P., U.E. Ruttimann, and M. Unser. 1998. A pyramid approach to subpixel registration based on intensity. *IEEE Trans. Image Process.* 7:27–41. https://doi.org/10.1109/83.650848

Thomas, Y., M. Peter, F. Mechali, J.-M. Blanchard, O. Coux, and V. Baldin. 2014. Kizuna is a novel mitotic substrate for CDC25B phosphatase. *Cell Cycle*. 13:3867–3877. https://doi.org/10.4161/15384101.2014.972882

Tinevez, J.-Y., N. Perry, J. Schindelin, G.M. Hoopes, G.D. Reynolds, E. Laplantine, S.Y. Bednarek, S.L. Shorte, and K.W. Eliceiri. 2017. TrackMate: An open and extensible platform for single-particle tracking. *Methods*. 115:80–90. https://doi.org/10.1016/j.ymeth.2016.09.016

Tsou, M.-F.B., W.-J. Wang, K.A. George, K. Uryu, T. Stearns, and P.V. Jallepalli. 2009. Polo kinase and separase regulate the mitotic licensing of centriole duplication in human cells. *Dev. Cell*. 17:344–354. https://doi.org/10.1016/j.devcel.2009.07.015

Tollervey, F., M.U. Rios, E. Zagoriy, J.B. Woodruff, and J. Mahamid. 2025. Native molecular architectures of centrosomes in *C. elegans* embryos. *Dev. Cell*. 60:885–900.e5. https://doi.org/10.1016/j.devcel.2024.12.002

Tsou, M.-F.B., A. Hayashi, and L.S. Rose. 2003. LET-99 opposes Galpha/GPR signaling to generate asymmetry for spindle positioning in response to PAR and MES-1/SRC-1 signaling. *Development*. 130:5717–5730. https://doi.org/10.1242/dev.00790

Varadi, M., D. Bertoni, P. Magana, U. Paramval, I. Pidruchna, M. Radhakrishnan, M. Tsenkov, S. Nair, M. Mirdita, J. Yeo, et al. 2024. AlphaFold protein structure database in 2024: providing structure coverage for over 214 million protein sequences. *Nucleic Acids Res.* 52:D368–D375. https://doi.org/10.1093/nar/gkad1011

von Tobel, L., T. Mikeladze-Dvali, M. Delattre, F.R. Balestra, S. Blanchoud, S. Finger, G. Knott, T. Müller-Reichert, and P. Gönczy. 2014. SAS-1 Is a C2 domain protein critical for centriole integrity in *C. elegans*. *PLoS Genet.* 10:e1004777. https://doi.org/10.1371/journal.pgen.1004777

Wang, C., H. Xu, S. Lin, W. Deng, J. Zhou, Y. Zhang, Y. Shi, D. Peng, and Y. Xue. 2020. GPS 5.0: An update on the prediction of kinase-specific phosphorylation sites in proteins. *Genomics Proteomics Bioinformatics*. 18:72–80. https://doi.org/10.1016/j.gpb.2020.01.001

Wang, S., D. Wu, S. Quintin, R.A. Green, D.K. Cheerambathur, S.D. Ochoa, A. Desai, and K. Oegema. 2015. NOCA-1 functions with gamma-tubulin and in parallel to patronin to assemble non-centrosomal microtubule arrays in *C. elegans*. *Elife*. 4:e08649. https://doi.org/10.7554/eLife.08649

Wong, S.S., J.M. Monteiro, C.-C. Chang, M. Peng, N. Mohamad, T.L. Steinacker, B. Xiao, S. Saurya, A. Wainman, and J.W. Raff. 2025. Centrioles generate two scaffolds with distinct biophysical properties to build mitotic centrosomes. *Sci. Adv.* 11:eadq9549. https://doi.org/10.1126/sciadv.adq9549

Wong, S.S., Z.M. Wilmott, S. Saurya, I. Alvarez-Rodrigo, F.Y. Zhou, K.-Y. Chau, A. Goriely, and J.W. Raff. 2022. Centrioles generate a local pulse of Polo/PLK1 activity to initiate mitotic centrosome assembly. *EMBO J.* 41:e110891. https://doi.org/10.15252/embj.2022110891

Woodruff, J.B. 2021. The material state of centrosomes: Lattice, liquid, or gel? *Curr. Opin. Struct. Biol.* 66:139–147. https://doi.org/10.1016/j.sbi.2020.10.001

Woodruff, J.B., O. Wueseke, V. Viscardi, J. Mahamid, S.D. Ochoa, J. Bunkenborg, P.O. Widlund, A. Pozniakovsky, E. Zanin, S. Bahmanyar, et al. 2015. Centrosomes. Regulated assembly of a supramolecular centrosome scaffold in vitro. *Science*. 348:808–812. https://doi.org/10.1126/science.aaa3923

Wueseke, O., D. Zwicker, A. Schwager, Y.L. Wong, K. Oegema, F. Jülicher, A.A. Hyman, and J.B. Woodruff. 2016. Polo-like kinase phosphorylation determines *Caenorhabditis elegans* centrosome size and density by biasing SPD-5 toward an assembly-competent conformation. *Biol. Open*. 5:1431–1440. https://doi.org/10.1242/bio.020990

Yoo, H., T. Kim, S. Ryu, D. Ko, J. Kim, H.J. Choi, Y. Shin, and K. Rhee. 2025. Enhancement of CEP215 dynamics for spindle pole assembly during mitosis. *J. Cell Sci.* 138:jcs263542. https://doi.org/10.1242/jcs.263542

Supplemental material

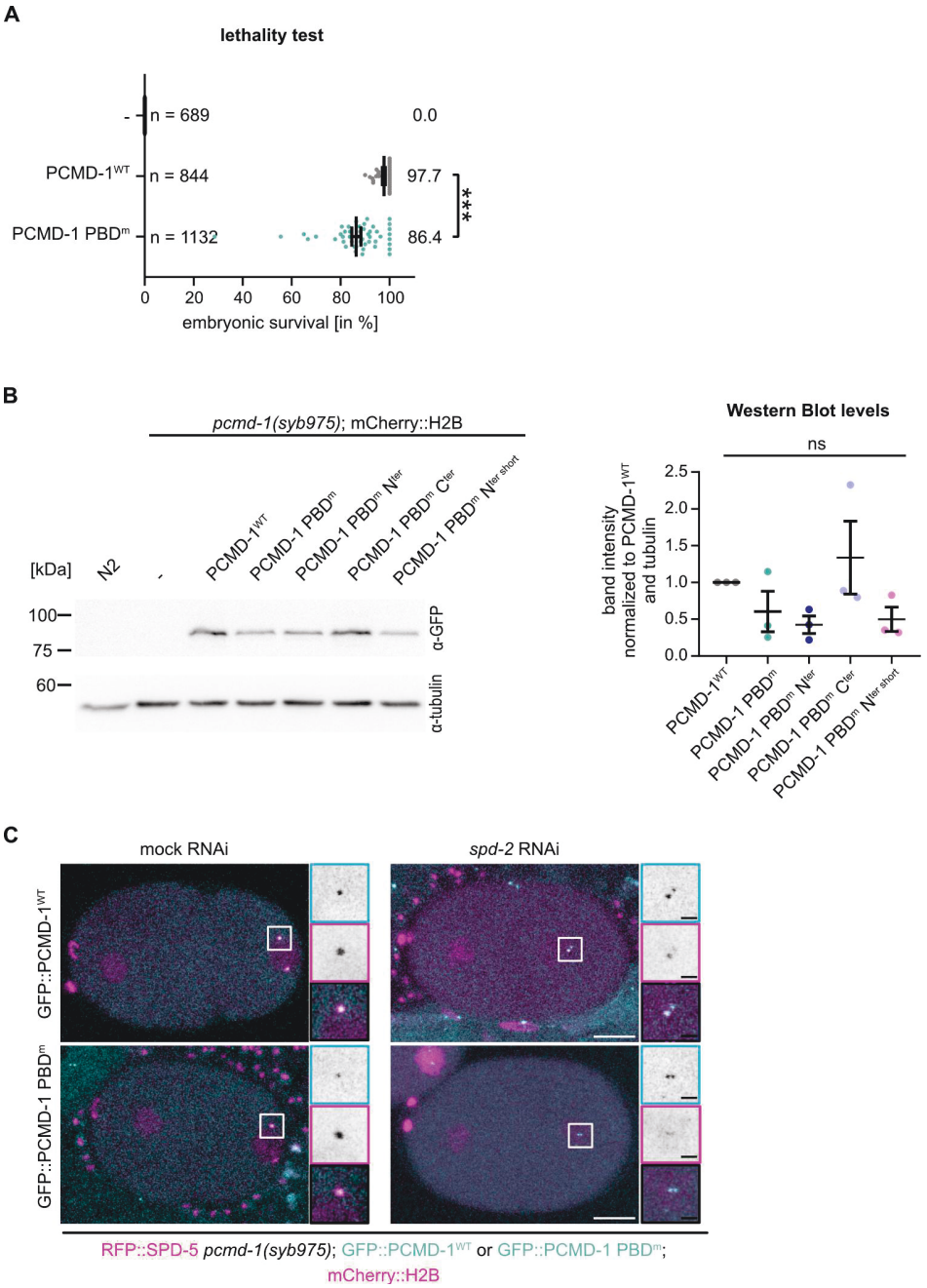

Figure S1. **PCMD-1-PBD^m does not affect SPD-5 recruitment to the PCM core. (A)** Survival rates of GFP::PCMD-1^{WT} and GFP::PCMD-1-PBD^m embryos at 25°C. *n* = number of embryos, P value from a Kruskal–Wallis test with Dunn post hoc. **(B)** Western blots of whole worm lysates expressing diverse GFP-tagged PCMD-1 constructs. Blotted are normalized mean expression levels ± SEM from *n* = 3 experiments. P value from a Friedman test. **(C)** Stills from movies showing RFP::SPD-5 recruitment to the PCM core in GFP::PCMD-1^{WT} (mock: *n* = 20, *spd-2* RNAi: *n* = 24) and GFP::PCMD-1-PBD^m (mock: *n* = 22, *spd-2* RNAi: *n* = 21) embryos after mock or *spd-2* RNAi treatment, *n* = number of centrosomes. White scale bar = 10 µm; black scale bar = 2 µm. P values: n.s. >0.05 > * >0.01 > ** >0.001 > ***. Source data are available for this figure: SourceData FS1.

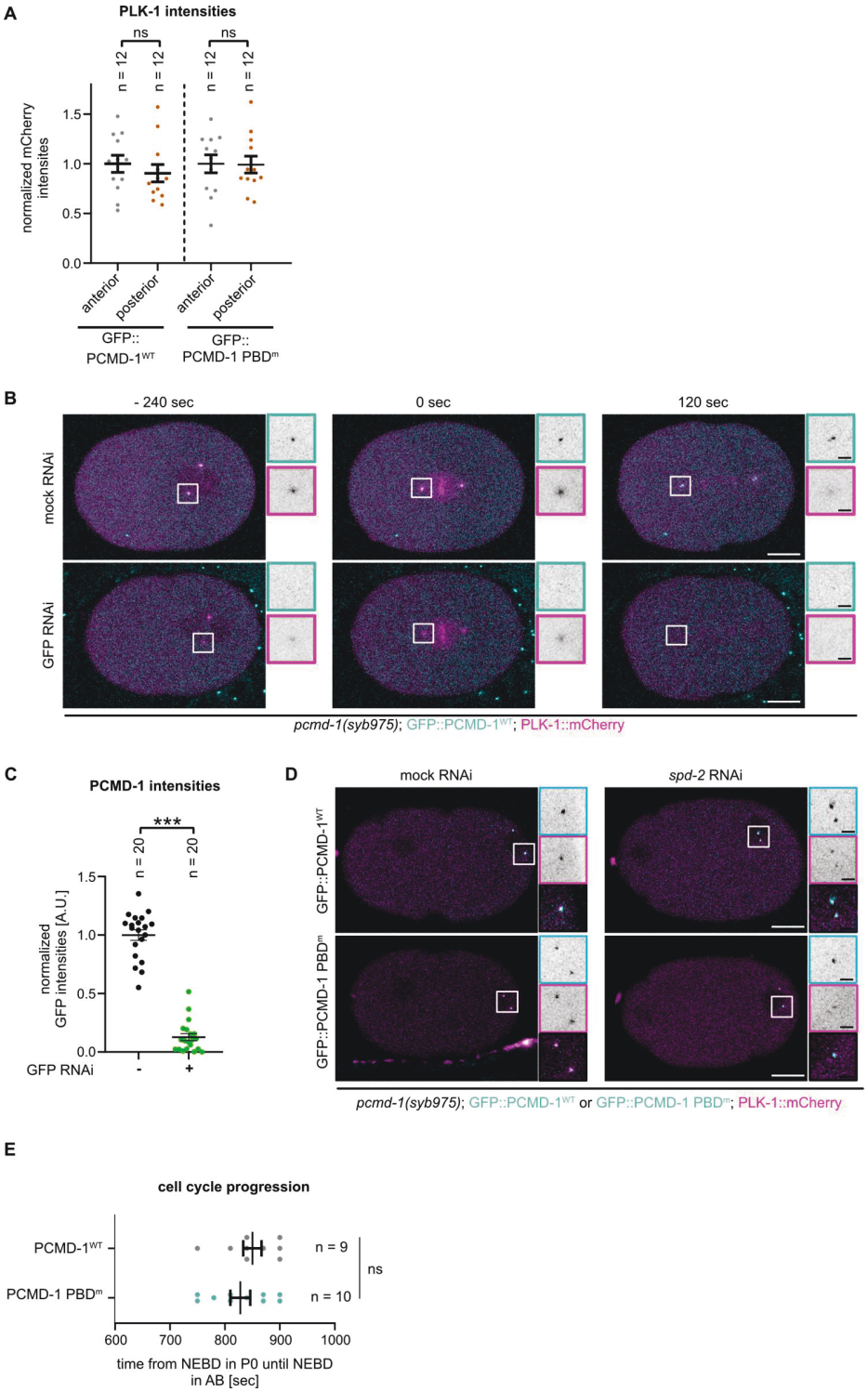

Figure S2. **PLK-1 levels at the centrosome follow the reduction of PCMD-1^{WT} levels. (A)** Normalized PLK-1::mCherry intensities at the anterior and posterior centrosomes at metaphase. P values from two sample *t* tests. *n* = number of analyzed centrosomes. **(B)** Stills of movies of mock and GFP RNAi-treated embryos expressing GFP::PCMD-1^{WT} and PLK-1::mCherry in the *pcmd-1(syb975)* background. Centrosomal areas are shown enlarged in insets. White scale bar = 10 µm; black scale bar = 2 µm. 0 s is metaphase. **(C)** Normalized GFP intensity values of mock or GFP RNAi-treated GFP::PCMD-1^{WT} embryos at metaphase. P value from a Wilcoxon rank-sum test. *n* = number of centrosomes. **(D)** Stills from movies showing PLK-1::mCherry recruitment to the PCM core in GFP::PCMD-1^{WT} (mock: *n* = 18, *spd-2* RNAi: *n* = 10) and GFP::PCMD-1-PBD^{m} (mock: *n* = 10, *spd-2* RNAi: *n* = 12) prophase embryos after mock or *spd-2* RNAi treatment. Centrosomal areas are shown enlarged in insets. White scale bar = 10 µm; black scale bar = 2 µm, *n* = number of centrosomes. **(E)** Cell cycle length measured from NEBD in the first cell cycle (P0) to the NEBD in the AB cell. P value from two sample *t* test. *n* = number of analyzed embryos. P values: n.s. >0.05 > * >0.01 > ** >0.001 > ***.

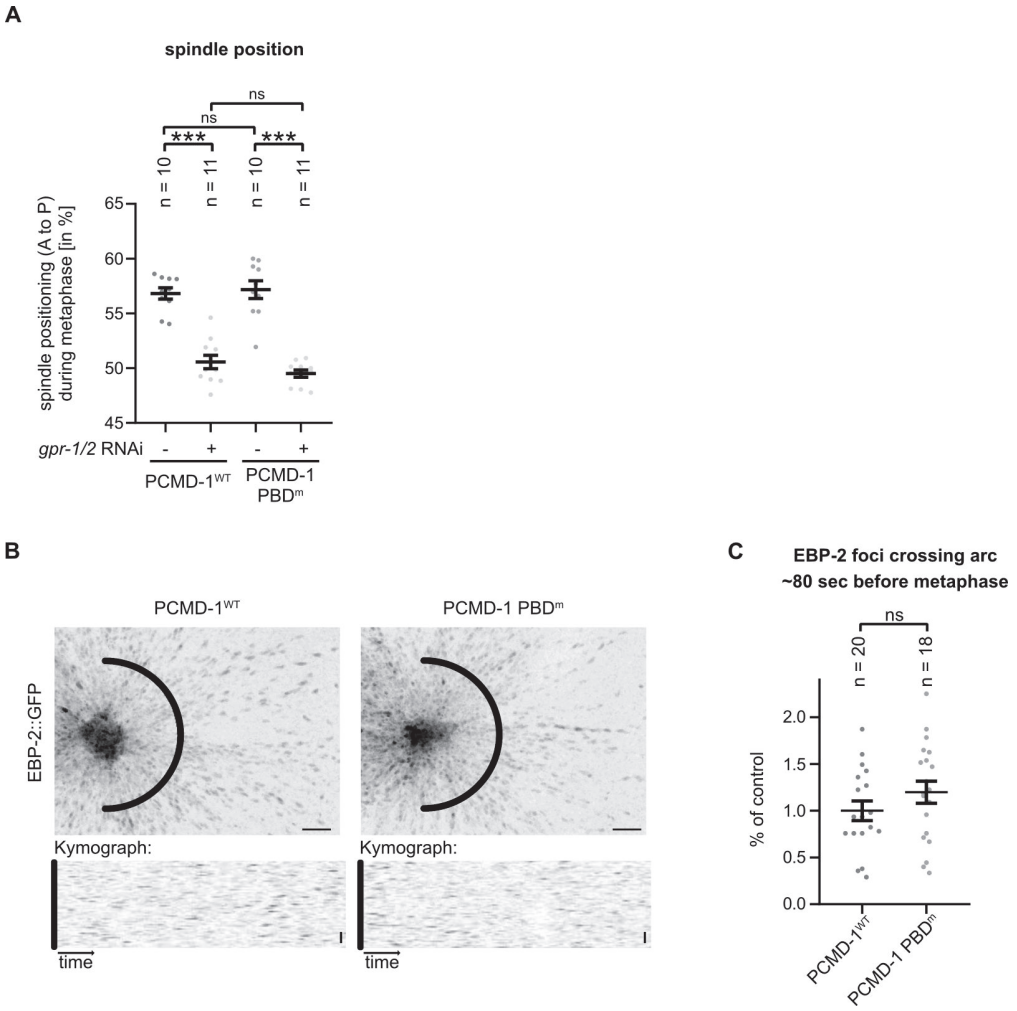

Figure S3. **Microtubule dynamics is not affected in PCMD-1 PBD^m embryos. (A)** Spindle position at metaphase of embryos expressing GFP::PCMD-1^{WT} or GFP::PCMD-1-PBD^m in combination with mCherry::H2B and RFP::SPD-5 and treated with mock or *gpr-1/2* RNAi. P values from ANOVA with subsequent Tukey HSD test. *n* = number of analyzed embryos. **(B)** Top: Projections of movies of the posterior pole ∼80 s before metaphase, of embryos expressing GFP::PCMD-1^{WT} or GFP::PCMD-1-PBD^m in combination with EBP-2::GFP and mCherry::H2B. Bottom: kymographs of the arc shown in the top images. Black scale bar = 2 µm. **(C)** Number of EBP-2::GFP foci crossing the arc over time in ∼80 s. P value from two sample *t* test. *n* = number of centrosomes. P values: n.s. >0.05 > * >0.01 > ** >0.001 > ***.

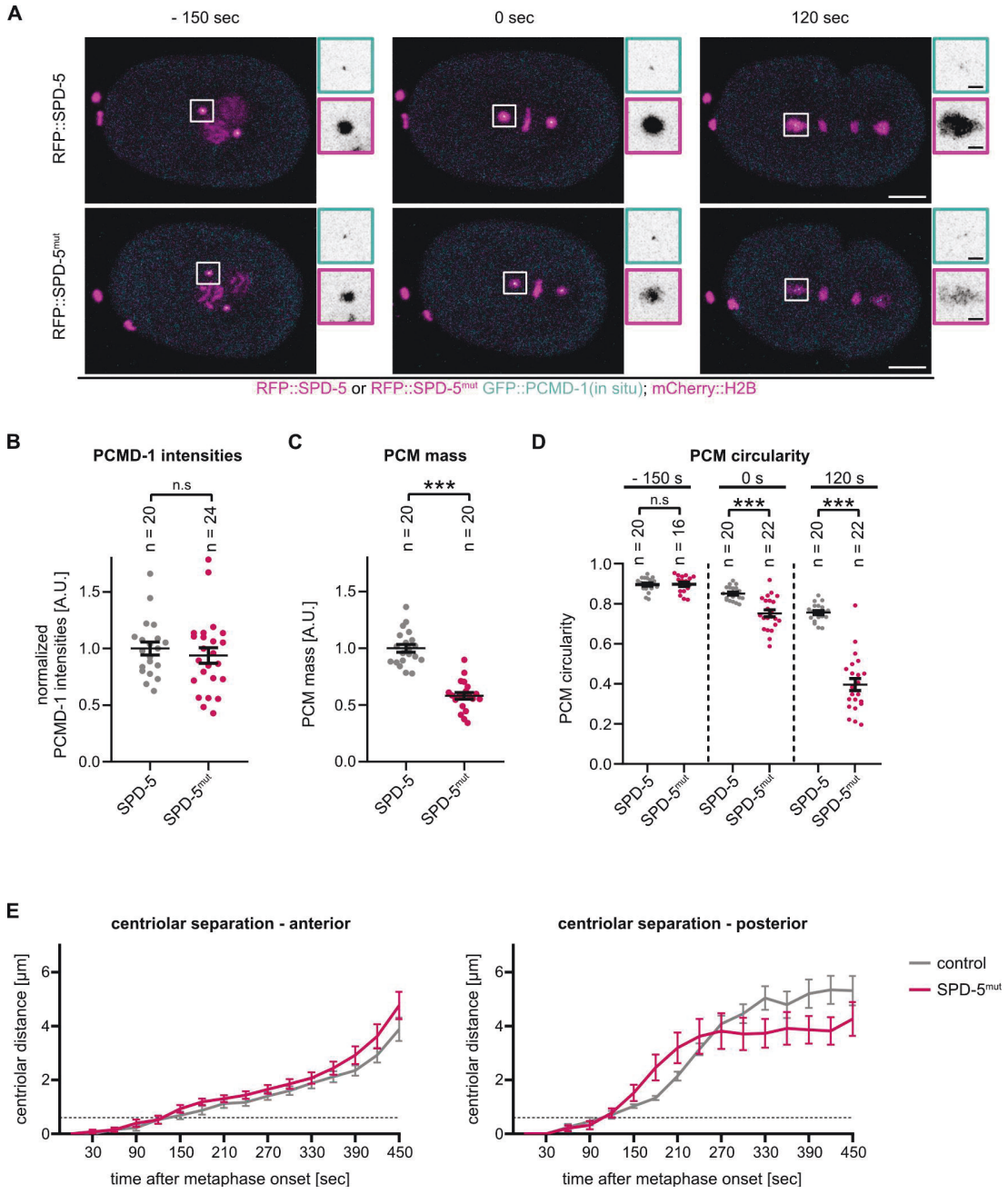

Figure S4. **PCM fragmentation caused by SPD-5(Δ734–918) does not affect PCMD-1 recruitment to the centrosome or centriole separation. (A)** Stills of time-lapse movies of embryos expressing RFP::SPD-5 or RFP::SPD-5^{mut} (Δ734–918) and endogenously tagged GFP::PCMD-1 in combination with mCherry::H2B. Centrosomal areas are shown enlarged in insets. White scale bar = 10 µm; black scale bar = 2 µm. **(B)** Normalized GFP intensities at the centrosome during metaphase. P value from a two sample *t* test. **(C)** Normalized PCM mass at the centrosome during metaphase. P value from two sample *t* test. **(D)** Quantification of PCM circularities at the indicated time points. P values from two sample *t* test and Welch two sample *t* test. **(E)** Quantification of the centriolar distance during the first cell division at the anterior and posterior spindle poles of control RFP::SPD-5 (*n* = 10, in gray) and RFP::SPD-5^{mut} (Δ734–918) (*n* = 10, in pink) embryos. Bold lines represent the mean ± SEM. Dashed lines indicate centrioles at a distance of 0.6 µm, defined as onset of centriole separation. For all movies, 0 s is metaphase. *n* = number of analyzed centrosomes. P values: n.s. >0.05 > * >0.01 > ** >0.001 > ***.

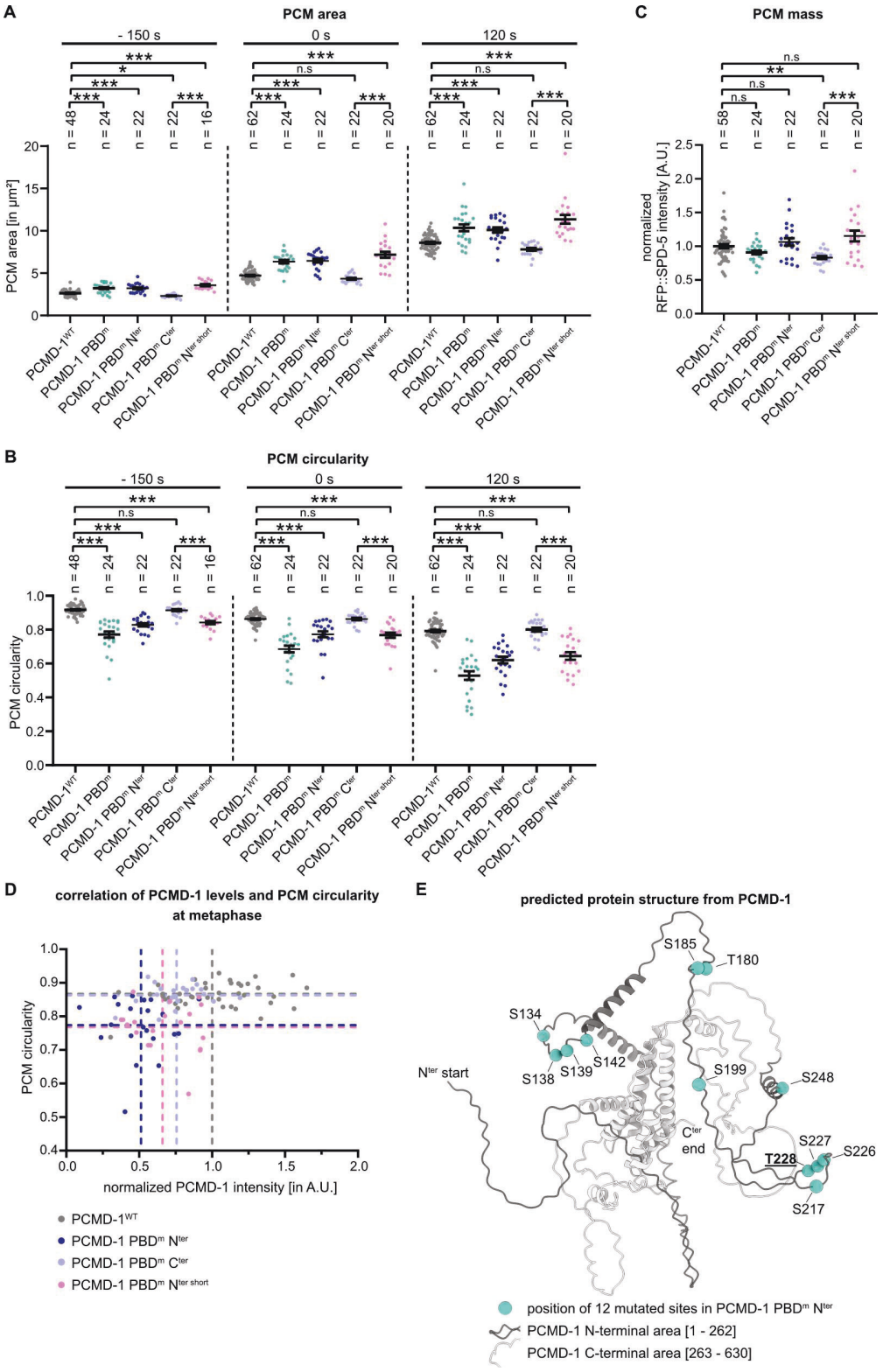

Figure S5. **PBD sites in the N-terminal part of PCMD-1 are needed to form a stable PCM scaffold. (A and B)** Quantification of PCM circularities and areas of GFP::PCMD-1^{WT}, PCMD-1-PBD^{m}, PCMD-1-PBD^{m}N^{ter}, PCMD-1-PBD^{m}C^{ter}, and PCMD-1-PBD^{m}N^{terShort} embryos at indicated time points. P values from Kruskal–Wallis test with Dunn post hoc. *n* = number of analyzed centrosomes. **(C)** Normalized PCM mass at the centrosomes during metaphase. P value from Kruskal–Wallis test with Dunn post hoc. **(D)** Scatter plot correlating PCMD-1 intensities and PCM circularities at metaphase of GFP::PCMD-1^{WT}, PCMD-1-PBD^{m}N^{ter}, PCMD-1-PBD^{m}C^{ter}, and PCMD-1-PBD^{m}N^{terShort}. Dashed lines indicate respective means. **(E)** AlphaFold schematics of PCMD-1^{WT} with the 12 mutant sites from PCMD-1-PBD^{m}N^{terShort}, the one remaining CDK-1 phosphorylation site is in bold and underlined. P values: n.s. >0.05 > * >0.01 > ** >0.001 > ***.

Video 1. **PCM scaffold dynamics in PCMD-1^{WT}.** Movie of the first cell division of a *C. elegans* embryo expressing GFP::PCMD-1^{WT} in combination with mCherry::H2B and RFP::SPD-5 in the *pcmd-1(syb975)* background. Images were taken every 30 s on an inverted Leica Stellaris 5 Point Scanning Confocal Microscope using a 100× HC PL APO oil immersion objective, and a maximum z-projection was made for visualization. The playback speed is 3 frames/s. Time point 0 indicates metaphase.

Video 2. **PCM scaffold dynamics in PCMD-1-PBD^{m}.** Movie of the first cell division of a *C. elegans* embryo expressing GFP::PCMD-1 PBD^{m} in combination with mCherry::H2B and RFP::SPD-5 in the *pcmd-1(syb975)* background. Images were taken every 30 s on an inverted Leica Stellaris 5 Point Scanning Confocal Microscope using a 100× HC PL APO oil immersion objective, and a maximum z-projection was made for visualization. The playback speed is 3 frames/s. Time point 0 indicates metaphase.

Video 3. **AlphaFold model with 12 mutated PBD-binding sites.** AlphaFold Protein Structure Database predicted 3D structure of PCMD-1, with dark gray indicating the N-terminal amino acids 1–262 and light gray indicating the C-terminal amino acids 263–630. The 12 PBD-binding sites of PCMD-1^{NterShort} are highlighted in petrol blue. Playback speed is 25 frames/s.

Provided online are Table S1 and Table S2. Table S1 shows mutated sites in PCMD-1-PBD^{m}, PCMD-1-PBD^{m}N^{ter}, PCMD-1-PBD^{m}N^{terShort}, PCMD-1-PBD^{m}C^{ter}, and CDK-1^{m} and primers and oligos used to generate these sites. Table S2 shows the *C. elegans* strains used.

3. Discussion

A functional centrosome is essential for accurate spindle formation and faithful chromosome segregation. If centrosome function is compromised, PCM fails to withstand microtubule-mediated pulling forces and can become scattered or fragmented, giving rise to extra, acentriolar MTOCs and multipolar spindles (Maiato and Logarinho 2014). Therefore, the PCM must form a strong, load-bearing matrix, yet it cannot remain static: it must assemble rapidly, remodel throughout mitosis, and disassemble again in a tightly controlled manner (Mittasch et al. 2020). This raises fundamental questions that are still incompletely answered: how is the PCM specifically targeted and organized at centrioles, and how can material properties support the PCM to support robust force transmission and dynamic remodeling simultaneously?

The identification of PCMD-1 provided an entry point into these questions (Erpf et al. 2019). PCMD-1 emerged as the long-sought centriolar-PCM bridge in *C. elegans*: in its absence, most centrosomes fail to recruit a detectable SPD-5 scaffold, and in the rare cases where PCM is assembled, it appears strongly disintegrated **(Figure 5C)** (Erpf et al. 2019). But how PCMD-1 executes this bridging role at the molecular level remained unclear. Key questions included how PCMD-1 itself is recruited to centrioles, how it recruits core PCM components, and how it helps to organize a mechanically competent mitotic scaffold.

In the first study (Stenzel et al. 2021), PCMD-1's bridging role was defined at the molecular level by showing that maternally provided PCMD-1 associates early with sperm centrioles, preceding all known PCM components, and that centriolar PCMD-1 is sufficient to recruit SPD-5 and PLK-1 to ectopic sites, thereby establishing PCMD-1 as a genuine tether between centrioles and PCM.

Building on this, the second study (Schreiner et al. 2025) dissects how PCMD-1 shapes the architecture and mechanics of the mitotic PCM. It shows that not only the presence of PCMD-1, but also its dosage at centrioles and its ability to dock PLK-1 are critical for the stabilization of the expanding SPD-5 scaffold. In addition, it reveals a so far unknown requirement for PCMD-1 in centriolar separation at mitotic exit.

Together, these findings reposition PCMD-1 from being merely a static bridge that seeds PCM assembly to a dynamic regulator that couples centriolar architecture, PCM material properties, and cell-cycle-dependent remodeling of the centrosome.

3.1 PCMD-1 bridges centrioles and PCM

Before the identification of PCMD-1 as a centrosomal bridge, centrosome assembly in the *C. elegans* zygote was viewed mainly through the lens of the canonical SPD-2/PLK-1/SPD-5

module known from mitotic centrosomes (Hamill et al. 2002, Pelletier et al. 2004, Woodruff et al. 2015, Wueseke et al. 2016). SPD-5 was established as the principal PCM scaffold, forming a thin interphase core around the sperm-derived “PCM naked” centrioles (McNally et al. 2012) that progressively expands at mitotic entry under the control of SPD-2 and PLK-1 (Woodruff et al. 2015, Ohta et al. 2021). How SPD-5 becomes loaded to the centrioles remained unclear. The discovery of PCMD-1 as a factor required for efficient loading of SPD-5 and PLK-1 onto the non-mitotic centrosome to form the PCM core suggested that PCMD-1 acts as a molecular platform for the PCM module (Erpf et al. 2019); however, its own recruitment dynamics at sperm-derived, initially PCM-less centrioles were not resolved. The finding that maternally provided PCMD-1 is one of the first components to associate with sperm centrioles after fertilization, preceding the accumulation of the SPD-5 core, therefore adds a crucial missing step to this hierarchy. It places PCMD-1 upstream of SPD-5 not only genetically, but also temporally, and identifies PCMD-1 as the earliest known bridge between the sperm centriole and the nascent PCM scaffold proteins.

3.1.1 Recruitment of PCMD-1 to centrioles

The question of how PCMD-1 is connected to the centriolar architecture brings SAS-7 into focus. SAS-7 has been identified as the outermost centriolar component in *C. elegans*, forming a paddlewheel structure at the centriole periphery (Sugioka et al. 2017). This unique positioning makes SAS-7 an attractive candidate for regulating the recruitment or stabilization of PCMD-1. Consistent with this view, SAS-7 perfectly aligns with PCMD-1 positioning and is required for efficient PCMD-1 recruitment during the first embryonic cell divisions. To dissect the underlying protein-protein interactions, a Y2H assay with centriolar candidates was performed. This revealed that PCMD-1 interacts with itself and SAS-4, but not with SAS-7. This raises the possibility that the relationship between PCMD-1 and SAS-7 may depend on local centrosomal specifications, such as PTMs, or may involve an indirect mechanism requiring additional mediators. One plausible scenario is that SAS-4, which has been shown to bind SAS-7 (Boxem et al. 2008 and this study) and PCMD-1, could facilitate such an indirect association. SAS-4 is recruited independently of PCMD-1 (Erpf et al. 2019), placing it upstream in the assembly hierarchy. The biochemical interaction between PCMD-1 and SAS-4 fits well with *in vivo* localization data: in early embryos, PCMD-1 and SAS-4 display nearly overlapping distributions at the ABp (posterior AB daughter at the four-cell stage) blastomere centrosome (Magescas et al. 2021). Moreover, recent ultrastructural mapping positions PCMD-1 in close proximity to SAS-4, with only HYLS-1 residing between them (Woglar et al. 2022), and HYLS-1 also being shown to be recruited by SAS-4 (Dammermann et al. 2009). A critical perspective that questions the idea of purely indirect recruitment via SAS-4 is provided by

studies on SAS-7-deficient mutants. In *sas-7*-mutated embryos, SAS-4 remains stably localized at the centrioles (Sugioka et al. 2017), while PCMD-1 disappears (this study). This observation argues against indirect recruitment of PCMD-1 via SAS-4 alone and highlights a more direct role for SAS-7. Together with subsequent ultrastructural work, which placed SAS-7 as the outermost component of the centriolar paddlewheel surrounding inner paddlewheel proteins, including PCMD-1 (Woglar et al. 2022), these findings support a model in which SAS-7 acts less as a classical docking receptor and more as a structural “shield” at the periphery of the centriole (Woglar et al. 2022). Because SAS-7 encases the centriole as the outermost layer, it is well positioned to stabilize proteins that occupy the paddlewheel region (Woglar et al. 2022). While core centriolar components are stably integrated into the centriole wall and do not readily disassemble (Dammermann et al. 2008, Loncarek and Bettencourt-Dias 2018), the more peripheral paddlewheel proteins might be intrinsically less stable and therefore require the encapsulating “shield” provided by SAS-7 to remain tightly associated. In this framework, SAS-7 does not need to bind PCMD-1 directly; instead, it creates a structural enclosure that limits dissociation and enhances retention of PCMD-1 and its partners at the centriole periphery. Consistent with this shielding model, *sas-7*-mutated embryos display a weak residual PCMD-1 signal at sperm-derived centrioles, which rapidly disappears during prophase, suggesting that SAS-7 is required predominantly for stabilizing rather than initiating PCMD-1 association with the paddlewheel region. An alternative explanation suggests that SAS-7 might recruit PCMD-1 indirectly via an additional, yet unidentified linker protein to bring it near SAS-4. However, this scenario appears less likely than the direct shielding model, as the available localization data do not support this (Woglar et al. 2022). Interestingly, in later cell divisions, PCMD-1 becomes less strictly dependent on SAS-7, suggesting that SAS-7 might be only crucial for the recruitment of PCMD-1 to the sperm-derived centrioles. Once a mature centriole and core PCM have been established in the zygote, PCMD-1 can still be recruited, but its long-term stabilization could be mediated by the persistent core PCM. In this view, the core PCM, once assembled around the sperm-derived centrioles in the zygote, is propagated to all future daughter centrioles and provides a SAS-7-independent platform that supports stabilized PCMD-1 localization at later developmental stages.

Next, the focus was on how PCMD-1 binds to centriole docking sites. In vertebrates and *Drosophila*, PCNT and Plp (the functional homologs of PCMD-1) contain a conserved C-terminal centriolar docking domain, the pericentrin-AKAP450 centrosomal targeting (PACT) domain (Gillingham and Munro 2000, Martinez-Campos et al. 2004, Erpf et al. 2019). As PCMD-1 is conserved only among nematodes and shows no obvious sequence homology to PCNT/Plp (Erpf et al. 2019), a PACT-like docking domain could not be delineated based on sequence alone. Moreover, at the time these experiments were designed, no structural

information beyond a single predicted CC domain was available. Therefore, the centriolar localization region of PCMD-1 was mapped by structure-function analysis of various protein truncations in the mutant endogenous *pcmd-1(t3421)* background. It revealed that neither the N-terminus of PCMD-1, PCMD-1^{N} (AA 2-117, including the predicted CC domain, and IDR 1 and 2), nor its central region, PCMD-1^{C1} (AA 118-342, including IDR 3, 4, and 5), was sufficient to target PCMD-1 to centrioles **(Figure 10A)**. By contrast, PCMD-1's C-terminal region, PCMD-1^{C2} (AA 343-630, including IDR 6) strongly localized at the centrioles **(Figure 10A)**. To test whether the C-terminal region directly engages known centriolar components, further Y2H experiments were performed, which demonstrated that PCMD-1^{C2} interacts with SAS-4, implying that the C-terminal part of PCMD-1 is recruited by SAS-4 to the centriole surface. Consistently, C-terminally tagged PCMD-1 was shown to be localized more proximally to SAS-4 than N-terminally tagged PCMD-1 (Woglar et al. 2022), further supporting a model in which the C-terminus of PCMD-1 mediates its centriolar docking. To determine whether the C2 region alone is responsible for centriolar localization, a construct lacking C2, PCMD-1$^{\Delta C2}$ (AA 2-342), was generated. Surprisingly, PCMD-1$^{\Delta C2}$ still exhibited a residual weak centriolar signal, suggesting that additional protein regions can contribute to low-level centriolar association. Notably, PCMD-1$^{\Delta C2}$ retains the predicted CC domain, a structural motif well known to promote protein oligomerization (Truebestein and Leonard 2016). Such CC-mediated homo-oligomerization might provide a low-affinity centriolar binding interface in the absence of the C-terminal docking site.

Indeed, the maintenance of sufficient PCMD-1 levels at the centriole is further enhanced by its tendency to self-interact, which is largely mediated by the CC domain. Oligomerization via CC domains is a reoccurring feature of centrosome scaffold proteins. Analogous examples are well documented, such as SPD-5 and SAS-6, where higher-order assemblies are critical for organizing PCM and centriole architecture (Qiao et al. 2012, Nakajo et al. 2022, Rios et al. 2024). For PCMD-1, deletion of the CC domain revealed that its self-interaction is completely abolished, whereas interaction is still detectable between PCMD-1$^{\Delta CC}$ (AA Δ86-117) and wild-type PCMD-1. This suggests that at least one interaction interface lies outside of the CC domain. *In vivo*, expressed PCMD-1$^{\Delta CC}$ leads to a pronounced reduction of PCMD-1 levels at centrioles and a slightly disorganized PCM, yet centrosomes remain largely functional. Together, these observations indicate that the CC region is not strictly essential for PCMD-1 activity but promotes its efficient accumulation at centrioles. In the context of the rapid embryonic divisions during the first *C. elegans* cell cycles, such CC-mediated multivalency is likely to facilitate the rapid build-up of a critical PCMD-1 concentration at centrioles within the narrow time window. Therefore, the relatively mild phenotype of the CC deletion suggests that this region acts as a robustness factor that optimizes centriolar assembly, rather than as an absolutely essential element of PCMD-1 function.

In summary, PCMD-1 recruitment to sperm-derived centrioles can be viewed as a multilayered process. Maternally provided PCMD-1 is one of the earliest known factors to associate with PCM-naked centrioles after fertilization, and this association is driven mainly by its C-terminal region via interaction with SAS-4, while the CC domain promotes its efficient accumulation **(Figure 10B)**. Once PCMD-1 and other paddlewheel proteins are in place, the surrounding SAS-7 layer likely acts as a structural cage that stabilizes this outer centriolar compartment during the rapid early embryonic divisions **(Figure 10B)**.

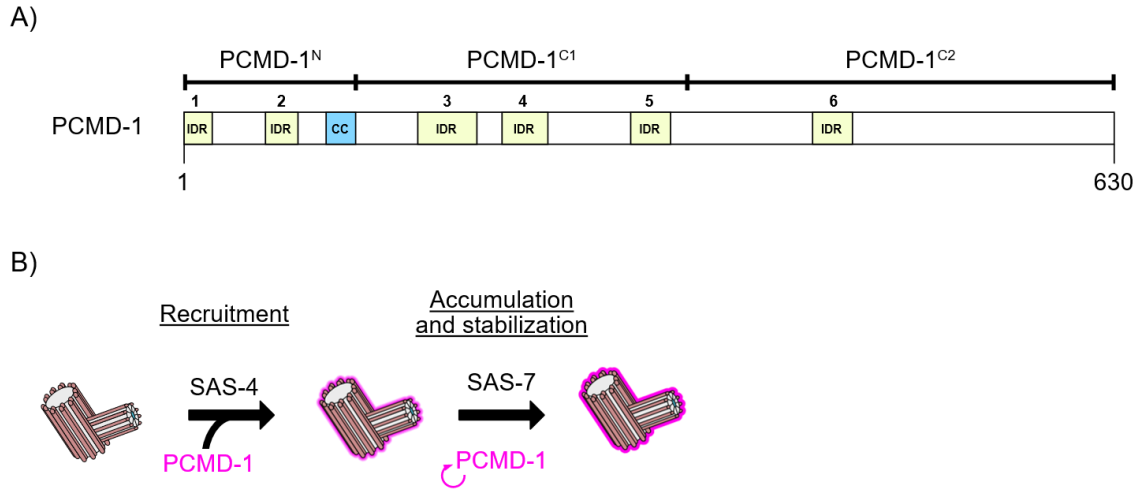

Figure 10: Centriolar recruitment of PCMD-1.
A) *Organization of the PCMD-1 protein with one predicted CC domain and six IDRs. Protein truncations of the structure-function analysis, PCMD-1^{N} (AA 2-117), PCMD-1^{C1} (AA 118-342), and PCMD-1^{C2} (AA 343-630), are shown.* ***B)*** *PCMD-1 is recruited to centrioles primarily through an interaction of its C-terminal domain with SAS-4. Subsequent CC-domain-driven self-association promotes the accumulation of PCMD-1, and its localization is ultimately stabilized by SAS-7, which likely acts as a shield (Woglar et al. 2022).*

Several key questions regarding the centriolar localization of PCMD-1 remain open. To understand the pronounced requirement for SAS-7 in early, but not later, embryonic divisions, a degron-based system could be used to acutely deplete SAS-7 at defined developmental stages and quantify the impact on PCMD-1 recruitment and maintenance at centrioles. Moreover, testing the proposed SAS-7 “shielding” model will be challenging but could be approached by FRAP analysis of the early PCMD-1 fraction in *sas-7* mutants. Thereby, it might be possible to differentiate whether SAS-7 loss primarily affects PCMD-1 retention rather than its initial recruitment. In addition to SAS-4/SAS-7 dependent mechanisms, centriolar microtubules may also contribute to PCMD-1 recruitment or stabilization. This idea is supported by the close spatial proximity of PCMD-1 to centriolar microtubules in ultrastructural maps (Woglar et al. 2022) and by the *in vivo* overlap of PCMD-1 with spindle microtubules observed in this study. *In vitro* microtubule co-sedimentation assays using different PCMD-1

regions could test whether microtubules constitute an additional interaction surface that helps to recruit or retain PCMD-1 at the centriole interface.

3.1.2 PCMD-1 recruits PCM components

The next question arising was how centriole-bound PCMD-1 contributes to the assembly of a functional PCM. The essential role of PCMD-1 in this process becomes particularly evident during early embryogenesis, when centrosomes must be rapidly converted into robust MTOCs. In *C. elegans*, the absence of PCMD-1 causes nearly all embryos to fail to efficiently recruit key PCM components at the onset of development. Consequently, they cannot build a stable SPD-5-based scaffold (Erpf et al. 2019), highlighting that PCMD-1 is indispensable for initiating PCM assembly at the centrosome. In the canonical view of mitotic PCM assembly, this scaffold is organized by the conserved SPD-2/PLK-1/SPD-5 module, in which centriolar SPD-2 recruits PLK-1 and thereby promotes the incorporation and expansion of the SPD-5 matrix around centrioles (Decker et al. 2011, Woodruff et al. 2015, Wueseke et al. 2016, Varadarajan and Rusan 2018). The identification of PCMD-1 as an additional centriole-proximal factor that is required for efficient SPD-5 loading (Erpf et al. 2019), therefore, raises the question of how PCMD-1 integrates into, and potentially modulates, this SPD-2/PLK-1/SPD-5 module.

To characterize the molecular mechanism by which PCMD-1 orchestrates PCM assembly, a series of interaction assays - including Y2H assays, co-immunoprecipitation, and *in vivo* translocation assays (TA) - testing PCM components were performed. These approaches demonstrate that PCMD-1 interacts directly with SPD-5, as well as with PLK-1. Strikingly, in TAs, PCMD-1 can independently translocate these two PCM components to an ectopic subcellular location in *C. elegans* embryos, demonstrating its strong recruiting capacity. Consistent with this, a recent study confirmed and refined these interaction networks by mapping the binding interfaces in more detail: the interaction between SPD-5 and PCMD-1 was pinpointed to PCMD-1's N-terminal region (AA 1-242) and the centriolar localization domain of SPD-5 (Nakajo et al. 2022), and the association of PCMD-1 with PLK-1 was narrowed down to PLK-1's C-terminal Polo-box-domains (PBDs) (Nakajo et al. 2022), which are required to bind PLK-1 to its interaction partners. To directly test whether PCMD-1 can recruit the core PCM rather than the PLK-1 phosphorylation-dependent mitotic scaffold, the PCM-maturation-deficient SPD-5^{4A} mutant was tested (Woodruff et al. 2015). In this mutant, four PLK-1 phosphorylation sites required for PCM maturation are rendered non-phosphorylatable so that SPD-5^{4A} still accumulates at the PCM core after fertilization but fails to form an expanded mitotic PCM scaffold (Woodruff et al. 2015, Ohta et al. 2021). In TAs, SPD-5^{4A} was efficiently recruited to ectopic sites by PCMD-1, even in a *spd-5*-depleted endogenous background. This demonstrates that PCMD-1-mediated docking does not depend

on these PLK-1 sites and can operate on a non-mature or also “PCM scaffold-inactive” version of SPD-5. This is consistent with the fact that the mutated residues lie outside the centriolar localization domain of SPD-5 (Nakajo et al. 2022) and support a model in which a centriolar pool of autoinhibited SPD-5 is first recruited and seeded at the PCM core by PCMD-1. Then, PLK-1, recruited by either PCMD-1 (this study) or SPD-2 (Decker et al. 2011), acts downstream to convert this PCM seed into an expanding PCM matrix. In this view, the spatial positioning of SPD-5 at centrosomes is primarily determined by PCMD-1, whereas the timing and extent of scaffold maturation are governed by PLK-1 signaling. Interestingly, while PCMD-1 efficiently recruits PCM proteins such as SPD-5 to an ectopic location in the TA, attempts to anchor centriolar proteins, including SAS-4 and SAS-7, were unsuccessful. This finding matches *in vivo* data showing that localization of SAS-4 and SAS-7 (Erpf et al. 2019 and this study) is independent of PCMD-1 during embryogenesis and, as a logical consequence, cannot be recapitulated by membrane tethering. Similarly, SAS-4$^{\Delta TCP}$, which is not recruited to the centrioles and therefore resides at the PCM (Cottee et al. 2013), also failed to be recruited to membranes in TAs. This suggests that either additional local environmental cues, like PTMs, or the TCP domain of SAS-4 are needed for their interaction. Altogether, these results highlight the remarkable selectivity of PCMD-1 during PCM assembly, specifically targeting distinct PCM proteins while excluding core centriolar components. Thus, they support a model in which PCMD-1 acts as a centriole-anchored adaptor that recruits the core PCM module: PCMD-1 binds non-mitotic and mitotic SPD-5 as well as PLK-1 and is even sufficient to recruit them to ectopic sites. Consequently, PCMD-1 provides a dedicated centriole-proximal platform that first seeds the initial PCM scaffold and later recruits mitotic PCM components, such as PLK-1. In early embryos, this adaptor function positions PCMD-1 as a key regulator that couples centriolar architecture to PCM formation and ensures that PCM assembly is initiated at the correct place and time.

However, these interaction networks are not limited to SPD-5 and PLK-1. Y2H assays have also identified additional PCMD-1 interactions with Polo-like kinase 2 (PLK-2; human Plk1; *Drosophila* Polo) and the PCM-associated protein TAC-1 (Nakajo et al. 2022), indicating that PCMD-1 can contact a broader set of PCM-associated regulators. PLK-2 and PLK-1 are both highly conserved and considered orthologous to human Plk1 (Brandt and Kim 2021). Moreover, PLK-2 has been shown to act redundantly with PLK-1 in the establishment of embryonic polarity (Nishi et al. 2008). However, in contrast to PLK-1, PLK-2 localizes predominantly to meiotic pairing centers at the nuclear envelope and later to the synaptonemal complex in the germline (Harper et al. 2011, Labella et al. 2011), although weaker PLK-2 signals have also been detected at centrosomes in proliferative germ cells (Harper et al. 2011). These observations raise two, not mutually exclusive, possibilities: PLK-2 may carry out as-yet uncharacterized centrosomal functions, potentially in germline-specific PCM regulation,

or the PCMD-1/PLK-2 interaction detected in Y2H primarily reflects the conserved PBD architecture of PLK-2 shared with PLK-1, without necessarily implying a major centrosomal role for PLK-2 *in vivo*. TAC-1, by contrast, belongs to the evolutionarily conserved TACC protein family (Bellanger and Gönczy 2003) and is a PCM- and spindle-associated microtubule regulator (Le Bot et al. 2003). Its interaction with PCMD-1 raises the possibility that PCMD-1 not only recruits the SPD-5 scaffold and Polo-like kinases but may also help position or stabilize microtubule-regulatory factors within the PCM. Although the physiological relevance of these interactions and their contribution to active recruitment remains to be established, they raise the possibility that PCMD-1 integrates additional kinase and microtubule-regulatory inputs into the PCM assembly process. How and if these connections influence centrosome architecture, organization, and function will require future investigation.

Before the identification of PCMD-1, SPD-2 was considered a putative centriolar organizer linking centrioles to PCM assembly in *C. elegans* (Varadarajan and Rusan 2018): it localizes close to the centriole wall and the PCM, recruits PLK-1, and promotes the incorporation and expansion of the SPD-5 scaffold (Kemp et al. 2004, Pelletier et al. 2004, Decker et al. 2011, Woodruff et al. 2015). Importantly, SPD-2 still localizes to centrioles in *pcmd-1(t3421)* embryos, even though its PCM-associated pool is reduced, indicating that SPD-2 recruitment to centrioles is largely PCMD-1 independent (Erpf et al. 2019). In this situation, SPD-2 very likely recruits the residual PCM fractions via its interaction with SPD-5 (Boxem et al. 2008, Erpf et al. 2019). Conversely, inhibition of SPD-2 alone leaves a residual SPD-5-positive PCM core, whereas simultaneous loss of PCMD-1 and SPD-2 abolishes PCM core formation and mitotic PCM expansion completely (Erpf et al. 2019). Furthermore, PCMD-1 localization to centrioles is independent of SPD-2 (Erpf et al. 2019). Together, these observations indicate that SPD-2 and PCMD-1 contribute to PCM assembly through largely independent, but cooperating activities. A simple model in which they act as a single joint recruitment complex appears unlikely, as no direct biochemical interaction between the two proteins was detected in the Y2H screen of this study. Instead, SPD-2 and PCMD-1 are best viewed as partially parallel routes: PCMD-1 provides a dedicated centriolar docking platform that directly couples SPD-5 and PLK-1 to the centriole surface, whereas SPD-2 channels PLK-1 activity and modulates assembly and mechanics of the SPD-5 scaffold. Such functional specialization is likely to be particularly important in the rapid embryonic cell cycles of the *C. elegans* zygote. Under these conditions, even modest perturbations in PCM recruitment can result in insufficient scaffold formation and defective spindle assembly, ultimately leading to embryonic lethality.

Having established that the C-terminal region of PCMD-1 provides the principal centriolar docking module, the next question was which parts of the protein are required for PCM recruitment and function. In this context, PCMD-1 functionality was defined by the ability of the PCMD-1 constructs **(Figure 10A)** to assemble a PCM scaffold and to rescue the embryonic

lethality of the *pcmd-1(t3421)* in the single-copy replacement background. Constructs that fail to localize to centrioles do not support PCM assembly and cannot restore viability. However, despite robust centriole localization, the C-terminal PCMD-1^{C2} alone is also unable to restore function, indicating that centriole attachment per se is not sufficient for PCMD-1 function. By contrast, constructs that localize at the centrioles and include the central region PCMD-1^{C1} almost fully restore protein function. These observations highlight the central region, which contains three of the predicted IDRs **(Figure 10A)**, as the key interface for engaging the PCM, in agreement with the previously mentioned mapping that placed the SPD-5-binding site of PCMD-1 within its N-terminal region (Nakajo et al. 2022).

3.1.3 Model: PCMD-1 bridges PCM components and centrioles

For PCMD-1 to function as a tether between centrioles and the PCM, it first needs to be anchored at the centriole surface. Maternally provided PCMD-1 associates with PCM-naked sperm-derived centrioles after fertilization, thereby licensing their SPD-5 core assembly. Centriolar association is driven primarily by the C-terminal region of PCMD-1 via direct interaction with SAS-4 and positions PCMD-1 immediately peripheral to the centriolar microtubules **(Figure 11B)** (Woglar et al. 2022). Moreover, the CC domain promotes local protein concentration. Once PCMD-1 and other paddlewheel proteins have been recruited, the surrounding SAS-7-layer might act as a structural cage that stabilizes this outer centriolar compartment **(Figure 11B)**. Together, the coordinated action of centriolar docking, self-organization, and SAS-7-dependent stabilization create a multilayered and partly redundant assembly mechanism that helps to ensure robust PCMD-1 centrosomal loading throughout embryonic development, especially during the rapid early embryonic divisions.

Anchored this way at the centriolar periphery, PCMD-1 employs its N-terminal region to interact with early PCM matrix proteins, most notably SPD-5 and PLK-1 **(Figure 11B)**. In this model, PCMD-1 first seeds a non-mitotic PCM core by recruiting an autoinhibited pool of SPD-5 to the centriole, thereby defining where a SPD-5-based scaffold can form, independently of its mitotic expansion. This centriolar SPD-5 pool provides a spatially confined “PCM seed” that is physically coupled to the centriole wall via PCMD-1. Upon mitotic entry, PLK-1 activity then converts this seed into an expanding PCM matrix: PLK-1 is probably brought to centrosomes through interactions with both PCMD-1 and SPD-2; it phosphorylates SPD-5 and thereby promotes scaffold assembly and enlargement around the centriole **(Figure 11B)**. In parallel, SPD-2 modulates the amount and mechanical properties of the SPD-5 matrix, while PCMD-1 continues to supply a centriolar docking platform for SPD-5 and PLK-1.

A key element of this recruitment platform might be the structural organization of PCMD-1 itself. Sequence analysis predicts that PCMD-1 contains large intrinsically disordered stretches **(Figure 11A)** (Erdős and Dosztányi 2024, Erdős et al. 2025). Disordered protein regions lack a fixed 3D conformation and can adopt different configurations depending on PTMs or binding partners, thereby supporting multivalent and condition-dependent interactions (Tompa and Fuxreiter 2008, Bah and Forman-Kay 2016). A comparable principle has been proposed for SPD-2, where phosphorylation of its unstructured N-terminus may tune its interaction profile in a context-dependent manner (Murph et al. 2022). The dual architecture of PCMD-1 fits neatly with its role at centrosomes: the more structured C-terminus provides a stable centriolar anchor, while the flexible, disordered central region can adapt to bind different PCM factors **(Figure 11A)**, such as non-mitotic and mitotic SPD-5 and PLK-1, and thereby support both the initial seeding of a core SPD-5 scaffold and its subsequent mitotic maturation and organization.

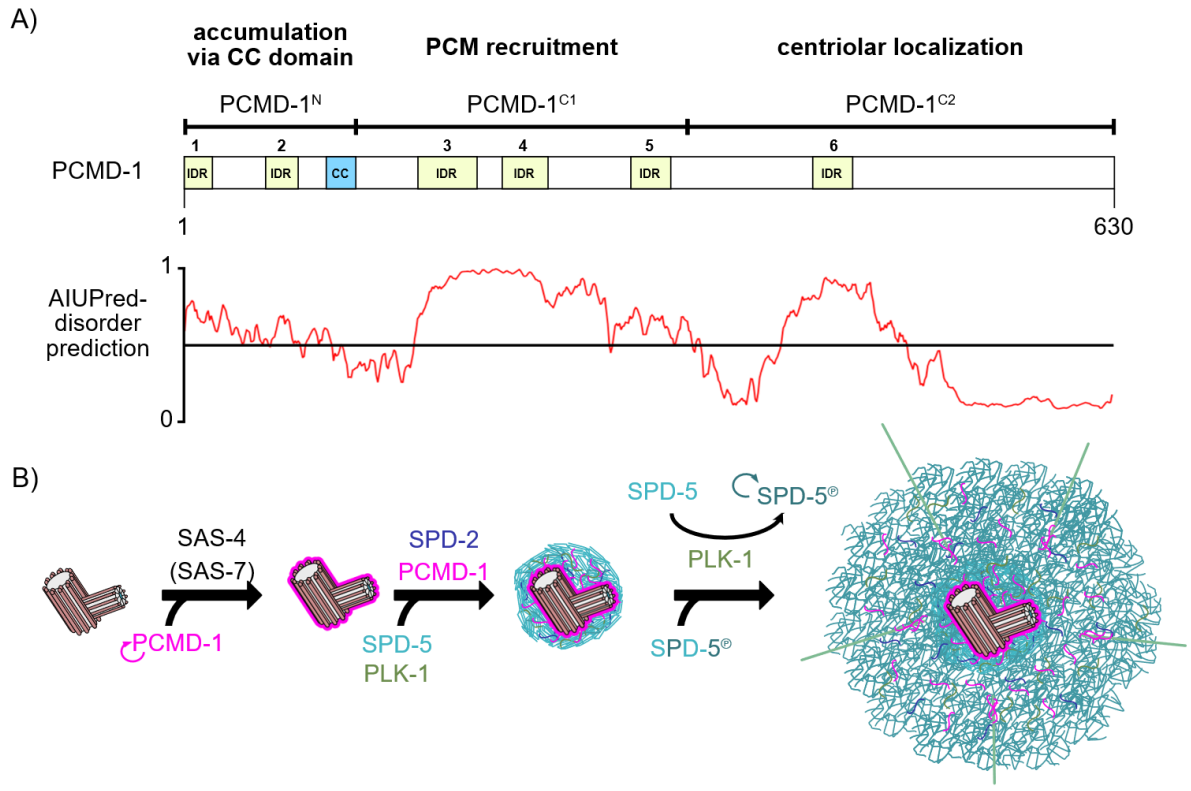

Figure 11: PCMD-1 bridges centrioles and PCM.
A) *Top: Organization of PCMD-1 with identified structure-functions. Bottom: Prediction of protein disorder of PCMD-1 generated by AIUPRED (Erdős and Dosztányi 2024, Erdős et al. 2025). Above 0.5 indicates disordered protein regions, below 0.5 indicates structured protein regions.* ***B)*** *PCMD-1 is recruited to centrioles via its C-terminal domain, dependent on SAS-4 and SAS-7. Once incorporated, it recruits the core PCM components PLK-1 and inactive SPD-5, in parallel with SPD-2. Their close proximity then allows PLK-1 to phosphorylate SPD-5, promoting its multimerization and the incorporation of additional SPD-5 molecules into the matrix, ultimately driving PCM maturation.*

The bridging function of PCMD-1 is closely mirrored by Plp in *Drosophila* and PCNT in vertebrates, such as human cells. Both Plp and PCNT are large CC proteins with a centriolar docking PACT domain at their C-terminus (Gillingham and Munro 2000, Martinez-Campos et al. 2004, Mennella et al. 2012). Upon C-terminal docking at the centriole, the long N-terminal regions of PCNT and Plp extend outward into the PCM, where they nucleate and organize the surrounding matrix (Lawo et al. 2012, Mennella et al. 2012). Like PCMD-1, Plp and PCNT selectively interact with PCM components; however, they are localized around the centrioles, emphasizing their specialized bridging functions (Buchman et al. 2010, Lawo et al. 2012, Mennella et al. 2012, Kim and Rhee 2014, Richens et al. 2015). All three proteins enable the PCM scaffold to be stably anchored to the underlying centriolar wall, and disruption of their function leads to abnormal PCM structure, if at all recruited, and defective mitotic spindle assembly. Although PCMD-1 lacks a recognizable PACT domain, its C-terminally mediated centriolar recruitment and proximal positioning suggest a functionally analogous mechanism. In agreement with this, ultrastructural analyses show that PCMD-1, Plp, and PCNT share the ability to position their C-termini close to the centrioles, with their N-termini projecting outwards (Lawo et al. 2012, Mennella et al. 2012, Woglar et al. 2022) - placing core PCM matrix components in proximity for phosphorylation (by PLK kinases) and subsequent expansion. Thus, despite evolutionary differences and the lack of a canonical PACT motif in PCMD-1, their core function as dynamic PCM bridges seems to be highly conserved.

3.2 PCM organization regulated by PCMD-1

In current models of mitotic PCM assembly in *C. elegans*, PCM organization is mainly attributed to SPD-2 and to a dynamic interplay between the kinase PLK-1 and the counteracting phosphatase PP2A, which altogether control SPD-5 incorporation, expansion, and disassembly at the centrosome (Woodruff et al. 2015, Wueseke et al. 2016, Enos et al. 2018, Magescas et al. 2019, Mittasch et al. 2020, Ohta et al. 2021, Rios et al. 2024, Amato et al. 2025). A contribution of PCMD-1 to PCM organization had already been suggested, as the few *pcmd-1(t3421)* embryos, which were able to recruit SPD-5, displayed a structurally highly abnormal PCM **(Figure 5B)** (Erpf et al. 2019). Yet, it was unclear whether PCM disorganization resulted from reduced PCM levels or whether PCMD-1 also exerts a distinct organizational role beyond tethering. In this work, the contribution of PCMD-1 to this framework is defined more precisely: both the abundance of PCMD-1 at centrosomes and its ability to dock PLK-1 emerge as key parameters for PCM architecture. When the interaction between PCMD-1 and PLK-1 is specifically hindered, PCM still assembles around centrioles but fails to form a properly organized and mechanically stable scaffold. This identifies the centrosomal

PCMD-1/PLK-1 module as an additional layer of regulation within the SPD-2/PLK-1/PP2A-centered network that governs mitotic PCM architecture.

The disruption of PBD-docking motifs in the PCMD-1 PBD^{m} (for PCMD-1 PBD mutant) leads to almost complete abolition of PLK-1 interaction in Y2H assays. Expressed *in vivo*, the centriolar recruitment of PCMD-1 PBD^{m} is strongly reduced but not abolished, and embryonic viability is only mildly compromised, arguing that a minimal pool of PCMD-1 still suffices to support basic centrosome function. Likewise, SPD-5 accumulates at centrosomes to near wild-type levels. Even in the absence of SPD-2, SPD-5 was still recruited, indicating that neither core PCM assembly nor scaffold expansion strictly depends on PLK-1 docking to PCMD-1. The most prominent defects instead lie in PCM architecture: the SPD-5 matrix fails to adopt a compact, cohesive organization and instead appears broadened, flared, and prone to fragmentation. Consistent with a mechanically fragile scaffold, this disorganized PCM responds strongly to alterations in pulling forces. When pulling forces are reduced, the PCM does not revert to a wild-type-like compact shape. During prometaphase and metaphase, no major improvement in PCM morphology is observed, and only a partial rescue becomes apparent in anaphase. Although residual pulling forces cannot be excluded, at least some restoration of PCM shape would be expected if pulling forces alone were responsible for the defect. Conversely, when pulling forces are increased, the broadened and flared PCM morphology is further exaggerated, revealing a weak scaffold that is unable to cope with elevated mechanical stress. Thus, PCMD-1 PBD^{m} represents the first separation-of-function condition for PCMD-1, in which its role in seeding PCM at centrioles is largely preserved, while its contribution to proper PCM organization is specifically compromised.

How does this PCMD-1 PBD^{m} phenotype relate to previous work on PCM organization? Earlier studies have shown that PCM stability is highly sensitive to both the molecular properties of the SPD-5 scaffold and to its regulation by mitotic kinases and phosphatases. On the regulatory side, inhibition of PLK-1 results in a structurally weak PCM scaffold that dissolves prematurely (Cabral et al. 2019). On the contrary, RNAi-mediated depletion of PP2A subunits leads to a more flexible, deformable PCM structure (Enos et al. 2018, Magescas et al. 2019, Amato et al. 2025). Both conditions are consistent with a SPD-5 scaffold whose phosphorylation state and intermolecular connectivity are improperly tuned (Amato et al. 2025). On the structural side, SPD-5 mutants have revealed how specific interaction modules contribute to scaffold robustness: SPD-5^{4A}, in which four key PLK-1 sites are rendered non-phosphorylatable, fails to form a mitotic PCM altogether (Woodruff et al. 2015). In contrast, its phospho-mimetic SPD-5^{4E} version gives rise to a distorted and stretched PCM with reduced total PCM mass (Amato et al. 2025). SPD-5$^{\Delta 734\text{-}918}$, which retains these specific phosphorylation sites but lacks a central CC domain providing multiple self-interaction interfaces, assembles a smaller, distorted PCM that fragments prematurely (Rios et al. 2024).

Interestingly, this SPD-5 mutant revealed PCM defects only from metaphase onwards (this study), when mechanical forces on the centrosome become the strongest. These conditions illustrate that most previously described PCM organization defects arise when either the quantity of SPD-5 in the scaffold or its intrinsic multimerization/phosphorylation state is directly perturbed.

The PCM scaffold in PCMD-1 PBD^{m} shares essential features with these mutants but also reveals a distinct mode of PCM destabilization. Similar to SPD-5 structural and regulatory mutants, the PCM in PCMD-1 PBD^{m} loses its compact, cohesive architecture and appears broadened, flared, and structurally fragile. However, in contrast to many SPD-5 mutants and kinase/phosphatase perturbations, the overall accumulation of SPD-5 at centrosomes remains the same, with SPD-5 being even recruited in the absence of SPD-2. Furthermore, in PCMD-1 PBD^{m}, the structural abnormality of the PCM occurs from the moment of its initial recruitment and is not solely a consequence of the structural weakness to microtubule-mediated pulling forces. Thus, inhibiting the binding of PLK-1 to PCMD-1 does not primarily impair PCM assembly but uncouples scaffold formation from its mechanical stabilization: a quantitatively normal SPD-5 scaffold is built but cannot be stably maintained under mitotic forces.

3.2.1 PCMD-1's dosage-dependent control of PCM organization

A central question arising from the PCMD-1 PBD^{m} phenotype is whether reduced centrosomal PCMD-1 levels alone are sufficient to account for PCM disorganization, or whether additional, PLK-1 docking-dependent mechanisms are involved. Previous analysis of a mutant version lacking self-interaction (PCMD-1$^{\Delta CC}$) already indicated that PCMD-1 levels are an essential parameter for PCM organization: deletion of the CC domain strongly reduces centrosomal PCMD-1 levels and leads to a disorganized PCM scaffold, while PCM recruitment is not, and embryonic viability is only mildly affected (Stenzel et al. 2021). In general, this suggests that the system can tolerate substantial reductions in PCMD-1 concentration without catastrophic loss of centrosome function, but that PCM morphology is noticeably compromised long before viability is severely impacted, at least under laboratory conditions. Whether such perturbations would be tolerated in natural environments remains unclear.

This view is supported by the stepwise reduction of centrosomal wild-type PCMD-1 levels, which revealed a clear dose-dependent contribution of PCMD-1 to PCM organization. Progressive depletion caused a gradual decrease of centrosomal PCMD-1 intensity, accompanied by a slight, but relatively consistent increase in PCM disorganization **(Figure 12)**. Notably, PCM morphology worsened only within a limited range: even under the

strongest depletion conditions, when centrosomal PCMD-1 was reduced to very low levels, PCM organization remained only mildly compromised and did not decline beyond a moderately disorganized state.

The observed PCMD-1 dosage effects illustrate a broader concept in cellular organization: protein abundance can act as a graded regulator of structural quality rather than as a simple on/off switch. Partial loss of a multivalent organizer does not abolish assembly but modulates how compact, robust, or deformable the resulting structure becomes. Conceptually, this is reminiscent of other cellular systems. A well-established and easy-to-imagine example is the dosage-dependent control of microtubule nucleation by γTuRCs, where altering the levels of activating microtubule-activating-proteins such as chTOG (*C. elegans* ZYG-9; *Drosophila* Msps) or TPX2 (*C. elegans* TPXL-2; *Drosophila* Tpx-2) directly scales the number of microtubules nucleated within a given volume and time (Consolati et al. 2020).

Interestingly, this dosage sensitivity does not apply uniformly to all PCMD-1-dependent functions. Even in gradually reduced PCMD-1 levels, the recruitment of SPD-5 to centrosomes was preserved, indicating that PCM mass is much less sensitive to PCMD-1 loss than PCM shape **(Figure 12)**. This suggests that very low amounts of PCMD-1 are sufficient to license PCM recruitment, whereas the structural matrix composition is more demanding and depends on higher PCMD-1 levels. In addition to its effect on PCM morphology, the strong reduction of PCMD-1 levels revealed that it is also required for efficient PLK-1 recruitment. Under these conditions, PLK-1 signals at centrosomes were reduced, which is consistent with PCMD-1 acting as a centriole-proximal docking platform for PLK-1 (Stenzel et al. 2021) and with the previously reported reduction of PLK-1 levels in *pcmd-1* mutants (Erpf et al. 2019). Although only a high-depletion condition was analyzed, these observations are compatible with the idea that PLK-1 recruitment might itself be sensitive to PCMD-1 dosage **(Figure 12)**. Nonetheless, this needs to be confirmed by measuring PLK-1 intensities under stepwise reduction of wild-type PCMD-1 levels.

How can these modest but reproducible morphology defects of the PCM be reconciled with largely preserved SPD-5 levels at centrosomes? One way to integrate the available data is to introduce a temporal component into the function of PCMD-1. Previous work has already established PCMD-1 as a key recruiter of the non-mitotic SPD-5 core at sperm-derived centrioles (Erpf et al. 2019). In this early phase after fertilization, PCMD-1 likely acts primarily as a seeding factor for PCM assembly: minimal amounts of centriolar PCMD-1 are sufficient to seed a core SPD-5 scaffold at the centriole surface, and subsequent growth and maturation of the PCM is then driven by a PLK-1- and SPD-5-dependent feedback loop (Erpf et al. 2019, Stenzel et al. 2021) that can, at least partially, proceed with only minimal additional PCMD-1 input. In such a scenario, bulk SPD-5 incorporation during mitotic PCM expansion would

become less sensitive to further reductions in PCMD-1 levels, explaining why SPD-5 mass remains largely stable even when PCMD-1 is strongly depleted. At the same time, PCMD-1 may exert a second, more subtle role during mitosis, namely in regulating how new SPD-5 molecules are incorporated within the expanding matrix. Super-resolution microscopy indicates that PCMD-1 also occupies marginal levels within the mitotic PCM (Erpf et al. 2019), so any further reduction in PCMD-1, combined with diminished PLK-1 recruitment, could disproportionately affect this organizational function. In this view, PCMD-1 would not primarily determine how much SPD-5 is added to the scaffold, but how well these SPD-5 molecules are spatially ordered and mechanically integrated into the existing network. Reducing PCMD-1 levels would then leave the overall amount of SPD-5 largely unchanged, while weakening the quality of its incorporation, resulting in a PCM that is measurably less compact and mechanically coherent, but still quantitatively assembled **(Figure 12)**.

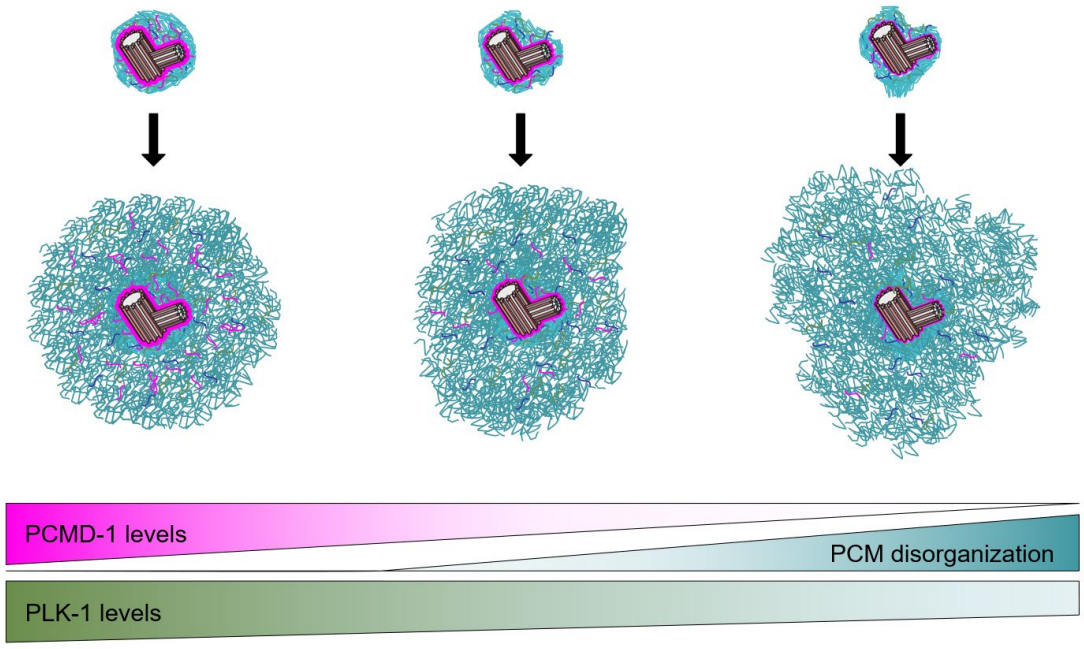

Figure 12: PCM organization depends on PCMD-1 levels.
Progressive reduction of centrosomal PCMD-1 levels (magenta) leads to decreased PLK-1 levels (green) and a slight increase in PCM disorganization (petrol blue). However, recruitment of total PCM mass appears to be unaffected by PCMD-1 reduction. This suggests that PCMD-1 primarily controls how SPD-5 molecules are organized and integrated into the existing scaffold, rather than how much SPD-5 is incorporated into it.

In mechanical terms, these observations suggest that decreasing PCMD-1 levels alter the material state of the PCM network, as the matrix forms in a broader and less compact manner, already during early mitotic stages. This appearance is reminiscent, at least superficially, of the PCM defects seen in the SPD-5$^{\Delta 734\text{-}918}$ mutant, where impaired oligomerization of SPD-5 has

been proposed to hinder proper incorporation of SPD-5 molecules into the scaffold (Rios et al. 2024). By analogy, the disorganized PCM observed upon PCMD-1 depletion may likewise reflect a defect in how SPD-5 molecules are incorporated within the matrix, rather than a simple reduction in SPD-5 mass. However, based solely on these data, this altered PCM state cannot be clearly attributed to reduced PCMD-1-mediated SPD-5 crosslinking or to the concomitant decrease in centrosomal PLK-1 levels, or to a combination of both.

3.2.2 PLK-1 docking to PCMD-1 is critical for PCM organization

The comparison between the PCMD-1 PBD^{m} phenotype and conditions with reduced PCMD-1 levels indicates that PCMD-1 performs more than a single, dosage-based function in PCM organization. In the PCMD-$1^{\Delta CC}$ mutant (Stenzel et al. 2021) or upon progressive depletion of PCMD-1, centrosomal PCMD-1 levels are strongly reduced and PCM morphology is clearly affected, yet PCM disorganization remains relatively mild. By contrast, in PCMD-1 PBD^{m}, PCM disorganization is markedly stronger, even if centrosomal PCMD-1 levels are similarly low **(Figure 13B)**. This suggests that PCMD-1 dosage alone cannot fully explain the observed PCM defects. Instead, two layers of PCMD-1 function can be distinguished: a first-order contribution provided by the overall amount of PCMD-1 available at centrioles, and a second-order contribution that is specifically compromised when PLK-1 docking to PCMD-1 is inhibited.

PLK-1 recruitment itself does not resolve this second-order effect. In PCMD-1 PBD^{m}, PLK-1 levels at centrosomes are reduced **(Figure 13B)** to the same extent as in strong PCMD-1 depletion, making it difficult to disentangle whether low centrosomal PLK-1 levels arise purely from reduced PCMD-1 dosage, from the loss of PLK-1 docking motifs, or from a combination of both. In general, it is assumed that PCMD-1 contributes only a fraction of the total centrosomal PLK-1 pool, with the remaining PLK-1 being recruited via the SPD-2-dependent branch (Erpf et al. 2019). In both conditions, low-PCMD-1 levels and PCMD-1 PBD^{m} mutant, PCMD-1 presumably fails to contribute its share of PLK-1, so that only the SPD-2-dependent pool remains. Because the experiments conducted here only measure the total centrosomal PLK-1 levels, they do not allow for discrimination between the relative contributions of “too little PCMD-1” versus “impaired docking”. Nevertheless, given that nearly all interaction between PLK-1 and PCMD-1 PBD^{m} is lost in Y2H, HEK cell recruitment assays, and bead-based binding assays, it seems most plausible to interpret the PCM phenotype of PCMD-1 PBD^{m} as the combined consequence of reduced PCMD-1 levels and strongly impaired PLK-1 docking.

If PCMD-1 and SPD-2 were the only relevant centriolar PLK-1 recruitment pathways, simultaneous impairment of both branches would be expected to abolish PLK-1 from

centrosomes altogether. However, when SPD-2 was depleted in the PCMD-1 PBD^{m} background, a very faint but reproducible PLK-1 signal remained at centrioles, indicating that a small residual pool of PLK-1 can still be maintained. This was surprising as the depletion of *spd-2* in the *pcmd-1(t3421)* mutant completely abolishes PLK-1 levels (Erpf et al. 2019). There are two putative explanations for this. One possibility is that PLK-1 can, once initially delivered, be recruited to and retained on the SPD-5-based PCM scaffold itself. In PCMD-1 PBD^{m} embryos, and even in the combined PCMD-1 PBD^{m}; *spd-2*(RNAi) condition, a small SPD-5-positive core PCM is still detectable at early stages in this study. Thus, even a low amount of core SPD-5 may suffice to engage - directly or indirectly - the PLK-1- and SPD-5-dependent feedback loop that normally drives PCM maturation after fertilization (Erpf et al. 2019), allowing a tiny fraction of PLK-1 to be captured and stabilized at centrosomes despite impaired docking to PCMD-1 and loss of SPD-2. By contrast, in *pcmd-1(t3421)*; *spd-2*-depleted embryos, where no SPD-5 core forms (Erpf et al. 2019), such scaffold-mediated recruitment and retention is not possible, and PLK-1 is consequently lost from centrosomes. A second possibility is that PCMD-1 PBD^{m} still retains a very weak ability to bind PLK-1: a faint interaction signal is detectable in Y2H assays, raising the formal possibility that few alternative docking sites contribute a small PLK-1 fraction, analogous to SPD-5, where distinct PLK-1 interaction sites are required for different functions (Ohta et al. 2021). However, because this residual interaction with PCMD-1 PBD^{m} is already very weak under conditions where PCMD-1 is expressed at wild-type levels in Y2H, it appears unlikely that the minimal PCMD-1 PBD^{m} levels *in vivo* account for the remaining centriolar PLK-1.

The question then arises how the interaction between PCMD-1 and PLK-1 contributes to PCM stability at a molecular level. As PLK-1 recruitment cannot account for the complete PCM disorganization phenotype, it could be that the modification of PCMD-1 by PLK-1 adds an additional regulatory layer. Indeed, kinase assays show that PCMD-1 is phosphorylated weakly by PLK-1 alone, but combining CDK-1 and PLK-1 activity induces a pronounced phosphorylation with a strong mobility shift. This suggests that CDK-1 acts as a priming kinase, creating docking-competent sites for PLK-1, and PLK-1 then performs the major phosphorylation events on PCMD-1. This behavior resembles the model proposed for SPD-2, in which CDK-1-dependent priming is thought to create a PLK-1 docking site that subsequently enables PLK-1 recruitment to the centrosome (Decker et al. 2011, Ohta et al. 2021). Together with the loss of the mobility shift in PCMD-1 PBD^{m}, these findings identify PCMD-1 as a bona fide CDK-1-primed PLK-1 substrate at the centrosome and extend its role beyond its previously described function as a centriole-proximal PLK-1 recruitment platform (Erpf et al. 2019, Stenzel et al. 2021). To exclude a direct role of CDK-1 in causing the PCM disorganization in PCMD-1 PBD^{m}, predicted CDK-1 consensus sites were rendered non-phosphorylatable. This CDK-1-site mutant did not display any of the phenotypes associated with PCMD-1 PBD^{m} or

PCMD-1 depletion. As all mutated residues in PCMD-1 PBD^{m} that also match CDK-1 consensus motifs were included in this CDK-1-site mutant, yet no phenotype was observed, this raises two possibilities: PCMD-1 may harbor additional CDK-1 sites *in vivo* that were not detected *in vitro*, or further priming kinases, such as Aurora A, may contribute to creating a PLK-1-competent phosphorylation state on PCMD-1. Regardless of these details, the absence of a phenotype in the CDK-1-site mutant argues that CDK-1 does not directly control PCMD-1 function at the centrosome. Instead, CDK-1 acts primarily as a priming kinase, whereas the critical regulatory input on PCMD-1 - and, by extension, on PCM stability - is exerted by PLK-1-mediated interaction or phosphorylation of PCMD-1.

A similar regulatory logic has been described for PCNT and its binding partner CDK5RAP2 (*C. elegans* SPD-5) in vertebrates. In interphase, PCNT is not phosphorylated by Plk1, yet it is already required to recruit CDK5RAP2 to centrosomes (Lee and Rhee 2011). Upon mitotic entry, PCNT becomes phosphorylated by Plk1, and this modification allows PCNT to recruit multiple PCM maturation factors, whereas unphosphorylatable mutants at specific Plk1 sites fail to accumulate these PCM components and do not support standard mitotic PCM assembly (Lee and Rhee 2011). Together with the PCNT-CDK5RAP2 interaction, which was shown to be likewise crucial for efficient PCM maturation (Kim and Rhee 2014), this indicates that PCNT phosphorylation and/or complex formation contribute to mitotic PCM organization, even though it remains difficult to disentangle whether the critical parameter is PCNT phosphorylation itself or the formation of a correctly modified PCNT/CDK5RAP2 complex. Conceptually, this parallels the PCMD-1 system: unphosphorylated PCMD-1 is sufficient to seed a core SPD-5 scaffold and support basic centrosome function, whereas PLK-1-dependent phosphorylation of PCMD-1 appears to be specifically required to convert this core into an organized and mechanically robust mitotic PCM. In both cases, a centriole-anchored scaffold protein first ensures that a PCM core can assemble in a phosphorylation-independent manner, but only its mitotically phosphorylated form is competent to organize PCM components into a compact, mechanically coherent matrix. For PCMD-1, this is reflected by the fact that impaired PLK-1 docking on PCMD-1 still allows substantial SPD-5 recruitment, yet leads to a broadened, fragile PCM, with normal PCM mass **(Figure 13B)**. Thus, PCMD-1 may represent the *C. elegans* counterpart of PCNT in this regard, combining a phosphorylation-independent seeding function with a PLK-1-dependent architectural role in organizing the mitotic PCM.

An alternative, though not mutually exclusive, model to PCMD-1 phosphorylation being the primary cause for the PCM-organizing function is that the efficient incorporation of SPD-5 molecules into the PCM matrix may require docking, or at least close proximity, of PLK-1 to PCMD-1 at the molecular level. In this view, PLK-1 would not only modify PCMD-1 but might also need to act from a PCMD-1-bound position to support proper SPD-5 engagement with the scaffold. To better understand how the PLK-1/PCMD-1 axis might influence SPD-5

incorporation into the PCM, the interaction between PCMD-1 and SPD-5 was examined in the PLK-1 docking-deficient background. In HEK cell and bead recruitment assays, the interaction between PCMD-1 PBD^{m} and SPD-5 was nearly abolished. This suggests that the association between PCMD-1 and SPD-5 is, at least in this system, dependent on PLK-1-mediated phosphorylation of PCMD-1 and/or on PLK-1 being in close proximity. This stands in contrast to the *in vivo* situation, where, even in a *spd-2*-depleted background that removes the redundant SPD-5 recruitment branch, recruitment of the SPD-5 PCM core is still observed in PCMD-1 PBD^{m} embryos (this data), but is completely abolished in the *pcmd-1(t3421)* mutant (Erpf et al. 2019). It might be that binding of SPD-5 to PCMD-1 in its native centrosomal context is possible due to a specialized environment - such as local protein concentration, or additional binding partners - that cannot be fully recapitulated in the HEK cell and bead recruitment assays. Nevertheless, the substantial loss of binding upon disruption of PLK-1 docking indicates that the interaction between PCMD-1 and SPD-5 is, at least to some extent, modulated by PLK-1, either through phosphorylation of PCMD-1 or by positioning PLK-1 in its immediate vicinity.

To further narrow down the region of PCMD-1 responsible for the PLK-1 docking-dependent contribution to PCM organization, PCMD-1 PBD^{m} was analyzed in chimeric protein versions in which only defined parts of the protein carried the PBD^{m} mutations, while the remaining regions were wild type **(Figure 13A)**. In this setting, the disorganized PCM phenotype could be restricted to the N-terminal side of PCMD-1 and even further to a more central region of PCMD-1, here called PCMD-1 PBD^{m} N$^{ter\ short}$ **(Figure 13A)**, which corresponds to the PCMD-1^{C1} **(Figure 10A)** region defined in the previous study (Stenzel et al. 2021). As PCMD-1 PBD^{m} N$^{ter\ short}$ reaches centrosomal levels comparable to the PCMD-1 PBD^{m} C^{ter}, and the latter does not show any abnormal PCM morphology, the contribution of reduced PCMD-1 dosage can be largely excluded for this mutant. Moreover, despite slightly increasing centrosomal PCMD-1 levels from PCMD-1 PBD^{m} N^{ter} to PCMD-1 PBD^{m} N$^{ter\ short}$, these constructs exhibit comparable, strongly disorganized PCMs. This indicates that, in this context, further changes in PCMD-1 levels no longer influence PCM architecture and that the phenotype largely reflects the pure consequence of impaired PLK-1 docking to the N-terminal region. Consistent with this view, PCMD-1 PBD^{m} N^{ter} and PCMD-1 PBD^{m} N$^{ter\ short}$ behave similarly in PLK-1 and SPD-5 recruitment assays, showing a comparable reduction in binding that is only slightly less severe than in PCMD-1 PBD^{m}. This is consistent with their intermediate phenotypic strength and shows that these chimeric mutants effectively uncouple the contribution of PCMD-1 levels from the effect of impaired PLK-1 docking. Notably, this mapping converges with the previous structural region analysis, which implicated the central region of PCMD-1 (PCMD-1^{C1}) in SPD-5-related functionality (Stenzel et al. 2021): the PBD-binding sites identified here fall exactly into this segment, suggesting that this part of PCMD-1 must

either be phosphorylated in a defined manner, or position PLK-1 in close proximity, to support efficient SPD-5 interaction and, consequently, proper PCM organization **(Figure 13B)**.

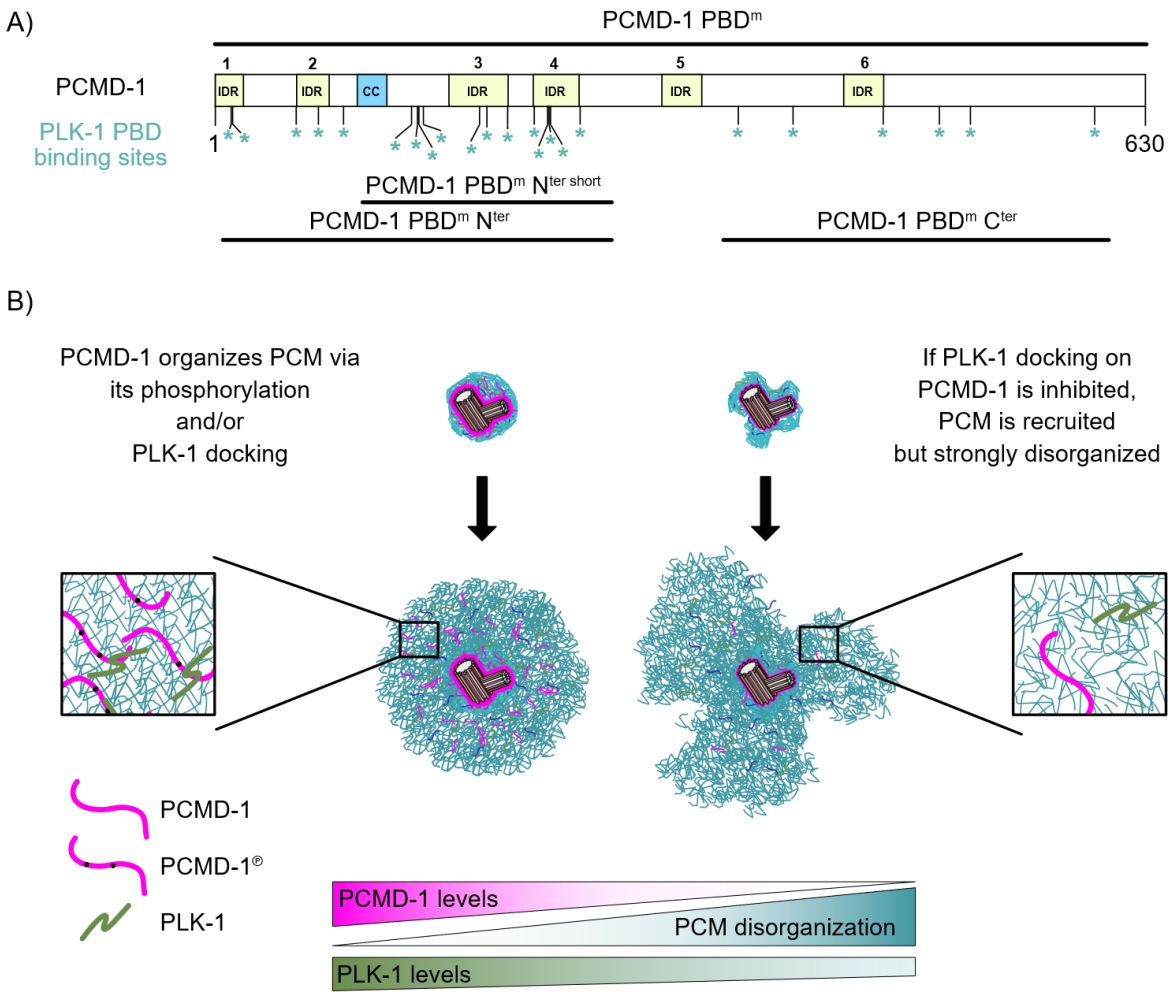

Figure 13: Docking of PLK-1 to PCMD-1 is required for PCM organization.
A) *Schematic representation of PCMD-1 PBD^{m} and the chimeric constructs PCMD-1 PBD^{m} N^{ter}, PCMD-1 PBD^{m} N$^{ter\ short}$, and PCMD-1 PBD^{m} C^{ter}. Only the mutated regions used in each chimera are shown. Predicted and mutated PLK-1 PBD-binding motifs are indicated below the protein by asterisks.* ***B)*** *PCMD-1 contributes to PCM stabilization by serving as a docking platform for PLK-1 and, potentially, by becoming phosphorylated through this interaction. This promotes efficient interaction with SPD-5 and thereby supports proper PCM organization. When PLK-1 docking to PCMD-1 is inhibited and PCMD-1 can no longer be phosphorylated, centrosomal PLK-1 levels drop (green) and the PCM becomes severely disorganized (petrol blue). As a consequence, SPD-5 incorporation and/or structuring within the matrix are likely impaired, leading to the formation of a disordered scaffold that fails to acquire mechanical stability.*

3.2.3 Model: A bifunctional role of PCMD-1 in PCM organization

These findings support a two-layered model of how PCMD-1, also in cooperation with PLK-1, could control PCM architecture:

On a first level, PCM disorganization can be understood as a quantitative consequence of lowering the number of PCMD-1 molecules available at centrosomes, and with them the amount of PLK-1 they can recruit. Because PCMD-1 serves as a docking platform for PLK-1 (Erpf et al. 2019, Stenzel et al. 2021), this quantitative loss in PCMD-1 molecules is accompanied by a proportional decrease in PLK-1 that can be positioned directly at the PCMD-1 interface, although it remains unclear whether this pool corresponds to the catalytically active fraction of PLK-1. When PCMD-1 abundance decreases, the SPD-2-mediated pathway can still bring PLK-1 to centrosomes (Decker et al. 2011, Erpf et al. 2019), but as total PLK-1 levels are reduced, less PLK-1 will act in the immediate vicinity of PCMD-1-bound SPD-5, and phosphorylation of this scaffold region becomes weaker. In addition, if phosphorylated PCMD-1 itself contributes to stabilizing the PCM scaffold, absolute PCMD-1 dosage would also determine how many such stabilizing units are present, in particular within the low-abundance PCM-associated pool (Erpf et al. 2019). In this regime, lowering PCMD-1 levels predominantly reduces the local PLK-1 input onto SPD-5 and the number of phosphorylation-competent PCMD-1 molecules that can reinforce the matrix. As a result, the PCM becomes moderately broadened and less compact, while the overall ability to recruit SPD-5 to centrosomes remains largely intact.

The second layer of disorganization is most clearly revealed by the PCMD-1 PBD^{m} $N^{ter\ short}$ mutant, in which PLK-1 is unable to dock to the N-terminal region of PCMD-1, and the PCM phenotype can no longer be explained by reduced PCMD-1 levels. This disorganization cannot be accounted for by reduced PLK-1 recruitment alone. Also, SPD-5 is still efficiently recruited to centrosomes after fertilization and during PCM expansion, arguing against a simple loss of SPD-5 binding as the primary defect. Instead, these observations point to a PLK-1 docking- and phosphorylation-dependent role of PCMD-1 in stabilizing the expanding PCM. One possibility is that phosphorylation of PCMD-1, particularly within its central region containing multiple IDRs, is required to maintain a specific conformation or charge state that promotes proper SPD-5 incorporation within the matrix. In this scenario, PLK-1-dependent modification of PCMD-1 would help to keep the SPD-5 scaffold in a stabilized, mechanically coherent state until metaphase **(Figure 14)**. After metaphase, PLK-1 levels at centrosomes decline while PP2A activity remains (Enos et al. 2018, Mittasch et al. 2020), which would lead to gradual dephosphorylation of PCMD-1; the protein would then revert to a less stabilizing conformation, allowing the SPD-5 matrix to loosen and ultimately disassemble **(Figure 14)**. In PCMD-1 mutants in which the central region cannot be phosphorylated, this stabilizing function would

be absent: SPD-5 can still be recruited, but its incorporation into a cohesive matrix is compromised.

An alternative, not mutually exclusive model for this second layer of regulation is that the incorporation of new SPD-5 molecules into the existing network requires a transient complex between PCMD-1 and PLK-1. In this view, a physical connection between PLK-1 and PCMD-1 would be needed to ensure that SPD-5 molecules recruited by PCMD-1 encounter PLK-1 in the correct spatial and temporal context to be phosphorylated at the relevant sites **(Figure 14)**. SPD-2 could still recruit sufficient amounts of PLK-1 to the centrosome in bulk, but without PLK-1 being locally presented by PCMD-1 at the SPD-5 docking interface, incorporation into a compact scaffold would be compromised.

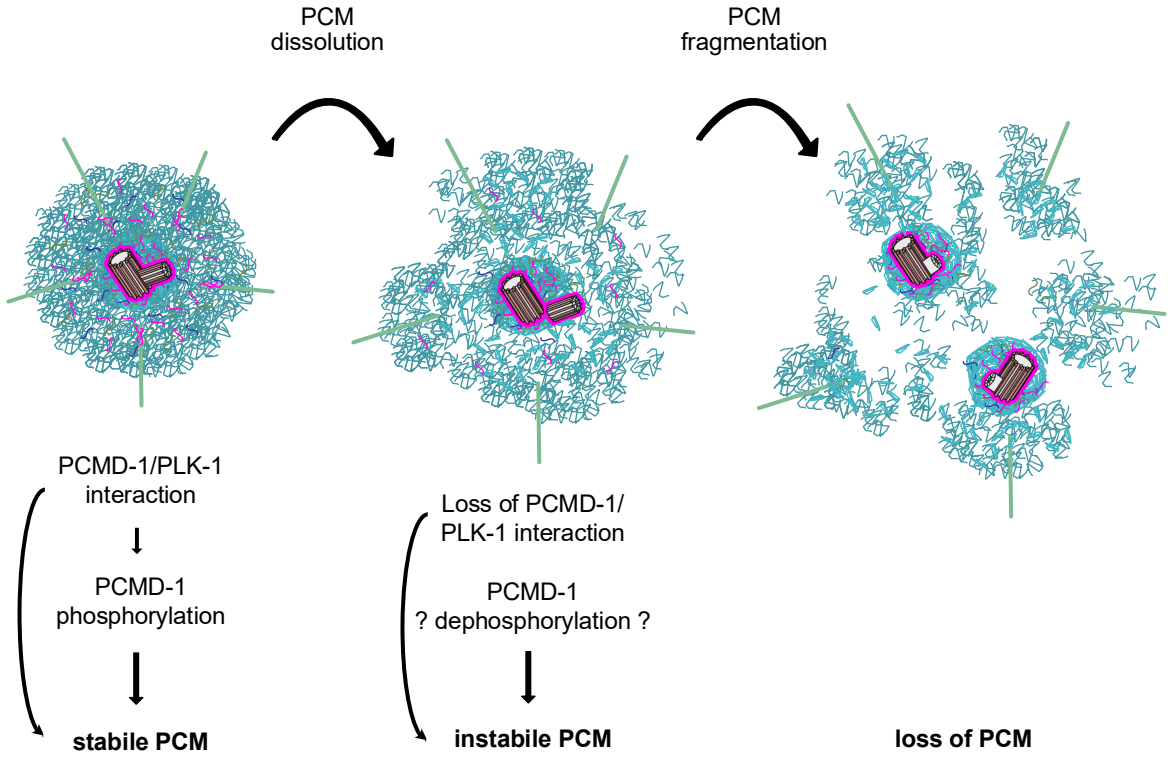

Figure 14: Proposed model of how PCMD-1 contributes to the mechanical properties of the PCM during mitosis.
Docking of PLK-1 to PCMD-1, and possibly phosphorylation of PCMD-1, are required to maintain a stable and organized PCM up to metaphase. Thereafter, PLK-1 levels decline while PP2A activity persists, leading to loss of the PCMD-1/PLK-1 interaction and progressive dephosphorylation of PCMD-1. This gradually destabilizes the PCM and renders it susceptible to fragmentation at the end of mitosis.

In this framework, the first-order phenotype reflects a disorganization of the PCM caused by reduced PCMD-1 dosage and the accompanying decrease in locally acting PLK-1, while SPD-5 recruitment remains largely intact. By contrast, the second-order phenotype emerges when PLK-1 can no longer dock to PCMD-1 despite normal PCMD-1 levels: under these

conditions, PCMD-1 can still seed SPD-5 at centrosomes, but cannot provide the docking- and phosphorylation-dependent stabilizing input, so that the SPD-5 scaffold assembles with essentially normal mass but in a distorted, mechanically weakened configuration. How this inner-core defect is reflected during early mitotic stages and propagates to the outer PCM shell during metaphase remains unclear, but the weak PCMD-1 signal throughout the PCM, seen by super-resolution microscopy (Erpf et al. 2019), suggests that a diffuse PCM-associated pool of PCMD-1 may contribute to stabilizing the outer layers.

How does this PCMD-1-based view of PCM organization relate to what is already known about the material properties of the PCM? In a recent study in *Drosophila*, mitotic PCM was shown to consist of two coexisting scaffold systems with distinct biophysical properties (Wong et al. 2025). In this model, Spd-2 radiating outwards from centrioles recruits Polo and Aurora-A to build a Polo-dependent Cnn scaffold that behaves as a more solid, load-bearing network, and an Aurora-A-dependent TACC scaffold that is more liquid-like and primarily concentrates centrosomal components (Wong et al. 2025). These two scaffolds can independently recruit PCM proteins, but both are required for proper centrosome assembly: the Cnn network provides mechanical robustness, whereas the TACC scaffold functions as a dynamic, concentrating layer (Wong et al. 2025). In *C. elegans*, it could be that SPD-5 and PCMD-1 also form two functionally and/or biophysically distinct scaffolds analogous to the Cnn and TACC scaffolds in *Drosophila*. SPD-5 appears to constitute the principal load-bearing PCM matrix, whose connectivity and mechanics are tuned by PLK-1-dependent phosphorylation and higher-order multimerization (Rios et al. 2024, Amato et al. 2025). Within this framework, PCMD-1 could function as a "mechanical modulator" that adjusts how rigid or compliant the SPD-5 network becomes. This could occur either directly by PCMD-1 or potentially indirectly via its reported interaction with the TACC homolog TAC-1 (Nakajo et al. 2022). The PCMD-1-driven network modulation might be achieved by locally enhancing PLK-1 activity at its interface, thereby promoting phosphorylation-dependent stabilization of the expanding scaffold. In such a scenario, PCMD-1 dosage and PLK-1-mediated modification would not primarily direct a SPD-5 scaffold assembly at all, but instead bias the PCM toward a more solid, cohesive state or toward a softer, more deformable architecture. This picture is consistent with recent observations on PCM material properties. Mechanical probing of the PCM has shown that it transitions from a strong, ductile state in metaphase to a weak, brittle state in anaphase. This change correlates with the departure of PLK-1 and SPD-2 from the scaffold and is promoted by PP2A phosphatase activity (Mittasch et al. 2020). Yet cryo-electron tomography data reveal that the underlying SPD-5 network remains structurally porous and interconnected throughout the cell cycle, with no obvious large-scale architectural rearrangement accompanying this mechanical transition (Tollervey et al. 2025). One way to reconcile these findings is that the "solid" SPD-5 matrix itself remains largely unchanged. At

the same time, the PCMD-1/PLK-1-dependent modification layer, which locally reinforces the scaffold, is progressively lost after metaphase as PLK-1 levels decline and PP2A-mediated dephosphorylation proceeds. In this view, PCMD-1 would act as a phosphorylation-dependent "stiffener" that stabilizes the PCM during early mitosis; once PLK-1 departs, PCMD-1's stabilizing input fades, and the scaffold softens without undergoing direct structural disassembly. Consistent with this interpretation, the PCMD-1 PLK-1 docking mutant displays a mechanically weakened, distorted PCM already before metaphase, effectively phenocopying the softened post-metaphase state at a stage when the wild-type scaffold should still be maximally reinforced. This premature loss of mechanical integrity in the absence of PLK-1/PCMD-1 interaction supports the idea that PLK-1-dependent modification of PCMD-1 is a key determinant of PCM stiffness during mitotic progression. At present, this analogy remains speculative, as the *C. elegans* PCM has not yet been formally resolved into discrete solid- and liquid-like scaffold layers (Raff 2019, Garcia-Baucells et al. 2025). However, the combination of normal SPD-5 mass with impaired mechanical robustness in PCMD-1 mutants supports the idea that PCMD-1 is a key candidate for a factor that modulates the material properties of mitotic PCM, in a way that may be functionally analogous to the multi-scaffold organization described in flies.

3.2.4 PCMD-1 affects centriolar separation

Proper centriolar disengagement and separation are essential prerequisites for centriole-to-centrosome conversion and for licensing a new round of centriole duplication (Tsou 2009, Kim et al. 2015, Kim et al. 2019). In *C. elegans*, mitotic centriolar separation has so far been discussed mainly in the context of PCM dynamics: according to current models, PCM holds centrioles together, and the timing of its assembly and disassembly dictates when centrioles separate **(Figure 15A)** (Dammermann et al. 2004, Cabral et al. 2013, Magescas et al. 2019). In this “passive release” framework, PCM is viewed primarily as a mechanical glue whose gradual loosening allows mother and daughter centrioles to drift apart once sufficient forces act on them.

The PCMD-1 PLK-1 docking mutant challenges this view. In PCMD-1 PBD^{m} N^{ter}, the PCM is structurally weak and brittle and fails to maintain a compact architecture under mitotic pulling forces. Based on the passive release model, one would predict that such a fragile PCM would promote earlier centriolar separation, because the mechanical barrier that holds the centrioles together is weakened. Instead, the opposite is observed: the onset of separation is delayed, and in turn, centrioles remain engaged for longer, despite the fragile PCM **(Figure 15A)**. Importantly, in this mutant, cortical pulling forces are not altered compared to wild type, indicating that the global force-generating machinery is intact. Instead, the defect appears to

lie in the coupling between the centriole and the PCM: forces generated by microtubules and acting on the PCM seem not to be efficiently transmitted to the centrioles. This behavior clearly contradicts a purely passive release model and suggests that PCMD-1 plays a more active and maybe multifaceted role in centriolar separation.

One possible interpretation of the delayed separation despite weakened PCM is that PCMD-1 acts as a relay that transmits microtubule-dependent forces from the PCM to the centrioles. PCMD-1 has been detected at all three structures that need to be mechanically connected for force transfer: at centrioles, within the PCM, and along microtubules (Erpf et al. 2019, Stenzel et al. 2021). This localization makes PCMD-1 an attractive candidate for a load-relay protein that links microtubules to the PCM scaffold and, through it, to the centrioles **(Figure 15B)**. In such a picture, centrioles would not simply “fall apart” once the PCM becomes weak but would instead require a defined pattern of PCM rupture and force transmission to be released from engagement. The PCM-organization defects in PCMD-1 PBD^{m} N^{ter} fit well with this idea: the SPD-5 scaffold is unable to resist mechanical stress, appearing broadened, flared, and prone to fragmentation. Conceptually, the PCM can be imagined as a net: if the mesh is well organized and its connections are robust, pulling on the periphery will effectively transmit forces to the center. If, however, the network is loose and its connections are weak, pulling forces will tear away peripheral parts without efficiently reaching the core. Applied to PCMD-1 PBD^{m} N^{ter}, this would mean that microtubule-generated forces fragment the unstable PCM but are not efficiently relayed to the centrioles, leading to delayed separation despite structural fragility. At the same time, this relay model cannot, on its own, account for all available observations. In SPD-5-depleted embryos, in which essentially no PCM scaffold is assembled, centrioles nevertheless separate during mitosis (Dammermann et al. 2004). If PCM rupture and force transmission via the SPD-5 matrix were required for separation, centrioles in such embryos would be expected to remain engaged. This discrepancy suggests that PCM-mediated force relaying is not the only mechanism capable of promoting centriolar separation and that additional, more directly centriolar factors must be involved.

This leads to a second, more speculative possibility: that PCMD-1 contributes to an active licensing step for centriolar disengagement, analogous to mechanisms described in vertebrate cells. In vertebrates, centriolar disengagement requires separase-dependent cleavage of PCNT after its phosphorylation by Plk1 (Lee and Rhee 2012, Kim et al. 2015). Although no disengagement step has yet been described in *C. elegans*, PLK-1 was recently implicated in directly regulating centriolar splitting: elevated PLK-1 levels were reported to trigger premature centriolar separation, even while centrioles remain spatially close and embedded within PCM (Chen et al. 2023), indicating that PLK-1 activity could directly tune a putative engagement state in this system as well. The delayed onset of separation in PCMD-1 PBD^{m} N^{ter} raises the possibility that a disengagement-like step may exist but is usually masked and only becomes

detectable when regulatory inputs such as PCMD-1/PLK-1 signaling are perturbed. In this context, it is tempting to speculate that PLK-1-dependent phosphorylation of PCMD-1 could be required to license a cleavage event analogous to PCNT processing in vertebrates. Supporting this idea, PCMD-1 harbors a predicted separase motif (Stenzel 2022), located within the N-terminal region affected by the PCMD-1 PBD^{m} N^{ter} mutations. This suggests that PCMD-1 could, in principle, act as part of a centriolar engagement linker, in which PLK-1 docking and phosphorylation on the N-terminal region primes PCMD-1 for later catalysis by separase **(Figure 15C)**. In the unphosphorylated docking mutant, such cleavage would be compromised, and PCMD-1 would remain as a persistent linker, prolonging centriolar engagement and delaying separation. However, this model faces an important caveat: previous work did not detect a requirement for separase in mitotic centriolar separation in *C. elegans* (Cabral et al. 2013). Whether this reflects technical limitations or the existence of separase-independent engagement mechanisms remains unclear. Thus, while the analogy to PCNT provides an attractive conceptual framework, a direct role for PCMD-1 as a separase substrate in mitotic centriolar disengagement remains speculative at this point.

Given these considerations, a third possibility is that PCM-mediated force transmission and a biochemical engagement linker cooperate to ensure timely centriolar separation, and that PCMD-1 contributes to both processes. This type of dual control is well supported in other systems. In vertebrates, centriole disengagement and separation involve both separase-mediated cleavage of engagement linkers and proper PCM organization; perturbing either component can affect the timing or fidelity of separation (Tsou 2009, Lee and Rhee 2012, Seo et al. 2015). Similarly, in *C. elegans'* initial centriolar separation, separase is required for the cleavage of a cohesion-like linker between centrioles. However, if separase is depleted, centrioles can still be forced apart by experimentally increasing microtubule pulling forces (Cabral et al. 2013). In that case, the biochemical linker and mechanical forces act as partially redundant mechanisms: either one alone can, under certain conditions, promote separation. A similar logic could apply to mitotic centriolar separation. Under normal conditions, strong microtubule-based forces acting on a robust PCM scaffold may be sufficient to separate centrioles without a strictly defined cleavage event, making a putative engagement linker irrelevant and therefore challenging to detect. If, however, force transmission to the centrioles is compromised, either because the PCM is too weak or because a relay protein such as PCMD-1 is misregulated, then a requirement for an additional licensing step could become evident. In PCMD-1 PBD^{m} N^{ter}, both aspects might be simultaneously affected: the PCM is structurally weakened and disorganized, compromising force relaying, and PCMD-1 can no longer dock PLK-1 and thus remains mainly unphosphorylated, which may in turn prevent the formation of a separase-dependent engagement-cleavage interface. In such a scenario, altering either PCM stability or linker function alone would have a limited impact on centriolar

separation, as the remaining mechanism could compensate. Only when both PCM integrity and PCMD-1-dependent regulation are perturbed, centrioles remain engaged for an extended period, which results in a robust delay of separation. This view is supported by the comparison with the SPD-5$^{\Delta 734\text{-}918}$ mutant, which displays a disorganized, mechanically fragile PCM (Rios et al. 2024) but does not show a significant delay or advance in centriolar separation (this study), suggesting that impaired PCM architecture alone is insufficient to alter separation timing when the engagement machinery is intact.

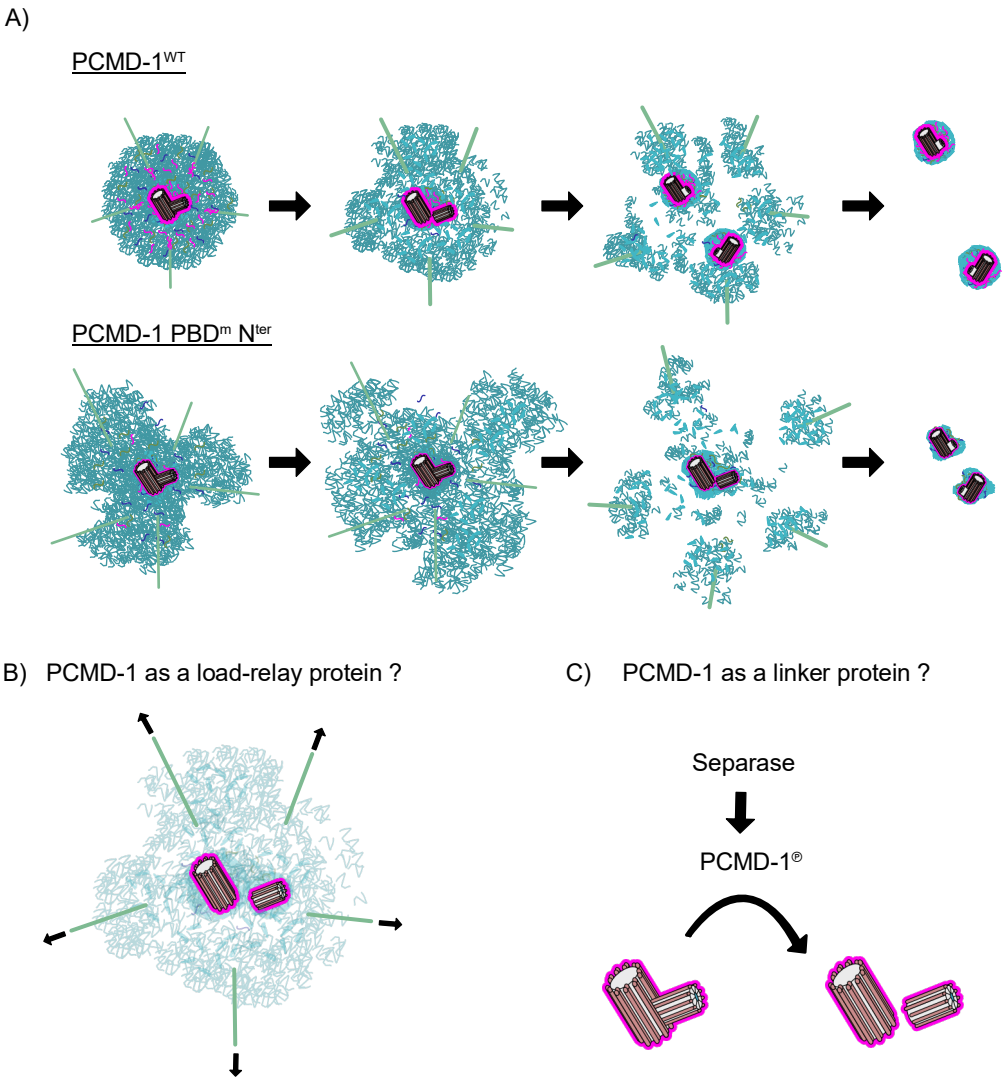

Figure 15: Centriolar separation during mitotic exit is affected by PCMD-1
A) *In PCMD-1^{WT}, the PCM forms a cohesive scaffold that holds mother and daughter centrioles together, and the timing of PCM dissolution and fragmentation determines when centrioles separate. When PLK-1 docking to the N-terminal region of PCMD-1 is blocked, centriolar separation is delayed, although the PCM is mechanically weakened and more easily torn apart.* ***B)*** *and* ***C)*** *represent putative, but not mutually exclusive, mechanisms by which PCMD-1 could affect centriole separation. PCMD-1 could act as a load-relay protein that transmits cortical pulling forces through the PCM to the centrioles (B), or PCMD-1 could function as a centriolar linker that must be phosphorylated in order to be cleaved by separase (C), analogous to what has been shown for human PCNT (Lee and Rhee 2012, Kim et al. 2015).*

To determine whether, analogous to vertebrates, centriolar separation in *C. elegans* can also be dissected into two functionally distinct steps, an initial disengagement followed by physical separation, super-resolution microscopy in wild-type and PCMD-1 PBD^{m} N^{ter} embryos throughout mitotic exit could resolve a discrete disengagement step. Quantitatively tracking the spatial relationship between mother and daughter centrioles might help to determine whether the timing of disengagement is altered in the docking mutant. In parallel, it would be interesting to repeat separase depletion as performed by Cabral and colleagues (Cabral et al. 2013) under conditions of reduced microtubule-mediated pulling forces, for example, as in *gpr-1/2*-depleted embryos (Panbianco et al. 2008): while separase loss alone has so far not produced an apparent mitotic centriolar separation defect, a decrease in pulling forces might unmask a hidden requirement for a biochemical engagement-cleavage step that is usually bypassed by high mechanical load. Along similar lines, combining separase RNAi with a PCM-disorder mutant, such as SPD-$5^{\Delta 734\text{-}918}$ (Rios et al. 2024), would test whether centrioles that typically separate with their own kinetics once released from an engagement linker now remain locked within a distorted PCM, mimicking aspects of the PCMD-1 PBD^{m} N^{ter} phenotype. Finally, mutating the predicted separase cleavage site in PCMD-1 (Stenzel 2022) would provide a direct handle on a potential engagement function. This mutant alone might behave close to wild type, but under reduced pulling forces, centrioles would be expected to remain engaged while the PCM slowly dissolves. Together, such experiments would help to establish whether mitotic centriole separation in *C. elegans* indeed comprises independent disengagement and separation phases, and whether PCMD-1 sits at the intersection of these mechanical and biochemical control layers.

Taken together, these observations extend the current model of centriolar separation in *C. elegans*. While previous work has emphasized the importance of PCM dynamics, the data presented here indicate that PCM behavior alone cannot fully account for the timing of centriolar separation. Instead, they point to an additional role for PCMD-1 in releasing daughter centrioles from their mothers, potentially as a component of a centriolar engagement system. This multi-layered role mirrors, at least conceptually, the diverse functions described for PCNT in vertebrate cells, where the same protein integrates PCM organization, Plk1 signaling, and centriole disengagement (Lawo et al. 2012, Kim et al. 2015, Kim et al. 2019).

3.3 Concluding remarks and outlook

The data presented in this work refine the current view of centrosome assembly in *C. elegans* by placing PCMD-1 at the center of three closely connected processes: centriole-PCM coupling, mitotic PCM stabilization, and timely centriolar separation.

Maternally provided PCMD-1 associates early with sperm-derived centrioles, preceding other PCM components. Importantly, PCMD-1 recruitment to ectopic sites is sufficient to nucleate both SPD-5 and PLK-1 localization, revealing its role as a functional tether that couples centriolar anchoring to PCM scaffold assembly. Therefore, PCMD-1 solves the long-standing question of how the SPD-5 matrix is physically coupled to sperm-derived centrioles: it provides a dedicated molecular handle on the centriole side and a multivalent PCM-binding surface on the other, functionally analogous to PCNT and Plp in vertebrates and flies (Lawo et al. 2012, Mennella et al. 2012).

Additionally, a bifunctional role of PCMD-1 in organizing the mitotic PCM was revealed. On the one hand, graded reduction of PCMD-1 levels uncovers a dosage-dependent contribution to PCM architecture, the matrix becomes slightly distorted and broader, consistent with reduced local PLK-1 input and fewer phosphorylation-competent PCMD-1 molecules reinforcing the scaffold. On the other hand, inhibition of PLK-1 docking to PCMD-1 uncouples PCM mass from PCM quality: SPD-5 is still robustly recruited, yet the scaffold expands into a severely disorganized, fragile network. This, together with biochemical data identifying PCMD-1 as a CDK-1-primed PLK-1 substrate, supports a model in which unmodified PCMD-1 is sufficient to seed a core SPD-5 scaffold, whereas PLK-1-dependent docking to PCMD-1 is specifically required to convert this core into a compact, load-bearing mitotic PCM. It remains poorly understood how linker proteins such as PCMD-1 regulate the biophysical properties of the PCM. The data presented here suggest that PLK-1-dependent PCMD-1 stabilization is temporally restricted to early mitosis: high PLK-1 activity maintains a rigid scaffold until metaphase, whereas declining PLK-1 levels in anaphase relieve this reinforcement, rendering the PCM softer and prone to disassembly. If true, the PLK-1 docking mutant PCM should phenocopy the softened wild-type anaphase state. Further biophysical characterization, by measuring PCM stiffness, elasticity, and structural dynamics as performed in Mittasch et al. 2020 or in Garcia-Baucells et al. 2025, will test this hypothesis and illuminate how PCMD-1 can regulate PCM mechanics.

The PLK-1 docking mutant reveals an additional, unexpected role of PCMD-1 in centriolar separation. Despite a weakened, brittle PCM that should favor passive release (Cabral et al. 2013), centrioles separate late rather than early. This argues that PCM mechanics alone cannot explain separation timing and suggests that PCMD-1 contributes, directly or indirectly, to a PLK-1-dependent licensing step for disengagement, potentially analogous to PCNT processing in vertebrate cells (Lee and Rhee 2012, Kim et al. 2015). It is important to gain deeper and more detailed insights into how centrioles separate during mitosis, especially whether a disengagement event similar to initial centriolar separation (Cabral et al. 2013) is present in *C. elegans*. Even though the presented data hints towards an engagement step, further analysis of separase function in defined PCMD-1 and PCM mutants under altered

microtubule-mediated pulling forces will be essential to dissect how mechanical forces and molecular licensing might cooperate for successful centriolar separation.

Gaining a more profound understanding of centrosome composition at both molecular and biophysical levels will be essential to elucidate how centrosomes simultaneously withstand mechanical forces while remaining dynamically competent for assembly and disassembly. Such insights are critical for understanding how defects in centrosomal function contribute to human diseases ranging from ciliopathies to chromosomal instability as observed in cancer cells (Nigg and Raff 2009).

Literature

Alberts, B., A. Johnson, J. Lewis, M. Raff, K. Roberts, and P. Walter. 2002a. Cytokinesis. Molecular Biology of the Cell. 4th edition. Garland Science.

Alberts, B., A. Johnson, J. Lewis, M. Raff, K. Roberts, and P. Walter. 2002b. Mitosis. Molecular Biology of the Cell. 4th edition. Garland Science.

Albertson, D. G. 1984. Formation of the first cleavage spindle in nematode embryos. Dev Biol **101**:61-72.

Alvarez-Rodrigo, I., T. L. Steinacker, S. Saurya, P. T. Conduit, J. Baumbach, Z. A. Novak, M. G. Aydogan, A. Wainman, and J. W. Raff. 2019. Evidence that a positive feedback loop drives centrosome maturation in fly embryos. Elife **8**.

Amato, M., J. H. Hwang, M. U. Rios, N. E. Familiari, M. K. Rosen, and J. B. Woodruff. 2025. Polo-Like Kinase 1 Phosphorylation Tunes the Functional Viscoelastic Properties of the Centrosome Scaffold. Advanced Science.

Arquint, C., and E. A. Nigg. 2016. The PLK4–STIL–SAS-6 module at the core of centriole duplication. Biochemical Society Transactions **44**:1253-1263.

Ashrafi, K., F. Y. Chang, J. L. Watts, A. G. Fraser, R. S. Kamath, J. Ahringer, and G. Ruvkun. 2003. Genome-wide RNAi analysis of *Caenorhabditis elegans* fat regulatory genes. Nature **421**:268-272.

Azimzadeh, J., and W. F. Marshall. 2010. Building the Centriole. Current Biology **20**:R816-R825.

Bah, A., and J. D. Forman-Kay. 2016. Modulation of Intrinsically Disordered Protein Function by Post-translational Modifications. J Biol Chem **291**:6696-6705.

Balestra, Fernando R., P. Strnad, I. Flückiger, and P. Gönczy. 2013. Discovering Regulators of Centriole Biogenesis through siRNA-Based Functional Genomics in Human Cells. Developmental cell **25**:555-571.

Bansbach, C. E., and D. Cortez. 2011. Defining genome maintenance pathways using functional genomic approaches. Critical Reviews in Biochemistry and Molecular Biology **46**:327-341.

Banterle, N., and P. Gönczy. 2017. Centriole Biogenesis: From Identifying the Characters to Understanding the Plot. Annual Review of Cell and Developmental Biology **33**:23-49.

Basto, R., J. Lau, T. Vinogradova, A. Gardiol, C. G. Woods, A. Khodjakov, and J. W. Raff. 2006. Flies without Centrioles. Cell **125**:1375-1386.

Begasse, M. L., and A. A. Hyman. 2011. The first cell cycle of the *Caenorhabditis elegans* embryo: spatial and temporal control of an asymmetric cell division. Results Probl Cell Differ **53**:109-133.

Bellanger, J.-M., and P. Gönczy. 2003. TAC-1 and ZYG-9 Form a Complex that Promotes Microtubule Assembly in *C. elegans* Embryos. Current Biology **13**:1488-1498.

Bettencourt-Dias, M., A. Rodrigues-Martins, L. Carpenter, M. Riparbelli, L. Lehmann, M. Gatt, N. Carmo, F. Balloux, G. Callaini, and D. Glover. 2005. SAK/PLK4 is required for centriole duplication and flagella development. Current Biology **15**:2199-2207.

Bianchi, S., K. Rogala, N. Dynes, M. Hilbert, S. Leidel, M. Steinmetz, P. Gönczy, and I. Vakonakis. 2018. Interaction between the *Caenorhabditis elegans* centriolar protein SAS-5 and microtubules facilitates organelle assembly. Molecular biology of the cell **29**:722-735.

Boudreau, V., R. Chen, A. Edwards, M. Sulaimain, and P. S. Maddox. 2019. PP2A-B55/SUR-6 collaborates with the nuclear lamina for centrosome separation during mitotic entry. Molecular biology of the cell **30**:876-886.

Boveri, T. 1888. Zellen-Studien. Jena, Verlag von Gustav Fischer.

Boveri, T. 1902. Das Problem der Befruchtung. G. Fischer.

Boveri, T. 2008. Concerning the Origin of Malignant Tumours by Theodor Boveri from 1914. Translated and annotated by Henry Harris. Journal of Cell Science **121**:1-84.

Boxem, M., Z. Maliga, N. Klitgord, N. Li, I. Lemmens, M. Mana, L. de Lichtervelde, J. D. Mul, D. van de Peut, M. Devos, N. Simonis, M. A. Yildirim, M. Cokol, H. L. Kao, A. S. de Smet, H. Wang, A. L. Schlaitz, T. Hao, S. Milstein, C. Fan, M. Tipsword, K. Drew, M. Galli, K. Rhrissorrakrai, D. Drechsel, D. Koller, F. P. Roth, L. M. Iakoucheva, A. K. Dunker, R. Bonneau, K. C. Gunsalus, D. E. Hill, F. Piano, J. Tavernier, S. van den Heuvel, A. A. Hyman, and M. Vidal. 2008. A protein domain-based interactome network for *C. elegans* early embryogenesis. Cell **134**:534-545.

Bracha, D., M. T. Walls, and C. P. Brangwynne. 2019. Probing and engineering liquid-phase organelles. Nature Biotechnology **37**:1435-1445.

Brandt, J. N., and Y. Kim. 2021. Targeting Polo-like kinase in space and time during *C. elegans* meiosis. Cell Cycle **20**:1519-1526.

Brenner, S. 1974. The genetics of *Caenorhabditis elegans*. Genetics **77**:71-94.

Brinkley, B. R. 1985. Microtubule Organizing Centers. Annual Review of Cell and Developmental Biology **1**:145-172.

Buchman, J. J., H. C. Tseng, Y. Zhou, C. L. Frank, Z. Xie, and L. H. Tsai. 2010. Cdk5rap2 interacts with pericentrin to maintain the neural progenitor pool in the developing neocortex. Neuron **66**:386-402.

Cabral, G., T. Laos, J. Dumont, and A. Dammermann. 2019. Differential Requirements for Centrioles in Mitotic Centrosome Growth and Maintenance. Dev Cell **50**:355-366 e356.

Cabral, G., S. S. Sans, C. R. Cowan, and A. Dammermann. 2013. Multiple mechanisms contribute to centriole separation in *C. elegans*. Curr Biol **23**:1380-1387.

Chalfie, M., Y. Tu, G. Euskirchen, W. W. Ward, and D. C. Prasher. 1994. Green Fluorescent Protein as a Marker for Gene Expression. Science **263**:802-805.

Chen, Y.-Z., V. Zimyanin, and S. Redemann. 2023. Loss of the mitochondrial protein SPD-3 elevates PLK-1 levels and dysregulates mitotic events. Life Science Alliance **6**:e202302011.

Colombo, K., S. W. Grill, R. J. Kimple, F. S. Willard, D. P. Siderovski, and P. Gönczy. 2003. Translation of polarity cues into asymmetric spindle positioning in *Caenorhabditis elegans* embryos. Science **300**:1957-1961.

Conduit, P. T., K. Brunk, J. Dobbelaere, C. I. Dix, E. P. Lucas, and J. W. Raff. 2010. Centrioles Regulate Centrosome Size by Controlling the Rate of Cnn Incorporation into the PCM. Current Biology **20**:2178-2186.

Conduit, Paul T., Z. Feng, Jennifer H. Richens, J. Baumbach, A. Wainman, Suruchi D. Bakshi, J. Dobbelaere, S. Johnson, Susan M. Lea, and Jordan W. Raff. 2014. The Centrosome-Specific Phosphorylation of Cnn by Polo/Plk1 Drives Cnn Scaffold Assembly and Centrosome Maturation. Developmental cell **28**:659-669.

Conduit, P. T., A. Wainman, and J. W. Raff. 2015. Centrosome function and assembly in animal cells. Nat Rev Mol Cell Biol **16**:611-624.

Consolati, T., J. Locke, J. Roostalu, Z. A. Chen, J. Gannon, J. Asthana, W. M. Lim, F. Martino, M. A. Cvetkovic, J. Rappsilber, A. Costa, and T. Surrey. 2020. Microtubule Nucleation Properties of Single Human γTuRCs Explained by Their Cryo-EM Structure. Dev Cell **53**:603-617.e608.

Cottee, M. A., N. Muschalik, Y. L. Wong, C. M. Johnson, S. Johnson, A. Andreeva, K. Oegema, S. M. Lea, J. W. Raff, and M. van Breugel. 2013. Crystal structures of the CPAP/STIL complex reveal its role in centriole assembly and human microcephaly. Elife **2**:e01071.

Couwenbergs, C., J.-C. Labbé, M. Goulding, T. Marty, B. Bowerman, and M. Gotta. 2007. Heterotrimeric G protein signaling functions with dynein to promote spindle positioning in *C. elegans*. Journal of Cell Biology **179**:15-22.

Dammermann, A., P. S. Maddox, A. Desai, and K. Oegema. 2008. SAS-4 is recruited to a dynamic structure in newly forming centrioles that is stabilized by the γ-tubulin–mediated addition of centriolar microtubules. Journal of Cell Biology **180**:771-785.

Dammermann, A., T. Müller-Reichert, L. Pelletier, B. Habermann, A. Desai, and K. Oegema. 2004. Centriole assembly requires both centriolar and pericentriolar material proteins. Dev Cell **7**:815-829.

Dammermann, A., H. Pemble, B. J. Mitchell, I. McLeod, J. R. Yates, C. Kintner, A. B. Desai, and K. Oegema. 2009. The hydrolethalus syndrome protein HYLS-1 links core centriole structure to cilia formation. Genes & Development **23**:2046-2059.

De Harven, E., and W. Bernhard. 1956. Etude au microscope electronique de l'ultrastructure du centriole chez les vertébrés. Zeitschrift für Zellforschung und Mikroskopische Anatomie **45**:378-398.

De Simone, A., F. Nédélec, and P. Gönczy. 2016. Dynein Transmits Polarized Actomyosin Cortical Flows to Promote Centrosome Separation. Cell Rep **14**:2250-2262.

Decker, M., S. Jaensch, A. Pozniakovsky, A. Zinke, K. F. O'Connell, W. Zachariae, E. Myers, and A. A. Hyman. 2011. Limiting amounts of centrosome material set centrosome size in *C. elegans* embryos. Curr Biol **21**:1259-1267.

Delattre, M. 2004. Centriolar SAS-5 is required for centrosome duplication in *C. elegans*. et al **6**:656-664.

Delattre, M., C. Canard, and P. Gönczy. 2006. Sequential Protein Recruitment in *C. elegans* Centriole Formation. Current Biology **16**:1844-1849.

Dickinson, D. J., and B. Goldstein. 2016. CRISPR-Based Methods for *Caenorhabditis elegans* Genome Engineering. Genetics **202**:885-901.

Dumont, J., and A. Desai. 2012. Acentrosomal spindle assembly and chromosome segregation during oocyte meiosis. Trends Cell Biol **22**:241-249.

Edgar, L. G., and J. D. McGhee. 1988. DNA synthesis and the control of embryonic gene expression in *C. elegans*. Cell **53**:589-599.

Encalada, S. E., J. Willis, R. Lyczak, and B. Bowerman. 2005. A spindle checkpoint functions during mitosis in the early *Caenorhabditis elegans* embryo. Mol Biol Cell **16**:1056-1070.

Enos, S. J., M. Dressler, B. F. Gomes, A. A. Hyman, and J. B. Woodruff. 2018. Phosphatase PP2A and microtubule-mediated pulling forces disassemble centrosomes during mitotic exit. Biology Open **7**.

Erdős, G., N. Deutsch, and Z. Dosztányi. 2025. AIUPred – Binding: Energy Embedding to Identify Disordered Binding Regions. Journal of Molecular Biology **437**:169071.

Erdős, G., and Z. Dosztányi. 2024. AIUPred: combining energy estimation with deep learning for the enhanced prediction of protein disorder. Nucleic Acids Research **52**:W176-W181.

Erpf, A. C., L. Stenzel, N. Memar, M. Antoniolli, M. Osepashvili, R. Schnabel, B. Conradt, and T. Mikeladze-Dvali. 2019. PCMD-1 organizes centrosome matrix assembly in *C. elegans*. Current Biology **29**:1324-1336. e1326.

Farrell, J. A., and P. H. O'Farrell. 2014. From egg to gastrula: how the cell cycle is remodeled during the *Drosophila* mid-blastula transition. Annu Rev Genet **48**:269-294.

Fawcett, D. W., and K. R. Porter. 1954. A study of the fine structure of ciliated epithelia. Journal of Morphology **94**:221-281.

Feng, Z., A. Caballe, A. Wainman, S. Johnson, A. F. M. Haensele, M. A. Cottee, P. T. Conduit, S. M. Lea, and J. W. Raff. 2017. Structural Basis for Mitotic Centrosome Assembly in Flies. Cell **169**:1078-1089.e1013.

Fire, A., S. Xu, M. K. Montgomery, S. A. Kostas, S. E. Driver, and C. C. Mello. 1998. Potent and specific genetic interference by double-stranded RNA in *Caenorhabditis elegans*. Nature **391**:806-811.

Friedland, A. E., Y. B. Tzur, K. M. Esvelt, M. P. Colaiácovo, G. M. Church, and J. A. Calarco. 2013. Heritable genome editing in *C. elegans* via a CRISPR-Cas9 system. Nature Methods **10**:741-743.

Frøkjaer-Jensen, C., M. W. Davis, C. E. Hopkins, B. J. Newman, J. M. Thummel, S. P. Olesen, M. Grunnet, and E. M. Jorgensen. 2008. Single-copy insertion of transgenes in *Caenorhabditis elegans*. Nat Genet **40**:1375-1383.

Gall, J. G. 2004. Early Studies on Centrioles and Centrosomes. Pages 1-15 Centrosomes in Development and Disease.

Galli, M., and D. O. Morgan. 2016. Cell Size Determines the Strength of the Spindle Assembly Checkpoint during Embryonic Development. Dev Cell **36**:344-352.

Garcia-Baucells, J., C. Bevilacqua, M. Rufin, C. Rumpf-Kienzl, A. Zampetaki, O. G. Andriotis, P. J. Thurner, R. Prevedel, S. Fürthauer, and A. Dammermann. 2025. Centrosome Softening As A Mechanical Adaptation For Mitosis. bioRxiv:2025.2009.2009.675178.

Giansanti, M. G., E. Bucciarelli, S. Bonaccorsi, and M. Gatti. 2008. *Drosophila* SPD-2 is an essential centriole component required for PCM recruitment and astral-microtubule nucleation. Current Biology **18**:303-309.

Gillingham, A. K., and S. Munro. 2000. The PACT domain, a conserved centrosomal targeting motif in the coiled-coil proteins AKAP450 and pericentrin. EMBO reports **1**:524-529-529.

Gönczy, P., S. Pichler, M. Kirkham, and A. A. Hyman. 1999. Cytoplasmic dynein is required for distinct aspects of MTOC positioning, including centrosome separation, in the one cell stage *Caenorhabditis elegans* embryo. J Cell Biol **147**:135-150.

Gottardo, M., G. Callaini, and M. G. Riparbelli. 2015. The *Drosophila* centriole - conversion of doublets into triplets within the stem cell niche. J Cell Sci **128**:2437-2442.

Gould, R. R., and G. G. Borisy. 1977. The pericentriolar material in Chinese hamster ovary cells nucleates microtubule formation. The Journal of cell biology **73**:601-615.

Green, R. A., E. Paluch, and K. Oegema. 2012. Cytokinesis in Animal Cells. Annual Review of Cell and Developmental Biology **28**:29-58.

Grill, S. W., P. Gönczy, E. H. Stelzer, and A. A. Hyman. 2001. Polarity controls forces governing asymmetric spindle positioning in the *Caenorhabditis elegans* embryo. Nature **409**:630-633.

Grill, S. W., J. Howard, E. Schäffer, E. H. K. Stelzer, and A. A. Hyman. 2003. The Distribution of Active Force Generators Controls Mitotic Spindle Position. Science **301**:518-521.

Guichard, P., V. Hamel, and P. Gönczy. 2018. The Rise of the Cartwheel: Seeding the Centriole Organelle. Bioessays **40**:1700241.

Habedanck, R., Y. D. Stierhof, C. J. Wilkinson, and E. A. Nigg. 2005. The Polo kinase Plk4 functions in centriole duplication. Nat Cell Biol **7**:1140-1146.

Hamill, D. R., A. F. Severson, J. C. Carter, and B. Bowerman. 2002. Centrosome Maturation and Mitotic Spindle Assembly in *C. elegans* Require SPD-5, a Protein with Multiple Coiled-Coil Domains. Developmental cell **3**:673-684.

Hannak, E., M. Kirkham, A. A. Hyman, and K. Oegema. 2001. Aurora-A kinase is required for centrosome maturation in *Caenorhabditis elegans*. Journal of Cell Biology **155**:1109-1116.

Harper, N. C., R. Rillo, S. Jover-Gil, Z. J. Assaf, N. Bhalla, and A. F. Dernburg. 2011. Pairing centers recruit a Polo-like kinase to orchestrate meiotic chromosome dynamics in *C. elegans*. Dev Cell **21**:934-947.

Hattersley, N., P. Lara-Gonzalez, D. Cheerambathur, J. S. Gomez-Cavazos, T. Kim, B. Prevo, R. Khaliullin, K.-Y. Lee, M. Ohta, R. Green, K. Oegema, and A. Desai. 2018. Employing the one-cell *C. elegans* embryo to study cell division processes. Pages 185-231 *in* H. Maiato and M. Schuh, editors. Methods in cell biology. Academic Press.

Hilbert, M., M. C. Erat, V. Hachet, P. Guichard, I. D. Blank, I. Flückiger, L. Slater, E. D. Lowe, G. N. Hatzopoulos, M. O. Steinmetz, P. Gönczy, and I. Vakonakis. 2013. *Caenorhabditis elegans* centriolar protein SAS-6 forms a spiral that is consistent with imparting a ninefold symmetry. Proceedings of the National Academy of Sciences **110**:11373-11378.

Hirsh, D., D. Oppenheim, and M. Klass. 1976. Development of the reproductive system of *Caenorhabditis elegans*. Developmental Biology **49**:200-219.

Holland, A. J., and D. W. Cleveland. 2009. Boveri revisited: chromosomal instability, aneuploidy and tumorigenesis. Nature Reviews Molecular Cell Biology **10**:478-487.

Holway, A. H., S. H. Kim, A. La Volpe, and W. M. Michael. 2006. Checkpoint silencing during the DNA damage response in *Caenorhabditis elegans* embryos. J Cell Biol **172**:999-1008.

Hyman, A. A., C. A. Weber, and F. Julicher. 2014. Liquid-liquid phase separation in biology. Annu Rev Cell Dev Biol **30**:39-58.

Hyman, A. A., and J. G. White. 1987. Determination of cell division axes in the early embryogenesis of *Caenorhabditis elegans*. J Cell Biol **105**:2123-2135.

Ichikawa, K., M. J. Shoura, K. L. Artiles, D. E. Jeong, C. Owa, H. Kobayashi, Y. Suzuki, M. Kanamori, Y. Toyoshima, Y. Iino, A. E. Rougvie, L. Wahba, A. Z. Fire, E. M. Schwarz, and S. Morishita. 2025. CGC1, a new reference genome for *Caenorhabditis elegans*. Genome Res **35**:1902-1918.

Inoué, S. 1953. Polarization optical studies of the mitotic spindle. Chromosoma **5**:487-500.

Izquierdo, D., W.-J. Wang, K. Uryu, and M.-Fu B. Tsou. 2014. Stabilization of Cartwheel-less Centrioles for Duplication Requires CEP295-Mediated Centriole-to-Centrosome Conversion. Cell Reports **8**:957-965.

Jaspersen, S. L., and M. Winey. 2004. The Budding Yeast Spindle Pole Body: Structure, Duplication, and Function. Annual Review of Cell and Developmental Biology **20**:1-28.

Jha, K., A. Woglar, C. Busso, G. N. Hatzopoulos, T. Favez, and P. Gönczy. 2025. *C. elegans* SAS-1 ensures centriole integrity and ciliary function, and operates with SSNA-1. PLoS Genetics **21**:e1011912.

Kamath, R. S., and J. Ahringer. 2003. Genome-wide RNAi screening in *Caenorhabditis elegans*. Methods **30**:313-321.

Kemp, C. A., K. R. Kopish, P. Zipperlen, J. Ahringer, and K. F. O'Connell. 2004. Centrosome maturation and duplication in *C. elegans* require the coiled-coil protein SPD-2. Developmental cell **6**:511-523.

Kemphues, K. J., and S. Strome. 1997. Fertilization and Establishment of Polarity in the Embryo.*in* D. L. Riddle, T. Blumenthal, B. J. Meyer, and J. R. Priess, editors. *C. elegans* II. Cold Spring Harbor Laboratory Press, Cold Spring Harbor (NY).

Kim, J., J. Kim, and K. Rhee. 2019. PCNT is critical for the association and conversion of centrioles to centrosomes during mitosis. J Cell Sci **132**.

Kim, J., K. Lee, and K. Rhee. 2015. PLK1 regulation of PCNT cleavage ensures fidelity of centriole separation during mitotic exit. Nat Commun **6**:10076.

Kim, S., and K. Rhee. 2014. Importance of the CEP215-pericentrin interaction for centrosome maturation during mitosis. PLOS ONE **9**:e87016.

Kim, W., R. S. Underwood, I. Greenwald, and D. D. Shaye. 2018. OrthoList 2: A New Comparative Genomic Analysis of Human and *Caenorhabditis elegans* Genes. Genetics **210**:445-461.

Kirkham, M. 2003. SAS-4 is a *C. elegans* centriolar protein that controls centrosome size. et al **112**:575-587.

Kitagawa, D., C. Busso, I. Fluckiger, and P. Gonczy. 2009. Phosphorylation of SAS-6 by ZYG-1 is critical for centriole formation in *C. elegans* embryos. Dev Cell **17**:900-907.

Klena, N., M. Le Guennec, A. M. Tassin, H. van den Hoek, P. S. Erdmann, M. Schaffer, S. Geimer, G. Aeschlimann, L. Kovacik, Y. Sadian, K. N. Goldie, H. Stahlberg, B. D. Engel, V. Hamel, and P. Guichard. 2020. Architecture of the centriole cartwheel-containing region revealed by cryo-electron tomography. EMBO J **39**:e106246.

Kohlmaier, G., J. Lončarek, X. Meng, B. F. McEwen, M. M. Mogensen, A. Spektor, B. D. Dynlacht, A. Khodjakov, and P. Gönczy. 2009. Overly Long Centrioles and Defective

Cell Division upon Excess of the SAS-4-Related Protein CPAP. Current Biology **19**:1012-1018.

Kotak, S., and P. Gönczy. 2013. Mechanisms of spindle positioning: cortical force generators in the limelight. Current Opinion in Cell Biology **25**:741-748.

Labbé, J. C., E. K. McCarthy, and B. Goldstein. 2004. The forces that position a mitotic spindle asymmetrically are tethered until after the time of spindle assembly. J Cell Biol **167**:245-256.

Labella, S., A. Woglar, V. Jantsch, and M. Zetka. 2011. Polo Kinases Establish Links between Meiotic Chromosomes and Cytoskeletal Forces Essential for Homolog Pairing. Developmental cell **21**:948-958.

Laos, T., G. Cabral, and A. Dammermann. 2015. Isotropic incorporation of SPD-5 underlies centrosome assembly in *C. elegans*. Current Biology **25**:648-649.

Lawo, S., M. Hasegan, G. D. Gupta, and L. Pelletier. 2012. Subdiffraction imaging of centrosomes reveals higher-order organizational features of pericentriolar material. Nature Cell Biology **14**:1148-1158.

Le Bot, N., M.-C. Tsai, R. K. Andrews, and J. Ahringer. 2003. TAC-1, a Regulator of Microtubule Length in the *C. elegans* Embryo. Current Biology **13**:1499-1505.

Lee, K., and K. Rhee. 2011. PLK1 phosphorylation of pericentrin initiates centrosome maturation at the onset of mitosis. J Cell Biol **195**:1093-1101.

Lee, K., and K. Rhee. 2012. Separase-dependent cleavage of pericentrin B is necessary and sufficient for centriole disengagement during mitosis. Cell Cycle **11**:2476-2485.

Leidel, S., M. Delattre, L. Cerutti, K. Baumer, and P. Gönczy. 2005. SAS-6 defines a protein family required for centrosome duplication in *C. elegans* and in human cells. Nature Cell Biology **7**:115-125.

Leidel, S., and P. Gönczy. 2003. SAS-4 Is Essential for Centrosome Duplication in *C. elegans* and Is Recruited to Daughter Centrioles Once per Cell Cycle. Developmental cell **4**:431-439.

Lettman, Molly M., Yao L. Wong, V. Viscardi, S. Niessen, S.-h. Chen, Andrew K. Shiau, H. Zhou, A. Desai, and K. Oegema. 2013. Direct Binding of SAS-6 to ZYG-1 Recruits SAS-6 to the Mother Centriole for Cartwheel Assembly. Developmental cell **25**:284-298.

Loncarek, J., and M. Bettencourt-Dias. 2018. Building the right centriole for each cell type. Journal of Cell Biology **217**:823-835.

Lu, Y., and R. Roy. 2014. Centrosome/Cell Cycle Uncoupling and Elimination in the Endoreduplicating Intestinal Cells of *C. elegans*. PLOS ONE **9**:e110958.

Ma, D., F. Wang, J. Teng, N. Huang, and J. Chen. 2023. Structure and function of distal and subdistal appendages of the mother centriole. Journal of Cell Science **136**.

Magescas, J., S. Eskinazi, M. V. Tran, and J. L. Feldman. 2021. Centriole-less pericentriolar material serves as a microtubule organizing center at the base of *C. elegans* sensory cilia. Current Biology **31**:2410-2417.e2416.

Magescas, J., J. C. Zonka, and J. L. Feldman. 2019. A two-step mechanism for the inactivation of microtubule organizing center function at the centrosome. Elife **8**.

Maheshwari, R., M. M. Rahman, S. Drey, M. Onyundo, G. Fabig, M. A. Q. Martinez, D. Q. Matus, T. Müller-Reichert, and O. Cohen-Fix. 2023. A membrane reticulum, the centriculum, affects centrosome size and function in *Caenorhabditis elegans*. Current Biology **33**:791-806.e797.

Maiato, H., and E. Logarinho. 2014. Mitotic spindle multipolarity without centrosome amplification. Nature Cell Biology **16**:386-394.

Malone, C. J., L. Misner, N. Le Bot, M. C. Tsai, J. M. Campbell, J. Ahringer, and J. G. White. 2003. The *C. elegans* hook protein, ZYG-12, mediates the essential attachment between the centrosome and nucleus. Cell **115**:825-836.

Mardin, B. R., and E. Schiebel. 2012. Breaking the ties that bind: new advances in centrosome biology. J Cell Biol **197**:11-18.

Martinez-Campos, M., R. Basto, J. Baker, M. Kernan, and J. W. Raff. 2004. The *Drosophila* pericentrin-like protein is essential for cilia/flagella function, but appears to be dispensable for mitosis. J Cell Biol **165**:673-683.

Matthews, L. R., P. Carter, D. Thierry-Mieg, and K. Kemphues. 1998. ZYG-9, a *Caenorhabditis elegans* protein required for microtubule organization and function, is a component of meiotic and mitotic spindle poles. J Cell Biol **141**:1159-1168.

McIntosh, J. R. 2021. Anaphase A. Semin Cell Dev Biol **117**:118-126.

McNally, F. J. 2013. Mechanisms of spindle positioning. J Cell Biol **200**:131-140.

McNally, Karen L. P., Amy S. Fabritius, Marina L. Ellefson, Jonathan R. Flynn, Jennifer A. Milan, and Francis J. McNally. 2012. Kinesin-1 Prevents Capture of the Oocyte Meiotic Spindle by the Sperm Aster. Developmental cell **22**:788-798.

Meaders, J. L., and D. R. Burgess. 2020. Microtubule-Based Mechanisms of Pronuclear Positioning. Cells **9**:505.

Medley, J. C., R. N. Yim, J. Dipanni, B. Sebou, B. Shaffou, E. Cramer, C. Wu, M. Kabara, and M. H. Song. 2023. Site-specific phosphorylation of ZYG-1 regulates ZYG-1 stability and centrosome number. iScience **26**:108410.

Meneely, P. M., C. L. Dahlberg, and J. K. Rose. 2019. Working with Worms: *Caenorhabditis elegans* as a Model Organism. Current Protocols Essential Laboratory Techniques **19**:e35.

Mennella, V., B. Keszthelyi, K. L. McDonald, B. Chhun, F. Kan, G. C. Rogers, B. Huang, and D. A. Agard. 2012. Subdiffraction-resolution fluorescence microscopy reveals a domain

of the centrosome critical for pericentriolar material organization. Nature Cell Biology **14**:1159-1168.

Meunier, S., and I. Vernos. 2012. Microtubule assembly during mitosis – from distinct origins to distinct functions? Journal of Cell Science **125**:2805-2814.

Mikeladze-Dvali, T., L. von Tobel, P. Strnad, G. Knott, H. Leonhardt, L. Schermelleh, and P. Gönczy. 2012. Analysis of centriole elimination during *C. elegans* oogenesis. Development **139**:1670-1679.

Mittasch, M., V. M. Tran, M. U. Rios, A. W. Fritsch, S. J. Enos, B. Ferreira Gomes, A. Bond, M. Kreysing, and J. B. Woodruff. 2020. Regulated changes in material properties underlie centrosome disassembly during mitotic exit. J Cell Biol **219**.

Morgan, D. O. 2007. The cell cycle: principles of control. New science press.

Moritz, M., M. B. Braunfeld, V. Guénebaut, J. Heuser, and D. A. Agard. 2000. Structure of the γ-tubulin ring complex: a template for microtubule nucleation. Nature Cell Biology **2**:365-370.

Murph, M., S. Singh, and M. Schvarzstein. 2022. A combined *in silico* and *in vivo* approach to the structure-function annotation of SPD-2 provides mechanistic insight into its functional diversity. Cell Cycle **21**:1958-1979.

Musacchio, A., and E. D. Salmon. 2007. The spindle-assembly checkpoint in space and time. Nature Reviews Molecular Cell Biology **8**:379-393.

Nakajo, M., H. Kano, K. Tsuyama, N. Haruta, and A. Sugimoto. 2022. Centrosome maturation requires phosphorylation-mediated sequential domain interactions of SPD-5. Journal of Cell Science **135**.

Nechipurenko, I. V., C. Berciu, P. Sengupta, and D. Nicastro. 2017. Centriolar remodeling underlies basal body maturation during ciliogenesis in *Caenorhabditis elegans*. Elife **6**:e25686.

Newport, J., and M. Kirschner. 1982. A major developmental transition in early *Xenopus* embryos: I. characterization and timing of cellular changes at the midblastula stage. Cell **30**:675-686.

Nigg, E. A., and A. J. Holland. 2018. Once and only once: mechanisms of centriole duplication and their deregulation in disease. Nat Rev Mol Cell Biol **19**:297-312.

Nigg, E. A., and J. W. Raff. 2009. Centrioles, centrosomes, and cilia in health and disease. Cell **139**:663-678.

Nishi, Y., E. Rogers, S. Robertson, and R. Lin. 2008. Polo kinases regulate *C. elegans* embryonic polarity via binding to DYRK2-primed MEX-5 and MEX-6. Development (Cambridge, England) **135**:687-697.

O'Connell, K. F. 1999. The centrosome of the early *C. elegans* embryo: inheritance, assembly, replication, and developmental roles. Pages 365-384 *in* R. E. Palazzo and G. P. Schatten, editors. Current Topics in Developmental Biology. Academic Press.

O'Toole, E., K. McDonald, A. Hyman, and T. Müller-Reichert. 2002. High-Voltage Electron Tomography of the Centrosome in *Caenorhabditis elegans*. Microscopy and Microanalysis **8**:880-881.

O'Connell, K. F. 2001. The *C. elegans zyg-1* Gene Encodes a Regulator of Centrosome Duplication with Distinct Maternal and Paternal Roles in the Embryo. et al **105**:547-558.

Oegema, K., and T. Hyman. 2006. Cell division. WormBook: The Online Review of *C. elegans* Biology.

Ohta, M., Z. Zhao, D. Wu, S. Wang, J. L. Harrison, J. S. Gómez-Cavazos, A. Desai, and K. F. Oegema. 2021. Polo-like kinase 1 independently controls microtubule-nucleating capacity and size of the centrosome. Journal of Cell Biology **220**.

Ong, J. Y., and J. Z. Torres. 2020. Phase Separation in Cell Division. Molecular Cell **80**:9-20.

Özlü, N., M. Srayko, K. Kinoshita, B. Habermann, E. T. O'Toole, T. Müller-Reichert, N. Schmalz, A. Desai, and A. A. Hyman. 2005. An Essential Function of the *C. elegans* Ortholog of TPX2 Is to Localize Activated Aurora A Kinase to Mitotic Spindles. Developmental cell **9**:237-248.

Palazzo, R. E., J. M. Vogel, B. J. Schnackenberg, D. R. Hull, and X. Wu. 2000. Centrosome maturation. Curr Top Dev Biol **49**:449-470.

Panbianco, C., D. Weinkove, E. Zanin, D. Jones, N. Divecha, M. Gotta, and J. Ahringer. 2008. A casein kinase 1 and PAR proteins regulate asymmetry of a PIP(2) synthesis enzyme for asymmetric spindle positioning. Dev Cell **15**:198-208.

Park, D. H., and L. S. Rose. 2008. Dynamic localization of LIN-5 and GPR-1/2 to cortical force generation domains during spindle positioning. Dev Biol **315**:42-54.

Peel, N., J. Iyer, A. Naik, M. P. Dougherty, M. Decker, and K. F. O'Connell. 2017. Protein Phosphatase 1 Down Regulates ZYG-1 Levels to Limit Centriole Duplication. PLoS Genetics **13**:e1006543.

Peel, N., N. R. Stevens, R. Basto, and J. W. Raff. 2007. Overexpressing Centriole-Replication Proteins *In Vivo* Induces Centriole Overduplication and De Novo Formation. Current Biology **17**:834-843.

Pelletier, L., E. O'Toole, A. Schwager, A. A. Hyman, and T. Muller-Reichert. 2006. Centriole assembly in *Caenorhabditis elegans*. Nature **444**:619-623.

Pelletier, L., N. Ozlu, E. Hannak, C. Cowan, B. Habermann, M. Ruer, T. Muller-Reichert, and A. A. Hyman. 2004. The *Caenorhabditis elegans* centrosomal protein SPD-2 is required for both pericentriolar material recruitment and centriole duplication. Curr Biol **14**:863-873.

Pickett-Heaps, J. D. 1969. The evolution of the mitotic apparatus: an attempt at comparative ultrastructural cytology in dividing plant cells. Cytobios **1**:257-280.

Pierron, M., A. Woglar, C. Busso, K. Jha, T. Mikeladze-Dvali, M. Croisier, and P. Gönczy. 2023. Centriole elimination during *Caenorhabditis elegans* oogenesis initiates with loss of the central tube protein SAS-1. The EMBO Journal **42**:e115076.

Pintard, L., and B. Bowerman. 2019. Mitotic Cell Division in *Caenorhabditis elegans*. Genetics **211**:35-73.

Policard, A., and M. Bessis. 1955. Étude au microscope électronique de la centrosphère des leucocytes des mammifères. Experimental Cell Research **8**:583-585.

Prosser, S. L., and L. Pelletier. 2017. Mitotic spindle assembly in animal cells: a fine balancing act. Nature Reviews Molecular Cell Biology **18**:187-201.

Qiao, R., G. Cabral, M. Lettman, A. Dammermann, and G. Dong. 2012. SAS-6 coiled-coil structure and interaction with SAS-5 suggest a regulatory mechanism in *C. elegans* centriole assembly. The EMBO Journal **31**.

Raff, J. W. 2019. Phase Separation and the Centrosome: A Fait Accompli? Trends Cell Biol **29**:612-622.

Richens, J. H., T. P. Barros, E. P. Lucas, N. Peel, D. M. Pinto, A. Wainman, and J. W. Raff. 2015. The *Drosophila* Pericentrin-like-protein (PLP) cooperates with Cnn to maintain the integrity of the outer PCM. Biol Open **4**:1052-1061.

Rios, M. U., M. A. Bagnucka, B. D. Ryder, B. Ferreira Gomes, N. E. Familiari, K. Yaguchi, M. Amato, W. E. Stachera, Ł. A. Joachimiak, and J. B. Woodruff. 2024. Multivalent coiled-coil interactions enable full-scale centrosome assembly and strength. Journal of Cell Biology **223**.

Rios, M. U., W. E. Stachera, N. E. Familiari, C. Brito, T. Surrey, and J. B. Woodruff. 2025. *In vitro* reconstitution of a minimal human centrosome scaffold capable of forming and clustering microtubule asters. J Cell Sci **138**.

Robbins, E., and N. K. Gonatas. 1964. The ultrastructure of a mammalian cell during the mitotic cycle. J Cell Biol **21**:429-463.

Sanchez, A. D., and J. L. Feldman. 2017. Microtubule-organizing centers: from the centrosome to non-centrosomal sites. Curr Opin Cell Biol **44**:93-101.

Sankaralingam, P., S. Wang, Y. Liu, K. Oegema, and K. O'Connell. 2024. The kinase ZYG-1 phosphorylates the cartwheel protein SAS-5 to drive centriole assembly in *C. elegans*. EMBO reports **25**:2698-2721.

Scheer, U. 2014. Historical roots of centrosome research: discovery of Boveri's microscope slides in Würzburg. Philosophical Transactions of the Royal Society B: Biological Sciences **369**:20130469.

Schmitt, M. T., J. Kroll, M. J. A. Ruiz-Fernandez, R. Hauschild, S. Ghosh, P. Kameritsch, J. Merrin, J. Schmid, K. Stefanowski, A. W. Thomae, J. Cheng, G. N. Öztan, P. Konopka, G. C. Ortega, T. Penz, L. Bach, D. Baumjohann, C. Bock, T. Straub, F. Meissner, E. Kiermaier, and J. Renkawitz. 2025. Protecting centrosomes from fracturing enables efficient cell navigation. Science Advances **11**:eadx4047.

Schöckel, L., M. Möckel, B. Mayer, D. Boos, and O. Stemmann. 2011. Cleavage of cohesin rings coordinates the separation of centrioles and chromatids. Nature Cell Biology **13**:966-972.

Scholey, J. M., G. Civelekoglu-Scholey, and I. Brust-Mascher. 2016. Anaphase B. Biology (Basel) **5**.

Schreiner, A., A. Heim, L. Pletschacher, L.-M. Alznauer, S. Schwenkert, F. Wolff, E. Zanin, and T. Mikeladze-Dvali. 2025. PCMD-1 stabilizes the PCM scaffold and facilitates centriole separation. Journal of Cell Biology **224**.

Sender, R., S. Fuchs, and R. Milo. 2016. Revised Estimates for the Number of Human and Bacteria Cells in the Body. PLoS Biol **14**:e1002533.

Seo, M. Y., W. Jang, and K. Rhee. 2015. Integrity of the Pericentriolar Material Is Essential for Maintaining Centriole Association during M Phase. PLOS ONE **10**:e0138905.

Srayko, M., A. Kaya, J. Stamford, and A. A. Hyman. 2005. Identification and Characterization of Factors Required for Microtubule Growth and Nucleation in the Early *C. elegans* Embryo. Developmental cell **9**:223-236.

Srinivasan, D. G., R. M. Fisk, H. Xu, and S. Van den Heuvel. 2003. A complex of LIN-5 and GPR proteins regulates G protein signaling and spindle function in *C. elegans*. Genes & development **17**:1225-1239.

Stenzel, L., A. Schreiner, E. Zuccoli, S. Üstüner, J. Mehler, E. Zanin, and T. Mikeladze-Dvali. 2021. PCMD-1 bridges the centrioles and the pericentriolar material scaffold in *C. elegans*. Development **148**.

Stenzel, L. K. 2022. Functional characterization of the centrosomal protein PCMD-1 in bridging the centrioles and the pericentriolar material in *C. elegans*. Dissertation. Ludwig-Maximilians-Universität, München.

Stevens, N. R., J. Dobbelaere, K. Brunk, A. Franz, and J. W. Raff. 2010. *Drosophila* Ana2 is a conserved centriole duplication factor. Journal of Cell Biology **188**:313-323.

Strnad, P., S. Leidel, T. Vinogradova, U. Euteneuer, A. Khodjakov, and P. Gönczy. 2007. Regulated HsSAS-6 levels ensure formation of a single procentriole per centriole during the centrosome duplication cycle. Developmental cell **13**:203-213.

Sugioka, K., D. R. Hamill, J. B. Lowry, M. E. McNeely, M. Enrick, A. C. Richter, L. E. Kiebler, J. R. Priess, and B. Bowerman. 2017. Centriolar SAS-7 acts upstream of SPD-2 to regulate centriole assembly and pericentriolar material formation. Elife **6**.

Sulston, J. E., and E. Schierenberg. 1983. The Embryonic Cell Lineage of the Nematode *Caenorhabditis elegans*. Developmental Biology **100**:64-119.

Tavernier, N., A. Noatynska, C. Panbianco, L. Martino, L. Van Hove, F. Schwager, T. Léger, M. Gotta, and L. Pintard. 2015. Cdk1 phosphorylates SPAT-1/Bora to trigger PLK-1 activation and drive mitotic entry in *C. elegans* embryos. The Journal of cell biology **208**:661-669.

Tollervey, F., M. U. Rios, E. Zagoriy, J. B. Woodruff, and J. Mahamid. 2025. Molecular architectures of centrosomes in *C. elegans* embryos visualized by cryo-electron tomography. Developmental cell **60**:885-900.e885.

Tompa, P., and M. Fuxreiter. 2008. Fuzzy complexes: polymorphism and structural disorder in protein–protein interactions. Trends in Biochemical Sciences **33**:2-8.

Toya, M., M. Terasawa, K. Nagata, Y. Iida, and A. Sugimoto. 2011. A kinase-independent role for Aurora A in the assembly of mitotic spindle microtubules in *Caenorhabditis elegans* embryos. Nature Cell Biology **13**:708-714.

Truebestein, L., and T. A. Leonard. 2016. Coiled-coils: The long and short of it. Bioessays **38**:903-916.

Tsou, M.-F. B., and T. Stearns. 2006. Controlling centrosome number: licenses and blocks. Current Opinion in Cell Biology **18**:74-78.

Tsou, M. F. B. 2009. Polo kinase and separase regulate the mitotic licensing of centriole duplication in human cells. et al **17**:344-354.

Uhlmann, F. 2001. Secured cutting: controlling separase at the metaphase to anaphase transition. The EMBO Reports **2**:487-492.

van den Heuvel, S. 2005. Cell-cycle regulation. WormBook: The Online Review of *C. elegans* Biology.

Varadarajan, R., and Nasser M. Rusan. 2018. Bridging centrioles and PCM in proper space and time. Essays in Biochemistry **62**:793-801.

Varmark, H., S. Llamazares, E. Rebollo, B. Lange, J. Reina, H. Schwarz, and C. Gonzalez. 2007. Asterless is a centriolar protein required for centrosome function and embryo development in *Drosophila*. Current Biology **17**:1735-1745.

Vasquez-Limeta, A., and J. Loncarek. 2021. Human centrosome organization and function in interphase and mitosis. Semin Cell Dev Biol **117**:30-41.

von Tobel, L., T. Mikeladze-Dvali, M. Delattre, F. R. Balestra, S. Blanchoud, S. Finger, G. Knott, T. Müller-Reichert, and P. Gönczy. 2014. SAS-1 is a C2 domain protein critical for centriole integrity in *C. elegans*. PLoS Genet **10**:e1004777.

Vulprecht, J., A. David, A. Tibelius, A. Castiel, G. Konotop, F. Liu, F. Bestvater, M. S. Raab, H. Zentgraf, and S. Izraeli. 2012. STIL is required for centriole duplication in human cells. Journal of Cell Science **125**:1353-1362.

Wicks, S. R., R. T. Yeh, W. R. Gish, R. H. Waterston, and R. H. Plasterk. 2001. Rapid gene mapping in *Caenorhabditis elegans* using a high density polymorphism map. Nat Genet **28**:160-164.

Wignall, S. M., and A. M. Villeneuve. 2009. Lateral microtubule bundles promote chromosome alignment during acentrosomal oocyte meiosis. Nat Cell Biol **11**:839-844.

Winey, M., and E. O'Toole. 2014. Centriole structure. Philosophical Transactions of the Royal Society B: Biological Sciences **369**:20130457.

Woglar, A., M. Pierron, F. Z. Schneider, K. Jha, C. Busso, and P. Gönczy. 2022. Molecular architecture of the *C. elegans* centriole. PLOS Biology **20**:e3001784.

Wolf, B., F. R. Balestra, A. Spahr, and P. Gönczy. 2018. ZYG-1 promotes limited centriole amplification in the *C. elegans* seam lineage. Dev Biol **434**:221-230.

Wong, S.-S., J. M. Monteiro, C.-C. Chang, M. Peng, N. Mohamad, T. L. Steinacker, B. Xiao, S. Saurya, A. Wainman, and J. W. Raff. 2025. Centrioles generate two scaffolds with distinct biophysical properties to build mitotic centrosomes. Science Advances **11**.

Woodruff, J. B. 2021. The material state of centrosomes: lattice, liquid, or gel? Curr Opin Struct Biol **66**:139-147.

Woodruff, J. B., B. Ferreira Gomes, P. O. Widlund, J. Mahamid, A. Honigmann, and A. A. Hyman. 2017. The Centrosome Is a Selective Condensate that Nucleates Microtubules by Concentrating Tubulin. Cell **169**:1066-1077.e1010.

Woodruff, J. B., O. Wueseke, and A. A. Hyman. 2014. Pericentriolar material structure and dynamics. Philosophical transactions of the Royal Society of London. Series B, Biological sciences **369**:20130459.

Woodruff, J. B., O. Wueseke, V. Viscardi, J. Mahamid, S. D. Ochoa, J. Bunkenborg, P. O. Widlund, A. Pozniakovsky, E. Zanin, S. Bahmanyar, A. Zinke, S. H. Hong, M. Decker, W. Baumeister, J. S. Andersen, K. Oegema, and A. A. Hyman. 2015. Centrosomes. Regulated assembly of a supramolecular centrosome scaffold *in vitro*. Science **348**:808-812.

Wu, J., and A. Akhmanova. 2017. Microtubule-Organizing Centers. Annu Rev Cell Dev Biol **33**:51-75.

Wueseke, O., J. Bunkenborg, M. Y. Hein, A. Zinke, V. Viscardi, J. B. Woodruff, K. Oegema, M. Mann, J. S. Andersen, and A. A. Hyman. 2014. The *Caenorhabditis elegans* pericentriolar material components SPD-2 and SPD-5 are monomeric in the cytoplasm before incorporation into the PCM matrix. Molecular biology of the cell **25**:2984-2992.

Wueseke, O., D. Zwicker, A. Schwager, Y. L. Wong, K. Oegema, F. Jülicher, A. A. Hyman, and J. B. Woodruff. 2016. Polo-like kinase phosphorylation determines *Caenorhabditis elegans* centrosome size and density by biasing SPD-5 toward an assembly-competent conformation. Biology Open **5**:1431-1440.

Zheng, X., L. M. Gooi, A. Wason, E. Gabriel, N. Z. Mehrjardi, Q. Yang, X. Zhang, A. Debec, M. L. Basiri, T. Avidor-Reiss, A. Pozniakovsky, I. Poser, T. Saric, A. A. Hyman, H. Li, and J. Gopalakrishnan. 2014. Conserved TCP domain of Sas-4/CPAP is essential for pericentriolar material tethering during centrosome biogenesis. Proc Natl Acad Sci U S A **111**:E354-363.

Zhu, F., S. Lawo, A. Bird, D. Pinchev, A. Ralph, C. Richter, T. Müller-Reichert, R. Kittler, A. A. Hyman, and L. Pelletier. 2008. The mammalian SPD-2 ortholog Cep192 regulates centrosome biogenesis. Current Biology **18**:136-141.

Zwicker, D., M. Decker, S. Jaensch, A. A. Hyman, and F. Julicher. 2014. Centrosomes are autocatalytic droplets of pericentriolar material organized by centrioles. Proc Natl Acad Sci U S A **111**:E2636-2645.

Acknowledgement

First, I want to express my sincere appreciation to Dr. Tamara Mikeladze-Dvali, for the opportunity to complete my PhD in her laboratory. Tamara, thank you for your trust, for all the support and mentorship you have given me. When this project became challenging, you never lost confidence in it or in me. You showed me that science rarely follows a straight line, and that the most surprising turns can lead to the most interesting questions. I will always (try) to carry that mindset with me.

I would also like to thank my TAC committee, Prof. Dr. Christof Osman, Dr. Daphne Cabianca, and Prof. Dr. David Keays, for their guidance and feedback throughout my PhD. In addition, I am grateful to the entire Zanin lab for the supportive environment during our lab meetings. In particular, I would like to thank Prof. Dr. Esther Zanin for accompanying my project from the very beginning with advice, discussions, and many new ideas. Thank you for your continuous support.

In particular, I want to express my deepest gratitude to my direct PhD colleague and dear friend, Zakiah Talib. Thank you for standing by me through all the ups and downs, for always listening, and for your patience, especially when the same experiment failed for the umpteenth time. Your support meant a lot to me, and I will miss our time together very much.

I would like to express my thanks to Dr. Friederike Wolf, meiner “Quasi-Kollegin”. During our shared time in the lab and well beyond, you supported me and were always available whenever I needed advice. Thank you for all your help and for the friendship that has resulted from it.

I also want to thank Beril Tiryakiler and Astrid Heim. I greatly enjoyed working with both of you, even though our time together in the lab was not as long as I would have liked. Many thanks to all the students in our lab during my time here, and to the colleagues in the Cell Biology Department, especially from the Mokranjac and Osman labs. I truly enjoyed our time together.

My heartfelt thanks go to my family and friends for their constant belief in me and for their patience and understanding during particularly stressful periods. I am especially grateful to my parents, Nina and Franz Schreiner. Mama, Papa - mein tiefster Dank gilt euch. Danke, dass ihr mich immer unterstützt habt, an mich geglaubt und jederzeit für mich da wart. All das hier wäre ohne euch nicht möglich gewesen!

My greatest personal thanks go to my husband, Christian Schletter. Throughout my PhD, you stood by my side, strengthened my confidence, encouraged me, and helped me through all the difficult moments. Even when my motivation dropped, yours didn’t, and that helped me more than you can imagine. A special thank you for your incredible support during the writing phase of this thesis, you kept everything else running, so I could focus on finishing.

The article “*PCMD-1 bridges the centrioles and the PCM scaffold in C. elegans*” (Stenzel et al. 2021) was reproduced with permission of Company of Biologists. The article “*PCMD-1 stabilizes the PCM scaffold and facilitates centriole separation*” (Schreiner et al. 2025) was reproduced with permission of Rockefeller University Press.

Curriculum Vitae

Personal details

Name	Alina Jessica Schreiner
Nationality	German

Education

06/2021 – 09/2025	PhD Candidate (Biology) Ludwig-Maximilians-Universität Munich, Germany
09/2018 – 05/2021	Master of Science in Molecular and Cellular Biology Ludwig-Maximilians-Universität Munich, Germany
09/2015 – 09/2018	Bachelor of Science in Biology Ludwig-Maximilians-Universität Munich, Germany